Studies on Direct Chemical Looping Combustion of Coal with Rice Straw using Electronic Waste Based Oxygen Carriers for Clean Energy Production

A thesis

Submitted in Partial Fulfilment of the Requirements for the Degree of

DOCTOR OF PHILOSOPHY

By

Barnali Bhui

Department of Chemical Engineering

Indian Institute of Technology Guwahati

Guwahati – 781039, Assam, India

February 2022

Dedicated

to

My Parents

And

My Mentor

Department of Chemical Engineering
Indian Institute of Technology Guwahati
Guwahati, Assam 781039

STATEMENT

I hereby declare that the matter embodied in this thesis entitled "**Studies on direct chemical looping combustion of coal with rice straw using electronic waste based oxygen carriers for clean energy production**" is the result of investigations carried out by me in the Department of Chemical Engineering, Indian Institute of Technology Guwahati, Assam, India under the supervision of **Dr. Prabu Vairakannu.**

In keeping with the general practice of reporting scientific observations, due acknowledgement has been made wherever the work described is based on the findings of other investigations.

Guwahati — **Barnali Bhui**

February, 2022 — (Roll No. 156107012)

Department of Chemical Engineering
Indian Institute of Technology Guwahati
Guwahati, Assam 781039

CERTIFICATE

It is certified that the work described in this thesis, entitled "**Studies on direct chemical looping combustion of coal with rice straw using electronic waste based oxygen carriers for clean energy production**", done by **Ms. Barnali Bhui** for the award of degree of philosophy is an authentic record of the results obtained from the research work carried out under my supervision in the department of Chemical Engineering, Indian Institute of Technology Guwahati, India and this work has not been submitted elsewhere for the award of any other degree or diploma.

This thesis in my opinion, has reached the standard fulfilling the requirements for the award of the degree of Doctor of philosophy in accordance with the regulations of the institute.

7/3/22

Date: February, 2022

(Dr. Prabu Vairakannu)
Associate Professor
Department of Chemical Engineering
Indian Institute of Technology Guwahati
Guwahati, 781039

ACKNOWLEDGEMENTS

It gives me immense pleasure to extend my sincere gratitude to acknowledge each individual who led me to the completion of the dissertation. I am highly obliged to all the people who have encouraged me during all these years.

First and foremost, I would like to express my sincere thanks to my thesis supervisor, **Dr. Prabu Vairakannu**, for providing relentless support and valuable guidance in various stages of my research journey. His positive attitude and encouragement boosted my inner confidence and helped me to excel even after multiple failures. I am fortunate that he took me under his wings and considered me working under his esteemed guidance. I am greatly indebted for sharing his profound knowledge with me. I have thoroughly enjoyed working with him and I strongly believe that he brought out the best in me in every aspect.

I am grateful to my doctoral committee members **Prof. Mahuya De** (Department of Chemical Engineering), **Prof Chandan Das** (Department of Chemical Engineering), **Prof. Kannan Pakshirajan** (Department of Biosciences and Bioengineering) for their valuable suggestions, intensive assessment, and their active cooperation during my research progress.

I would like to acknowledge all the centres for providing me instrumental facilities for the characterization purposes such as the Analytical Lab Facility (Department of Chemical Engineering), Central Instrument Facility (CIF), Guwahati Biotech Park (for ultimate analysis) and IIT Kharagpur for the X-ray Fluorescence (XRF) analysis.

I am grateful to all the staff and faculty members of the Chemical Engineering Department for showering their profound knowledge as soon as I enrolled myself as the research scholar in this institute.

I would like to thank my friends, labmates and my well-wishers for providing me healthy research environment. Finally, I would like to thank my family for showering their endless love, care and encouragement throughout my life. They have always pushed me to set goals and helped me to achieve them.

Barnali Bhui

Abstract

Chemical looping combustion (CLC) is a promising technology paving the way for inherent CO_2 capture. As Indian coals are either enriched in ash content or have high sulphur, their utilization in the CLC technology under direct fuelled conditions is challenging. Alternatively, the blending of biomass with these coals can enhance fuel reactivity. In this context, the present study is focused on the co-utilization of Indian coals (mainly varying in ash content) and rice straw (RS) in the CLC process using low cost metal oxides in a fixed bed reactor under CO_2 based in-situ gasification mode of operation. A high ash coal (HAC) with 33% ash and a low ash coal (LAC) with 3% ash are used with RS. The intrinsic reactivity of ash, char, and volatile matter of the solid fuels with the oxygen carriers are assessed individually.

To commercialize the CLC based carbon capture technology, low-cost oxygen carriers are essential for economical operation. Electronic waste contains enormous metal components, which can be a potential source for the production of oxygen carriers. Thus, mixed oxygen carrier particles obtained from a printed circuit board (PCB) based electronic wastes are used in the present study. A series of thermochemical processes such as pyrolysis, gasification and combustion are conducted for the extraction of metals from the PCB board. The performance of the oxidized PCB based oxygen carrier (OPCB) is compared with commercial Fe_2O_3. The XRF analysis showed that the obtained OPCB contains 21% Fe_2O_3, 22.8% CuO and 3% NiO, 9.6% CaO and 33.6% inert supports (Al_2O_3, SiO_2, TiO_2). The experimental results showed that by using OPCB oxygen carriers, the CO_2 yield has increased by 4.6% for LAC, 3.9% for HAC, and 4.2% for RS, compared to the commercial Fe_2O_3 metal oxides. This is due to the chemical looping oxygen uncoupling nature (CLOU) of CuO, which releases oxygen molecules combusting the fuel directly. Further, the generated OPCB based metal oxides have a

higher surface area of 7.11m^2/g, leading to higher reactivity with fuels, compared to the commercial Fe_2O_3 particles having a surface area of 2.52 m^2/g.

The co-combustion of RS with HAC using commercial Fe_2O_3 metal oxides in the CLC process enhanced the CO_2 yield from 81.2% to 86.3%. Similarly, using OPCB with the blend of HAC-RS, the CO_2 yield is increased from 86.1% to 90.9% in the blend. Further, the char conversion is increased from 89.6% (HAC-OPCB) to 93.2% for the HAC-RS-OPCB blend. The interaction between the coals and RS is further studied to evaluate their synergistic effects, the char-oxygen carrier interaction, and activation energy using a thermogravimetric analyzer (TGA) under N_2 and CO_2 atmosphere. Among the kinetic models considered, the shrinking core model is found to be the best fit for all the cases. The activation energy is reduced by 18-25% using the coals-RS blend for both the oxygen carriers. However, the OPCB further reduced the activation energy of the reaction mixture by 7-25%, compared to the commercial Fe_2O_3.

Using the OPCB based oxygen carriers, Aspen Plus simulations are performed to examine the feasibility of commercial implementation of this technology by integrating the CLC system with a combined cycle power plant having a net capacity of 150 MW for electricity generation. The effect of co-firing on the net thermal efficiency of the power plants is analyzed. Further, economic analyses are carried out for the proposed system, and the levelized cost of electricity (LCOE) is estimated for the power plants using various fuels. It is found that the use of electronic waste-based oxygen carriers achieved almost an equivalent net thermal efficiency of 42.4% based on the combined cycle power plants, compared to the commercial Fe_2O_3 based power plants. Further, the economic analysis has shown that the levelized cost of electricity (LCOE) of the CLC integrated combined cycle power system employed with electronic waste-based oxygen carriers is 85.9 $/MWh, which is the lowest among other power systems. The LCOE using the

OPCB metal oxides is found to be lower than the commercial Fe_2O_3 and CuO by 8.9 $/MWh and 15.3 $/MWh, respectively.

It can be concluded that the oxygen carriers prepared from the discarded e-waste displayed higher reactivity with coal, RS, and their blends at 900°C than the commercial Fe_2O_3. Further, the blending of coal with RS demonstrated a better performance than that of the unblended conditions. Thus, the electronic-based oxygen carriers and the co-processing of Indian coals with RS in the CLC process can be the alternative strategy to implement the technology economically feasible for large-scale applications.

Keywords: Chemical looping combustion, e-waste as an oxygen carrier, co-gasification, CO_2 capture, kinetic analysis, energy analysis, economic analysis

Table of contents

List of Tables

List of Figures

CHAPTER 1

Introduction

CHAPTER 1

INTRODUCTION

The chapter presents a brief introduction to the energy supply scenario in India. The adverse effects of CO_2 escalation due to the conventional power generating systems are discussed. An advanced emerging technology termed as chemical looping combustion (CLC) is highlighted which has an ability to capture CO_2 inherently. The research formulation is based on the scope and significance of the CLC process. Finally, the basic outline of the doctoral work is discussed.

1.1. Current scenario of energy production in India

The demand for energy supply has been accelerated due to the rapid economic development. Fossil fuel supplies 85% of the global energy. India holds third rank globally in the coal production sector (Sharma and Kautish, 2020). Chikkatur et al. (2009) claimed that fossil fuel (coal) alone contributes to 70% of the total electricity production in India. Coal-based electricity production is inexpensive compared to other energy sources. The world bank data and statistics for India (2019) indicated that the electricity supply to 90% of the Indian population had elevated the CO_2 emissions to a higher level of 1.8 metric tonnes per capita in 2016 (Figure 1.1). The liberation of anthropogenic CO_2 during the fossil fuel combustion causes global climate change, acid rain, ozone layer depletion issues due to the escalation of global warming. Ortega-Ruiz et al. (2020) evaluated that the global temperature has increased by 1.5°C due to greenhouse gas emissions. Lu et al. (2020) asserted that the global mean temperature would further increase by 1.3-1.7°C by the end of the 21st century. The major aim of the electricity sector should be transitioned towards cleaner power production such that the electricity

access can be increased without any detrimental impact on the environment. Dubash et al. (2018) claimed that the CO_2 emissions in India would reach 3.8 Gt - 3.9 Gt by 2030 if the energy is harnessed only from the conventional power production units.

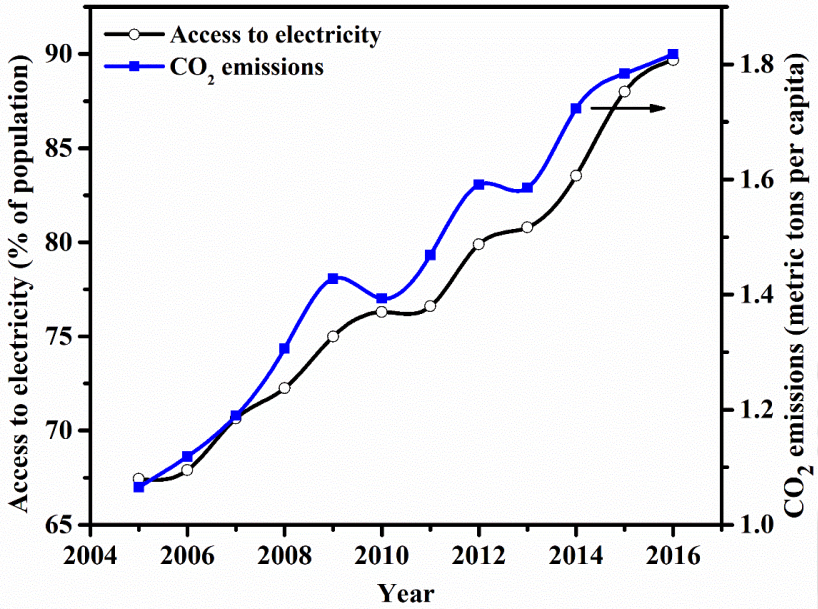

Figure 1.1. Relation between access to electricity to the Indian population and CO_2 emissions (World Bank Data and Statistics for India, 2019).

The CO_2 concentration in the atmosphere has shoot up to 400 ppm, which is the primary reason for global warming (Gai et al., 2016). It is estimated that the CO_2 concentration would reach up to 530 ppm by 2050 and 1360 ppm by the end of the 21st century (Lu et al., 2020). Several technologies are reported in the literature to capture the CO_2 including pre-combustion, post-combustion and oxy-fuel combustion approaches. The major demerit is that these technologies are energy-intensive. As a consequence, the net thermal efficiency of the power plants is reduced (Farooqui et al., 2018, Shahrestani and Rahimi, 2014). Chemical looping combustion (CLC) is a promising carbon capture and storage (CCS) technology with inherent CO_2 capture (Yaqub and Oboirien, 2020). The estimated cost of CO_2 capture is 20 \$/ton CO_2 for the CLC process, 28-41 \$/ton CO_2 for the pre-

combustion process and 36-67 $/ton CO_2 for the oxy-fuel process (Adanez et al., 2012). Hence the CLC technology needs to be implemented for the efficient and economic operation of CCS.

1.2. Carbon capture and storage (CCS) potential in India

The main purpose of carbon capture and storage (CCS) is to avoid CO_2 emission from the power generation sectors into the atmosphere. This technology attempts to mitigate the climate change issues via three steps: capture, transport and storage (Romanak & Dixon, 2022). This technology can reduce CO_2 emissions upto 0.1 tonnes CO_2/MWh thus, it is an important measure to control carbon emission (Mishra et al., 2015). Zoback & Gorelick (2012) estimated that 27 Gt of CO_2 needs to be stored worldwide, while only 40 Mt is only stored annually. The annual emission of CO_2 displayed a 3.1% compounded annual growth rate during the last three decades (Vishal et al., 2021). This has rendered CCS as an immediate measure to limit the increasing CO_2 concentration. India is among 24 developing countries with CCS activity and acknowledging the importance of CCS (Gupta & Paul, 2019). CO_2 once compressed to 110 bar is either sent to geological or ocean for storage for millions of years (Holloway et al., 2007). It comprises of CO_2 injecting either in to depleted oil and gas fields, saline aquifers, basalt formations or in unminable coal beds (Chao et al., 2021, Cruz et al., 2021), thereby preventing CO_2 emission into the environment. Viebahn et al. (2014) suggested that a reliable storage capacity assessment is required in India since theoretical storage capacity is much higher than the practical capacity. This occurred mainly due to the lack of geological data.

The Deccan volcanic province is one of the largest stable sink of CO_2 in India (Shackley & Verma, 2008). Singh et al. (2006) also suggested that CO_2 storage in basalt formation is a suitable option in India since basalt thickness ranges from few hundred meters to

thousand of meters. Table 1.1 highlights the existing CO_2 capture storage capacities in India. Dooley et al. (2005) estimated CO_2 storage capacity of 104 Gt in India in 2005. The capacity was split into 102 Gt from aquifers, 2 Gt from gas fields and 2 Gt from coal fields. (Garg & Shukla, 2009) suggested that CO_2 can be stored in the saline aquifers and in the coalfields situated in the Gondwana basins. Saline aquifers contains sedimentary rocks with dissolved salts, thus they are not suitable for agriculture and human consumption, but viable option for storage. Oil and gas fields can trap CO_2 for a longer duration of time (Garg & Shukla, 2009, Singh et al., 2006). Singh et al. (2006) assessed that 200 GT of CO_2 (out of 572 BT) can be stored in basalt formations, while 12 BT in unminable coal seams and depelted oil reservoirs. National Aluminium company (NALCO), Oil and Natural gas corporation Limited (ONGC), Bharat heavy Electricals Ltd. (BHEL), National thermal power corporation limited (NTPC) have initiated the setup for CCS (Shackley & Verma, 2008), (Kumar et al., 2019), (Mishra et al., 2015). National aluminium company (NALCO) has successfully demonstrated CO_2 sequestration plant. NALCO sequestered CO_2 in open pond using algal technology. The algae were produced by using flue gas of the plant and then further used to capture CO_2 with a capturing capacity of 36-54 ton of CO_2/acre/year (Sharma, 2018). Indian fertilizer sector are also adopting the CCS technology since the capture CO_2 will be utilized to produce urea and ammonia (Shackley & Verma, 2008). A pilot scale (500 MW) has been commissioned to capture CO_2 using amine based capture. It has been further integrated with an oil fired boiler and biomass gasifier to produce H_2 and CH_4. This plant has successfully operated for 4000hrs with CO_2 capture efficiency of 90-93% (Sethi & Vyas, 2017). ONGC has also planned to store 1200 tonnes CO_2 at its Ankleswar oil field with a rate of 440,000 tonnes/ year (Shackley & Verma, 2008).

The present scenario shows that India is applying various strategies to reduce the CO_2 emission. However, implementation of CCS in large scale further requires proper site specific assessments and stronger commitments in India. Hence, more in-depth assessments are required to identify the cost-optimal sites for CO_2 capture. The storage potential is still poorly defined with only a few broad assessments completed. It suffers several challenges such as lack of R&D effort, poor geological CO_2 storage data, energy penalty and environmental issues.

Table 1.1. Overview of existing CO_2 storage capacity (in Gt) in India.

Storage facilities	(Dooley et al., 2004)	(Singh et al., 2006)	(Holloway et al., 2008)
Saline aquifers	102	360	142
Enhanced oil recovery	2	7	1.1
Enhanced coal bed methane recovery	2	5	0.34
Basalts	-	200	-
Total	104	572	143.44

1.3. Carbon capture technologies

The CCS is one of the comprehensive technology which will allow the continuous usage of fossil fuels for power generation. It is classified as post-combustion, pre-combustion and oxy-fuel combustion capture technology (Mukherjee et al., 2019, Yadav & Mondal, 2022). Figure 1.2 presents the overview of the three main technologies for CO_2 capture. These processes require huge investment and has high energy penalty.

1.3.1. Post-combustion capture technology

The post-combustion capture means that the CO_2 is captured after the combustion of the fossil fuel by absorption (wet and dry), membrane separation, cryogenic distillation, and

adsorption processes (Figure 1.2a). Thus, it is attractive for retrofitting existing thermal plants. CO_2 is commercially absorbed over a solvent (mono-ethanolamine) and then it is exposed to high temperature to strip off the CO_2 from the solvent. The amine-based chemical absorption process appears to be the most suitable method to treat larger volumes of flue gases (Chen et al., 2014, Romanak & Dixon, 2022). It is an energy intensive process due to the solvent generation, and thus suffers significant losses in the energy output of the power plant (Mukherjee et al., 2019, Kanniche et al., 2010).

1.3.2. Pre-combustion capture technology

In this technology, CO_2 capture takes place before combustion. It involves the primary oxidation of the solid fuel with air/oxygen and steam to produce syngas (Figure 1.2b). In a water gas shift reactor, this stream is transformed to H_2 and CO_2. The physical absorption-based techniques are used to separate the generated H_2 from the CO_2. Generation of syngas is advantageous as it can be used in a combined cycle to produce energy or as a feedstock for chemical synthesis. However, this technology is expensive and thus reduces the overall plant efficiency (Olabi et al., 2022, Erlach et al., 2011).

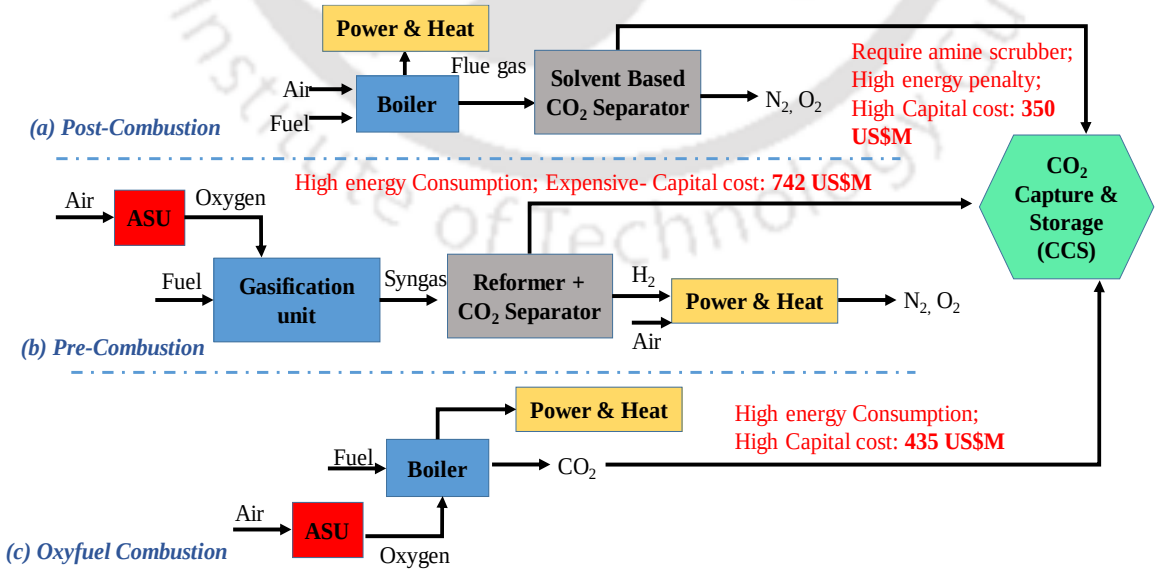

Figure 1.2. Layout of existing CCS technologies.

1.3.3. Oxy-fuel capture technology

This technology utilizes pure oxygen instead of air for the combustion of fossil fuels (Figure 1.2c). Thus, the flue gas stream contains a rich stream of CO_2 and H_2O with no N_2 dilution. This requires high energy input since oxygen is separated by cryogenic processes in the air separation unit (Tebbiche et al., 2021, Akash et al., 2016).

1.4. Chemical looping combustion (CLC)

CLC technology has been emerged as an advanced oxy-fuel process where the oxidant is supplied by the solid oxygen carriers. The attractive feature of the CLC is the inherent separation of CO_2 from other gases without any treatment. The CLC process is carried out using two interconnected reactors, namely, a fuel reactor (FR) and an air reactor (AR). Solid fuel is mixed thoroughly with oxygen carrier particles (metal oxides) in the FR with the supply of gasifying agents (steam/CO_2). The metal oxide particles oxidize the syngas, which is generated during the in-situ gasification of the solid fuel in the FR. The reduced metal oxide particles in the FR are then transported to the AR for the re-oxidation process. Thus, a continuous cyclic loop operation is maintained between the two reactors.

Solid fuels (coal/biomass) are abundant and low-cost energy sources for power production. The direct utilization of solid fuels in the CLC operation without using an additional gasification unit is economical and reduces the complexity of the process. Figure 1.3 shows the schematic layout of the CLC process using solid fuel. Coal/ biomass is directly introduced into the FR along with the oxygen carrier in a stoichiometric ratio. The use of biomass with coal is beneficial since biomass is considered as the 4th most available energy source after the three fossil energy sources (coal, crude oil and natural gas) (Situmorang et al., 2021). The co-utilization of coal with biomass provides several

social, economic, and environmental advantages (Wang et al., 2014, Mcilveen-Wright et al., 2011). The biomass based gasification will result in negative carbon emission (since it absorbs CO_2 for growth) and thus provides an option to stabilize the greenhouse gas emissions. The total power production through various energy sources is 377 GW in India (as on 31.01.2021) of which 53.1% of the total is contributed by coal. And 24.5% of the energy is generated from renewable energy sources (biomass, wind, solar etc.) Steam/CO_2 is used as the in-situ gasifying agent in the FR to convert the solid fuel into syngas. A portion of the outlet stream from the FR is recycled to the FR for the gasification of solid fuels (Wei et al., 2021). The outlet gas from the FR is mainly composed of CO_2 and H_2O, which upon condensation, produces pure CO_2.

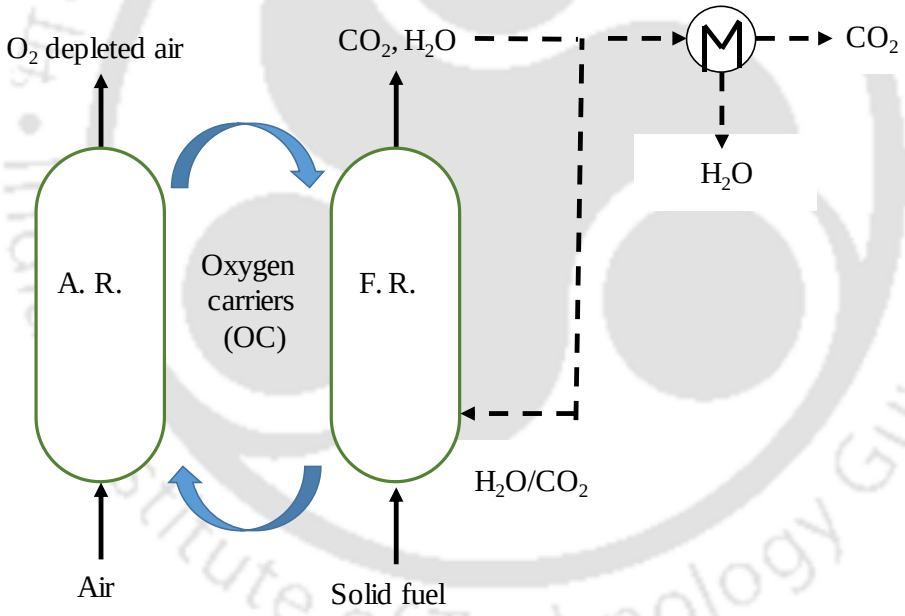

Figure 1.3. Schematic diagram of the CLC process.

1.4.1. Oxygen carriers

Oxygen carriers play a vital role in the performance of the CLC process. NiO, Fe_2O_3, CuO, Mn_2O_3, and Co_3O_4 are extensively used metal oxides in the CLC process. The oxygen carriers are prepared by using commercial pure oxides (Fe_2O_3, CuO, NiO etc)

and inerts (Al_2O_3, SiO_2, TiO_2 etc.) in different possible combinations (40/60, 30/70,60/40 etc.) (Adánez et al., 2004). Till date, chemical looping operation using solid and gaseous fuels are conducted for more than 11000 h in more than 49 pilot plants (Lyngfelt, 2020). The desirable properties for oxygen carriers are: (a) sufficient oxygen transport capacity, (b) favourable thermodynamics to convert fuels to CO_2 and H_2O, (c) high reactivity and stability during reduction and oxidation cycles, (c) resistant towards agglomeration, sintering and carbon deposition, (d) low attrition rate, (e) environmental friendly and (f) economical. CuO, Mn_2O_3, and Co_3O_4 exhibit chemical looping oxygen uncoupling behaviour (CLOU) releasing lattice oxygen at elevated temperatures. Cu-based oxygen carriers demonstrated a better performance in the CLC process than Mn, and Co-based oxygen carriers due to their higher oxygen transport capacity (Song et al., 2014). However, CuO has not been considered as a commercially viable oxygen carrier to date due to its low melting point. NiO has higher reactivity with fuels but it is carcinogenic and expensive. Hence, its usage is not preferred in large-scale applications. Fe_2O_3 is considered as a viable oxygen carrier due to its high oxygen transport capacity, high-temperature stability, abundant nature, low cost and non-toxic nature (Zhu et al., 2020). Thus, Fe-based oxygen carriers are feasible to utilize in the CLC process for continuous cycle operation. Low-cost oxygen carriers are preferred as a part of them are disposed of along with the fuel ash during the CLC operation. The interaction between the fuel elements (volatiles and char) and the typical oxygen carriers are shown in Table 1.2.

Table 1.2. List of chemical reactions occurring between the oxygen carriers and the solid fuel in FR and AR.

Process	Oxygen carrier	FR reactions	AR reactions
Char gasification		$C(s) + CO_2(g) \rightarrow 2CO(g)$	
		$C(s) + H_2O(g) \rightarrow CO(g) + H_2(g)$	
Water gas shift reaction		$CO(g) + H_2O(g) \rightarrow CO_2(g) + H_2(g)$	
iG-CLC	Fe_2O_3	$CO(g) + 3Fe_2O_3(s) \rightarrow CO_2(g) + 2Fe_3O_4(s)$	$4Fe_3O_4(s) + O_2(g) \rightarrow 6Fe_3O_4(s)$
		$H_2(g) + 3Fe_2O_3(s) \rightarrow H_2O(g) + 2Fe_3O_4(s)$	
		$CH_4(g) + 12Fe_2O_3(s) \rightarrow CO_2(g) + 2H_2O(g) + 8Fe_3O_4(s)$	
iG-CLC	NiO	$CO(g) + NiO(s) \rightarrow CO_2(g) + Ni(s)$	$NiO(s) + 0.5O_2(g) \rightarrow Ni(s)$
		$H_2(g) + NiO(s) \rightarrow H_2O(g) + Ni(s)$	
		$CH_4(g) + 4NiO(s) \rightarrow CO_2(g) + 2H_2O(g) + 4Ni(s)$	
CLOU	CuO	$4CuO(s) \rightarrow 2Cu_2O(s) + O_2(g)$	$2Cu_2O(s) + O_2(g) \rightarrow 4CuO(s)$
		$Char(s) + O_2(g) \rightarrow CO_2(g)$	
		$Volatiles\ (H_2, CO, CH_4)(g) + O_2(g) \rightarrow CO_2(g) + H_2O(g)$	

The annual e-waste production (more than 50 million tons) has caused several environmental and human health issues due to land and water pollution (Chen et al., 2021). Qiu et al. (2020) reported that the e-waste production is three times faster than municipal waste generation. This has increased the landfilling, and thus affected the environment and human health (Yang et al., 2021). It is reported that only one-fifth of the total e-waste generated is sent for recycling, while the rest is discarded into the open landfills (Sahle-Demessie et al., 2021). The present study intends to provide a solution to two prime issues i.e. e-waste management and CO_2 emission control for a sustainable environment. With the rapid advancement in the electronic industries, electronic gadget production has tremendously increased worldwide while their lifespan has decreased (Akram et al., 2019). Existing electronic equipment such as mobile phones, fax machines, desktops, calculators, audio and video players, etc. become obsolete while their upgraded version arrived in the market. The typical lifetime of a central processing unit in computers is 2-5 years, and annually 17 million desktops are discarded globally (Yamane et al., 2011). Further, the increase in population growth has escalated the electronic usage, which leads to the abundant production of electronic wastes.

Ádám et al. (2021) have claimed that the e-waste production would exceed 74 million metric tonnes by 2030. Asia contributed 24.9 million metric tonnes of e-waste out of 53.6 million metric tonnes of total e-waste produced globally in 2019. The printed circuit board (PCB) is considered as the main component for every electronic device (Zhang et al., 2013). The presence of valuable metals in the PCB has become the primary reason to recycle it. The waste electrical and electronic equipment (WEEE) contains 40% metal, 30% plastic and 30% refractory oxides (Cui and Forssberg, 2003). Out of the total stock of the generated WEEE, 3% of waste constitutes PCB (Flandinet et al., 2012). PCB recycling becomes difficult because of the presence of heavy and hazardous metals such

as mercury, lead, cadmium etc. (Salbidegoitia et al., 2015). However, the proper utilization of e-waste could improve the lives of human beings due to the reduction in land and water pollution. The rapid obsolescence of electronic waste has created huge junk and plays a major role in land, air pollution (Mcilveen-Wright et al., 2006). Discarded devices such as phones, audio players, printed circuit board, television, calculators, etc. are toxic-laden products that should either be recycled or treated before landfilling (Morf et al., 2007). Landfill storage of e-wastes causes groundwater contamination. Thus, an alternative way needs to be carved to handle the e-waste and prevent any damage to the environment. The most efficient technique is to convert these e-wastes into value added product. In the present study, the metals are extracted from these e-wastes and utilized as the oxygen carrier in the CLC process. Till date, no work has been reported regarding the e-waste utilization as oxygen carrier in the CLC process.

1.5. Motivation

In view of the importance of the implementation of the carbon capture and storage (CCS) technology, the chemical looping combustion process is considered for the inherent separation of CO_2 for storage. The motivation for the thesis is discussed below:

- Feasibility study for the utilization of high ash coal in the CLC process is essential for the efficient production of electricity with carbon capture. As Indian coal contains ash content as high as 40%, its utilization in the thermal power plants creates ash handling issues. Especially the use of high ash coal in the CLC process leads to agglomeration issues with metal oxides. To address these issues, an experimental study on the CLC technology with high ash coal is essential.
- As coal, a fossil fuel has been continuously utilized for power production, it becomes a depleting energy source (Nawaz and Ali, 2020). Till date, fossil fuels fulfill our

huge energy demand for electricity production. Hence the energy demand-supply gap is widening due to rapid industrialization (Buragohain et al., 2010). Thus, the utilization of renewable fuels along with fossil fuels becomes compulsory to meet our energy demands. Hence the co-combustion and co-gasification of coal with biomass will be a promising alternative technology for energy generation. Relying on biomass can reduce the dependency on fossil fuel, increase the life span of coal reserves and reduce the global greenhouse gas emission (Mcilveen-Wright et al., 2006). However, the heavy usage of biomass is limited due to its high moisture content, low bulk density and low calorific value, compared to coal. The utilization of biomass as the sole fuel in the combustor also poses threats such as corrosion and fouling issues (Pronobis, 2006). Thus, the co-feeding of coal and biomass is preferred to overcome the operational issues due to use of biomass alone in the combustor.

1.6. Organization of the Thesis

The complete thesis is organized into seven chapters. The basic outline of each chapter is discussed below:

Chapter 1 provides a brief insight into the global CO_2 emissions and their effect on the environment. The issue of reducing CO_2 emission by the CLC technology has been addressed.

Chapter 2 provides the literature review of the CLC process using different oxygen carriers with various reactor configurations. The knowledge gap is highlighted.

Chapter 3 focuses on the materials and methods implemented in the present study. The methodology adopted to assess the CLC behaviour of Indian coals is explained. Several key parameters that are evaluated are explained. The power plant simulation

methodology based on Aspen simulation for the estimation of the net thermal efficiency and the cost of electricity is explained.

Chapter 4 investigates the experimental results based on the CLC of coal, rice straw and their blends with Fe_2O_3 as the oxygen carrier using a fixed bed reactor and a thermogravimetric analysis (TGA). Further, the estimated kinetic parameters are compared using different reaction models.

Chapter 5 examines the experimental results of the extraction of oxygen carriers from discarded e-waste such as printed circuit boards (PCB). The chemical composition of the syngas and volatiles obtained using PCB during the metal extraction process is reported. Further, the performance of the metal oxides obtained from PCB is tested using the solid fuels (coal, rice straw) and their blends under the CO_2 atmosphere.

Chapter 6 deals with the techno-economic analysis of the CLC integrated combined cycle based on coal, rice straw and their mixture as feed using Fe_2O_3, CuO and oxidized e-waste as oxygen carriers. The effect of utilization of e-waste based metal oxides on the net thermal efficiency and levelized cost of electricity is explained.

Chapter 7 presents the overall conclusions and the scope for future study.

References

Ádám, B., Göen, T., Scheepers, P. T. J., Adliene, D., Batinic, B., Budnik, L. T., Duca, R. C., Ghosh, M., Giurgiu, D. I., Godderis, L., Goksel, O., Hansen, K. K., Kassomenos, P., Milic, N., Orru, H., Paschalidou, A., Petrovic, M., Puiso, J., Radonic, J., Au, W. W. (2021). From inequitable to sustainable e-waste processing for reduction of impact on human health and the environment. *Environmental Research*, *194*, 110728.

Adanez, J., Abad, A., Garcia-labiano, F., Gayan, P., & Diego, L. F. De. (2012). Progress in chemical-looping combustion and reforming technologies. *Progress in Energy and Combustion Science*, *38*, 215–282.

Adánez, J., De Diego, L. F., García-Labiano, F., Gayán, P., Abad, A., & Palacios, J. M. (2004). Selection of oxygen carriers for chemical-looping combustion. *Energy and Fuels*, *18*, 371–377.

Akash, A. R., Rao, A. B., & Chandel, M. K. (2016). Prospects of Implementing CO_2 Capture and Sequestration (CCS) in the Proposed Supercritical Coal Power Plants in India. *Energy Procedia*, *90*, 604–612.

Akram, R., Fahad, S., Hashmi, M. Z., Wahid, A., Adnan, M., Mubeen, M., Khan, N., Ishaq, M., Rehmani, A., & Awais, M. (2019). Trends of electronic waste pollution and its impact on the global environment and ecosystem. *Environmental Science and Pollution Research*, *26*, 16923–16938.

Buragohain, B., Mahanta, P., & Moholkar, V. S. (2010). Biomass gasification for decentralized power generation: The Indian perspective. *Renewable and Sustainable Energy Reviews*, *14*, 73–92.

Chao, C., Deng, Y., Dewil, R., Baeyens, J., & Fan, X. (2021). Post-combustion carbon capture. *Renewable and Sustainable Energy Reviews*, *138*, 110490.

Chen, Q., Rao, A., & Samuelsen, S. (2014). H_2 coproduction in IGCC with CCS via coal and biomass mixture using advanced technologies. *Applied Energy*, *118*, 258–270.

Chen, Y., Liang, S., Xiao, K., Hu, J., & Hou, H. (2021). A cost-effective strategy for metal recovery from waste printed circuit boards via crushing pretreatment combined with pyrolysis : Effects of particle size and pyrolysis temperature. *Journal*

of Cleaner Production, *280*, 124505.

Chikkatur, A. P., Sagar, A. D., & Sankar, T. L. (2009). Sustainable development of the Indian coal sector. *Energy*, *34*, 942–953.

Cruz, T. T. da, Perrella Balestieri, J. A., de Toledo Silva, J. M., Vilanova, M. R. N., Oliveira, O. J., & Ávila, I. (2021). Life cycle assessment of carbon capture and storage/utilization: From current state to future research directions and opportunities. *International Journal of Greenhouse Gas Control*, *108*, 103309.

Cui, J., & Forssberg, E. (2003). Mechanical recycling of waste electric and electronic equipment : a review. *Journal of Hazardous Materials*, *99*, 243–263.

Dubash, N. K., Khosla, R., Rao, N. D., & Bhardwaj, A. (2018). India's energy and emissions future: an interpretive analysis of model scenarios. *Environmental Research Letters*, *13*, 074018.

Erlach, B., Schmidt, M., & Tsatsaronis, G. (2011). Comparison of carbon capture IGCC with pre-combustion decarbonisation and with chemical-looping combustion. *Energy*, *36*, 3804–3815.

Farooqui, A., Bose, A., Ferrero, D., Llorca, J., & Santarelli, M. (2018). Techno-economic and exergetic assessment of an oxy-fuel power plant fueled by syngas produced by chemical looping CO_2 and H_2O dissociation. *Journal of CO_2 Utilization*, *27*, 500–517.

Flandinet, L., Tedjar, F., Ghetta, V., & Fouletier, J. (2012). Metals recovering from waste printed circuit boards (WPCBs) using molten salts. *Journal of Hazardous Materials*, *213–214*, 485–490.

Gai, S., Yu, J., Yu, H., Eagle, J., Zhao, H., Lucas, J., Doroodchi, E., & Moghtaderi, B.

(2016). Process simulation of a near-zero-carbon-emission power plant using CO_2 as the renewable energy storage medium. *International Journal of Greenhouse Gas Control*, *47*, 240–249.

Garg, A., & Shukla, P. R. (2009). Coal and energy security for India: Role of carbon dioxide (CO_2) capture and storage (CCS). *Energy*, *34*, 1032–1041.

Gupta, A., & Paul, A. (2019). Carbon capture and sequestration potential in India: A comprehensive review. *Energy Procedia*, *160*, 848–855.

Holloway, S., Garg, A., Kapshe, M., Deshpande, A., Pracha, A. S., & Khan, S. R. (2008). A regional assessment of the potential for CO_2 storage in the Indian subcontinent. *IEA GHG R&D Program*.

Holloway, S., Pearce, J. M., Hards, V. L., Ohsumi, T., & Gale, J. (2007). Natural emissions of CO_2 from the geosphere and their bearing on the geological storage of carbon dioxide. *Energy*, *32*(7), 1194–1201.

J. Dooley, Kim, S., Edmonds, J., Friedman, S., & Wise, M. (2005). A first-order global geological CO_2-storage potential supply curve and its application in a global integrated assessment model, Elsevier Science Ltd, Oxford,. *In Greenhouse Gas Control Technologies*, *7*, 573–581.

J.J.Dooley, S.H.Kim, J.A.Edmonds, Friedman, S. J., & M.A.Wise. (2004). A first-order global geological CO_2-storage potential supply curve and its application in a global integrated assessment model. *Greenhouse Gas Control Technologies*, *1*, 573–581.

Kanniche, M., Gros-Bonnivard, R., Jaud, P., Valle-Marcos, J., Amann, J. M., & Bouallou, C. (2010). Pre-combustion, post-combustion and oxy-combustion in thermal power plant for CO_2 capture. *Applied Thermal Engineering*, *30*, 53–62.

Kumar, R., Jilte, R., Nikam, K. C., & Ahmadi, M. H. (2019). Status of carbon capture and storage in India's coal fired power plants: A critical review. *Environmental Technology and Innovation*, *13*, 94–103.

Lu, H., He, L., Adhikari, H., & Maeda, E. (2020). Patch aggregation trends of the global climate landscape under future global warming scenario. *International Journal of Climatology*, 2674–2685.

Lyngfelt, A. (2020). Chemical Looping Combustion: Status and Development Challenges. *Energy and Fuels*, *34*(8), 9077–9093.

Mcilveen-wright, D. R., Huang, Y., Rezvani, S., Mondol, J. D., Redpath, D., Anderson, M., Hewitt, N. J., & Williams, B. C. (2011). A Techno-economic assessment of the reduction of carbon dioxide emissions through the use of biomass co-combustion. *Fuel*, *90*, 11–18.

Mcilveen-Wright, D. R., Pinto, F., Armesto, L., Caballero, M. A., Aznar, M. P., & Cabanillas, A. (2006). A comparison of circulating fluidised bed combustion and gasification power plant technologies for processing mixtures of coal , biomass and plastic waste. *Fuel Processing Technology*, *87*, 793–801.

Mishra, M. K., Khare, N., & Agrawal, A. B. (2015). Scenario analysis of the CO_2 emissions reduction potential through clean coal technology in India's power sector: 2014-2050. *Energy Strategy Reviews*, *7*(2015), 29–38.

Morf, L. S., Tremp, J., Gloor, R., Schuppisser, F., Stengele, M., & Taverna, R. (2007). Metals, non-metals and PCB in electrical and electronic waste - Actual levels in Switzerland. *Waste Management*, *27*, 1306–1316.

Mukherjee, A., Okolie, J. A., Abdelrasoul, A., Niu, C., & Dalai, A. K. (2019). Review of

post-combustion carbon dioxide capture technologies using activated carbon. *Journal of Environmental Sciences (China)*, *83*, 46–63.

Olabi, A. G., Obaideen, K., Elsaid, K., Wilberforce, T., Sayed, E. T., Maghrabie, H. M., & Abdelkareem, M. A. (2022). Assessment of the pre-combustion carbon capture contribution into sustainable development goals SDGs using novel indicators. *Renewable and Sustainable Energy Reviews*, *153*, 111710.

Ortega-ruiz, G., Mena-nieto, A., & García-ramos, J. E. (2020). Is India on the right pathway to reduce CO_2 emissions? Decomposing an enlarged Kaya identity using the LMDI method for the period 1990 – 2016. *Science of the Total Environment*, *737*, 139638.

Pronobis, M. (2006). The influence of biomass co-combustion on boiler fouling and efficiency. *Fuel*, *85*, 474–480.

Qiu, R., Lin, M., Ruan, J., Fu, Y., Hu, J., Deng, M., Tang, Y., & Qiu, R. (2020). Recovering full metallic resources from waste printed circuit boards : A refined review. *Journal of Cleaner Production*, *244*, 118690.

Romanak, K., & Dixon, T. (2022). CO_2 storage guidelines and the science of monitoring: Achieving project success under the California Low Carbon Fuel Standard CCS Protocol and other global regulations. *International Journal of Greenhouse Gas Control*, *113*, 103523.

Sahle-demessie, E., Mezgebe, B., Dietrich, J., Shan, Y., Harmon, S., & Lee, C. C. (2021). Material recovery from electronic waste using pyrolysis : Emissions measurements and risk assessment. *Journal of Environmental Chemical Engineering*, *9*, 104943.

Salbidegoitia, J. A., Fuentes-ordóñez, E. G., González-marcos, M. P., & González-

velasco, J. R. (2015). Steam gasification of printed circuit board from e-waste : Effect of coexisting nickel to hydrogen production. *Fuel Processing Technology*, *133*, 69–74.

Sethi, V. K., & Vyas, S. (2017). An Innovative Approach for Carbon Capture & Sequestration on a Thermal Power Plant through Conversion to Multi-Purpose Fuels - A Feasibility Study in Indian Context. *Energy Procedia*, *114*, 1288–1296.

Shackley, S., & Verma, P. (2008). Tackling CO_2 reduction in India through use of CO_2 capture and storage (CCS): Prospects and challenges. *Energy Policy*, *36*, 3554–3561.

Shahrestani, M. M., & Rahimi, A. (2014). Evolution, fields of research, and future of chemical-looping combustion (CLC) process: A review. *Environmental Engineering Research*, *19*, 299–308.

Sharma, N. (2018). Silver bullet or bitter pill? Reassessing the scope of CO_2 capture and storage in India. *Carbon Management*, *9*, 311–332.

Sharma, R., & Kautish, P. (2020). Examining the nonlinear impact of coal and oil-based electricity production on CO_2 emissions in India. *The Electricity Journal*, *33*, 106775.

Singh, A.K., Mendhe, V. A., & Garg, A. (2006). CO_2 storage potential of geologic formations in India. *8th Greenhouse Gas Technology Conference, Trondheim, Norway*.

Singh, Ajay K., Mendhe, V. A., & Garg, A. (2006). CO_2 Storage Potential of Geologic Formations in India. *In 8th Greenhouse Gas Technology Conference, Trondheim, Norway*.

Situmorang, Y. A., Zhao, Z., Chaihad, N., Wang, C., Anniwaer, A., Kasai, Y., Abudula, A., & Guan, G. (2021). Steam gasification of co-pyrolysis chars from various types of biomass. *International Journal of Hydrogen Energy*, *46*, 3640–3650.

Song, H., Shah, K., Doroodchi, E., Wall, T., & Moghtaderi, B. (2014). Reactivity of Al_2O_3 - or SiO_2 - supported Cu - , Mn - , and Co-based oxygen carriers for chemical looping air separation. *Energy & Fuels*, *28*, 1284–1294.

Tebbiche, I., Mocellin, J., Huong, L. T., & Pasquier, L.-C. (2021). Circular Economy and Carbon Capture, Utilization, and Storage. In *Biomass, Biofuels, Biochemicals*. Elsevier Inc.

The world Bank. (2019). *World BankData and Statistics for India*. World Bank Data and Statistics for India.

Viebahn, P., Vallentin, D., & Höller, S. (2014). Prospects of carbon capture and storage (CCS) in India's power sector - An integrated assessment. *Applied Energy*, *117*, 62–75.

Vishal, V., Verma, Y., Chandra, D., & Ashok, D. (2021). International Journal of Greenhouse Gas Control A systematic capacity assessment and classification of geologic CO_2 storage systems in India. *International Journal of Greenhouse Gas Control*, *111*, 103458.

Wang, G., Zhang, J., Shao, J., & Ren, S. (2014). Characterisation and model fitting kinetic analysis of coal/biomass co-combustion. *Thermochimica Acta*, *591*, 68–74.

Wei, G., Zhou, H., Huang, Z., Zheng, A., & Zhao, K. (2021). Reaction performance of Ce-enhanced hematite oxygen carrier in chemical looping reforming of biomass pyrolyzed gas coupled with CO_2 splitting. *Energy*, *215*, 119044.

Yadav, S., & Mondal, S. S. (2022). A review on the progress and prospects of oxy-fuel carbon capture and sequestration (CCS) technology. *Fuel*, *308*, 122057.

Yamane, L. H., Moraes, V. T. De, Crocce, D., Espinosa, R., Alberto, J., & Tenório, S. (2011). Recycling of WEEE : Characterization of spent printed circuit boards from mobile phones and computers. *Waste Management*, *31*, 2553–2558.

Yang, Q., Cao, J., Yang, F., Liu, Y., Chen, M., Qin, R., Chen, L., & Yang, P. (2021). Amyloid-like aggregates of bovine serum albumin for extraction of gold from ores and electronic waste. *Chemical Engineering Journal*, *416*, 129066.

Yaqub, Z. T., & Oboirien, B. O. (2020). Process modelling of chemical looping combustion of paper, plastics, paper/plastic blend waste, and coal. *ACS Omega*, *5*, 22420–22429.

Zhang, S., Yoshikawa, K., Nakagome, H., & Kamo, T. (2013). Kinetics of the steam gasification of a phenolic circuit board in the presence of carbonates. *Applied Energy*, *101*, 815–821.

Zhu, X., Imtiaz, Q., & Donat, F. (2020). Chemical looping beyond combustion – a perspective. *Energy & Environmental Science*, *13*, 772–804.

Zoback, M. D., & Gorelick, S. M. (2012). Earthquake triggering and large-scale geologic storage of carbon dioxide. *Proceedings of the National Academy of Sciences of the United States of America*, *109*, 10164–10168.

CHAPTER 2

Literature Review

CHAPTER 2

LITERATURE REVIEW

An extensive review of the CLC process implemented with different solid feedstock, oxygen carriers and reactor configurations is performed in the present chapter. Durable and reactive oxygen carriers for solid fuels are highlighted. Further, the performance of the reported CLC integrated power plants is analyzed based on their net thermal efficiency with CO_2 capture. Based on the literature gap, the objectives and scope of the thesis are reported.

2.1. Process overview

The chemical looping combustion (CLC) process can effectively utilize solid, liquid and gaseous fuels. In the present study, the direct use of solid fuels in the CLC process is performed. The solid fuel based CLC process can be carried out by direct and indirect methods (Figure 2.1). The direct process is further categorized into in-situ gasification process (iG-CLC) and chemical looping oxygen uncoupling process (CLOU) process.

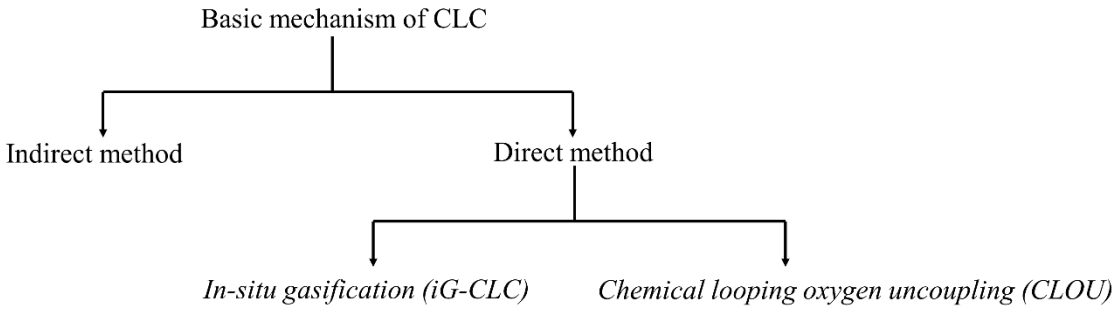

Figure 2.1. Classification of the CLC process.

2.1.1. Indirect CLC method

The indirect method involves two processes such as (i) gasification of solid fuel into syngas in a gasifier unit and (ii) CLC of the generated syngas. An additional gasifier unit

is used to convert solid fuels into syngas (Eq. 2.1), which is further sent to the CLC system for the metal oxy-combustion process (Figure 2.2). The metal oxides readily react with syngas in the fuel reactor (FR) (Eq. 2.2), and the obtained metal particles in the reduced form are transported to the air reactor (AR) for regeneration.

$$\text{Gasifier: } \text{Coal} + CO_2/H_2O \rightarrow \text{syngas} \quad (2.1)$$

$$\text{Fuel reactor (FR): } \text{syngas} + MeO \rightarrow Me + CO_2 + H_2O \quad (2.2)$$

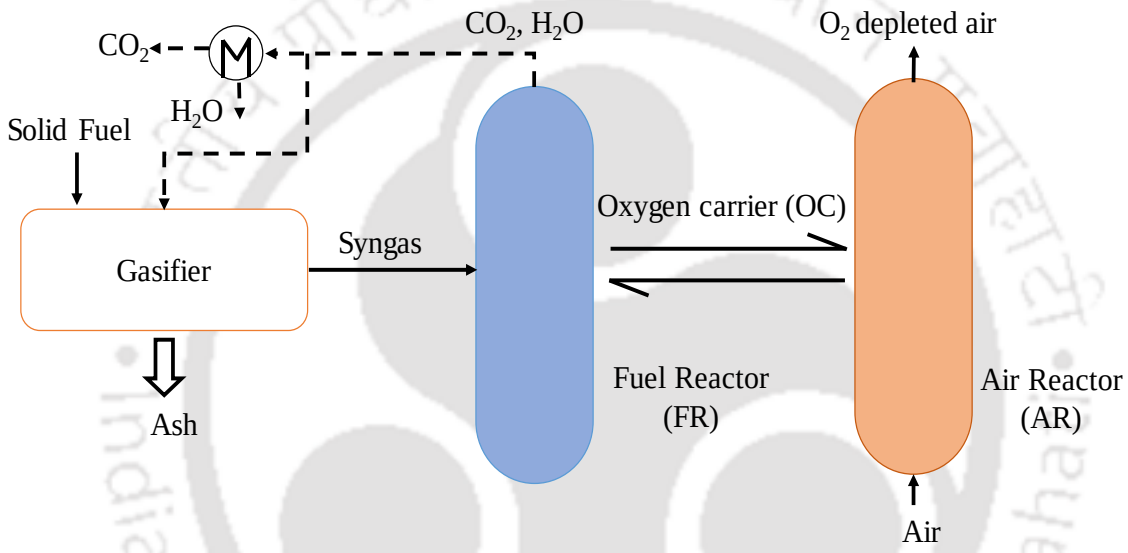

Figure 2.2. Schematic diagram of an indirect method in the CLC process.

2.1.2. Direct CLC method

The direct method involves the simultaneous occurrence of both the processes such as (i) coal gasification and (ii) syngas metal oxy-combustion in a single reactor. Chen et al. (2016) discussed the chemical reactions that occurred between solid fuels and metal oxides. These reactions include (a) devolatilization/gasification of fuel, (b) interaction of metal oxide with syngas and char and (c) homogeneous water gas shift reaction. This method can be carried out in two ways, which are based on the choice of metal oxides.

As discussed earlier, the direct method is classified into (i) chemical looping with oxygen uncoupling (CLOU), and (ii) in-situ gasification chemical looping combustion (ig-CLC). Leion et al. (2009) found that the use of oxygen carriers such as nickel, ilmenite, etc. could result in a low conversion rate of solid fuel due to the rate-limiting step of char gasification reaction. In the CLOU technology, the metal oxides release their oxygen molecule in the gas phase at higher operating temperatures and, this gas phase oxygen burns solid fuels directly. Metal oxides such as Cu, Mn, Co possess the CLOU characteristics.

$$2Me_xO_y \rightarrow 2Me_xO_{y-1} + O_2 \quad (2.3)$$

$$Coal \rightarrow Volatiles + Char \quad (2.4)$$

$$Volatiles + O_2 \rightarrow CO_2 + H_2O \quad (2.5)$$

$$Char + O_2 \rightarrow CO_2 \quad (2.6)$$

This technology is highly efficient due to the direct combustion of solid fuel with the gas phase oxygen. However, the following drawbacks are reported for the CLOU based metal oxides in the literature.

(i) Cobalt oxide is expensive and toxic (Frick et al., 2015).

(ii) Mn-based oxides release oxygen at a lower rate. The re-oxidation of Mn_2O_3 occurs at lower temperatures where the reaction rate is too slow (Rydén et al., 2011).

(iii) Cu-based metal oxide is expensive and has a short lifetime due to high attrition rate (0.04 wt%/h) (Adanez et al., 2012). Furthermore, Cu has the low melting point (1085°C) that could lead to agglomeration issues in the CLC reactors (Qin et al., 2012).

Another method of the CLC technology is referred to as in-situ gasification technology (iG-CLC). Due to the absence of an additional gasifier, iG-CLC process captures CO_2 at

relatively low cost (Abad et al., 2018). The solid fuel is gasified by a gasifying medium (steam or recirculated CO_2) to convert the char into CO, since char gasification is the limiting step. The produced CO then subsequently gets oxidized by the oxygen carriers into CO_2 and H_2O. However, an oxygen polishing step is usually required due to the presence of unconverted volatiles and char (Wang et al., 2021). A carbon stripper is usually employed to prevent the transportation of unconverted char from FR to AR (Abad et al., 2015). In this method, sequential chemical reactions such as pyrolysis (Eq. 2.7), char gasification (Eq. 2.8), metal-oxy combustion of syngas (Eq. 2.9) etc., occur simultaneously. As this technology eliminates the use of a gasifier, the operational cost of the CLC process can be reduced. Ohlemüller et al. (2015) and Adanez et al. (2012) explained the iG-CLC reaction mechanism as follows,

$$\text{Coal (s)} \rightarrow \text{volatiles (g)} + \text{char (s)} \quad (2.7)$$

$$C + H_2O/CO_2 \rightarrow CO + H_2 \quad (2.8)$$

$$\text{Volatiles (g)} + \text{MeO (s)} \rightarrow CO_2(g) + H_2O\ (g) \quad (2.9)$$

As discussed earlier, carbon capture and storage (CCS) technologies will reduce the CO_2 emission from the industries. However, transport sector for CO_2 capture technologies is quite complex. H_2 when used as a fuel reduces the CO_2 emission. Further, this can be utilized in power generation and for the production of various chemical feedstocks such as ammonia, methanol etc. (Adanez et al., 2012). The conventional way to generate syngas from hydrocarbons is usually through steam reforming (Mattisson et al., 2018). Steam methane reforming (SMR) was the most widely used for H_2 production and requires enormous heat input for H_2 purification (Luo et al., 2018). However, CLR has superior characteristics over SMR since the former can capture carbon inherently (Tang et al., 2015). Further, high CO/H_2 ratio is achieved using the CLR technique, which can further be used to produce chemicals. Hydrogen production using chemical looping

processes can be categorized into two sections: (a) chemical looping gasification (CLG) and (b) chemical looping reforming (CLR). Figure 2.3 shows the overview of CLR and CLG using solid fuels. The main difference between CLG and CLR is that former process produces syngas from solid fuels (Figure 2.3a), while pure H_2 is obtained using CLR as shown in Figure 2.3(b). CLG produces a gas mixtures (CO, H_2, CH_4 etc), thus requires additional gas separation technique to separate H_2. However, CLR concept employs three reactors and produces rice stream of H_2. They both follows the same principles as CLC. However, heat management for CLG and CLR cases will be difficult since they release less heat than the CLC case due to incomplete combustion (Yu et al., 2019).

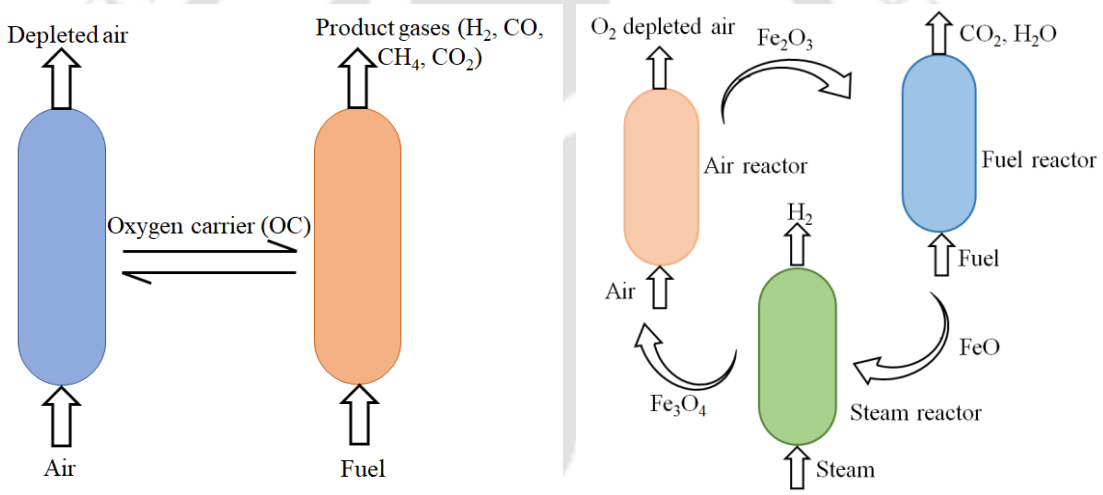

Figure 2.3. Schematic diagram of (a) CLG and (b) CLR.

2.2. Data evaluation

The reactivity of solid fuel during the CLC process is defined in terms of solid fuel conversion, gas conversion, CO_2 yield, oxygen demand, etc. These terms are explained as follows,

2.2.1. CO_2 yield

It is defined as the degree of the conversion of carbonaceous fuel into CO_2 due to interactions with metal oxides in the FR (Wang et al., 2016).

$$CO_2 \text{ yield} = \frac{F_{CO_2}}{F_{CO} + F_{CO_2} + F_{CH_4}} \tag{2.10}$$

where 'F' denotes the molar flow rate of individual gas species at the FR outlet.

2.2.2. Gas conversion (η_{gas})

It denotes the reactivity of the generated syngas from solid fuels with metal oxides in the FR. The second term of Eq. (2.11) is referred to as the oxygen demand (OD). The OD is defined as the ratio of the quantity of the oxygen required for the complete conversion for the unconverted gas at the exit of FR to the oxygen needed for the complete conversion of the total carbonaceous gases obtained during the gasification of solid fuels (Linderholm et al., 2016, Schmitz & Linderholm, 2016).

$$\eta_{gas} = 1 - \frac{0.5x_{CO} + 2x_{CH_4} + 0.5x_{H_2}}{\varphi_0 (x_{CO} + x_{CO_2} + x_{CH_4})} \tag{2.11}$$

Where φ_0 is the stoichiometric oxygen required for the complete combustion of carbonaceous gases, and x_i denotes the volume fraction of gaseous species 'i'.

2.2.3. Solid fuel conversion (η_{SF})

It is defined as the conversion of carbon (in the form of char and volatiles) in the solid fuel into carbonaceous gas in the AR and FR (Pérez-Vega et al., 2016).

$$\eta_{SF} = \frac{(F_{CH_4} + F_{CO} + F_{CO_2})_{out,FR} + (F_{CO_2AR})}{\dot{m}_{SF}.(f_{C,SF} / M_C)} \tag{2.12}$$

$\dot{m}_{SF}$(g/s) is the mass flow rate of solid fuel; $f_{C,SF}$ is the fraction of total carbon in solid fuel; M_C (g/mol) is the molar mass of solid fuel.

2.2.4. Char conversion

It is defined as the conversion of fixed carbon (char) in solid fuels into gaseous products (Pérez-Vega et al., 2016).

$$X_{char,FR} = \frac{(F_{CO_2} + F_{CO} + F_{CH_4})_{out,FR} - F_{C,vol}}{F_{C,fix} - F_{C,elut}} \quad (2.13)$$

Where 'F' denotes the flow rate of the gas species at the exit of the FR; $F_{C,vol}$ is the flow rate of the carbonaceous species in the volatile matter; $F_{C,fix}$ is the flow rate of fixed carbon; $F_{C,elut}$ is the flow rate of elutriated carbon.

2.2.5. Combustion efficiency

It is defined as the ratio of the utilized oxygen for the combustion of solid fuels to the total supplied oxygen in the form of metal oxides for the complete combustion. The degree of the combustion of solid fuel in the FR can be calculated as per the following equation (I. Adánez-Rubio et al., 2014).

$$\eta_{comb,FR} = 1 - \frac{2F_{CH_4} + 0.5F_{CO} + 0.5F_{H_2}}{(\Omega_{SF}.\dot{m}_{coal})/M_C} \quad (2.14)$$

Ω_{SF} is the stoichiometric mass of the O_2 required for the conversion of unit kg of solid (kg/kg); M_C is the molecular weight of solid fuel.

2.2.6. Carbon capture efficiency (η_{CC})

It is a measure of the leakage of carbon gas from the FR into the AR (Ma et al., 2015, Abad et al., 2015). The high carbon capture efficiency of the CLC process denotes the minimum seepage of carbon gas into the AR. It is defined as the ratio of the flow rate of carbonaceous gas leaving the FR to the total flow rate of the carbon gas exiting both the reactors.

$$\eta_{CC} = \frac{F_{CO_2,FR} + F_{CO,FR} + F_{CH_4,FR}}{F_{CO_2,FR} + F_{CO,FR} + F_{CH_4,FR} + F_{CO_2,AR}} \quad (2.15)$$

2.3. Choice of reactors

The configurations of the CLC reactors are briefly discussed in this section. It is essential to design the CLC reactors with a better contacting pattern for the efficient conversion of solid fuels. Fixed bed, bubbling fluidized bed, circulating fluidized bed and spouting fluidized bed conditions are reported in the literature for the CLC operation as shown in Figure 2.4. The fixed bed condition of the CLC reactors has the following advantages and disadvantages.

(i) Fixed bed condition is proved to be an advantageous configuration over a fluidized bed configuration if the CLC process is integrated with a combined cycle power plant. As the outlet stream of a fixed bed reactor is free of fine particles, the surface coatings of gas turbines cannot be damaged by the carry-over particles (Warnecke, 2000).

(ii) Cyclone separator, non-mechanical loop seals and energy required for fluidization can be eliminated in a reactor operating under fixed bed conditions (Kimball et al., 2013).

(iii) Hot spots are generated in the packed bed conditions due to the uneven temperatures. The existence of high-temperature spots at various locations of a reactor causes agglomeration and decomposition of metal oxides with ash particles of solid fuels. However, the generation of hot spots can be eliminated in a fluidized bed reactor.

Circulating, bubbling and spouted fluidized bed reactors can be used for the operation of the FR. A circulating fluidized bed reactor (CFBR) operates under a fast fluidized bed regime, which enhances the interaction between metal oxide, coal and gasifying medium (Ohlemüller et al., 2015, Perreault et al., 2016). Due to higher fluidization velocity in FR, metal particles are usually carried along with the gas stream to the reactor's outlet. These particles are separated from the outlet gas stream by using a cyclone separator and, are

recirculated to the feed point. Low-velocity bubbling bed fluidization is preferred for the operation of the AR and the FR, which lead to a higher residence time of fuel particles in reactors (Thon et al., 2014, Rydén et al., 2011).

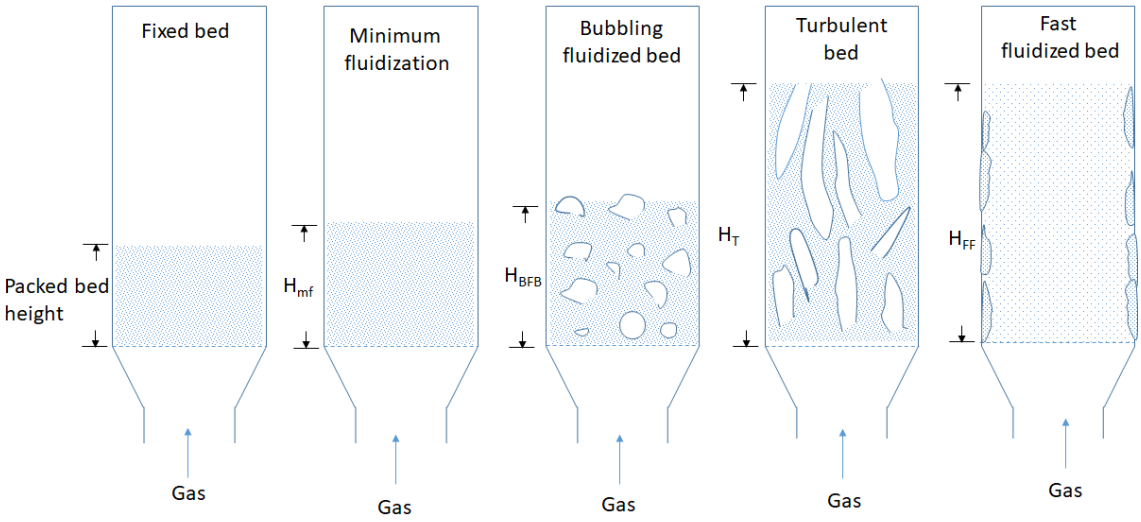

Figure 2.4. CLC reactor configurations (H: height; mf: minimum fluidization; bfb: bubbling fluidized bed; t turbulent bed; ff: fast fluidized bed).

Fluidized bed reactors possess high mixing rate and uniform temperature distribution (Johansson et al., 2003, Song & Shen, 2018). In general, the main challenge lies in the design of fuel reactor since complete conversion of fuel is desired. Figure 2.4 shows the typical bed configurations for the FR based on the inlet gas flowrate. The main advantage of a packed bed reactor are that separation of gas and particles are intrinsically avoided and compact reactor size when compared to fluidized bed configurations. Generation of hot spots result in incomplete decomposition and particle agglomeration in the fixed bed reactor configuration (Walter et al., 2021). Thus, fluidized bed condition was preferred over fixed bed operation for gasification solid fuels (Hasanzadeh et al., 2021, Han & Kim, 2008). The fluidized bed reactor ensures high heat transfer rates with excellent mixing, low tar and high syngas yield. They suffer agglomeration and sintering issues during

multiple cycle operations. Thus, the fluidized bed configuration is mostly used for the pilot scale studies using chemical looping operation ash shown in Table 2.1.

Table 2.1. Overview of chemical looping units using different reactor configurations (CFB: Circulating fluidized bed, BFB: bubbling fluidized bed)

Fuel	Oxygen carrier	Power (kW_{th})	Location	Reactor configuration in FR	Operation time (h)	References
Coal, petcoke	Ilmenite, perovskite	10	Chalmers University of Technology, Sweden	BFB	253	Berguerand & Lyngfelt (2008)
Coal, petcoke	Iron ore	100	Chalmers University of Technology, Sweden	BFB	116	Linderholm & Schmitz (2016)
Coal, biomass	NiO, Fe_2O_3	10	Southeast University, China	Spouted bed	130	Shen et al. (2009)
Coal	Ilmenite, CuO	25	Hamburg University of Technology, Germany	BFB	80	Thon et al. (2014)
Coal, biomass	Ilmenite, Iron ore	1000	Darmstadt, Germany	CFB	>100	Ströhle et al. (2014)
Coal	Fe_2O_3	25	Ohio State University, USA	Moving bed	>680	Kim et al. (2013)
Biomass	Ilmenite	10-5	VTT Technical research Centre, Finland	BFB	-	Pikkarainen et al. (2016)
Coal	Iron ore	10	IFP Energies Nouvelles, France	BFB	52	Sozinho et al. (2012)

Chemical looping units operating with 10-100 kW_{th} power are categorized into lab-scale units, while >100k Wth are categorized into pilot scale units (Adánez et al., 2018). The

FR is usually operated in a bubbling fluidized mode, while AR in fast fluidized mode to achieve satisfactory conversion. Bituminous coals are mostly investigated, however, petcoke, biomass etc. were preferred for higher reactivity. Coals achieved % CO_2 capture at 960℃, while biomass attained at 930℃. Thus, most of the existing CLC plants use interconnected fluidized bed for long operation time. Fluidization is preferred over fixed bed since it is mature and has been used for decades in conventional gasification processes also. Wilk and Hofbauer (2013) performed reforming of PE, PP, PS, PET in steam fluidized bed. They obtained high calorific value syngas of 27.2 MJ/Nm^3 at 850℃. Similarly, Arena et al. (2009) achieved calorific value of 9.2 MJ/Nm^3 at 831℃ using PE and Saebea et al. (2020) attained 11.36 9.2 MJ/Nm^3 at 900℃ in a bubbling fluidized bed reactor using steam as a gasifying agent. Maric et al. (2020) performed gasification of automotive shredder residue (ASR) in a fluidized bed reactor to estimate the liberation of polychlorinated dibenzo-p-dioxins/dibenzofurans (PCDD/PCDF) from the flue gas. They detected very low emissions of PCDD/PCDF (only 0.17ng/kg_{ASR}) at 900℃. Choi et al. (2021) gasified polyethylene terephthalate (PET) in a bubbling fluidized bed reactor without facing any operational issues. The product gas contained 22% H_2, 25% CO and 7mg/m^3 tar at 844℃. These results suggest that bubbling fluidized bed reactor should be preferred for gasification of the plastic waste based materials.

2.4. Metal oxides

Oxygen carriers play a vital role in the performance of the CLC process. They are responsible for transferring the lattice oxygen from one reactor to another. NiO, Fe_2O_3, CuO, Mn_2O_3, and Co_3O_4 are extensively used metal oxides in the CLC process. The oxygen carriers are prepared by using commercial pure oxides (Fe_2O_3, CuO, NiO etc) and inerts (Al_2O_3, SiO_2, TiO_2 etc.) in different possible combinations (40/60, 30/70,60/40 etc.) (Adánez et al., 2004). Table 2.2 highlights the key properties of oxygen carriers.

Lifetime of oxygen carriers is the mean time that a particle can be kept in reduction/oxidation atmosphere without experiencing any attrition (Adanez et al., 2012).

Table 2.2. Main properties of oxygen carriers.

Oxygen carrier	Oxygen transport capacity (OTC) (%)	Mechanical strength (N)	Lifetime (h)	Attrition rate (%/h)	Melting point (°C)	References
NiO	21	1.1	40000	0.0023	1955	Mattisson et al. (2006), Leion et al. (2009)
CuO	10	2.4	2400	0.04	1326	Mattisson et al. (2009), Dai & Whitty (2019)
Fe_2O_3	3.3	5.8	280-1000	5.1-12.7 (%)	1565	Siriwardane et al. (2015a), Guo et al. (2014)
Ilmenite	2.1-4	1.0-2.2	700-1300	0.076	1050	Lyngfelt (2020), Cuadrat et al. (2012)

NiO showed high reactivity with an oxygen transport capacity (OTC) and lifetime of 21% and 40000h but its usage is limited since it is expensive and toxic (Fang et al., 2021). It is advantageous to use chemical looping oxygen uncoupling (CLOU) based oxygen carriers (Cu, Co, Mn-based) since they have the ability to release molecular oxygen at elevated temperatures (800-1000°C) (Patzschke et al., 2021). However, they have some limitations. CuO have displayed high reaction rate with no thermodynamic restriction for complete fuel conversion into CO_2 and H_2O. However, it cannot be tested at higher operating temperatures due to the low melting point of metallic Cu (1085°C). The main issue with Mn-based oxygen carriers are high fractions of fines are generated, thereby decreasing their lifetime (Larring et al., 2015). Similarly, Co-based oxides are expensive

and toxic. Fe_2O_3 is one of the attractive option among these metal oxides due to its low cost and environmental compatibility (Qasim et al., 2021). They have received most of the attention even though they have a lower OTC of 3%. Ilmenite has OTC somewhat higher than pure Fe_2O_3 with good fluidization behaviour and stability.

Metal oxides play a dual role both as oxygen supplier and catalyst. The gasification efficiency of coal and biomass is influenced by the presence of suitable metal oxides in the CLC process. The conversion of solid fuel, char, volatiles, and gasified products in the CLC process depends on the choice of metal oxide and gasifying medium (CO_2/H_2O). Table 2.3 shows the reactivity of solid fuels with different metal oxides using thermo-gravimetric (TGA) studies. It can be seen that CuO as the metal oxide achieved a higher weight loss in the range of 30-40% of the reaction mixture due to the CLOU nature, which leads to liberate gas phase oxygen (Cao et al., 2006). Red mud demonstrated higher mass loss than hematite ores due to the presence of alkali and alkaline earth metals (Chen et al., 2016). Bimetallic oxygen carriers such as $CoFe_2O_4$ resulted in 3% additional mass due to the presence of Co and Fe. The presence of Fe_2O_3 in sewage sludge ash resulted in a 6% mass loss in hard coal.

It is reported in the literature that nickel, manganese, copper, iron, cobalt, etc. are the major oxygen carriers for the CLC operation. However, these metal oxides have some disadvantages. Nickel oxide exhibits a low oxidation rate in the AR, and furthermore, this metal oxide is toxic and expensive (Tseng et al., 2014, Adanez et al., 2012). Cobalt and nickel-based oxygen carriers have thermodynamic limitations for the complete conversion of H_2 and CO (Pröll et al., 2009). Thus, low-cost and environmental-friendly metal oxides are preferred for the economic operation of the CLC process.

Table 2.3. TGA studies on the weight loss characteristics of solid fuel during CLC operation.

Fuel	Oxygen carrier	Operating condition	Weight loss of (MeO+fuel)	References
Sub-bituminous coal char	Hematite and red mud	950ºC, Ar 10°C/min	Hematite: 5.45% Red mud: 8.64%	Chen et al. (2016)
Bituminous coal	copper oxide-iron oxide-alumina	850 ºC, Ar	49.28%	Siriwardane et al. (2016)
Hard coal	Sewage sludge ash	900 ºC, Ar	~6%	Ksepko (2014)
Bituminous coal	$CoFe_2O_4$ Fe_2O_3	900 ºC, N_2, 25°C/min	$CoFe_2O_4$:9.1% Fe_2O_3 :6.03%	Wang et al. (2014)
Wood	CuO	1000°C, CO_2 /N_2 30°C/min	CO_2: 39.34% N_2: 36.87%	Cao et al. (2006)

2.4.1. Iron-based metal oxides

Iron-based oxygen carriers exist in the form of hematite (Fe_2O_3), magnetite (Fe_3O_4) and wustite (FeO). These metal oxides are inexpensive, non-toxic and possess non-agglomeration characteristics at higher operating temperatures (Cormos, 2010). The reaction between Fe_2O_3 and syngas is as follows. The hematite form of iron oxides is reduced to the magnetite form.

$$3Fe_2O_3 + CO \rightarrow 2Fe_3O_4 + CO_2 \quad (2.16)$$

$$3Fe_2O_3 + H_2 \rightarrow 2Fe_3O_4 + H_2O \quad (2.17)$$

Sewage sludge ash was proposed as the oxygen carrier as it comprises of SiO_2, P_2O_5, Fe_2O_3, and Al_2O_3 (Ksepko, 2014). Iron oxides in the sewage sludge can act as metal oxides, and SiO_2, Al_2O_3 particles present in the ash content could eliminate

agglomeration issues. Xiao et al. (2010) confirmed that iron-based oxygen carrier is highly suitable for high pressure and high-temperature operations due to the non-agglomeration property.

I. Pyrite cinder

Pyrite cinder comprises of iron oxides (~ 87%) with minor amount of calcium and magnesium-based oxides (Alp et al., 2009). It is a waste product of sulfuric acid manufacturing plants. Zhang et al. (2015) used pyrite cinder as the metal oxides for the CLC process of coal under an inert and reactive atmosphere. Their results showed that there are no sintering and agglomeration problems even at higher operating temperatures (950°C). Thus, pyrite cinder can be effectively used for the metal oxy-combustion of solid fuel.

II. Natural Hematite

Natural hematite can be obtained as a waste from steel manufacturing industries. It mainly contains Fe_2O_3 (~ 81%) as the active phase along with inert metals such as Al_2O_3 and SiO_2 (Song et al., 2013). As discussed earlier, inert components in metal oxides are beneficial for the prevention of sintering problems for long-term usage (Song et al., 2012). This metal oxide accelerates the rate of char conversion, and furthermore, the heat transfer capacity between the CLC reactors can be enhanced (Ge et al., 2016). Song et al. (2013) reported a higher carbon capture efficiency using hematite as the oxygen carriers using bituminous coal (82%), compared to anthracite coal (65%). This might be due to the presence of a higher percentage of volatile matter in low-rank coals, which are beneficial for the CLC operation.

III. Red mud

Red mud is a mixture of metals such as Fe_2O_3, TiO_2, SiO_2, $CaCO_3$, and NaOH (Bao et al., 2016). It can be obtained as a side product from Bayer's process during alumina production. It is reported that 55-70% of red mud could be generated with bauxite as the feed (Mendiara et al., 2012). The reactivity of red mud oxides with gaseous fuels showed that it could be completely re-oxidized without any agglomeration problems even at 950°C (Chen et al., 2015, Ortiz et al., 2011). Mendiara et al. (2013) observed higher reactivity of coal with red mud than ilmenite at 900°C.

IV. Ilmenite

Ilmenite ($FeO.TiO_2$) is one of the low cost metal oxides, which inherently contain unreactive rutile (TiO_2) as an inert support. During the oxidation process, pseudobrookite ($Fe_2O_3.TiO_2$) is the highest oxidation state of the ilmenite (Eq. 2.28-2.29) (Pröll et al., 2009). It exhibits higher reactivity towards coal than methane (Berguerand, 2008). Low agglomeration tendency, high CO_2 capture efficiency, high melting point (1367 ºC) and high mechanical strength are the several advantages of ilmenite reported in the literature. However, ilmenite has a low oxygen transfer capacity, which could affect the rate of fuel conversion (Mendiara et al., 2013, Linderholm et al., 2011). Furthermore, ilmenite showed low reactivity at the initial stages of CLC; however, the reactivity increased after several cycles of oxidation and reduction processes (Cuadrat et al., 2011). Ilmenite achieved a solid conversion efficiency of 40%, 89% and 93% using hard coal, bituminous coal, and lignite, respectively (Ströhle et al., 2015, Abad et al., 2015). This shows that the presence of the higher proportion of volatile matter in low-rank coals causes higher reactivity of solid fuels in the CLC process.

$$2FeTiO_3 + 0.5O_2 \rightarrow Fe_2O_3 + 2TiO_2 \qquad (2.18)$$

$$4FeTiO_3 + O_2 \rightarrow 2Fe_2TiO_5 + 2TiO_2 \quad (2.19)$$

Coal needs low-cost oxygen carriers for the CLC operation due to the problem associated with the separation of metal particles from ash content. Many researchers have been working on low-cost oxygen carriers to make this technology economically viable. There are several low cost metal oxides in the form of natural ores and industrial waste products that are tested in the CLC process. Table 2.4 provides a detailed analysis of the performance of the CLC process based on the iron-based metal oxides in terms of the combustion efficiency, carbon capture and CO_2 yield under iG-CLC condition. It concludes that FR operating temperature of about 900-950°C is sufficient to achieve desirable conversion. The char conversion using char as fuel increased from 5% to 23% when operating temperature increased from 820-910°C (Rajendran et al., 2016). The particle size of OC too plays a critical role in the CLC process. It is seen that 35% of particles gets elutriated when particle size of OC +74-125µm are chosen (Cuadrat et al., 2011). Thus, Ströhle et al. (2015) observed the lowest solid conversion (40%) even after operating CLC at 1050°C. However, fuel size does not affect the CLC performance. Cuadrat et al. (2011) observed that only the residence time gets reduced from 23min to 11min when coal particle size changed from +200-300µm to +74-125µm, while the values of the key parameters remain unchanged. The gas conversion (96.7%) is found to be the highest when 90% hematite is mixed with 10% NiO (Song et al., 2012). The solid fuel conversion increased by 4.1% with the addition of NiO. Thus, the mixed metal oxides proved to display higher reactivity than the single metal oxides. Ilmenite, natural iron ore, perovskite, pyrite cinder, hematite, bauxite are the low-cost metal oxides, which showed higher conversion rates with solid fuels. The gas conversion efficiency of the iron-based metal oxides was found in the range of 79.0-98.0% and CO_2 yield in the range of 73.7-99.9%. Bauxite showed higher gas conversion efficiency in the range of 87.0-98.0%

using coal chars. Hematite is also found as a suitable metal oxide showing the CO_2 yield of ~93.0% using bituminous coals. Next to bauxite and hematite, ilmenite achieved gas conversion efficiency in the range of 70.0-87.0% with 87.0-94.9% carbon capture efficiency (η_{CC}). Ilmenite showed better performance during the redox reactions as its oxygen transport capacity had not changed significantly even after a prolonged period of operation (Abad et al., 2011). Furthermore, ilmenite showed 89-92% combustion efficiency using bituminous coal as the fuel. Hematite also showed higher combustion efficiency as equivalent to the performance of ilmenite.

2.4.2. Manganese based metal oxides – pyrolusite

Manganese-based ores are mainly produced in metallurgical industries. Pyrolusite possesses a higher oxygen transfer capacity than ilmenite (Arjmand et al., 2012). Due to its CLOU nature, a higher rate of char conversion can be achieved. Furthermore, Frohn et al. (2013) reported a higher instantaneous rate of char gasification using manganese ores when compared to ilmenite. Perreault et al. (2016) concluded that pyrolusite is an appropriate CLC metal oxide that retains its stability even after several oxidation and reduction cycles. They found that pyrolusite, an ore with higher content of manganese oxide, has a reactivity almost three times higher than ilmenite.

Table 2.4. The reactivity of iron-based oxygen carriers in terms of solid fuel conversion for CLC operation in a fluidized bed operation.

Fuel	Oxygen Carrier (OC)	FR Operating conditions	Gas conversion efficiency (η_{gas})	Char conversion (X_{char})	Solid fuel conversion (η_{SF})	Combustion efficiency (η_{comb})	Carbon capture efficiency (η_{CC})	References
Bituminous coal (100 µm)	Ilmenite (+100–300 µm)	BFB 991°C, Steam	-	84.7%	87%	89.2%	-	Abad et al. (2015)
Bituminous coal (+100–300 µm)	Ilmenite (+100–300 µm)	CFB 970°C, Steam	-	79.2%	88.5%	89.3%	~83%	Pérez-Vega et al. (2016)
Bituminous coal (74-125 µm)	Ilmenite (200-800 µm)	FFB 950°C, Steam	86%	-	-	92%	-	Cuadrat et al. (2011)
Swedish wood char (200-1000 µm)	Ilmenite (171 µm)	CFB Steam	~94%	-	~89%	-	94.4%	Linderholm et al. (2014)
Hard coal (25-125 µm)	Ilmenite (25-90 µm)	CFB 1050°C, Steam and CO_2	-	-	~40%	-	~80%	Ströhle et al. (2015)

(BFB: Bubbling fluidized bed, CFB: Circulating fluidized bed, FFB: Fast fluidized bed)

Table 2.4 continued

Fuel	Oxygen Carrier (OC)	Operating conditions	Gas conversion efficiency (η_{gas})	Char conversion (X_{char})	Solid fuel conversion (η_{SF})	Combustion efficiency (η_{comb})	Carbon capture efficiency (η_{CC})	References
Bituminous coal (45 µm)	Ilmenite and a manganese ore (140 µm)	CFB 970 °C, Steam	90%	-	73.7%	-	98.5%	Linderholm et al. (2016)
Bituminous coal	Hematite (150-250 µm)	BFB 1000°C, Steam and N_2	-	-	-	86%	95%	Ma et al. (2018)
Lignite coal (600-1000 µm)	Iron ore (150-350 µm)	fluidized bed 900°C, CO_2	-	-	91%	-	81%	Rajendran et al. (2016)
Bituminous coal (200-450 µm)	90% hematite (54-350 µm) and 10% Ni (300-450 µm)	SFB, 950°C, Steam and N_2	96.7%	-	81.2%	-	87.2%	Song et al. (2012)

(BFB: Bubbling fluidized bed, CFB: Circulating fluidized bed, FFB: Fast fluidized bed)

2.4.3. Electronic waste (e-waste)

E-waste could be a major source of metal extraction. The extracted metals can be used as low cost oxygen carriers for the CLC operation. Printed circuit boards (PCB) are considered as the main component for every electronic device. The presence of valuable metals in e-waste has become the primary reason to recycle it. PCB mainly consists of glass fiber, metallic layers (mainly Cu) and epoxy resins (polymer). Thermochemical treatment (pyrolysis and gasification) is a viable method to separate metal particles from e-waste. The presence of heavy metals and hazardous materials such as mercury, lead, cadmium etc. in the e-waste is not beneficial for utilization (Salbidegoitia et al., 2015). The pyrolysis and gasification of e-waste produce a high quality syngas, and the obtained residue after gasification is mainly the metallic contents. These metals can be considered for oxygen carriers in the CLC process. Table 2.5 shows the chemical composition of various e-waste materials. It can be observed that e-waste contains Fe, Cu, Ni in significant amount, compared to other metals. The metallic content varied from 18% to 80%, depending on the nature of e-wastes. It is observed that utilizing PCB in the CLC process as oxygen carrier serves both the purposes since the typical PCB contains 40-70% ash (metals and non-metals). Thus, PCB was preferred over e-waste materials.

Dilmaç et al. (2020) assessed the electric arc furnace slag as oxygen carrier with syngas in a fluidized bed reactor at 800℃. The syngas conversion was found to be more than 85%. The oxygen carrier was stable till 15 consecutive cycles. Staničić et al. (2021) gasified automotive shredder residue (ASR) (containing 23% Fe in ash) under steam atmosphere. They observed the formation of copper ferrites, zinc ferrites and antimony oxides in the metal rich ash residues. They concluded that the high content of Fe in the residue is beneficial since it may act as oxygen carrier in the CLC process. Thus, the waste materials with high metallic fraction need to be deeply investigated for their usage

in the CLC process. Hammache et al. (2020) investigated the CLC performance using industrial waste material (waste from fluid catalytic cracking process) at 1100℃. It is operated in a fixed bed reactor using coal char as the fuel. Due to higher content of alumina and silica, the industrial waste was found to be attrition resistant. Thus, the waste demonstrated better stability than hematite. Adánez-Rubio et al. (2018) used a mixture of 34% CuO and 66% Mn_3O_4 oxygen carrier particles and tested it using different biomasses (pine sawdust, olive stone, almond shell). They obtained a maximum CO_2 yield of 97.8% and char conversion of 96.6% for pine sawdust at 850℃. They concluded that the CLC reactions can occur even at lower operating temperature due to the mixed metal oxides containing CLOU materials as the oxygen carriers. Similarly, Pérez-Vega et al. (2020) examined the CLOU performance using Mn-Fe mixture with coal. They achieved the CO_2 yield of above 95% in a fluidized bed reactor. Complete coal combustion (99.4%) was attained at 925℃ (fuel reactor temperature). Due to the CLOU nature, the reactivity was found to be lower than ilmenite.

Table 2.5. Composition analysis of e-waste.

Type	Cu	Fe	Ni	Al	Pb	Zn	Others	References
Tv board	10	28	0.3	10	1	-	50.7	Cui & Zhang (2008)
PC board	20	7	1	5	1.5	-	65.5	Pant et al. (2012)
Mobile phone	13	5	0.1	1	0.3	-	81.6	Cui & Zhang (2008)
DVD player	5	62	0.1	2	0.3	-	30.6	Cui & Zhang (2008)
Audio player	21	23	0.03	1	0.14	-	54.8	Cui & Zhang (2008)
PCB	20	8	2	-	2	1	67.0	Qiu et al. (2020)
USB port	76	-	0.7	-	1.3	0.6	21.3	Pant et al. (2012)

2.4.4. Mixed metal oxides

It is observed that careful selection of metal oxides is required to achieve higher CLC performance. Thus, mixed metal oxides are preferred over mingle metal oxides since it increases the reactivity and selectivity (Sun et al., 2018, Liu et al., 2021, Siriwardane et al., 2016). Patzschke et al. (2021) investigated the Cu-Mn oxide since the limitations posed by Cu are balanced by Mn based oxygen carrier. Mn-based oxygen carriers are less prone to sintering and has the ability to release oxygen at lower temperature than Cu-based oxygen carriers. These metal oxides demonstrated high resistance towards agglomeration during 50 redox cycles in a fluidized bed reactor using methane as the fuel. Niu et al. (2018) used Cu-Fe oxide with sawdust in a fluidized bed reactor. They obtained carbon conversion of 97.5% at 900°C. They also observed that with increase in Cu content, increased the tar conversion due to its higher reactivity. Addition of Fe_2O_3 reduced the sintering issues when compared to CuO based cases. Similarly, Siriwardane et al. (2015b) and Yang et al. (2015) also observed the positive synergistic effect of Cu-Fe oxide due to the formation of copper ferrites. Hu et al. (2015) modified Fe-Zr oxide with K_2CO_3 for hydrogen production. Addition of K_2CO_3 increased the reaction rate due to its catalyst activity. The maximum hydrogen production was found to be 1.73 L/g. Thus, new functional materials such as perovskites (ABO_3) are currently investigated where A is either alkali, alkaline or rare earth metals, while B is a transition metal (Rydén et al., 2008). It is advantageous to use perovsiktes due to the presence of alkali and alkaline earth metals and have high thermal and mechanical stability (Shen et al., 2015). Calcium magnetite ($CaMnO_3$) are mostly studied perovskite till date (Shafiefarhood et al., 2015). Siriwardane et al. (2016) explored the interaction of barium ferrite and calcium ferrite with coal in a fixed bed reactor. They observed that these ferrites increased the synthesis gas yields. These ferrites were found to be more reactive towards carbon than

the generated syngas. Thus, mixed metal oxides are proved to be superior than single metal oxides since carbon deposition, agglomeration are limited.

2.5. Effect of process parameters and solid fuel properties on the CLC process

Temperature, pressure, gasifying medium, inherent properties of solid fuels are the various operating process parameters that could significantly affect the performance of the CLC process. These effects are explained in the following section.

2.5.1. Effect of temperature and pressure

The operating temperature and pressure have an essential role in the performance of the CLC process. Table 2.6 highlights the significance of the process parameters of the CLC operation. The conversion efficiency of carbon can be enhanced with an increase in the operating temperature of reactors. A low operating temperature of an FR causes carbon slip into the AR (Spinelli et al., 2016, Song et al., 2013). Bidwe et al. (2011) found that the increase in the operating temperature of CLC reactors from 900 ºC to 950 ºC enhanced the fuel conversion efficiency from 42.0% to 65.0% using ilmenite as the oxygen carrier. At low temperatures, the volatile matters of solid fuels mainly react with metal oxides. And the char gasification leads to high conversion efficiency in the CLC process at high temperatures (Cuadrat et al., 2011). Spinelli et al. (2016) found that the char conversion was increased from 82.4% to 96.7% with an increase in the operating temperature of reactors from 880 ºC to 940 ºC using CuO as the oxygen carrier. This may be due to the expansion of the pore volume of solid reactants that would increase the surface area of fuel causing higher reactivity. Therefore, higher operating temperature of reactors can enhance the gasification rate; however, it may alter the reactivity of oxygen carriers due to the agglomeration and sintering problems.

Xiao et al. (2012) reported that the increase in the partial pressure of steam in feed gas had enhanced the rate of char gasification; however, at the medium operating pressure of 6 atm., the char conversion rate becomes low due to the saturation of char active sites with the adsorbed steam molecules. Furthermore, high operating pressures can prevent the release of volatiles that could result in the deposition of tar on metal oxides (García et al., 2006, Nordness et al., 2016). Thus, high-pressure operating conditions of the CLC can reduce the combustion efficiency (η_{comb}) of metal oxides. Wang et al. (2016) confirmed these pressure effects by their CLC experimental studies using biomass with Mn_2O_3 as the metal oxides. They operated the CLC reactors in the pressure range of 1-10 atm and reported the adverse effect on the conversion rate of solid fuels due to the deposition of carbon on metal oxides.

2.5.2. Effect of solid fuel properties

The proportion of fixed carbon, volatile matter (gas and tar), ash and moisture content in solid fuels greatly influences the performance of the CLC process. Coal contains 2-40% of ash content; whereas biomass has a low ash content of ~ 0.1-10% (by weight). Hence, the co-combustion technology can reduce the ash handling issues when compared to coal. Low rank coals contain high moisture and high volatile matter content with a low energy density (Rajendran et al., 2016). A higher conversion rate can be achieved by using high volatile solid fuels in the CLC operation (Bhattacharya, 2006, Mendiara et al., 2013). Pinewood (biomass) and lignite (coal) in the CLOU process have shown higher combustion efficiency (96-100%), compared to bituminous coal (70%) (Zhao et al., 2015, Leion et al., 2009). Thus, biomass can be considered as a suitable feed for blending with coal for the benefit of the CLC process.

Biomass contains a higher quantity of alkali and alkaline earth metals. These substances exhibit catalytic activity for char gasification reactions. A higher proportion of potassium and calcium in the biomass ash content can enhance the gasification rate (Yang et al., 2007). Hence, the blending of biomass with coal can be beneficial for enhancing the gasification efficiency of solid fuels. However, higher alkali content of biomass can lead to ash agglomeration issues and may affect the solid circulation rate between CLC reactors (Rubio et al., 2014). Furthermore, the high chlorine content of biomass can lead to corrosion problems in CLC reactors. Silica in coal prevents the sintering issues of metal oxides. However, it has a negative effect on the iron-based oxygen carriers due to the formation of iron silicates (Song et al., 2013, Adánez et al., 2004). Hence, the blending of biomass and coal has both beneficial and inhibitory effects. Thus, the selection of biomass and coal for mixing should be based on their composition, which is crucial for efficient gasification.

2.5.3. Effect of gasifying agents

The iG-CLC process requires gasifying agents to convert solid fuel into syngas. CO_2, steam and recirculated flue gas are the various medium for gasification (Lyngfelt et al., 2014). Steam as the gasifying agent amplified the conversion of solid fuel with higher gasification rate, compared to CO_2 gas (Yi et al., 2016, Luo et al., 2013). CO_2 gasification (Boudouard reaction) is highly endothermic in nature, compared to steam gasification. The reactivity of steam with coal is almost four times higher than the CO_2 gas (Molina et al., 1998). However, Mendiara et al. (2013) reported that the CO_2 as the gasifying medium reduces the energy penalty of the iG-CLC technology. It is reported that the fluidization of solid fuel and metal oxide particles using steam is energy-intensive. The recirculation of flue gas for solid fuel gasification can eliminate the steam production process. Adánez et al. (2015) reported that the recovery of sensible heat could be

increased from 81.4% to 98.7% in the case of CO_2 gasification, compared to steam gasification as a considerable amount of heat is lost due to steam condensation. Thus, CO_2 gas can be considered as a potential gasification agent for the economic operations of the CLC process.

2.6. Synergetic effects of co-utilization of coal and biomass

Co-combustion is one of the potential options for enhancing the reactivity of metal oxides with solid fuels. Coal contains a higher proportion of fixed carbon that could not effectively undergo CLC reaction with metal oxides. Alternatively, biomass contains 80% volatile matter with low ash content, which has potential catalytic species for char gasification. Therefore, the co-combustion of coal and biomass is beneficial for not only enhancing the chemical reactivity of metal oxides but also for reducing the carbon footprint (Cormos, 2010). Furthermore, the co-utilization of coal and biomass enhances the ignition property of solid fuels by reducing the activation energy required for combustion and gasification reactions (Zhou et al., 2016). The co-combustion of biomass and coal causes higher reactivity of char due to the presence of alkaline minerals such as Si, K, Ca, Mn, etc. (Massoudi et al., 2016). The catalytic activity of mineral contents in biomass is found in the order of $K_2CO_3 > Na_2CO_3 > KCl > NaCl > CaCl_2$ (Liu et al., 2016). Luo et al. (2013) estimated the weight loss of coal and candlenut wood under the CO_2 atmosphere. They found a higher weight loss rate under co-gasification conditions due to the presence of suitable catalytic species in biomass. Xu et al. (2014) found a positive synergistic effect on the co-combustion of lignite and biomass mixed in the ratio of 4:1. The yield of char decreased with an increase in the ratio of biomass to coal, and furthermore, the quality of syngas is improved under co-gasification conditions. The higher ratio of oxygen and hydrogen to the carbon ((O+H)/C) of biomass had resulted in the generation of $H^{\bullet}$ and $O^{\bullet}H$ radicals, which favoured the cracking of higher

hydrocarbons (tar) into gas (Krerkkaiwan et al., 2013, Song et al., 2014). The yield of tar is reduced from 43 g/m^3 to 2.4 g/m^3 using iron-based catalysts (Li et al., 2014). Hence, the co-processing of coal and biomass is beneficial for enhancing the reactivity of metal oxides.

Gu et al. (2011) conducted a comparative study of the combustion behaviour of sawdust with coal in a spouted bed reactor using natural iron ore as the oxygen carrier. They found that the alkali (Na_2O, K_2O) content in the biomass led to the de-fluidization and agglomeration of particles due to the low melting point of alkali. However, under co-combustion conditions, higher combustion efficiency is estimated due to the release of the higher quantity of volatiles (Jayaraman et al., 2017). Wei et al. (2016) reported that the char reactivity is increased with the addition of sawdust to coal due to the presence of K_2O in their mineral matters. Masnadi et al. (2015) obtained a similar result by blending switchgrass and coal at 800°C. However, a low reactivity is observed at 900°C due to the evaporation of alkali. Coal ash minerals such as silica and alumina have interacted with potassium and resulted in the formation of a complex compound, $KAlSiO_4$. Thus, the optimum temperature should be maintained to retain the catalytic activity of ash contents. Habibi et al. (2012) reported that the molar ratio of K/Al should be greater than one for higher catalytic activity, and this condition can be maintained by adjusting the ratio of biomass to coal under co-combustion conditions.

Table 2.6. Effect of operating conditions (temp./pressure/gasifying agent/effect of ash, tar etc.) on the performance of the CLC process.

Fuel	Ash (%)	Oxygen carrier	Type of bed	Gasifying medium	Pressure (bar)	Temperature (°C)	Results	References
Bituminous coal	7.8	Iron ore	Fast fluidized bed	Steam	1-5	950	CO_2 yield 1 bar-92.1%, 5 bar-97.2%	Xiao et al. (2012)
Bituminous coal	25.8	Fe_2O_3 waste from steel industry	Fixed bed reactor	Steam-N_2	1-5	970	CO_2 yield 1 bar-92.03% 5 bar-100%	Zhang et al. (2011)
Bituminous coal	4.7	Hematite	Spout fluidized bed	Steam	1	880-970	CO_2 yield 82%-880°C 93%-970°C	Song et al. (2013)
Bituminous coal	8.8	Ilmenite	Bubbling fluidized bed	Steam	1	820-950	η_{comb} 37%-880°C 92%-950°C	Cuadrat et al. (2011)
Coal char	14.7	Ilmenite ore	Bubbling fluidized bed	Steam	1-6	950	η_{comb} 1 bar-92.7% 6 bar -84.2%	Chen et al. (2016)

2.7. Comparison of performance of CLC based power plants

In thermal power plant industries, the CLC system can replace the conventional boilers for the combustion of solid fuel. The incorporation of the CLC system in power plants can increase the net thermal efficiency. Table 2.7 shows the comparative evaluation of the CLC integrated combined cycle, fuel cell cycle and steam turbine systems with conventional power plants. It can be noted that the CLC integrated combined cycle power system achieved a net thermal efficiency in the range of 38-42%, which is 4-5% higher than the conventional power systems. Zhu et al. (2015) compared various operations for the CO_2 capture based on coal gasification process such as IGCC with CO_2 capture, CLC and calcium looping process (CLP) using Aspen Software. They observed a maximum net thermal efficiency of 39.7% in the CLC process. It is found that the CLC based power plant achieved a higher efficiency by 3.1% and 2.1% than the IGCC process and the CLP process, respectively. Mukherjee et al. (2015a) performed energy analysis with different metal oxides such as CuO, Fe_2O_3, NiO and Mn_2O_3 using syngas as the fuel for electricity generation in a combined cycle. They observed that the iron-based oxygen carrier achieved the highest efficiency of 34.3%. Shijaz et al. (2017) showed that a conventional in-situ gasification based combined cycle system achieved 35.8% net efficiency with 94% CO_2 capture. However, with the implementation of the CLC technology, the net thermal efficiency of the power plant is increased to 40.2% with 100% CO_2 capture. Similarly, Prabu (2015) assessed an increase in the net efficiency from 25% to 29.4% in the CLC based combined cycle using syngas obtained from underground coal gasification (UCG). The net efficiency is further increased to 32.5% at supercritical conditions of the steam turbine.

Table 2.7. Comparison of the performance of CLC and conventional and based power plants.

Fuel	Oxygen carrier (OC)	Technique	Methodology	Power plant system	Net efficiency		CO_2 capture efficiency		References
					CLC	Conventional	CLC	Conventional	
Coal	Fe_2O_3	CLC (1100°C) And OFC (1300°C)	Aspen Software	Combined cycle	39.7%	35.2%	100.0%	-	Mukherjee, et al. (2015b)
Bituminous coal	Fe_2O_3	CLC (800°C), IGCC (>1450°C)	ChemCAD Software	Combined cycle	38.7%	-	~99.0%	-	Petrescu & Cormos (2017)
Coal	NiO Fe_2O_3	CLC	Aspen Software	Steam cycle	NiO -45.9% Fe_2O_3- 47.4%	-	-	-	Petriz-Prieto et al. (2016)
Lignite coal	Ilmenite	IG-CLC	Aspen Software	Combined cycle	Lignite-39.0%	35.4%	Lignite-89.1%	-	Fan et al. (2017)
Sawdust	Ilmenite	CLC 650-900°C	ChemCAD software	Combined cycle	42.5%	36.9%	99.6%	90.7%	Cormos (2015)
Coal	CuO	CLC	Simulation study	Ultra-supercritical steam cycle	42.0%	37.0%	95.6%	91.6%	Spinelli et al. (2016)

(CLC: Chemical looping combustion, OFC: Oxy-fuel combustion; IGCC: Integrated gasification combined cycle, IG: In-situ gasification, SOFC: Solid oxide fuel cell)

Table 2.7 continued

Fuel	Oxygen carrier (OC)	Technique	Methodology	Power plant system	Net efficiency		CO_2 capture efficiency		References
					CLC	Conventional	CLC	Conventional	
Coal	NiO	IGCC-CLC	Aspen Software	Combined cycle	39.7%	36.6%	99.9%	86.9%	Zhu et al. (2015)
Syngas from pine bark	CaO	CLC-SOFC	Aspen Software	Combined cycle	55.8%	-	100.0%	-	Aghaie et al. (2016)
Coal syngas		IGCC-CLC	Aspen Software	Combined cycle	40.2%	35.8%	99.9%	94%	Shijaz et al. (2017)
Coal syngas	CuO CoO Fe_2O_3 NiO	IGCC-CLC 750°C	Aspen Software	Combined cycle	CuO-33.3% CoO-33.4% Fe_2O_3-34.3% NiO -34%	-	CuO ~100.0% CoO ~99.0% Fe_2O_3~100.0% NiO ~99.0%	-	Mukherjee et al. (2015a)
UCG coal syngas	NiO	CLC	Simulation study	Subcritical steam cycle	29.4%	~25.0%	-	-	Prabu (2015)
UCG coal syngas	NiO	CLC	Simulation study	Supercritical steam cycle	32.5%	-	-	-	Prabu (2015)

(CLC: Chemical looping combustion, OFC: Oxy-fuel combustion; IGCC: Integrated gasification combined cycle, IG: In-situ gasification, SOFC: Solid oxide fuel cell)

The chemical looping reforming (CLR) process can be integrated with fuel cells for electricity production. The net thermal efficiency of the CLC integrated proton exchange membrane fuel cell (PEM) and solid oxide fuel cell (SOFC) based power systems was estimated in the range of 45-55% (Aghaie et al., 2016, Vairakannu & Kumari, 2016) which is 8-9% higher than the efficiency of combined cycle power plants (Fan et al., 2017, Mukherjee et al., 2015a). Cormos (2015) obtained 42.5% net efficiency by using sawdust and ilmenite in the direct solid fuelled CLC method. However, the net efficiency of the power plant is reduced to 38% for a gasifier integrated CLC process. Similar observations were obtained by Spinelli et al. (2016). Thus the direct solid fuelled based CLC unit would increase the efficiency of the thermal power plant. Overall, the incorporation of the CLC technology in thermal power plant industries is beneficial to achieve higher net thermal efficiency for electricity production with CO_2 capture.

2.8. Conclusions

CLC has proved to be a promising technology due to its low energy penalty, compared to other CO_2 capture technologies. The direct solid fuel based CLC process favors the mutual benefits of enhancing the gasification of char with chemical looping reactivity with metal oxides. Further, the co-utilization of coal and biomass in the CLC technology could improve the performance of the process with the implementation of a carbon negative system. The following conclusions can be drawn from the literature review.

(i) Natural ores (ilmenite, red mud), sewage sludge, etc. are low-cost metal oxides, which are suitable for the economic operation of the CLC process. Furthermore, CLOU-based oxygen carriers can enhance the conversion of solid fuels. However, these metal oxides are expensive and hence, further investigations are necessary for the identification of low-cost CLOU-based oxygen carriers. E-waste based oxygen

carriers are thus proposed, which can handle the e-waste and will also make the CLC process economical.

(ii) The blending of coal and biomass is beneficial to achieve higher conversion of solid fuels. The catalytic activity of inorganic substances (ash), a higher proportion of volatile matter, and carbon-neutral impact of biomass are the specific advantages of the co-utilization of coal and biomass.

(iii) CLC based power generating systems gained a 4 to 5% increase in the net thermal efficiency, compared to conventional power systems with 100% CO_2 capture.

2.9. Research gaps

Based on the literature review, the research gaps are found to be:

1. Detailed experimental studies of the CLC process were reported in the literature using various feedstock such as coal, biomass, coke etc. However, the CLC performance of the high ash Indian coal and its blend with biomass has not been reported. The effect of coal ash on the performance of the CLC process is not explored. Further, the kinetic analysis of high ash coal (volatiles, char) with oxygen carriers is not found in the literature reported for different reaction models.
2. Low cost oxygen carriers in a lab-scale configuration are studied extensively. Various wastes from industries are tested as the oxygen carriers in the CLC process. They exhibited good reactivity due to the presence of Fe. In order to enhance the reactivity, many researchers used mixed metal oxides in the CLC process. Till date, mixed metal oxides from any waste materials have not been explored. E-waste based oxygen carrier can be considered as a low cost metal oxide due to its higher content of Fe and Cu.
3. A compendious analysis has been conducted in the literature to estimate the net thermal efficiency of the CLC based power plant using solid fuels. The impact of co-

combustion of solid fuels with different metal oxides on electricity production and levelized cost of electricity (LCOE) is not compared.

2.10. Objectives and scope of the thesis

The main aim of this thesis is to study the chemical looping combustion behavior of Indian coals under the CO_2 atmosphere. Further, the effective utilization of Indian coals in the in-situ gasification based CLC technology has not been reported. The metal oxides used in the CLC process should be low cost as a fraction of them is carried away along with the ash residue. With the above research gap, the following objectives are framed,

(i) Laboratory scale experimental studies on the CLC based in-situ gasification of solid fuels with and without co-feed conditions in a fixed bed reactor using Indian coals,

(ii) Extraction and utilization of metals as the oxygen carriers from discarded e-waste and testing their performance during the CLC operation,

(iii) Impact of utilization of high ash Indian coal with the extracted metal oxides from e-waste on the cost of electricity in the CLC based thermal power plants.

The scope of the present work is as follows,

(i) Two types of Indian coals, namely, high ash coal (33% ash) and low ash coal (3% ash) are used in the CLC operation. A biomass, rice straw, is used as a co-feed along with coals to improve the combustion efficiency of the CLC process.

(ii) Assessment of the process parameters using Fe_2O_3 as the oxygen carrier with CO_2 as the gasification agent. Evaluation of CO_2 yield, syngas conversion, char conversion, metal oxidation

(iii) Metal extraction from a printed circuit board (PCB) by a series of thermochemical processes such as pyrolysis, gasification and combustion.

(iv) Utilization of the extracted metal oxides (a mixture of CuO, Fe_2O_3, Ni) in the CLC operation with solid fuel feedstock.

(v) Thermogravimetric analysis of the CLC behavior of the solid fuels with Fe_2O_3 and e-waste based metal oxides. Estimation of the kinetic parameters for the CLC based reaction using various models proposed in the literature.

(vi) Estimation of net thermal efficiency, levelized cost of electricity (LCOE) of CLC integrated combined cycle power plants using different metal oxides (pure Fe_2O_3, CuO and oxidized e-waste) by Aspen plus software.

References

Abad, A., Mendiara, T., de Diego, L. F., García-Labiano, F., Gayán, P., & Adánez, J. (2018). A simple model for comparative evaluation of different oxygen carriers and solid fuels in iG-CLC processes. *Fuel Processing Technology*, *179*, 444–454.

Abad, Alberto, Adánez, J., Gayán, P., Diego, L. F. De, García-labiano, F., & Sprachmann, G. (2015). Conceptual design of a 100 MW_{th} CLC unit for solid fuel combustion. *Applied Energy*, *157*, 462–474.

Abad, Alberto, Pérez-vega, R., Diego, L. F. De, García-labiano, F., Gayán, P., & Adánez, J. (2015). Design and operation of a 50 kW_{th} Chemical Looping Combustion (CLC) unit for solid fuels Chemical Looping with Oxygen Uncoupling. *Applied Energy*, *157*, 295–303.

Adánez-Rubio, I., Abad, A., Gayán, P., De Diego, L. F., García-Labiano, F., & Adánez, J. (2014). Biomass combustion with CO_2 capture by chemical looping with oxygen uncoupling (CLOU). *Fuel Processing Technology*, *124*, 104–114.

Adánez-Rubio, Iñaki, Pérez-Astray, A., Mendiara, T., Izquierdo, M. T., Abad, A., Gayán,

P., de Diego, L. F., García-Labiano, F., & Adánez, J. (2018). Chemical looping combustion of biomass: CLOU experiments with a Cu-Mn mixed oxide. *Fuel Processing Technology*, *172*, 179–186.

Adanez, J., Abad, A., Garcia-labiano, F., Gayan, P., & Diego, L. F. De. (2012). Progress in chemical looping combustion and reforming technologies. *Progress in Energy and Combustion Science*, *38*, 215–282.

Adánez, J., Abad, A., Mendiara, T., Gayán, P., de Diego, L. F., & García-Labiano, F. (2018). Chemical looping combustion of solid fuels. *Progress in Energy and Combustion Science*, *65*, 6–66.

Adánez, J., De Diego, L. F., García-Labiano, F., Gayán, P., Abad, A., & Palacios, J. M. (2004). Selection of oxygen carriers for chemical-looping combustion. *Energy and Fuels*, *18*, 371–377.

Aghaie, M., Mehrpooya, M., & Pourfayaz, F. (2016). Introducing an integrated chemical looping hydrogen production, inherent carbon capture and solid oxide fuel cell biomass fueled power plant process configuration. *Energy Conversion and Management*, *124*, 141–154.

Alp, I., Deveci, H., Yazıcı, E. Y., Türk, T., & Süngün, Y. H. (2009). Potential use of pyrite cinders as raw material in cement production : Results of industrial scale trial operations. *Journal of Hazardous Materials*, *166*, 144–149.

Arena, U., Zaccariello, L., & Mastellone, M. L. (2009). Tar removal during the fluidized bed gasification of plastic waste. *Waste Management*, *29*, 783–791.

Arjmand, M., Leion, H., Lyngfelt, A., & Mattisson, T. (2012). Use of manganese ore in chemical-looping combustion (CLC)- Effect on steam gasification. *International*

Journal of Greenhouse Gas Control, *8*, 56–60.

Bao, J., Chen, L., Liu, F., Fan, Z., Nikolic, H. S., & Liu, K. (2016). Evaluating the effect of inert supports and alkali sodium on the performance of red mud oxygen carrier in chemical looping combustion. *Industrial & Engineering Chemistry Research*, *55*, 8046–8057.

Berguerand, N., & Lyngfelt, A. (2008). Design and operation of a 10 kW_{th} chemical-looping combustor for solid fuels - Testing with South African coal. *Fuel*, *87*, 2713–2726.

Bhattacharya, S. P. (2006). Gasification performance of Australian lignites in a pressurized fluidized bed gasifier process development unit under air and oxygen-enriched air blown conditions. *Process Safety and Environmental Protection*, *84*, 453–460.

Bidwe, A. R., Mayer, F., Hawthorne, C., Charitos, A., Schuster, A., & Scheffknecht, G. (2011). Use of ilmenite as an oxygen carrier in chemical looping combustion-batch and continuous dual fluidized bed investigation. *Energy Procedia*, *4*, 433–440.

Cao, Y., Casenas, B., & Pan, W. (2006). Redox reaction kinetics and product characterization with coal, biomass, and solid waste as solid fuels and CuO as an oxygen carrier. *Energy and Fuels*, *20*, 1845–1854.

Chen, C., Han, L., & Bollas, G. M. (2016). Dynamic simulation of fixed-bed chemical-looping combustion reactors integrated in combined cycle power plants. *Energy Technology*, *4*, 1209–1220.

Chen, L., Bao, J., Kong, L., Combs, M., Nikolic, H. S., Fan, Z., & Liu, K. (2016). The direct solid-solid reaction between coal char and iron-based oxygen carrier and its

contribution to solid-fueled chemical looping combustion. *Applied Energy*, *184*, 9–18.

Chen, L., Zhang, Y., Liu, F., & Liu, K. (2015). Development of a cost-effective oxygen carrier from red mud for coal-fueled chemical-looping combustion. *Energy and Fuels*, *29*, 305–313.

Choi, S. E., Kim, S. S., Choi, E., Kim, J. H., Choi, Y., Kang, J., Kwon, O., & Kim, D. W. (2021). Diamine vapor treatment of viscoelastic graphene oxide liquid crystal for gas barrier coating. *Scientific Reports*, *11*, 1–11.

Cormos, C. (2010). Evaluation of energy integration aspects for IGCC-based hydrogen and electricity co-production with carbon capture and storage. *International Journal of Hydrogen Energy*, *35*, 7485–7497.

Cormos, C. (2015). Biomass direct chemical looping for hydrogen and power co-production : Process configuration, simulation, thermal integration and techno-economic assessment. *Fuel Processing Technology*, *137*, 16–23.

Cuadrat, A., Abad, A., Adánez, J., De Diego, L. F., García-Labiano, F., & Gayán, P. (2012). Behavior of ilmenite as oxygen carrier in chemical-looping combustion. *Fuel Processing Technology*, *94*, 101–112.

Cuadrat, Ana, Garcı, F., Gaya, P., Diego, L. F. De, Abad, A., & Ada, J. (2011). Kinetics of redox reactions of ilmenite for chemical looping combustion. *Chemical Engineering Science*, *66*, 689–702.

Cui, J., & Zhang, L. (2008). Metallurgical recovery of metals from electronic waste: A review. *Journal of Hazardous Materials*, *158*, 228–256.

Dai, J., & Whitty, K. J. (2019). Predicting and alleviating coal ash-induced deactivation

of CuO as an oxygen carrier for chemical looping with oxygen uncoupling. *Fuel*, *241*, 1214–1222.

Dilmaç, Ö. F., Dilmaç, N., & Doruk, E. T. (2020). Performance of electric arc furnace slag as oxygen carrier in chemical-looping combustion process. *Fuel*, *265*, 117014.

Fan, J., Hong, H., Zhu, L., Jiang, Q., & Jin, H. (2017). Thermodynamic and environmental evaluation of biomass and coal co-fuelled gasification chemical looping combustion with CO_2 capture for combined cooling , heating and power production. *Applied Energy*, *195*, 861–876.

Fang, S., Deng, Z., Lin, Y., Huang, Z., Ding, L., Deng, L., & Huang, H. (2021). Nitrogen migration in sewage sludge chemical looping gasification using copper slag modified by NiO as an oxygen carrier. *Energy*, *228*, 120448.

Frick, V., Rydén, M., Leion, H., Mattisson, T., & Lyngfelt, A. (2015). Screening of supported and unsupported Mn-Si oxygen carriers for CLOU (chemical-looping with oxygen uncoupling). *Energy*, *93*, 544–554.

Frohn, P., Mattisson, T., & Lyngfelt, A. (2013). On the high-gasification rate of Brazilian manganese ore in chemical-looping combustion (CLC) for solid fuels. *Fuel*, *59*, 4346–4354.

García-labiano, F., Adánez, J., Diego, L. F. De, Gayán, P., & Abad, A. (2006). Effect of pressure on the behavior of copper-, iron-and nickel-based oxygen carriers for Chemical-Looping Combustion. *Energy & Fuels*, *1*, 26–33.

Ge, H., Guo, W., Shen, L., Song, T., & Xiao, J. (2016). Biomass gasification using chemical looping in a 25 kW_{th} reactor with natural hematite as oxygen carrier. *Chemical Engineering Journal*, *286*, 174–183.

Gu, H., Shen, L., Xiao, J., Zhang, S., & Song, T. (2011). Chemical looping combustion of biomass/coal with natural iron ore as oxygen carrier in a continuous reactor. *Energy and Fuels*, *25*(1), 446–455.

Guo, L., Zhao, H. bo, Ma, J. chen, Mei, D. feng, & Zheng, C. guang. (2014). Comparison of Large-Scale Production Methods of Fe_2O_3/Al_2O_3 Oxygen Carriers for Chemical-Looping Combustion. *Chemical Engineering and Technology*, *37*, 1211–1219.

Habibi, R., Kopyscinski, J., Masnadi, M. S., Lam, J., Grace, J. R., Mims, C. A., & Hill, J. M. (2013). Co-gasification of biomass and non-biomass feedstocks: Synergistic and inhibition effects of switchgrass mixed with sub-bituminous coal and fluid coke during CO_2 gasification. *Energy and Fuels*, *27*(1), 494–500.

Hammache, S., Means, N., Burgess, W., Howard, B., & Smith, M. (2020). Investigation of low-cost oxygen carriers for chemical looping combustion at high temperature. *Fuel*, *273*, 117746.

Han, J., & Kim, H. (2008). The reduction and control technology of tar during biomass gasification/pyrolysis: An overview. *Renewable and Sustainable Energy Reviews*, *12*, 397–416.

Hasanzadeh, R., Mojaver, M., Azdast, T., & Park, C. B. (2021). Polyethylene waste gasification syngas analysis and multi-objective optimization using central composite design for simultaneous minimization of required heat and maximization of exergy efficiency. *Energy Conversion and Management*, *247*, 114713.

Hu, S., Yu, Z., Li, C., Wang, Z., Guo, S., Huang, J., & Fang, Y. (2015). Reaction characteristics research of coal char chemical looping gasification for hydrogen production with an Fe-Zr oxygen carrier modified by K_2CO_3. *Journal of Fuel Chemistry and Technology*, *43*, 386–392.

Jayaraman, K., Kok, M. V., & Gokalp, I. (2017). Thermogravimetric and mass spectrometric (TG-MS) analysis and kinetics of coal-biomass blends. *Renewable Energy*, *101*, 293–300.

Johansson, E., Lyngfelt, A., Mattisson, T., & Johnsson, F. (2003). Gas leakage measurements in a cold model of an interconnected fluidized bed for chemical-looping combustion. *Powder Technology*, *134*, 210–217.

Kim, H. R., Wang, D., Zeng, L., Bayham, S., Tong, A., Chung, E., Kathe, M. V., Luo, S., McGiveron, O., Wang, A., Sun, Z., Chen, D., & Fan, L. S. (2013). Coal direct chemical looping combustion process: Design and operation of a 25-kW_{th} sub-pilot unit. *Fuel*, *108*, 370–384.

Kimball, E., Hamers, H. P., Cobden, P., Gallucci, F., & Van Sint Annaland, M. (2013). Operation of fixed-bed chemical looping combustion. *Energy Procedia*, *37*, 575–579.

Krerkkaiwan, S., Fushimi, C., Tsutsumi, A., & Kuchonthara, P. (2013). Synergetic effect during co-pyrolysis/gasification of biomass and sub-bituminous coal. *Fuel Processing Technology*, *115*, 11–18.

Ksepko, E. (2014). Sewage sludge ash as an alternative low-cost oxygen carrier for chemical looping combustion. *Journal of Thermal Analysis and Calorimetry*, *116*, 1395–1407.

Larring, Y., Braley, C., Pishahang, M., Andreassen, K. A., & Bredesen, R. (2015). Evaluation of a Mixed Fe–Mn Oxide System for Chemical Looping Combustion. *Energy & Fuels*, *29*, 3438–3445.

Leion, H., Lyngfelt, A., & Mattisson, T. (2009). Solid fuels in chemical-looping

combustion using a NiO-based oxygen carrier. *Chemical Engineering Research and Design*, *87*, 1543–1550.

Leion, H., Mattisson, T., & Lyngfelt, A. (2009). Using chemical-looping with oxygen uncoupling (CLOU) for combustion of six different solid fuels. *Energy Procedia*, *1*, 447–453.

Linderholm, C., Cuadrat, A., & Lyngfelt, A. (2011). Chemical-looping combustion of solid fuels in a 10 kW_{th} pilot- Batch tests with five fuels. *Energy Procedia*, *4*, 385–392.

Linderholm, C., & Schmitz, M. (2016). Chemical-looping combustion of solid fuels in a 100 kW_{th} dual circulating fluidized bed system using iron ore as oxygen carrier. *Journal of Environmental Chemical Engineering*, *4*, 1029–1039.

Linderholm, C., Schmitz, M., Knutsson, P., Ka, M., & Lyngfelt, A. (2014). Use of low-volatile solid fuels in a 100 kW_{th} chemical-looping combustor. *Energy & Fuels*, *28*, 5942–5952.

Linderholm, C., Schmitz, M., Knutsson, P., & Lyngfelt, A. (2016). Chemical-looping combustion in a 100-kW_{th} unit using a mixture of ilmenite and manganese ore as oxygen carrier. *Fuel*, *166*, 533–542.

Liu, G., Wang, H., Veksha, A., Giannis, A., Lim, T. T., & Lisak, G. (2021). Chemical looping combustion-adsorption of HCl-containing syngas using alkaline-earth coated iron ore composites for simultaneous purification and combustion enhancement. *Chemical Engineering Journal*, *417*, 129226.

Liu, X., Chen, M., & Wei, Y. (2016). Assessment on oxygen enriched air co-combustion performance of biomass/bituminous coal. *Renewable Energy*, *92*, 428–436.

Luo, M., Wang, S., Wang, L., Lv, M., Qian, L., & Fu, H. (2013). Experimental investigation of co-combustion of coal and biomass using chemical looping technology. *Fuel Processing Technology*, *110*, 258–267.

Luo, M., Yi, Y., Wang, S., Wang, Z., Du, M., Pan, J., & Wang, Q. (2018). Review of hydrogen production using chemical-looping technology. *Renewable and Sustainable Energy Reviews*, *81*, 3186–3214.

Lyngfelt, A. (2020). Chemical Looping Combustion: Status and Development Challenges. *Energy and Fuels*, *34*(8), 9077–9093.

Lyngfelt, A., & Linderholm, C. (2014). Chemical-looping combustion of solid fuels - Technology overview and recent operational results in 100 kW_{th} unit. *Energy Procedia*, *63*, 98–112.

Ma, J., Tian, X., Wang, C., Chen, X., & Zhao, H. (2018). Performance of a 50 kW_{th} coal-fuelled chemical looping combustor. *International Journal of Greenhouse Gas Control*, *75*, 98–106.

Ma, J., Zhao, H., Tian, X., Wei, Y., Rajendran, S., & Zhang, Y. (2015). Chemical looping combustion of coal in a 5 kW_{th} interconnected fluidized bed reactor using hematite as oxygen carrier. *Applied Energy*, *157*, 304–313.

Maric, J., Berdugo Vilches, T., Pissot, S., Cañete Vela, I., Gyllenhammar, M., & Seemann, M. (2020). Emissions of dioxins and furans during steam gasification of Automotive Shredder residue; experiences from the Chalmers 2–4-MW_{th} indirect gasifier. *Waste Management*, *102*, 114–121.

Masnadi, M. S., Grace, J. R., Bi, X. T., Lim, C. J., & Ellis, N. (2015). From fossil fuels towards renewables: Inhibitory and catalytic effects on carbon thermochemical

conversion during co-gasification of biomass with fossil fuels. *Applied Energy*, *140*, 196–209.

Massoudi Farid, M., Jeong, H. J., & Hwang, J. (2016). Kinetic study on coal–biomass mixed char co-gasification with H_2O in the presence of H_2. *Fuel*, *181*, 1066–1073.

Mattisson, T., Johansson, M., & Lyngfelt, A. (2006). The use of NiO as an oxygen carrier in chemical looping combustion. *Fuel*, *85*, 736–747.

Mattisson, T., Keller, M., Linderholm, C., Moldenhauer, P., Rydén, M., Leion, H., & Lyngfelt, A. (2018). Chemical-looping technologies using circulating fluidized bed systems: Status of development. *Fuel Processing Technology*, *172*, 1–12.

Mattisson, T., Leion, H., & Lyngfelt, A. (2009). Chemical looping with oxygen uncoupling using CuO/ZrO_2 with petroleum coke. *Fuel*, *88*, 683–690.

Mendiara, T., Abad, A., Diego, L. F. de, García-Labiano, F., Gayán, P., & Adánez, J. (2012). Use of an Fe-based residue from alumina production as an oxygen carrier in chemical-looping combustion. *Energy & Fuels*, *26*, 1420–1431.

Mendiara, T., García-Labiano, F., Gayán, P., Abad, A., De Diego, L. F., & Adánez, J. (2013). Evaluation of the use of different coals in chemical looping combustion using a bauxite waste as oxygen carrier. *Fuel*, *106*, 814–826.

Mendiara, T., Gayán, P., Abad, A., Diego, L. F. De, & Adánez, J. (2013). Performance of a bauxite waste as oxygen-carrier for chemical-looping combustion using coal as fuel. *Fuel Processing Technology*, *109*, 57–69.

Molina, A., Mondragón, F., Mondrago, F., & Mondragón, F. (1998). Reactivity of coal gasification with steam and CO_2. *Fuel*, *77*(15), 1831–1839.

Mukherjee, S., Kumar, P., Yang, A., & Fennell, P. (2015a). A systematic investigation

of the performance of copper-, cobalt-, iron-, manganese- and nickel-based oxygen carriers for chemical looping combustion technology through simulation models. *Chemical Engineering Science*, *130*, 79–91.

Mukherjee, S., Kumar, P., Yang, A., & Fennell, P. (2015b). Energy and exergy analysis of chemical looping combustion technology and comparison with pre-combustion and oxy-fuel combustion technologies for CO_2 capture. *Journal of Environmental Chemical Engineering*, *3*, 2104–2114.

Niu, P., Ma, Y., Tian, X., Ma, J., & Zhao, H. (2018). Chemical looping gasification of biomass: Part I. screening Cu-Fe metal oxides as oxygen carrier and optimizing experimental conditions. *Biomass and Bioenergy*, *108*, 146–156.

Nordness, O., Han, L., Zhou, Z., & Bollas, G. M. (2016). High-pressure chemical-looping of methane and synthesis gas with Ni and Cu oxygen carriers. *Energy and Fuels*, *30*, 504–514.

Ohlemüller, P., Alobaid, F., Gunnarsson, A., Ströhle, J., & Epple, B. (2015). Development of a process model for coal chemical looping combustion and validation against 100kW_{th} tests. *Applied Energy*, *157*, 433–448.

Ortiz, M., Gayán, P., De Diego, L. F., García-Labiano, F., Abad, A., Pans, M. A., & Adánez, J. (2011). Hydrogen production with CO_2 capture by coupling steam reforming of methane and chemical-looping combustion: Use of an iron-based waste product as oxygen carrier burning a PSA tail gas. *Journal of Power Sources*, *196*(9), 4370–4381.

Pant, D., Joshi, D., Upreti, M. K., & Kotnala, R. K. (2012). Chemical and biological extraction of metals present in E waste: A hybrid technology. *Waste Management*, *32*(5), 979–990.

Patzschke, C. F., Boot-Handford, M. E., Song, Q., & Fennell, P. S. (2021). Co-precipitated Cu-Mn mixed metal oxides as oxygen carriers for chemical looping processes. *Chemical Engineering Journal*, *407*, 127093.

Pérez-Vega, R., Abad, A., García-Labiano, F., Gayán, P., de Diego, L. F., & Adánez, J. (2016). Coal combustion in a 50 kW_{th} chemical looping combustion unit: Seeking operating conditions to maximize CO_2 capture and combustion efficiency. *International Journal of Greenhouse Gas Control*, *50*, 80–92.

Pérez-Vega, R., Abad, A., Gayán, P., García-Labiano, F., Izquierdo, M. T., de Diego, L. F., & Adánez, J. (2020). Coal combustion via chemical looping assisted by oxygen uncoupling with a manganese-iron mixed oxide doped with titanium. *Fuel Processing Technology*, *197*, 106184.

Perreault, P., Rifflart, S., Nguyen, E., & Patience, G. (2016). Pyrolusite : An alternative oxygen carrier for chemical looping combustion. *Fuel*, *185*, 630–638.

Petrescu, L., & Cormos, C. (2017). Environmental assessment of IGCC power plants with pre-combustion CO_2 capture by chemical & calcium looping methods. *Journal of Cleaner Production*, *158*, 233–244.

Petriz-Prieto, M. A., Rico-ramirez, V., Gonzalez-Alatorre, G., Gómez-Castro, F. I., & Diwekar, U. M. (2016). A comparative simulation study of power generation plants involving chemical looping combustion systems. *Computers & Chemical Engineering*, *84*, 434–445.

Pikkarainen, T., Hiltunen, I., & Teir, S. (2016). Piloting of bio-CLC for BECCS. *In: 4th International Conference on Chemical Looping*.

Pröll, T., Mayer, K., Bolhàr-Nordenkampf, J., Kolbitsch, P., & Mattisson, T. (2009).

Natural minerals as oxygen carriers for chemical looping combustion in a dual circulating fluidized bed system. *Energy Procedia*, *1*(1), 27–34.

Qasim, M., Ayoub, M., Ghazali, N. A., Aqsha, A., & Ameen, M. (2021). Recent Advances and Development of Various Oxygen Carriers for the Chemical Looping Combustion Process: A Review. *Industrial and Engineering Chemistry Research*, *60*, 8621–8641.

Qin, C., Yin, J., Liu, W., An, H., & Feng, B. (2012). Behavior of CaO/CuO based composite in a combined calcium and copper chemical looping process. *Industrial and Engineering Chemistry Research*, *51*(38), 12274–12281.

Qiu, R., Lin, M., Ruan, J., Fu, Y., Hu, J., Deng, M., Tang, Y., & Qiu, R. (2020). Recovering full metallic resources from waste printed circuit boards : A refined review. *Journal of Cleaner Production*, *244*, 118690.

Rajendran, S., Wong, M., Stokie, D., & Bhattacharya, S. (2016). Performance of a Victorian brown coal and iron ore during chemical looping combustion in a 10 kW_{th} alternating fluidized bed. *Fuel*, *183*, 245–252.

Rydén, M., Lyngfelt, A., & Mattisson, T. (2011). Combined manganese/iron oxides as oxygen carrier for chemical looping combustion with oxygen uncoupling (CLOU) in a circulating fluidized bed reactor system. *Energy Procedia*, *4*, 341–348.

Rydén, M., Lyngfelt, A., Mattisson, T., Chen, D., Holmen, A., & Bjørgum, E. (2008). Novel oxygen-carrier materials for chemical-looping combustion and chemical-looping reforming; $La_xSr_{1-x}Fe_yCo_{1-y}O_{3-\delta}$ perovskites and mixed-metal oxides of NiO, Fe_2O_3 and Mn_3O_4. *International Journal of Greenhouse Gas Control*, *2*, 21–36.

Saebea, D., Ruengrit, P., Arpornwichanop, A., & Patcharavorachot, Y. (2020). Gasification of plastic waste for synthesis gas production. *Energy Reports*, *6*, 202–207.

Salbidegoitia, J. A., Fuentes-Ordóñez, E. G., González-Marcos, M. P., González-Velasco, J. R., Bhaskar, T., & Kamo, T. (2015). Steam gasification of printed circuit board from e-waste : Effect of coexisting nickel to hydrogen production. *Fuel Processing Technology*, *133*, 69–74.

Schmitz, M., & Linderholm, C. J. (2016). Performance of calcium manganate as oxygen carrier in chemical looping combustion of biochar in a 10 kW_{th} pilot. *Applied Energy*, *169*, 729–737.

Shafiefarhood, A., Stewart, A., & Li, F. (2015). Iron-containing mixed-oxide composites as oxygen carriers for Chemical Looping with Oxygen Uncoupling (CLOU). *Fuel*, *139*, 1–10.

Shen, L., Wu, J., Xiao, J., Song, Q., & Xiao, R. (2009). Chemical-looping combustion of biomass in a 10 kW_{th} reactor with iron oxide as an oxygen carrier. *Energy and Fuels*, *23*, 2498–2505.

Shen, Q., Zheng, Y., Luo, C., Ding, N., Zheng, C. G., & Thern, M. (2015). Effect of A/B-site substitution on oxygen production performance of strontium cobalt based perovskites for CO_2 capture application. *RSC Advances*, *5*, 39785–39790.

Shijaz, H., Attada, Y., Patnaikuni, V. S., Vooradi, R., & Anne, S. B. (2017). Analysis of integrated gasification combined cycle power plant incorporating chemical looping combustion for environment-friendly utilization of Indian coal. *Energy Conversion and Management*, *151*, 414–425.

Siriwardane, R., Benincosa, W., Riley, J., Tian, H., & Richards, G. (2016a). Investigation of reactions in a fluidized bed reactor during chemical looping combustion of coal/ steam with copper oxide-iron oxide-alumina oxygen carrier. *Applied Energy*, *183*, 1550–1564.

Siriwardane, R., Riley, J., Tian, H., & Richards, G. (2016b). Chemical looping coal gasification with calcium ferrite and barium ferrite via solid-solid reactions. *Applied Energy*, *165*, 952–966.

Siriwardane, R., Tian, H., Miller, D., & Richards, G. (2015). Fluidized bed testing of commercially prepared MgO-promoted hematite and CuO–Fe_2O_3 mixed metal oxide oxygen carriers for methane and coal chemical looping combustion. *Applied Energy*, *157*, 348–357.

Song, T., & Shen, L. (2018). Review of reactor for chemical looping combustion of solid fuels. *International Journal of Greenhouse Gas Control*, *76*, 92–110.

Song, T., Shen, T., Shen, L., Xiao, J., Gu, H., & Zhang, S. (2013). Evaluation of hematite oxygen carrier in chemical-looping combustion of coal. *Fuel*, *104*, 244–252.

Song, T., Wu, J., Zhang, H., & Shen, L. (2012). Characterization of an Australia hematite oxygen carrier in chemical looping combustion with coal. *International Journal of Greenhouse Gas Control*, *11*, 326–336.

Song, Y., Tahmasebi, A., & Yu, J. (2014). Co-pyrolysis of pine sawdust and lignite in a thermogravimetric analyzer and a fixed-bed reactor. *Bioresource Technology*, *174*, 204–211.

Sozinho, T., Pelletant, W., Gauthier, T., & Stainton, H. (2012). Main results of the 10 kW_{th} coal pilot plant operation. *In 2nd Int. Conf. on Chemical Looping*.

Spinelli, M., Peltola, P., Bischi, A., Ritvanen, J., Hyppänen, T., & Romano, M. C. (2016). Process integration of chemical looping combustion with oxygen uncoupling in a coal-fired power plant. *Energy*, *103*, 646–659.

Staničić, I., Cañete Vela, I., Backman, R., Maric, J., Cao, Y., & Mattisson, T. (2021). Fate of lead, copper, zinc and antimony during chemical looping gasification of automotive shredder residue. *Fuel*, *302*, 121147.

Ströhle, J., Orth, M., & Epple, B. (2014). Design and operation of a 1MW_{th} chemical looping plant. *Applied Energy*, *113*, 1490–1495.

Ströhle, J., Orth, M., & Epple, B. (2015). Chemical looping combustion of hard coal in a 1 MW_{th} pilot plant using ilmenite as oxygen carrier. *Applied Energy*, *157*, 288–294.

Sun, Z., Chen, S., Russell, C. K., Hu, J., Rony, A. H., Tan, G., Chen, A., Duan, L., Boman, J., Tang, J., Chien, T. Y., Fan, M., & Xiang, W. (2018). Improvement of H_2-rich gas production with tar abatement from pine wood conversion over bi-functional $Ca_2Fe_2O_5$ catalyst: Investigation of inner-looping redox reaction and promoting mechanisms. *Applied Energy*, *212*, 931–943.

Tang, M., Xu, L., & Fan, M. (2015). Progress in oxygen carrier development of methane-based chemical-looping reforming: A review. *Applied Energy*, *151*, 143–156.

Thon, A., Kramp, M., Hartge, E., Heinrich, S., & Werther, J. (2014). Operational experience with a system of coupled fluidized beds for chemical looping combustion of solid fuels using ilmenite as oxygen carrier. *Applied Energy*, *118*, 309–317.

Vairakannu, P., & Kumari, G. (2016). CO_2-Oxy underground coal gasification integrated proton exchange membrane fuel cell operating in a chemical looping mode of reforming. *International Journal of Hydrogen Energy*, *41*(44), 20063–20077.

Walter, J. P., Brune, A., Seidel-Morgenstern, A., & Hamel, C. (2021). Model-based analysis of fixed-bed and membrane reactors of various scale. *Chemie-Ingenieur-Technik*, *93*(5), 819–824.

Wang, B., Gao, C., Wang, W., Kong, F., & Zheng, C. (2014). TGA-FTIR investigation of chemical looping combustion by coal with $CoFe_2O_4$ combined oxygen carrier. *Journal of Analytical and Applied Pyrolysis*, *105*, 369–378.

Wang, K., Yu, Q., Zuo, Z., Hou, L., & Qin, Q. (2016). Redox performance of Cu-based oxygen carrier used in chemical looping air separation combined oxy-fuel combustion technology. *Applied Thermal Engineering*, *98*, 440–448.

Wang, P., Howard, B., & Means, N. (2021). Investigation of reactivities of bimetallic Cu-Fe oxygen carriers with coal in high temperature in-situ gasification chemical-looping combustion (iG-CLC) and chemical-looping with oxygen uncoupling (CLOU) using a fixed bed reactor. *Fuel*, *285*, 119012.

Warnecke, R. (2000). Gasification of biomass: Comparison of fixed bed and fluidized bed gasifier. *Biomass and Bioenergy*, *18*, 489–497.

Wei, J., Guo, Q., Chen, H., Chen, X., & Yu, G. (2016). Study on reactivity characteristics and synergy behaviours of rice straw and bituminous coal co-gasification. *Bioresource Technology*, *220*, 509–515.

Wilk, V., & Hofbauer, H. (2013). Co-gasification of plastics and biomass in a dual fluidized-bed steam gasifier: Possible interactions of fuels. *Energy and Fuels*, *27*(6), 3261–3273.

Xiao, R., Chen, L., Saha, C., Zhang, S., & Bhattacharya, S. (2012). Pressurized chemical-looping combustion of coal using an iron ore as oxygen carrier in a pilot-scale unit.

International Journal of Greenhouse Gas Control, *10*, 363–373.

Xu, C., Hu, S., Xiang, J., Zhang, L., Sun, L., Shuai, C., Chen, Q., He, L., & Edreis, E. M. A. (2014). Interaction and kinetic analysis for coal and biomass co-gasification by TG – FTIR. *Bioresource Technology*, *154*, 313–321.

Yang, J. B., Cai, N. S., & Li, Z. S. (2007). Reduction of iron oxide as an oxygen carrier by coal pyrolysis and steam char gasification intermediate products. *Energy and Fuels*, *21*(6), 3360–3368.

Yang, W., Zhao, H., Wang, K., & Zheng, C. (2015). Synergistic effects of mixtures of iron ores and copper ores as oxygen carriers in chemical-looping combustion. *Proceedings of the Combustion Institute*, *35*, 2811–2818.

Yi, B., Zhang, L., Yuan, Q., Yan, S., & Zheng, C. (2016). The evolution of coal char structure under the oxy-fuel combustion containing high H_2O. *Fuel Processing Technology*, *152*, 294–302.

Yu, Z., Yang, Y., Yang, S., Zhang, Q., Zhao, J., Fang, Y., Hao, X., & Guan, G. (2019). Iron-based oxygen carriers in chemical looping conversions: A review. *Carbon Resources Conversion*, *2*, 23–34.

Zhang, S., Rajendran, S., Henderson, S., Zeng, D., & Xiao, R. (2015). Use of pyrite cinder as an iron-based oxygen carrier in coal-fueled chemical looping combustion. *Energy & Fuels*, *29*, 2645–2655.

Zhang, S., Saha, C., Yang, Y., Bhattacharya, S., & Xiao, R. (2011). Use of Fe_2O_3-containing industrial wastes as the oxygen carrier for chemical-looping combustion of coal: effects of pressure and cycles. *Energy & Fuels*, *25*, 4357–4366.

Zhao, H., Guo, L., & Zou, X. (2015). Chemical-looping auto-thermal reforming of

biomass using Cu-based oxygen carrier. *Applied Energy*, *157*, 408–415.

Zhou, C., Liu, G., Wang, X., Qi, C., & Hu, Y. (2016). Combustion characteristics and arsenic retention during co-combustion of agricultural biomass and bituminous coal. *Bioresource Technology*, *214*, 218–224.

Zhu, L., Jiang, P., & Fan, J. (2015). Comparison of carbon capture IGCC with chemical-looping combustion and with calcium-looping process driven by coal for power generation. *Chemical Engineering Research and Design*, *104*, 110–124.

CHAPTER 3

Materials & Method

CHAPTER 3

MATERIALS AND METHODOLOGY

The present chapter describes the materials and methodology of the research work. The feed material, operating conditions, reactor configuration, and the methodology of the CLC process are explained. The pre and post combustion characterization of feed and metal oxides using various analytical equipment are discussed. Further, this chapter illustrates the process methodology of the flow sheeting for estimating the gross electricity by integrating the CLC process in a combined cycle power plant. The operating conditions, basic energy and economic analysis methodology, and assumptions are highlighted along with the Aspen plus model validation.

3.1. Fuels

The properties of solid feedstocks (coal, rice straw, e-wastes) are characterized by proximate and ultimate analysis. The estimated properties are shown in Table 3.1. The heating value of the solid fuels is found using a bomb calorimeter. Indian coal reserves vary in their fuel composition with location, either rich in ash content or possessing high sulfur content. In the present study, three solid fuels are used in the CLC process.

i. Coals found in Assam, a north-eastern state of India, contain low ash (LAC) but are enriched with sulphur content. These coals have higher calorific value among other fuels.

ii. A high ash coal (HAC) is obtained from Jharkhand coal mines, India and this coal contains 33% ash content. Both HAC and LAC are reduced into a fine powder of size 213 μm using crushers.

iii. A biomass, rice straw (RS), is collected from the local market of Guwahati, India and crushed into particles of size in the range of 1-3 mm. RS contains a significant amount of volatile matter, but the fixed carbon is low.

These three solid fuels are used in the CLC process. The particles size of coals (LAC and HAC) are -250 to +212µm, while RS is 1-3mm. The metal oxy-combustion process is performed with and without co-combustion conditions. RS is mixed with coals at 1:1 ratio by weight and the synergistic effects are assessed. The higher heating value (HHV) of LAC, HAC and RS are found to be 32.8 MJ/kg, 22.1 MJ/kg and 17.2 MJ/kg, respectively.

Table 3.1. Proximate and ultimate analysis of fuels.

Analysis	Composition	Low ash coal (LAC)	High ash coal (HAC)	Rice straw (RS)	E-waste (EW)
Proximate Analysis (wt. %, wet basis)	Moisture	11.2	2.1	18.0	0.1
	Volatile matter	34.7	18.8	59.0	28.1
	Ash	2.1	33.0	12.0	69.3
	Fixed carbon	52.0	46.1	11.0	2.5
Ultimate Analysis (wt. %, dry and ash free basis)	C	78.3	60.4	47.9	18.2
	H	5.5	2.5	6.3	1.6
	O	12.1	34.9	44.4	10.2
	N	2.4	2.2	1.2	0.5
	S	1.7	-	0.2	0.2
Heating value (MJ/kg)		32.8	22.1	17.6	11.6

3.2. Oxygen carriers

3.2.1. Fe_2O_3

Fe_2O_3 is purchased from Sigma Aldrich (99.99% purity) with a particle size less than 5µm. Fe_2O_3 is preferred over other oxygen carriers since it is low cost and has sufficient oxygen transport capacity. It has a high melting point and non-toxicity nature (Feng et

al., 2020). Further, it is reported that the coal ash fusion temperature is increased in the presence of Fe_2O_3 (Ni et al., 2010). Also, the quantity of tar formed during gasification is low in the presence of Fe_2O_3, which is thus a potential catalyst for tar cracking reactions (Ge et al., 2016). In addition, the sintering and agglomeration tendency of Fe_2O_3 are negligible (Berguerand & Lyngfelt, 2010). Hence, it is advantageous to use Fe_2O_3 for coal direct CLC process.

3.2.2. Oxidized e-waste

E-waste (EW) can be utilized as the oxygen carrier in the CLC process due to its metallic content as discussed in Chapter 2. Figure 3.1 shows the stepwise preparation of oxygen carrier from a printed circuit board (PCB). The PCB from a discarded computer is selected to prepare the e-waste based oxygen carriers for the CLC process. The proximate and ultimate analysis of PCB is given in Table 3.1. The calorific value of PCB is found as 11.6 MJ/kg. It is observed that the PCB remarkably contains various metal components. Epoxy resins in the PCB is the source of volatile content (Jie et al., 2008). The resins are used as flame retardants, waterproof materials and additives in the e-waste to increase its lifespan (Li et al., 2010).

The list of steps followed for metal extraction is shown in Figure 3.1. The PCB taken from a discarded computer is dismantled to separate its base plate from the mounted pieces on the mainboard. It is then sent for the pyrolysis process. After the removal of volatiles, the pyrolyzed solid residue mostly contains metals and char along with flame retardants. Further, the char content in the residue is gasified using CO_2 gas. The gasified residue is combusted using air to convert metals into their respective oxides. The combustion process is continued till there is no CO_2 detected in the outlet gas. The final residue obtained after combustion contains mainly a mixture of metal oxides, which are

the potential oxygen carriers for the CLC process. This can further be mixed with solid fuels (coal/ biomass) to produce rich CO_2.

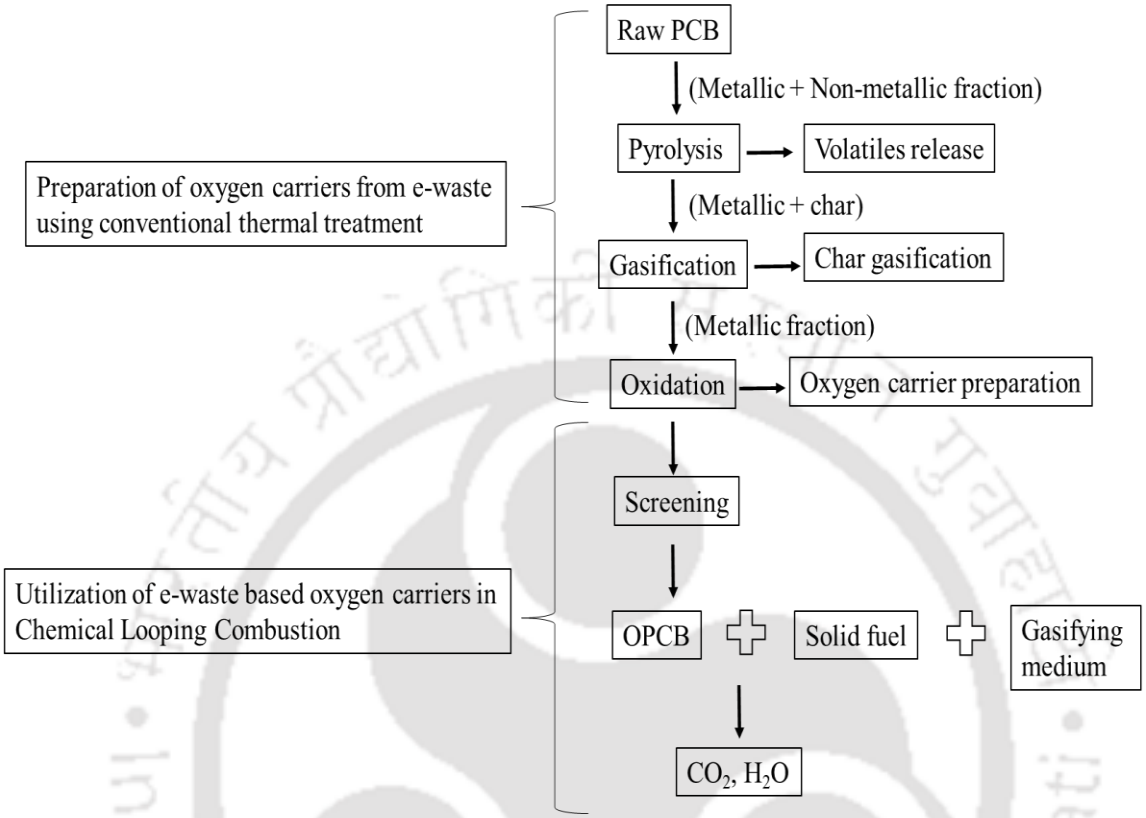

Figure 3.1. Process flowchart for the oxygen carrier preparation from e-waste (PCB).

3.3. Experimental setup

Experiments are conducted using a laboratory-scale fixed bed reactor under atmospheric pressure in a batch-wise operating mode. The schematic diagram of the experimental setup is shown in Figure 3.2. The reactor is electrically heated using an external furnace and the operating temperature is measured using a K-type thermocouple, which is fixed at the centre of the reactor. The feed mixture containing coal, biomass and metal oxides is stored in the hopper located at the top of the reactor. After reaching the desired operating temperature of the reactor at 900°C, the feed mixture (fuel and oxygen carrier) is allowed to discharge into the reactor using an on/off valve. Simultaneously, the feed gas, CO_2, is supplied through the gas feed line (bottom of the reactor). The volatile gases

are released quickly, and a carbon rich char bed is formed in the reactor. The released volatiles react with the metal oxides and produce a CO_2 enriched stream. The flow rate of the flue gas is measured using a bubble flow meter. It is collected at every 10 minutes interval and stored in vacutainer tubes. Once the reduction process is complete, a part of the residue is collected for characterization, while the rest is again introduced to the air reactor for oxidation. This technique has been applied during multiple cycle operation. The chemical composition of the flue gas is analyzed using gas chromatography (Model: CP-3800; Make M/s Varian, Netherland). The fixed bed reactor experiments are performed with solid fuels with and without metal oxides. The experiments performed without metal oxides are referred to as non-CLC experiments, whereas the CLC experiments are conducted with metal oxides. The complete list of experiments is shown in Table 3.2 which highlights the fuel-oxygen carrier ratio, inlet gas flowrate etc.

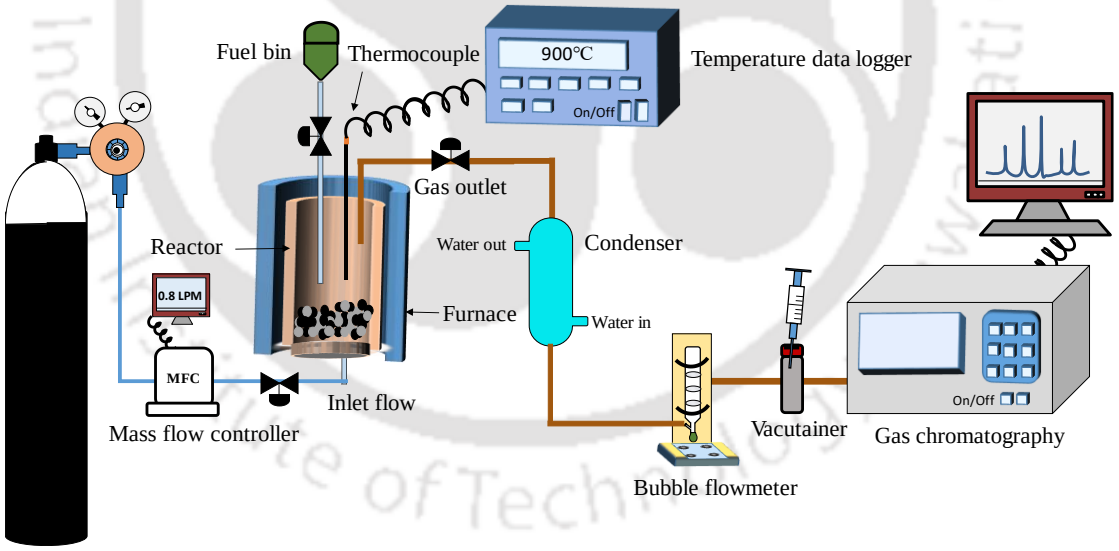

Figure 3.2. Schematic diagram of the fixed bed reactor experimental setup.

Table 3.2. Various cases of experiments conducted in the present study *(* Operated for 3 consecutive cycles)*

Case No.	Fuels	Quantity of fuel and OC	Residence time (min.)	Temperature, °C	Operating conditions		
					Fuel reactor		Air reactor
					Ratio of fuel: metal oxide (by mass)	Inlet gas flow rate (L/min)	Inlet gas flow rate (L/min)
1.	LAC	60g		350-950°C	-	0.3 L/min -N_2	-
2.	LAC	60g		350-1000°C	-	0.3 L/min -CO_2	-
3.	RS	60g		350-1000°C	-	0.3 L/min -CO_2	-
4.	LAC-RS	60g		350-1000°C	-	0.3 L/min -CO_2	-
5.	HAC	60g		350-950°C	-	0.3 L/min -N_2	-
6.	HAC	60g		350-1000°C	-	0.3 L/min -CO_2	-
7.	HAC-RS	60g		350-1000°C	-	0.3 L/min -CO_2	-
8.	LAC:Fe_2O_3	5 g LAC, 325 g Fe_2O_3	100	900	1:65	0.8 L/min - CO_2	0.8 L/min - Air
9.	RS:Fe_2O_3	5 g RS, 200 g Fe_2O_3	100	900	1:40	0.8 L/min - CO_2	0.8 L/min - Air
10.	LAC-RS:Fe_2O_3	5 g LAC-RS, 275 g Fe_2O_3	100	900	1:55	0.8 L/min - CO_2	0.8 L/min - Air

Table 3.2 continued

Case No.	Fuels	Quantity of fuel and OC	Residence time (min.)	Temperature, ℃	Operating conditions		
					Fuel reactor		Air reactor
					Ratio of fuel: metal oxide (by mass)	Inlet gas flow rate (L/min)	Inlet gas flow rate (L/min)
11.	HAC:Fe_2O_3	5 g HAC, 225 g Fe_2O_3	100	900	1:45	0.8 L/min - CO_2	0.8 L/min - Air
12.	HAC-RS:Fe_2O_3	5 g HAC, 225 g Fe_2O_3	100	900	1:45	0.8 L/min - CO_2	0.8 L/min - Air
13.	PCB	100g	50	900	-	0.8 L/min - $N_2/CO_2/O_2$	-
14.	HAC-OPCB	5 g HAC, 50-250 g OPCB	95	900	1:10, 1:20, 1:30, 1:40, 1:50	0.8 L/min - CO_2	0.8 L/min - Air
15.	LAC-OPCB	5 g HAC, 50-300 g OPCB	100	900	1:10, 1:20, 1:30, 1:60	0.8 L/min - CO_2	0.8 L/min - Air
16.	RS-OPCB	5 g RS, 50-200 g OPCB	80	900	1:10, 1:20, 1:30, 1:40	0.8 L/min - CO_2	0.8 L/min - Air
17.	HAC-RS-OPCB*	5 g HAC-RS, 225 g OPCB	85	900	1:45	0.8 L/min - CO_2	0.8 L/min - Air
18.	LAC-RS-OPCB	5 g LAC-RS, 225 g OPCB	95	900	1:50	0.8 L/min - CO_2	0.8 L/min - Air

3.4. Characterization techniques

3.4.1. Proximate analysis

The proximate analysis provides the percentage composition of moisture, volatile matter, inorganic residue (ash) and fixed carbon in the fuels. The moisture content (ASTM D 3173-03), volatile matter (ASTM-3175-07), ash content (ASTM-3174-04) in the solid fuels are evaluated as per the ASTM methods (Saydut et al., 2008).

3.4.2. Ultimate analysis

The ultimate analysis provides the elemental composition of carbon, hydrogen, nitrogen, sulphur and oxygen. The ASTM D 3176-09 method is followed for the analyses. This analysis is performed in Biotech Park, IIT Guwahati.

3.4.3. Bomb calorimeter

The gross calorific value (GCV) of the solid fuels is measured using a Bomb calorimeter as per the Indian standard (IS: 1359- 1959) method (Model: CC01/M3, Make: M/s Toshniwal Technologies Pvt. Ltd, India).

3.4.4. Brunauer-Emmett-Teller (BET) analysis

BET analysis estimates the surface area of the solid fuels (Model: TriStar II, Make: Micromeretics, USA). The samples are kept at 110 ˚C overnight to remove the moisture from the fuel surface. Nitrogen gas is used as the adsorbate for the analysis at 77 K. The surface area obtained from the analysis is expressed in m^2/g of solid.

3.4.5. X-ray diffraction (XRD)

XRD is used to identify the crystalline components present in the powdered sample (Model: Smartlab, Make: Rigaku Technologies, Japan). The formation of any complex compounds after the thermal process could be identified using XRD analysis. The reduction and oxidation pathways can be identified by this analysis. The interaction of

oxygen carriers with fuel ash could also be detected. The fuel samples are scanned with a step size of 0.03° with a 2Θ angle in the range of 10-80°. It is analyzed in the Central Instrumental Facilities (CIF) of IIT Guwahati.

3.4.6. X-ray fluorescence (XRF)

XRF analysis quantifies the metals in the OPCB and its respective oxides present in the oxidized e-waste. A 4g of powdered OPCB sample is mixed with boric acid (binding agent) and compressed into small discs. The pelletization is done by using the hydraulic press method (Bouraoui et al., 2015). It is analyzed in IIT Kharagpur (Model: Pan Analytical, Make: Axios FAST XRF spectrometer, Netherland).

3.4.7. Fourier transform infrared spectroscopy (FTIR)

Table 3.3. FTIR spectra bands of functional groups.

Functional groups	Wavenumber (cm^{-1})
O-H stretching	4000-3500
C-H aliphatic (aliphatic hydrocarbon)	3000-2800
C=O (aromatic ester)	1900-1650
C=C (aromatic hydrocarbon)	1500-1400
C-O (aromatic ester)	1200-1050
C-O-C (aromatic ether)	1270-820
Si-O-Al	900-670
Ca-O	525
Fe-Ca	1064
N-H	1695

The functional groups present in fuels and their respective ash samples are characterized by FTIR analysis. The IR spectrum is recorded in the range 4000-500 cm^{-1} by the KBr pellet method. The mass ratio of 1:100 (sample: KBr) is maintained for the analysis. Table 3.3 highlights the functional groups and their respective wavenumbers (Lin et al., 2019, Singh & Zondlo, 2017, Meng et al., 2014). It is analyzed in the Department of

Chemical Engineering, IIT Guwahati (Model: IRAffinity-1, Make: M/s Shimadzu, Japan).

3.4.8. Gas chromatography-mass spectrometer (GC-MS)

The tar composition is analyzed using a GC-MS under a helium atmosphere. A 200 mg of coal tar is dissolved in dichloromethane, and the solution is filtered using filter papers (100 nm pore size). About 1µL of the filtered solution is injected into the GC-MS for analysis. The injector temperature is set to 280℃. The oven temperature is held at 60℃ for 3 minutes. It is then increased to 320℃ at 5℃/min (Jiang et al., 2007, Morgan et al., 2008, Shi et al., 2010). It is analyzed in the Department of Chemical Engineering, IIT Guwahati (Model: 450-GC, 240-MS, Make: M/s Varian, Netherland).

3.4.9. Field emission scanning electron microscope (FESEM)

FESEM images (Model: Sigma 300, Make: M/s Zeiss, United Kingdom) provide the surface morphology of the solid fuels. The detailed information about sintering, agglomeration can be confirmed by this analysis. It has the ability to magnify 10x to 3,00,000x. The interaction of coal, biomass with oxygen carriers after the reduction process can be analyzed using FESEM images. This equipment is found in the Central Instrumental Facilities (CIF) of IIT Guwahati.

3.4.10. Gas chromatography (GC)

The gas chromatography technique is used to find the composition of the gas from the reactor outlet. Argon is used as the carrier gas for the analysis. A standard gas calibration chart is prepared to estimate the composition of the unknown samples. The standard gas canister is purchased from Chemix. Gas samples are analyzed using a gas chromatograph (Model: CP-3800; Make M/s Varian, Netherland).

3.4.11. Thermogravimetric analyser (TGA)

Thermo-gravimetric analysis (TGA) is conducted for the CLC and non-CLC process of the coal under non-isothermal conditions in the temperature range of 25-1000°C at a heating rate of 10°C/min under CO_2/N_2 atmosphere. Further, the reactivity of char (coal and rice straw) with oxygen carriers (Fe_2O_3, OPCB) are tested for estimating the solid-solid interaction under an inert atmosphere using a TGA (Model: TG 209 F1 Libra; Make M/s Netzsch, Germany).

3.4.11.1 Synergistic effect of coal and biomass

The synergistic effect of the coals (LAC, HAC) and biomass (RS) is assessed by comparing the estimated weight loss based on individual fuel behaviour in unblended conditions (theoretically) and the actual weight loss (W_{act}) under blended conditions (Equation 3.1) using a coal-biomass mixture of 1:1 ratio by weight. The theoretical weight loss (W_{theo}) is predicted by using the individual weight loss of coal and RS estimated under the unblended condition and is given as,

$$W_{theo} = x_1 W_1 + x_2 W_2 \quad (3.1)$$

x_i denotes the mass fraction of each component (0.5 for each case); W_i is the weight loss of individual fuels in unblended conditions. The difference in weight loss between W_{theo} and W_{act} indicates a measure of synergistic effect on the co-blending of coal and RS.

3.4.11.2. Kinetic studies using TGA Data

The activation energy is estimated using different models such as the reaction order model and shrinking core model (SCM). The Coats-Redfern method is used for fitting the various models considered to determine the thermo-kinetic parameters. Table 3.4 describes the different reaction models, such as the shrinking core model and volumetric

models to determine the activation energy. The integral form of the Coats–Redfern equation is as follows,

$$\ln\left[\frac{G(\alpha)}{T^2}\right] = \ln\left[\frac{AR}{\beta E}\right] - \frac{E}{RT} \quad (3.2)$$

Where G(α) is the integral form, T is the absolute temperature in K, E is the activation energy, β is the heating rate (10 K/min), A is the pre-exponential factor. The activation energy is obtained by plotting ln $(G(\alpha)/T^2)$ and 1/T and the slope of the straight line gives the value of E/R.

Table 3.4. Different reaction models for the estimation of kinetic parameters.

Model	Integral form G (α)
Shrinking core model (SCM)	
Contracting volume	$1-(1-\alpha)^{1/3}$
Reaction models	
First order	$-ln(1-\alpha)$
Second order	$(1-\alpha)^{-1}-1$
Third order	$[(1-\alpha)^{-2}-1]/2$

The pre-exponential factor (A) and activation energy (E) can be calculated with the plot of ln $(G(\alpha)/T^2)$ versus 1/T. These values are calculated at three different temperature intervals in the range of 350-600°C for volatiles reactivity, 600-800°C for higher hydrocarbon reactivity and 800-1000°C for char reactivity.

3.5. Data evaluation

The fuel reactor performance is analyzed by three key parameters such as (a) CO_2 yield (η_{CO_2}), (b) gas conversion (η_{gc}) and (c) char conversion (X_{char}). H_2, CO, CH_4 and CO_2 are the main gases detected at the reactor outlet.

3.5.1. CO_2 yield

CO_2 yield is defined as the degree of conversion of carbonaceous gas into CO_2 in the FR (Adánez et al., 2018, Wang et al., 2016, Kolbitsch et al., 2010). The carbon in the coal exists either in the form of volatiles or fixed carbon in char. It denotes the amount of CO_2 produced during the CLC process. It is the ratio of CO_2 to the unconverted gases at the reactor outlet. Higher the CO_2 production, higher the efficiency of the CLC process.

$$\eta_{CO_2} = \frac{F_{CO_{2_{out}}} - F_{CO_{2_{in}}}}{F_{CO_{2_{out}}} + F_{CO} + F_{CH_4} - F_{CO_{2_{in}}}} \tag{3.3}$$

3.5.2. Syngas conversion

The syngas conversion (Eq. 3.4) provides the degree of reactivity between the syngas generated in FR and the metal oxides. The second term of Eq. (3.4) is the oxygen demand, which is defined as the ratio of oxygen required for the complete oxidation of the unconverted carbonaceous gases at the FR exit to the total amount of carbon at the reactor outlet. It denotes the total amount of oxygen needed by the volatiles and the gasified products and this is supplied by the oxygen carrier. Higher the gas conversion, lower is the unconverted gases at the fuel reactor outlet. (Linderholm et al., 2016, Xiao et al., 2012).

$$\eta_{gc} = 1 - \frac{0.5F_{CO} + 0.5F_{H_2} + 2F_{CH_4}}{F_{CO_{2_{out}}} + F_{CO} + F_{CH_4} - F_{CO_{2_{in}}}} \tag{3.4}$$

'F' is the molar flow rate of individual species evolved during the pyrolysis reaction.

3.5.3. Char conversion

The char conversion (X_{char}) in the FR is estimated by using Eq. 3.5. In order to estimate the char conversion, it is essential to estimate the unreacted fixed carbon left in the CLC process (Adánez et al., 2018). Hence, the solid residue obtained from the FR is burnt in the reactor using air (AR) at 900°C. The resultant CO_2 gas is a measure of the quantity of fixed carbon in the residue.

$$X_{char} = \frac{f_{C,fix} \cdot m_{fuel} - M_C F_{CO_2,AR} \cdot t}{f_{C,fix} \cdot m_{fuel}} \quad (3.5)$$

Where $f_{C,fix}$ is the weight fraction of fixed carbon in the fuel; m_{fuel} is the initial mass of the fuel taken for the CLC process; M_C is the molecular weight of carbon; $F_{CO_2,AR}$ is the average molar flow rate of CO_2 gas at the exit during the run hour 't'.

3.6. CLC based power plant simulation using Aspen plus

In the present study, the energy and techno-economic analysis for the CLC integrated gasification combined cycle (IGCC) power plant are performed using Indian coals with RS under co-combustion conditions. The basic operating parameters such as operating pressure, temperature, mass flow rate of solid feed and metal oxides used in the Aspen plus simulation are listed in Table 3.5. The CLC reactors are operated at 30 bar with 900°C/1000°C in the fuel reactor/air reactor, respectively. Steam turbines are operated at different pressures of 170.5 bar, 83.3 bar and 17.7 bar. The mass flow rates of the fuel used are estimated based on their total heating values with a basis of 150 MW. LAC, HAC and RS mass flow rates to the fuel reactor are found as 4.57 kg/s, 6.78 kg/s and 8.52 kg/s, respectively. The coals and biomass (RS) are the non-conventional components and are decomposed in a RYield reactor. These components are transferred to an RGibbs reactor, which estimates their product composition based on the minimum Gibbs free

energy of each component. In this model, a counter-current MHeatX module is used for simulating the heat recovery steam generator (HRSG).

Table 3.5. Design specifications of the various components in the CLC based power system.

Unit	Description
Fuel	Mass flow rate: LAC - 4.57 kg/s; HAC - 6.78 kg/s; RS - 8.52 kg/s. Inlet temperature: 25°C, Inlet pressure: 1bar
Oxygen carriers	Oxidized e-waste, Fe_2O_3, CuO
Air	21% O_2 and 79% N_2 on volume basis Inlet temperature: 25°C, Inlet pressure: 1bar
Chemical looping combustion unit	Fuel reactor: 900 °C/ 30 bar Air reactor: 1000 °C/ 30 bar
Desulfurization unit	H_2S removal >99%
Steam turbine and HRSG	Three pressure levels (High Pressure/Medium Pressure/Low Pressure): 170.5 bar/83.3 bar/17.7 bar Reheat temperature: 540°C Condenser pressure: 0.045 bar Isentropic efficiency: 0.88 Mechanical efficiency: 0.99
CO_2 compression and drying	Delivery pressure: 110 bar Compressor efficiency: 0.88
Compressor/ gas turbine/ pump	Isentropic efficiency: 0.88 Mechanical efficiency: 0.99

3.6.1. Process configuration

A general conceptual schematic of the CLC process using coal/biomass as solid fuels and OPCB as oxygen carriers is shown in Figure 3.3. The methodology proposed by Mukherjee et al. (2015) is followed in this power plant study. Conventional gasifiers are

usually operated at high temperature (1300°C-1600°C) and high pressure (30-35 bar) (Chen et al., 2015, Mun et al., 2016). Álvaro et al. (2015) observed the optimum pressure of 20 bar for syngas based CLC operation. Retrofitting conventional gasifier with CLC fuel reactor will reduce the plant installation cost, thereby reducing the plant operation cost. Thus, high operating pressure was chosen for the simulation study. The major components of the process flow sheeting are CLC reactors (fuel reactor and air reactor), turbines, compressors, heat exchangers, heat recovery steam generator (HRSG), carbon capture and storage unit (CCS). The operating parameters of steam turbines are taken from the studies of Prabu (2015). The e-waste base metal oxide is mainly a mixture of CuO, Fe_2O_3 and NiO along with the trace amount of other oxides. The solid fuels are directly introduced into the FR along with the oxygen carriers. CO_2 is used as the gasifying agent for char gasification in the FR. A portion of the CO_2 gas stream from the carbon capture and storage unit (CCS) is recycled into the FR. The hot flue gas from the FR is sent to the HRSG unit to recover the heat in the form of steam. The flue gas is then sent to a desulphurization unit to convert the released H_2S into ZnS by reacting with zinc titanate as shown in the following reactions (3.6-3.7).

$$ZnTiO_3 + H_2S \rightarrow ZnS + H_2O + TiO_2 \quad (3.6)$$

$$2ZnS + 3O_2 \rightarrow 2ZnO + SO_2 \quad (3.7)$$

Finally, the gas stream is enriched with CO_2 and H_2O with a trace amount of other gases. After the removal of water from the flue gas, the stream is directly sent to the multi-stage CO_2 compression unit to compress the gas to 110 bar for storage.

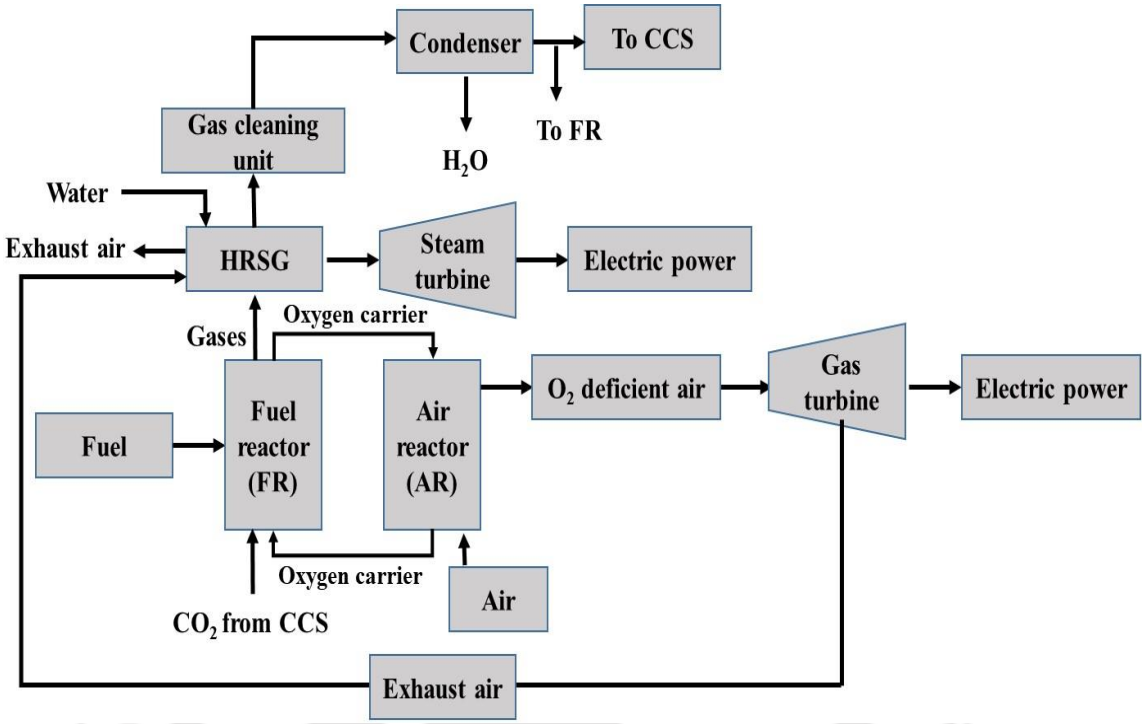

Figure 3.3. Conceptual diagram of the direct coal fuelled CLC based combined cycle power plants (CCS: Carbon capture and storage; HRSG: Heat Recovery Steam Generator).

The following assumptions are considered in the power plant simulation:

- The property method chosen for the gas-solid modelling is Peng-Robinson cubic equation of state with Boston-Mathias alpha function (Zhu et al., 2016, Jiang et al., 2019).
- The simulations are operated in a steady state.
- HCOALGEN and COALIGT property models are used to estimate the enthalpies and densities respectively (Mohamed et al., 2020).
- Solid fuels and their ash are assigned to the unconventional category, while the oxygen carriers are selected as solid type materials.
- OPCB is a mixed oxygen carrier and the trace quantity of resins and carbon residue are ignored.

- Pump, compressors, turbines have isentropic efficiency of 0.88 and mechanical efficiency of 0.99 (Prabu, 2015).
- Negligible char left in the air reactor (AR).
- Ash is considered as a non-reactive component.
- Negligible heat loss and pressure drop in the reactors.

3.6.2. Gross and net electricity power calculation

The gross efficiency (η_{gross}) of power plants is calculated from the following equation,

$$\eta_{gross} = \frac{P_{gross}}{\dot{m}_{fuel} \times HHV_{fuel}} \times 100\% \quad (3.8)$$

P_{gross} is the gross power produced (MW), $\dot{m}_{fuel}$ is the mass flow rate of fuel (kg/s), HHV is the calorific value of the feed (MJ/kg).

The net electric power produced (P_{net}) is estimated as,

$$P_{net} = (P_{GT} + P_{ST}) - (P_{CCS} + P_{FWP} + P_{ACU}) \quad (3.9)$$

P_{GT}, P_{ST} are the electric power generated from gas and steam turbines (MW), respectively. P_{CCS}, P_{FWP} and P_{ACU} are the electric power consumed in the CO_2 compression, feed water pump and air compressor units (MW), respectively.

The net efficiency of the power plants (η_{net}) is estimated from the following equation,

$$\eta_{net} = \frac{P_{net}}{\dot{m}_{fuel} \times HHV_{fuel}} \times 100\% \quad (3.10)$$

3.6.3. Techno-economic analysis of the power plants

The cost of fuels and metal oxides considered in the present study for economic analysis is shown in Table 3.6. The levelized cost of electricity (LCOE) is evaluated for each case

of the power plants using different fuels and metal oxides. LCOE estimation includes the power plant capital cost, fuel cost, operation and maintenance cost, storage cost, etc. LCOE is calculated by the following Eq. (3.11-3.15).

Table 3.6. Basic parameters considered in the economic analysis.

Components	Price	References
Low ash coal (LAC)	Rs 3288/ton	Mishra et al. (2019)
High ash coal (HAC)	Rs 1757/ton	Mishra et al. (2019)
Rice straw (RS)	Rs 1840/ton	Hiloidhari et al. (2012)
Fe_2O_3	55 $/ton	Khan & Shamim (2021)
CuO	5000 $/ton	Zhou et al. (2015)
Owners cost	0.15×total installed cost	Mishra et al. (2019)
Land purchase, surveying etc.	0.05×total installed cost	Mishra et al. (2019)
Ash disposal	11.3$/ton	Tang & You (2018)
Annual discount rate	7%	Tang & You (2018)
Plant life	25 years for coal 20 years for RS	Cormos (2012) Al-Qayim et al. (2015)

$$\text{LCOE} = \frac{\text{Annual capital cost (ACC)} + \text{Total operating \& maintenance cost}}{\text{Net electricity produced}} \quad (3.11)$$

$$\text{ACC} = \text{Total capital cost (TC)} \times \text{capital recovery factor (CRF)} \quad (3.12)$$

$$\text{CRF} = \frac{r(1+r)^t}{(1+r)^t - 1} \quad (3.13)$$

$$C_E = C_B \times \left(\frac{Q}{Q_B}\right)^M \quad (3.14)$$

$$\text{Specific capital investment (gross/ net)} = \frac{\text{Total invested cost}}{\text{Power output (gross/ net)}} \quad (3.15)$$

The equipment cost (CLC reactors, turbines) are calculated by Eq. (3.14). C_B and Q_B are the cost and capacity of a known equipment, while C_E and Q_E are the corresponding values to be estimated for the required equipment in the present study (Khallaghi et al., 2020). M is the scaling factor ranging from 0.6 to 0.7 (Khallaghi et al., 2020, Zhou et al., 2015). The plant life for the CLC process using coal is assumed to be 25 years, while for biomass, it is assumed to be 20 years due to fouling, slagging and corrosion issues (Zang et al., 2018).

References

Adánez, J., Abad, A., Mendiara, T., Gayán, P., de Diego, L. F., & García-Labiano, F. (2018). Chemical looping combustion of solid fuels. *Progress in Energy and Combustion Science*, *65*, 6–66.

Al-Qayim, K., Nimmo, W., & Pourkashanian, M. (2015). Comparative techno-economic assessment of biomass and coal with CCS technologies in a pulverized combustion power plant in the United Kingdom. *International Journal of Greenhouse Gas Control*, *43*, 82–92.

Berguerand, N., & Lyngfelt, A. (2010). Batch testing of solid fuels with ilmenite in a 10 kW_{th} chemical-looping combustor. *Fuel*, *89*(8), 1749–1762.

Bouraoui, Z., Jeguirim, M., Guizani, C., Limousy, L., Dupont, C., & Gadiou, R. (2015). Thermogravimetric study on the influence of structural, textural and chemical properties of biomass chars on CO_2 gasification reactivity. *Energy*, *88*, 703–710.

Chen, S., Lior, N., & Xiang, W. (2015). Coal gasification integration with solid oxide fuel cell and chemical looping combustion for high-efficiency power generation with inherent CO_2 capture. *Applied Energy*, *146*, 298–312.

Cormos, C. (2012). Evaluation of syngas-based chemical looping applications for hydrogen and power co-generation with CCS. *International Journal of Hydrogen Energy*, *37*, 13371–13386.

Feng, Y., Wang, N., Guo, X., & Zhang, S. (2020). Dopant screening of modified Fe_2O_3 oxygen carriers in chemical looping hydrogen production. *Fuel*, *262*, 116489.

Ge, H., Guo, W., Shen, L., Song, T., & Xiao, J. (2016). Biomass gasification using chemical looping in a $25kW_{th}$ reactor with natural hematite as oxygen carrier. *Chemical Engineering Journal*, *286*, 174–183.

Hiloidhari, M., Baruah, D., Mahilary, H., Baruah, D. C., & Camellia, L. (2012). GIS based assessment of rice (Oryza sativa) straw biomass as an alternative fuel for tea (Camellia sinensis L.) drying in Sonitpur district of Assam , India. *Biomass and Bioenergy*, *4*, 160–167.

Jiang, J., Wang, Q., Yingyu, W., Tong, W., & Xiao, B. (2007). GC/MS analysis of coal tar composition produced from coal pyrolysis. *Bulletin of the Chemical Society of Ethiopia*, *21*(2), 229–240.

Jiang, P., Berrouk, A. S., & Dara, S. (2019). Biomass Gasification Integrated with Chemical Looping System for Hydrogen and Power. Coproduction Process – Thermodynamic and Techno-Economic Assessment. *Chemical Engineering and Technology*, *42*, 1153–1168.

Jie, G., Ying-shun, L., & Mai-xi, L. (2008). Product characterization of waste printed circuit board by pyrolysis. *Journal of Analytical and Applied Pyrolysis*, *83*, 185–189.

Jiménez Álvaro, Á., López Paniagua, I., González Fernández, C., Rodríguez Martín, J.,

& Nieto Carlier, R. (2015). Simulation of an integrated gasification combined cycle with chemical looping combustion and carbon dioxide sequestration. *Energy Conversion and Management*, *104*, 170–179.

Khallaghi, N., Hanak, D. P., & Manovic, V. (2020). Techno-economic evaluation of near-zero CO_2 emission gas-fired power generation technologies: A review. *Journal of Natural Gas Science and Engineering*, *74*, 103095.

Khan, M. N., & Shamim, T. (2021). Techno-economic assessment of a plant based on a three reactor chemical looping reforming system. *International Journal of Hydrogen Energy*, *41*, 22677–22688.

Li, J., Duan, H., Yu, K., Liu, L., & Wang, S. (2010). Characteristic of low-temperature pyrolysis of printed circuit boards subjected to various atmosphere. *Resources, Conservation and Recycling*, *54*, 810–815.

Lin, B., Zhou, J., Qin, Q., Song, X., & Luo, Z. (2019). Thermal behavior and gas evolution characteristics during co-pyrolysis of lignocellulosic biomass and coal: A TG-FTIR investigation. *Journal of Analytical and Applied Pyrolysis*, *144*, 104718.

Meng, F., Yu, J., Tahmasebi, A., Han, Y., Zhao, H., Lucas, J., & Wall, T. (2014). Characteristics of chars from low-temperature pyrolysis of lignite. *Energy and Fuels*, *28*, 275–284.

Mishra, N., Bhui, B., & Vairakannu, P. (2019). Comparative evaluation of performance of high and low ash coal fuelled chemical looping combustion integrated combined cycle power generating systems. *Energy*, *169*, 305–318.

Mohamed, U., Zhao, Y., Huang, Y., Cui, Y., Shi, L., Li, C., Pourkashanian, M., Wei, G., Yi, Q., & Nimmo, W. (2020). Sustainability evaluation of biomass direct

gasification using chemical looping technology for power generation with and w/o CO_2 capture. *Energy*, *205*, 117904.

Morgan, T. J., George, A., Álvarez, P., Millan, M., Herod, A. A., & Kandiyoti, R. (2008). Characterization of molecular mass ranges of two coal tar distillate fractions (creosote and anthracene oils) and aromatic standards by LD-MS, GC-MS, probe-MS and size-exclusion chromatography. *Energy and Fuels*, *22*, 3275–3292.

Mukherjee, S., Kumar, P., Yang, A., & Fennell, P. (2015). Energy and exergy analysis of chemical looping combustion technology and comparison with pre-combustion and oxy-fuel combustion technologies for CO_2 capture. *Journal of Environmental Chemical Engineering*, *3*, 2104–2114.

Mun, T. Y., Tumsa, T. Z., Lee, U., & Yang, W. (2016). Performance evaluation of co-firing various kinds of biomass with low rank coals in a 500 MW_{th} coal-fired power plant. *Energy*, *115*, 954–962.

Ni, J., Zhou, Z., Yu, G., Liang, Q., & Wang, F. (2010). Molten slag flow and phase transformation behaviors in a slagging entrained-flow coal gasifier. *Industrial and Engineering Chemistry Research*, *49*, 12302–12310.

Prabu, V. (2015). Integration of in-situ CO_2 -oxy coal gasification with advanced power generating systems performing in a chemical looping approach of clean combustion. *Applied Energy*, *140*, 1–13.

Saydut, A., Duz, M. Z., Tonbul, Y., Baysal, A., & Hamamci, C. (2008). Separation of liquid fractions obtained from flash pyrolysis of asphaltite. *Journal of Analytical and Applied Pyrolysis*, *81*, 95–99.

Shi, Q., Yan, Y., Wu, X., Li, S., Chung, K. H., Zhao, S., & Xu, C. (2010). Identification

of dihydroxy aromatic compounds in a low-temperature pyrolysis coal tar by gas chromatography-mass spectrometry (GC-MS) and Fourier transform ion cyclotron resonance mass spectrometry (FT-ICR MS). *Energy and Fuels*, *24*(10), 5533–5538.

Singh, K., & Zondlo, J. (2017). Characterization of fuel properties for coal and torrefied biomass mixtures. *Journal of the Energy Institute*, *90*, 505–512.

Tang, Y., & You, F. (2018). Life cycle environmental and economic analysis of pulverized coal oxy-fuel combustion combining with calcium looping process or chemical looping air separation. *Journal of Cleaner Production*, *181*, 271–292.

Zang, G., Jia, J., Tejasvi, S., Ratner, A., & Silva, E. (2018). Techno-economic comparative analysis of biomass integrated gasification combined cycles with and without CO_2 capture. *International Journal of Greenhouse Gas Control*, *78*, 73–84.

Zhou, C., Shah, K., & Moghtaderi, B. (2015). Techno-economic assessment of integrated chemical looping air separation for oxy-fuel combustion : An Australian case study. *Energy & Fuels*, *29*, 2074–2088.

Zhu, L., Wang, F., & Zhang, Z. (2016). Thermodynamic evaluation of a conceptual process for coal gasification coupled with chemical looping air separation. *Chemical Engineering and Processing: Process Intensification*, *106*, 33–41.

CHAPTER 4

Experimental Studies on Chemical Looping Combustion of Coals with Rice Straw using Fe_2O_3 as the Oxygen Carrier

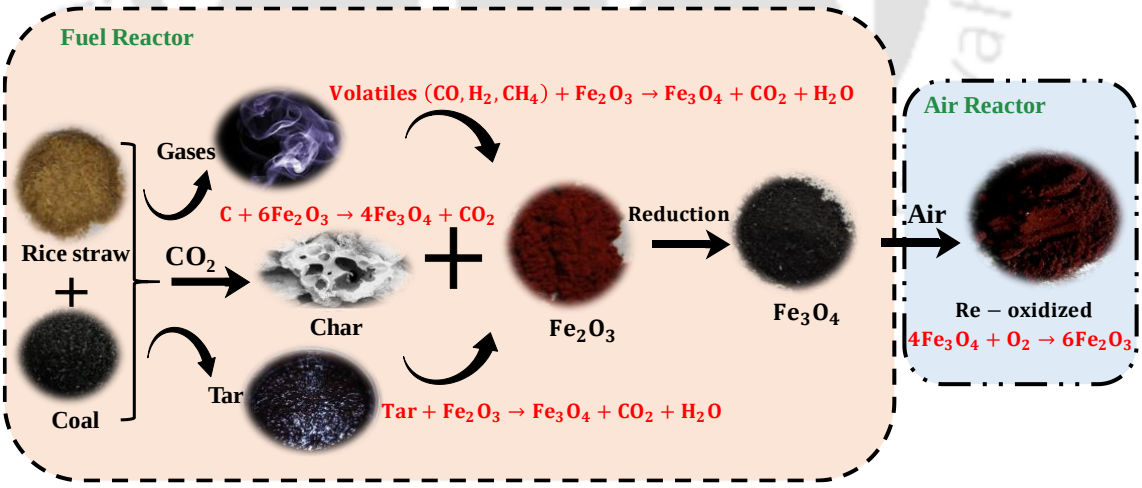

CHAPTER 4

EXPERIMENTAL STUDIES ON CHEMICAL LOOPING COMBUSTION OF COALS WITH RICE STRAW USING Fe_2O_3 AS THE OXYGEN CARRIER

The present work assesses the feasibility of co-utilization of coal and biomass (rice straw) in the chemical looping combustion (CLC) process using pure Fe_2O_3 as the oxygen carrier. The overall performance of the CLC process is evaluated by estimating the key parameters such as syngas conversion, CO_2 yield, and char conversion. The intrinsic reactivity of char and volatile matter of the solid fuels with Fe_2O_3 is assessed individually using TGA by evaluating the activation energy.

The present chapter evaluates the CLC performance of Fe_2O_3 using Indian coals (LAC, HAC) and biomass (rice straw) under CO_2 and air atmosphere for the reduction and oxidation process. This chapter is categorized into two sub-sections viz. Chapter 4A and Chapter 4B. Chapter 4A explains the interaction of low ash Indian coal and rice straw with Fe_2O_3, while Chapter 4B describes the findings of the co-CLC process using high ash Indian coal and rice straw with Fe_2O_3 under the CO_2 atmosphere.

CHAPTER 4A

EXPERIMENTAL STUDIES OF LAC, RS AND THEIR BLEND USING Fe_2O_3 AS THE OXYGEN CARRIER

4.1. Experimental details

The set of experiments conducted using LAC fuel are discussed in Table 4.1. The product gas obtained during pyrolysis and gasification of LAC and RS in an inert and reactive atmosphere is analyzed (Exp. 1, Exp. 2, Exp. 3, Exp. 4). Further, the CLC reactivity is investigated using LAC, RS and their blend with pure Fe_2O_3 oxygen carrier in isothermal mode (900°C).

Table 4.1. Experimental details of assessing LAC, RS and their blend based fuels in a fixed bed reactor.

Case	Fuels	Operating conditions	
		Fuel reactor (Temperature, Flow, Fuel: Fe_2O_3)	Air reactor
Expt. 1	LAC	350-950°C, 0.3 LPM-N_2	-
Expt. 2	LAC	350-1000°C, 0.3 LPM-CO_2	-
Expt. 3	RS	350-1000°C, 0.3 LPM-CO_2	-
Expt. 4	LAC-RS	350-1000°C, 0.3 LPM-CO_2	-
Expt. 5	LAC	900°C, 0.8 LPM-CO_2, 1:65	900°C, 0.8 LPM-Air
Expt. 6	RS	900°C, 0.8 LPM-CO_2, 1:40	900°C, 0.8 LPM-Air
Expt. 7	LAC-RS	900°C, 0.8 LPM-CO_2, 1:55	900°C, 0.8 LPM-Air

The operating temperature is fixed as per the studies of Wang et al. (2017), Ma et al. (2018) and Pérez-Vega et al. (2020). They concluded that with an increase in the operating temperature, the CLC performance increases. Moreover, higher oxidation temperature promotes higher thermal plant efficiency due to higher turbine inlet temperature. The LAC is mixed with Fe_2O_3 in a stoichiometric ratio of 1:65, while RS is

mixed at 1:40 mass ratio. As the LAC and RS are mixed in equal mass ratios (1:1), 1:55 ratio is maintained for LAC-RS blend fuels. CO_2 is used as the gasifying agent for the in-situ gasification of solid fuels.

4.2. Results and discussion

4.2.1. LAC pyrolysis (Expt. 1)

The pyrolysis of LAC under nitrogen atmosphere shows a significant production of H_2, CO, CH_4 gases and a small proportion of other hydrocarbons due to the release of volatiles and tar thermal cracking reactions (Figure 4.1). The pyrolysis gases started evolving after 300°C. A sustained gas stream with the production of valuable calorific gases can be noted. Hydrogen and methane gas are estimated with the highest concentrations of 25% and 12% by volume, respectively. The average outlet gas concentrations are found to be 12.2% H_2, 6.2% CO and 6.8% CH_4. The liberation of C_2H_4, C_2H_6 (0-5%) is mainly due to the tar cracking reactions.

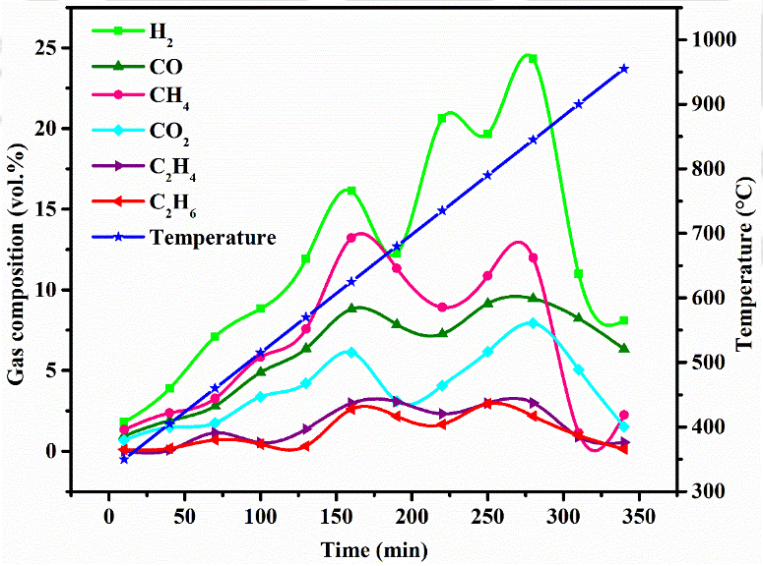

Figure 4.1. Gas composition obtained during the pyrolysis of LAC (on N_2 free basis).

4.2.2. CO_2 gasification of LAC, RS and their blend (Expt. 2, Expt. 3, Expt. 4)

The release of volatiles from LAC and RS is initiated at 350°C as seen in the earlier case (Expt. 1). Figure 4.2 shows the composition of the gaseous products obtained from LAC, RS and their blend during the CO_2 gasification. The results indicate the temperature has a significant effect on the progress of the gasification process.

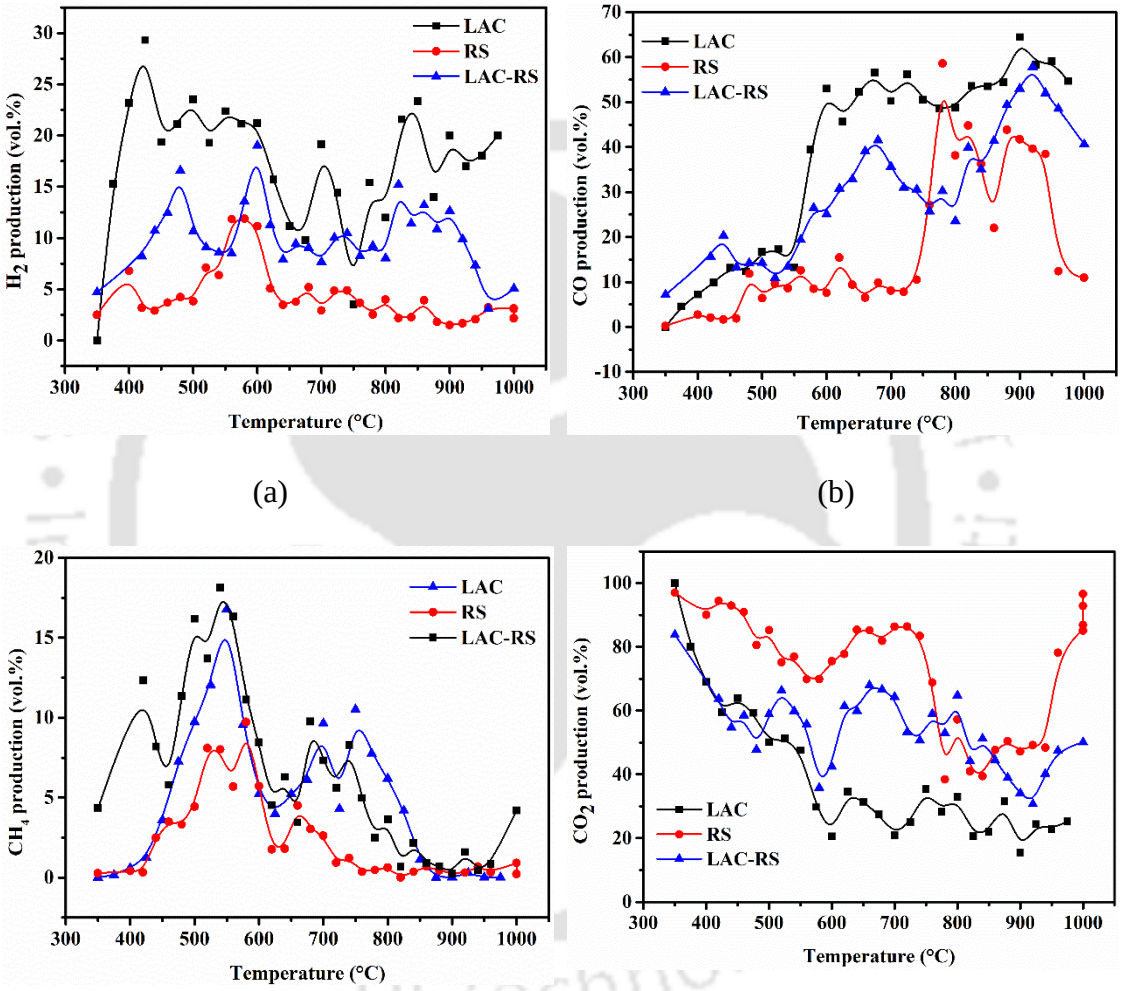

Figure 4.2. Comparison of outlet gas composition of (a) H_2, (b) CO, (c) CH_4 and (d) CO_2 during the CO_2 gasification of LAC, RS and their blend in CO_2 atmosphere.

The governing reactions are water-gas shift reaction (Eq. 4.1), methanation (Eq. 4.2), dry reforming reaction (Eq. 4.3), and Boudouard reaction (Eq. 4.4). The H_2 gas is generated between 500-650°C during RS gasification, while it is released into two distinct regions

for LAC i.e. 350-600℃ and 750-900℃. This resulted in an increase in the average H_2 concentration for LAC (17.3%), compared to RS (4.8%). Due to the cracking and reforming reaction, CH_4 concentration is obtained in the range of 3-8% in all three fuels. The Boudouard reaction plays a key role in the generation of CO (Reaction 4.4) at temperatures above 700°C. Both LAC and RS follow the same trend showing 40-60% of CO release at 750-950℃. It can be noticed the production of high quantity of CO gas of about 40-60% by volume at temperatures above 600°C. Figure 4.3 shows the calorific value of the product gas obtained under the CO_2 atmosphere. It can be observed that the calorific value of LAC syngas is found in the range of 8-10 MJ/Nm^3, while RS produced the syngas with 4-6 MJ/Nm^3. Mixing LAC and RS produced syngas with a calorific value in the range of 6-8 MJ/Nm^3. Thus, utilizing a blend of LAC-RS produces higher quality syngas than RS alone.

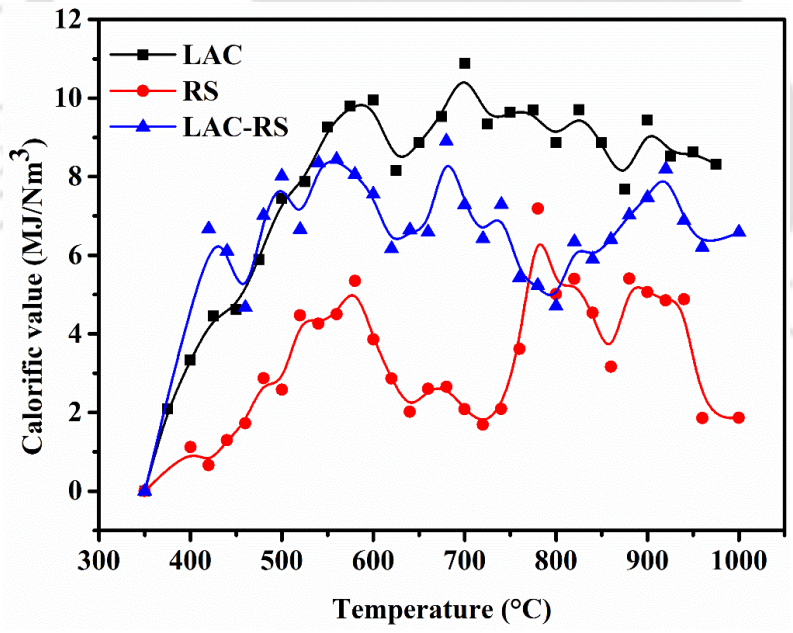

Figure 4.3. Calorific value of the product gas obtained during the CO_2 gasification of LAC, RS and their blend.

$$CO + H_2O \rightarrow CO_2 + 2H_2 \quad (4.1)$$

$$C + 2H_2 \rightarrow CH_4 \quad (4.2)$$

$$CH_4 + CO_2 \rightarrow 2CO + 2H_2 \quad (4.3)$$

$$C + CO_2 \rightarrow 2CO \quad (4.4)$$

$$^1/_2\, C_2H_6 + CO_2 \rightarrow 2CO + {}^3/_2\, H_2 \quad (4.5)$$

4.2.3. CLC reactivity of LAC and RS with Fe_2O_3 (Expt. 5 and Exp. 6)

The CLC of fuels are conducted in isothermal mode at 900°C. Figure 4.4 shows the profile of the gas composition obtained under the CO_2 atmosphere using LAC and RS in the presence of Fe_2O_3. The in-situ gasification of direct solid fuelled CLC involves three successive reactions. Firstly, the LAC/RS is converted into gaseous species, and then those gas components interact with Fe_2O_3 for metal-oxy fuel combustion (Eq. 1.1-1.7). Thirdly, a fraction of coal particles can directly react with metal oxide and may get partially/fully oxidized into gas (Eq. 1.8). Figure 4.4(a) shows the gas composition obtained during LAC based CLC process, while the RS based CLC gas composition is shown in Figure 4.4(b). The unconverted gases are found within the range of 10%. On an average, the unconverted H_2 and CO gas are found to be 0.4% and 4.1% for LAC- Fe_2O_3, respectively. Due to higher reactivity of rice straw than LAC, the average unreacted gases are found less around 0.3% H_2 and 3.6% CO. The liberation of CH_4 and higher hydrocarbons are found to be negligible for both the cases.

The reduced metal oxides obtained from the in-situ gasification CLC experiment are used for the re-oxidation process. The oxidation of the reduced metal particles is carried out at 900°C using atmospheric air at 0.8 litre per minute (LPM). Figures 4.4(c) and 4.4(d) show the gas composition at the outlet of the air reactor during the oxidation reaction for LAC and RS, respectively. The product gases mainly consist of CO_2 and air with negligible CO and CH_4. A 5-10% CO_2 is noticed along with the oxygen depleted air. This is due to

the combustion of deposited carbon/unconverted char during the CLC. Based on the quantity of CO_2 release during the oxidation reaction, the char conversion is evaluated by using Eq. (3.5). The oxidation of reduced Fe_2O_3 particles is performed for 85 minutes to achieve complete oxidation.

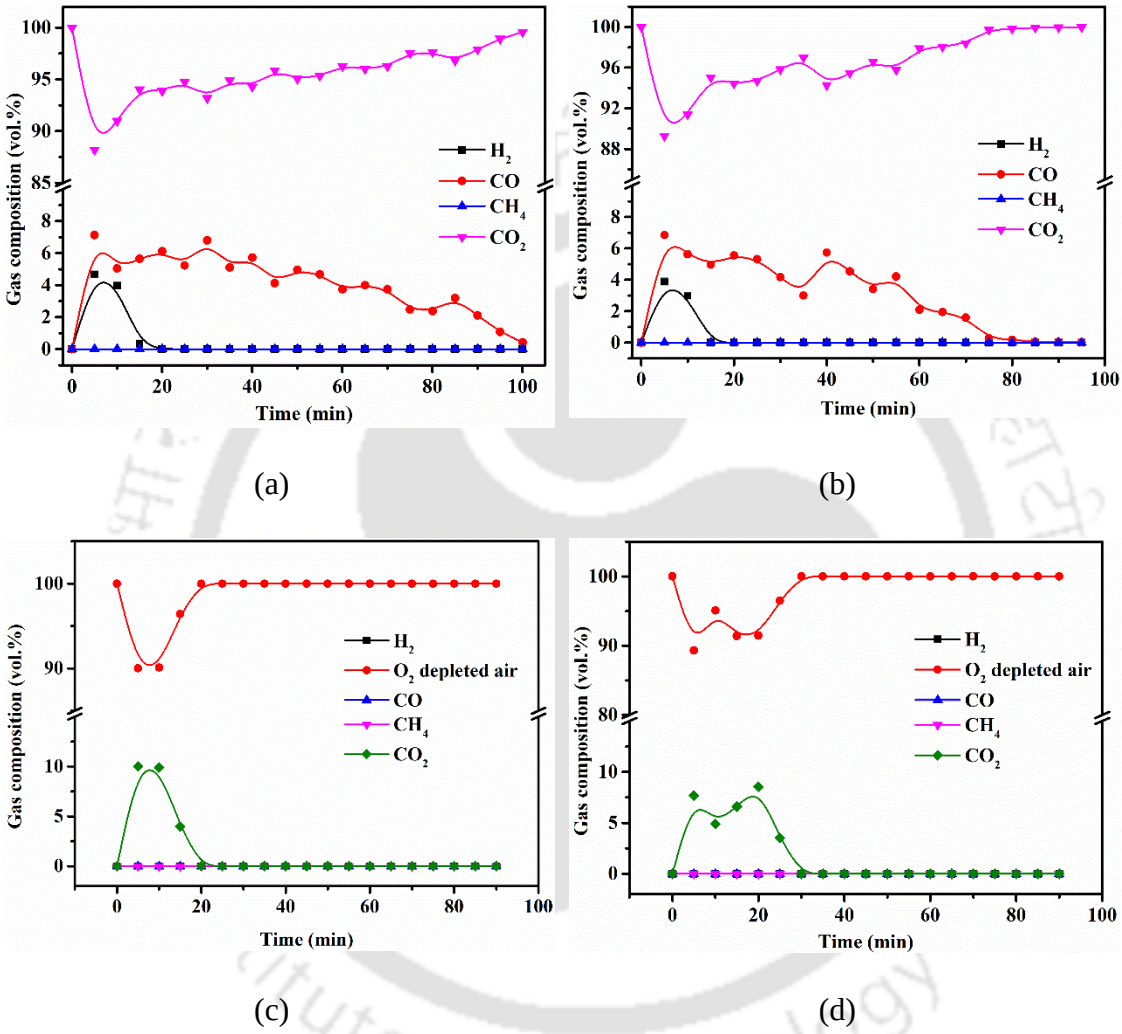

Figure 4.4. Gas composition obtained during (a) CLC of LAC-Fe_2O_3, (b) CLC of RS-Fe_2O_3, (c) oxidation of LAC-Fe_2O_3 based residue and (d) oxidation of RS-Fe_2O_3 based residue.

4.2.4. CLC reactivity during co-gasification of LAC and RS with Fe_2O_3 (Expt. 7)

Figure 4.5 shows the gas composition obtained using the blend of LAC-RS mixed at 1:1 ratio. The unconverted gases are found in the range of 0.1% H_2 and 3.5% CO. The LAC-

RS blend reduced the unconverted CO by 11.9%, compared to LAC at unblended conditions. Hence, the co-utilization of LAC and RS proved to be beneficial when compared to coal alone as the feedstock.

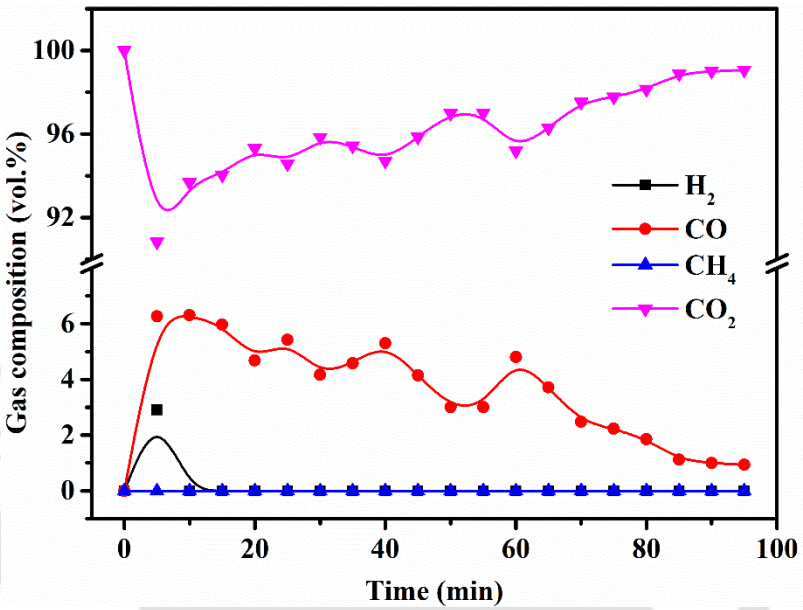

Figure 4.5. Gas composition obtained during the CLC of LAC-RS with Fe_2O_3 under CO_2 atmosphere.

4.2.5. Determination of gas conversion, CO_2 yield and char conversion

The gas conversion, CO_2 yield and char conversion are calculated for the conducted experiments under the CLC mode of operation and displayed in Figure 4.6. The extent of LAC and RS conversion into CO_2 is quantified by the CO_2 yield (Eq. 3.4). The average CO_2 yield and gas conversion are found to be 85.8% and 89.1% for LAC-Fe_2O_3, respectively, due to the reactivity of Fe_2O_3 with the volatile matters and char. Similarly, the CO_2 yield and gas conversion for RS-Fe_2O_3 are 89.6% and 92.4%, respectively. High gas conversion indicates the minimum amount of unconverted gases (H_2, CO, CH_4) at the fuel reactor (FR) outlet. Under the co-CLC conditions, the average CO_2 yield has increased to 88.1%, and the gas conversion has reached as high as 91.3%. The char conversion in FR (evaluated using Eq. (3.5)) is estimated as 90.9% for LAC-Fe_2O_3 and

93.5% for RS-Fe_2O_3. Higher char conversion resulted in higher CO_2 yield. The blending of LAC and RS improved the char conversion by 2%.

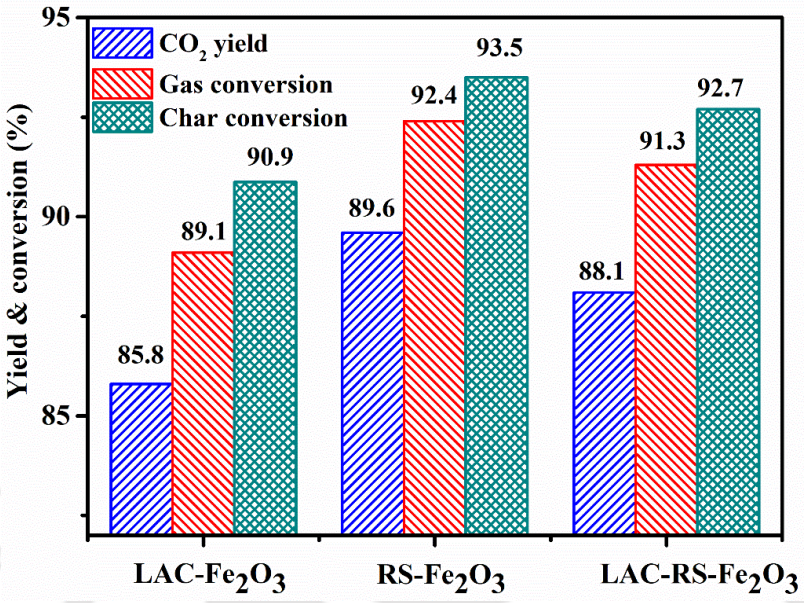

Figure 4.6. Comparison of gas conversion, char conversion and CO_2 yield under blended and unblended conditions of LAC-RS (Expt. 5, Expt. 6, Expt. 7).

4.2.6. Post characterization of the non-CLC and CLC residue

4.2.6.1. FTIR analysis of raw LAC, char and tar

The char and the tar obtained during the N_2 pyrolysis experiment (Expt. 1) are used for the FTIR spectra analysis. Figure 4.7 shows the comparison of the spectra of raw coal, char and tar. The spectra of raw coal show the presence of aliphatic, aromatic, phenol and silica groups while in the case of char, only weaker functional groups with low intensity of OH are observed along with C. The C-C functional group present in the raw coal is not detected in tar and char samples due to the conversion of these groups into CO_2, CO and CH_4 as volatiles. In the case of tar, it can be seen the presence of C=O, C-O and C=C functional groups and these species undergo chemical reaction under CO_2 atmosphere.

C=C are generally heavier hydrocarbons which are resistant to heat, thus appear in tar samples (Cai et al., 2008). This could be evidenced from the GC-MS analysis of tar.

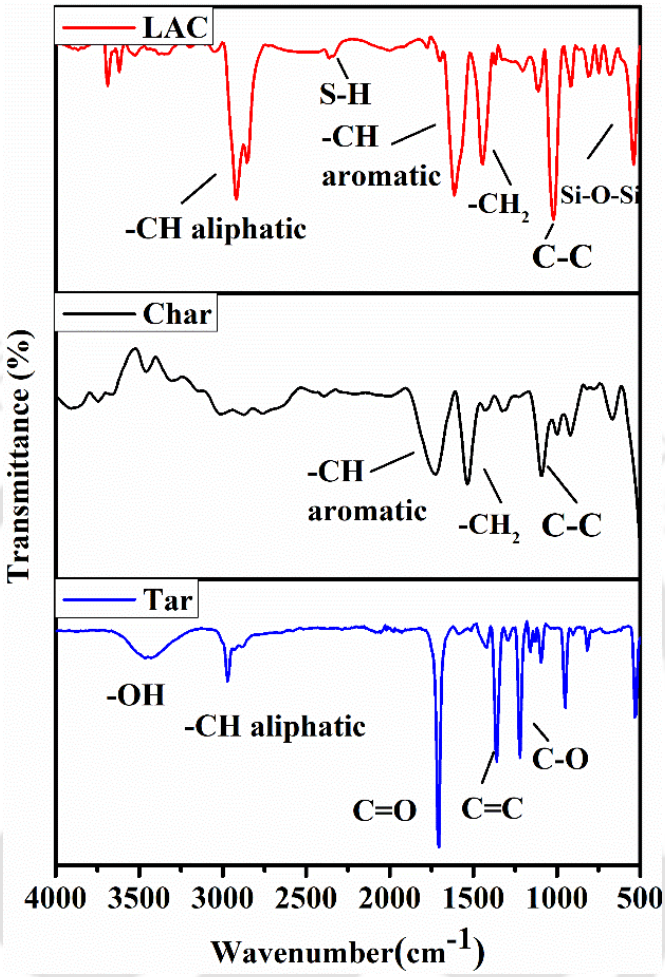

Figure 4.7. FTIR spectra analysis of pure LAC, char and tar under N_2 atmosphere.

4.2.6.2. GC-MS analysis of LAC based tar

GC-MS analysis of the LAC tar content obtained under both N_2 (pyrolysis) and CO_2 (gasification) atmosphere is carried out for finding the presence of different chemical species. Table 4.2 shows the detected components of the tar content obtained from both the atmospheres. It is observed that the percentage of alkane content is lower than alkene in both the tar contents. Further, aliphatic components are absent in both the atmosphere.

Table 4.2. Comparative study of the composition of LAC based tar in N_2 and CO_2 atmosphere.

Components	Retention time	Percentage composition (%)	
		N_2 atm.	CO_2 atm.
1-pentene,2,4,4-trimethyl	3.38	7.49	6.88
2,3,5-trimethylphenol	4.35	0.18	0.13
C3 alkyl	10.25	0.35	0.056
Trimethylnaphthalene	12.26	0.82	0.13
C2 alkyl phenol	13.57	0.32	0.23
Acenaphthylene	13.81	0.45	0.059
Dimethylnaphthalene	14.04	0.33	0.1
Methylacenaphthene	14.37	1.09	1.04
Tetramethylnaphthalene	14.62	0.78	0.19
6-isopropoxydihydroindole	14.75	0.35	0.22
Biphenyl acenaphthene	15.90	1.16	0.75
C3 alkyl phenol	16.10	0.50	0.07
n-C16 alkane	17.73	0.057	0.01
C3-alkyl naphthalene	16.52	0.90	0.01
Azafluorene	17.21	1.85	0.75
Pentamethyl-2,3-dihydro-1H-indene	38.79	0.94	0.07
6-isopropyl-1,4 dimethylnapthalene	45.03	1.99	1.70
9H-fluorene,9-methylene	47.45	2.21	1.27
Quinoline	11.96	0.70	-
Alkyl indene	13.00	0.32	-
Xanthene	17.50	0.43	-
Fluorenamine	18.92	1.32	-
Naphthalenecarbonitrile	19.76	0.46	-

This may be due to the decomposition of these groups into hydrocarbon based volatiles (CH_4, C_2H_4, C_2H_6 etc.) at lower temperatures by thermal cracking reactions (Zhang et al., 2018). The percentage composition of higher hydrocarbons, aromatics, phenols etc. is

found low in tar obtained under CO_2 atmosphere, compared to N_2 based tar. It is observed that components such as dibenzofuran, naphthalene etc. are present in the N_2 based tar, and these are found negligible in the CO_2 environment. This is due to the reactivity of CO_2 with tar content over a temperature range during the in-situ gasification process.

4.2.6.3. FESEM and BET analysis

The FESEM analysis of raw LAC and its pyrolyzed char is shown in Figure 4.8. Figure 4.8(b) shows the porous structure of the pyrolyzed char. The BET surface area is in good agreement with the FESEM analysis, as mentioned in Table 4.3. The raw LAC has a surface area of about 1.16 m^2/g, which increased to 5.34 m^2/g for the char sample. Thus, almost 4 to 5 times increase in the total surface area is estimated.

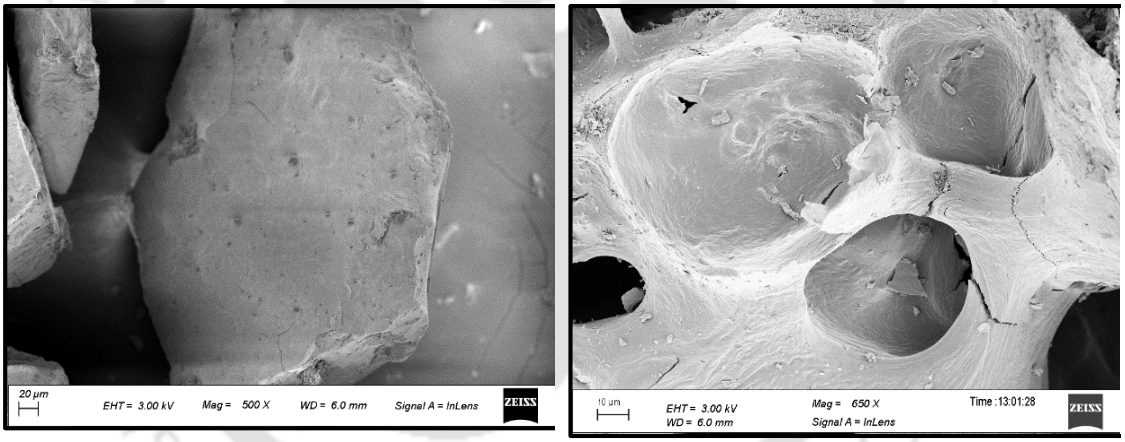

(a) (b)

Figure 4.8. FESEM images of (a) raw LAC, and (b) pyrolyzed LAC.

Further, the FESEM images of Fe_2O_3 particles after reduction and re-oxidation reactions are presented in Figure 4.9. The reduced particles from the fuel reactor are found spherical in shape. The discrete particles of Fe_2O_3 are observed in all the cases. The grain size of the particles remains the same, indicating no agglomeration and sintering issues. It is seen that the addition of biomass increased the porosity of LAC during the co-CLC process. This can be noticed from the BET analysis.

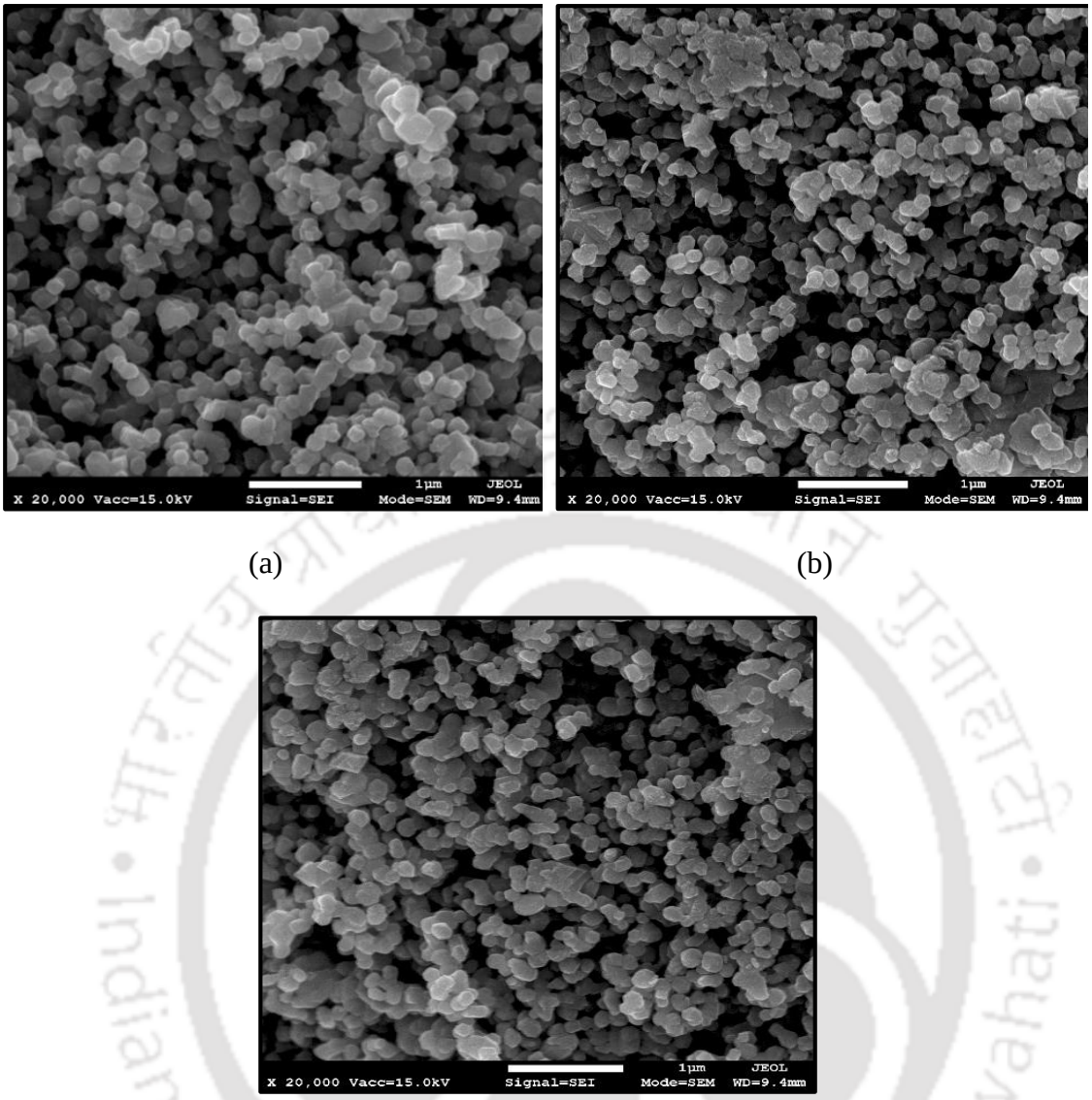

Figure 4.9. FESEM images of residue obtained from (a) LAC-Fe_2O_3, (b) RS- Fe_2O_3, (c) LAC-RS-Fe_2O_3.

Table 4.3 compares the BET surface area of the fresh Fe_2O_3 with the re-oxidized residues. The re-oxidized residue contains Fe_2O_3 and ash, with a minor content of unconverted carbon. The BET surface area of the re-oxidized Fe_2O_3 increased from 2.5 m^2/g to 3.1 m^2/g for LAC-Fe_2O_3 and 3.4 m^2/g for RS-Fe_2O_3, respectively (Table 4.3). The blending of LAC and RS has resulted in a BET surface area of 3.2 m^2/g. The reduced Fe_2O_3 particles have a higher surface area than the fresh Fe_2O_3 due to the phase transition from

Fe_2O_3 to Fe_3O_4. The reduction and oxidation may have resulted in the formation of new pores, which resulted in an increase in the surface area.

Table 4.3. BET Surface area of fresh and reduced residues.

Sample	Surface area (m^2/g)	Pore volume ($\times 10^{-3}$ cm^3/g)	Pore diameter (nm)
Raw coal	1.16	5.51	5.08
Pyrolyzed LAC	5.34	3.36	4.59
Gasified LAC	13.52	19.8	4.13
Fresh Fe_2O_3	2.52	5.23	9.34
LAC- Fe_2O_3-AR	3.07	6.11	6.21
RS- Fe_2O_3-AR	3.43	5.77	4.49
LAC-RS-Fe_2O_3- AR	3.24	5.85	6.83

Figure 4.10. Photographs of (a) fresh LAC, (b) fresh RS, (c) fresh Fe_2O_3, (d) reduced form of Fe_2O_3 obtained during CLC (e) re-oxidized Fe_2O_3 obtained from air reactor.

Figure 4.10 shows the photographs of the fresh, reduced and re-oxidized Fe_2O_3 particles indicating the colour variation in different forms. The snapshot of raw feedstock such as LAC, RS and fresh Fe_2O_3 is shown in Figure 4.10 (a-c). Figure 4.10 (c) are found red in colour and these particles are turned into black colour (Figure 4.10d) upon reduction in the FR. This colour variation may represent the reduction of Fe_2O_3 into Fe_3O_4. The re-oxidized Fe_2O_3 (Figure 4.10e) particles are shown to be dark brown in colour, which indicates successful oxidation.

4.2.6.4. XRD analysis

X-ray powder diffraction of fresh, reduced and oxidized Fe_2O_3 particles are examined as shown in Figure 4.11. The residue obtained after the CLC reaction from the FR outlet displays the crystalline peaks of Fe_3O_4, Al_2O_3, SiO_2 and Fe_2O_3 (Figure 4.11a). The phase identification are found similar to the reported literature (Qin et al., 2016, Song et al., 2012, Zhang et al., 2011). Liu et al. (2020) performed XRD analysis of Fe_2O_3 mixed in 40% coal ash. They observed the formation of Fe_2SiO_4, $FeAl_2O_4$, $KAlSiO_4$ due to ash-Fe_2O_3 interaction. However, no such peaks are seen during the reduction and oxidation stage, which indicate the negligible fusion of ash with oxygen carriers, thus unaffecting the oxygen carrier reactivity. The absence of Fe3C peak indicates the absence of coal tar deposition over the Fe_2O_3 particles (Wang et al., 2019). As Fe_2O_3 particles are 99% pure, no other impurity peaks are observed, as shown in Figure 4.11(b). Overall, the XRD analysis showed that the CLC residue containing the reduced Fe_2O_3 particles is efficiently oxidized in the air atmosphere.

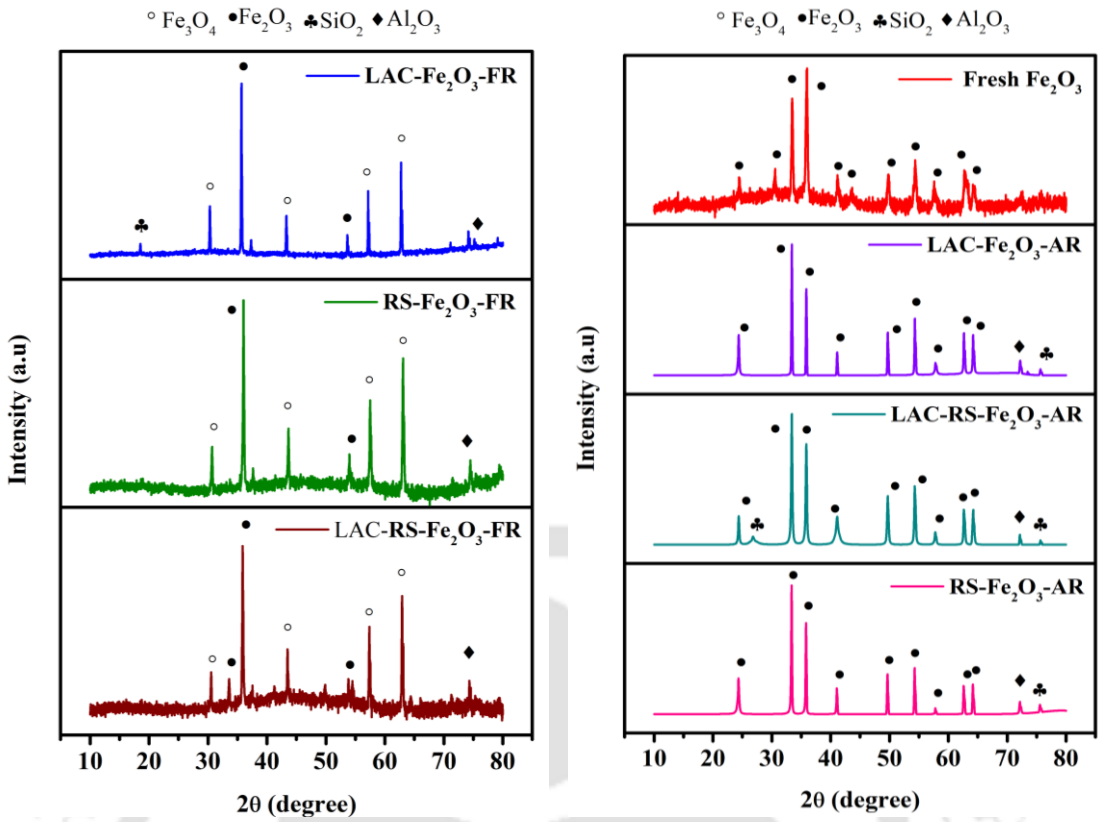

(a) (b)

Figure 4.11. XRD analysis of LAC, RS and their blend under (a) reduction and (b) oxidation atmosphere.

4.2.6.5. TGA analysis

TGA analysis is conducted for estimating the reactivity of LAC, RS and their blend under N_2 and CO_2 atmosphere with and without the presence of iron oxides. Non-isothermal condition is maintained in a temperature range of 30 to 1000°C. Further, the reactivity of char with Fe_2O_3 under an inert atmosphere is estimated in order to calculate the solid-solid reactivity.

A. Pyrolysis and gasification of individual fuels- LAC and RS

Figure 4.12 displays the TGA and DTG curves of raw LAC and RS under N_2 and CO_2 atmosphere. The mass loss is characterized into three zones of temperature, i.e., 25-100°C, 200-400°C (for RS) or 400-600°C (for LAC) and 800-1000°C.

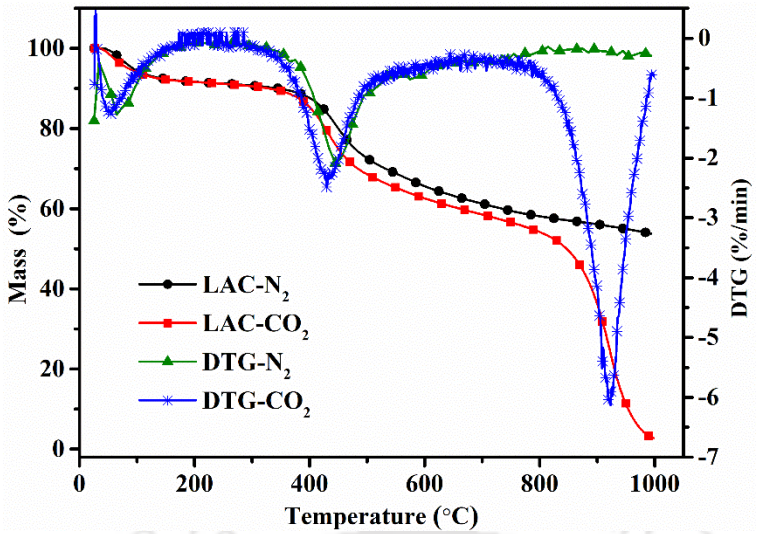

(a)

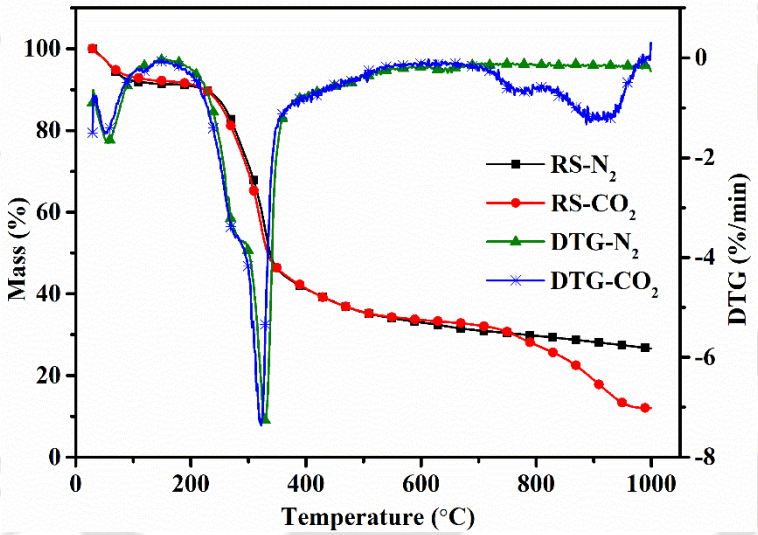

(b)

Figure 4.12. TGA and DTG curves of (a) LAC and (b) RS under N_2 and CO_2 atmosphere.

The first zone is related to the inherent moisture present in the feed. The mass loss due to the LAC volatiles is 26.7% observed between 350°C and 650°C. It is apparent that the RS releases its volatiles at 200-400°C earlier than LAC at 350-650°C. It is evident that the decomposition of hemicellulose and cellulose from the RS resulted in the mass loss at 200-400°C. Due to the higher content of volatiles in RS, a significant mass loss of 49.6% happens between 200-400°C. Further, a drastic mass reduction is shown under the

CO_2 atmosphere due to the Boudouard reaction in the temperature interval between 800 and 1000°C. Due to higher content of fixed carbon in LAC than RS, LAC experienced the higher mass loss of 51.3% at 800-1000°C. The mass loss for RS is accounted 15.3% at 800-1000°C.

B. Effect of the addition of RS with LAC in the CLC process

Figure 4.13 shows the TGA and DTG curves of LAC with Fe_2O_3 under N_2 and CO_2 atmosphere. The distinct mass loss peaks due to the CLC reactions of LAC-Fe_2O_3 are observed at 400-560°C, 650-730°C, 750-820°C in N_2 atmosphere, and 400-560°C, 600-700°C, 800-1000°C in CO_2 atmosphere. Similar mass loss peaks are found for the CLC reaction based on the RS-Fe_2O_3 mixture. As discussed, the onset of volatiles release from RS is earlier than LAC. Hence, in the temperature range of 200-400°C for RS-Fe_2O_3 and 400-560°C for LAC-Fe_2O_3, the reactivity of lighter volatiles with Fe_2O_3 can be noticed. The reactivity of lighter and heavier hydrocarbons (mainly from tar) is observed mainly between 600-800°C. RS-Fe_2O_3 displayed an additional mass loss at 800-900°C even in the N_2 atmosphere due to the ash interaction with the char particles. A broader peak at 800-1000°C is observed due to the char gasification and further CO oxidation by the Fe_2O_3 particles.

C. Effect of RS ash on LAC

In order to assess the effect of rice straw ash (RSA) on the LAC conversion, the ash content is produced from RS by being burnt in a muffle furnace. Further, the reactivity of the obtained RSA is tested with LAC in the TGA. Figure 4.14 shows the TGA curve highlighting the interaction of rice straw ash (RSA) with LAC under N_2 and CO_2 atmosphere. LAC-RSA blend observed a total mass loss of 28% and 50% under N_2 and CO_2 atmosphere, respectively. Moreover, the addition of LAC char with RSA has resulted

in 18% mass loss even in N_2 atmosphere at 800-1000℃. It can be inferred that the RSA could interact with char and enhance the rate of gasification.

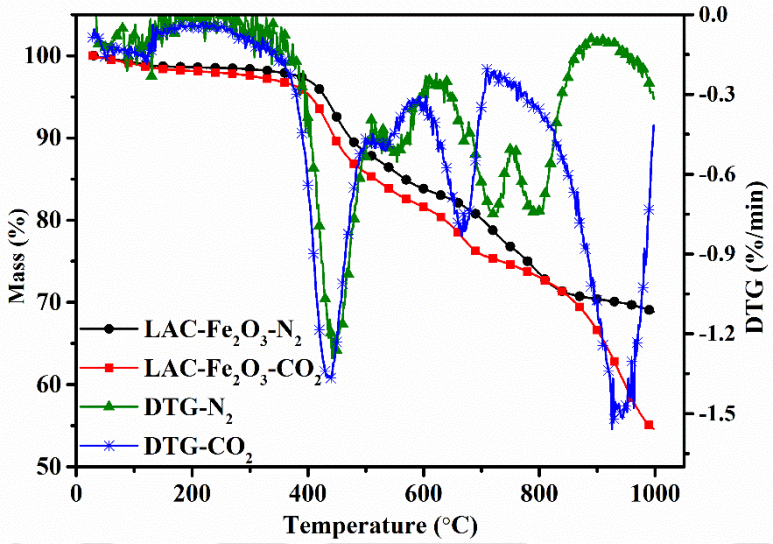

(a)

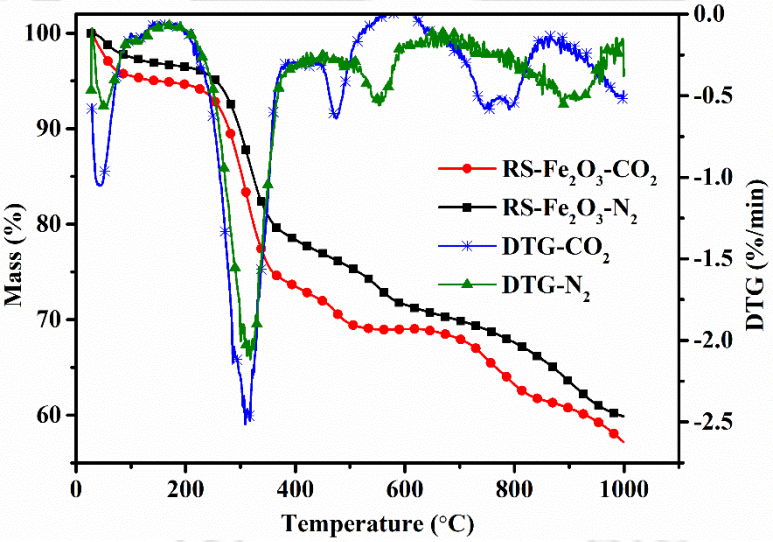

(b)

Figure 4.13. TGA and DTG curve of (a) LAC-Fe_2O_3 and (b) RS-Fe_2O_3 under N_2 and CO_2 atmosphere.

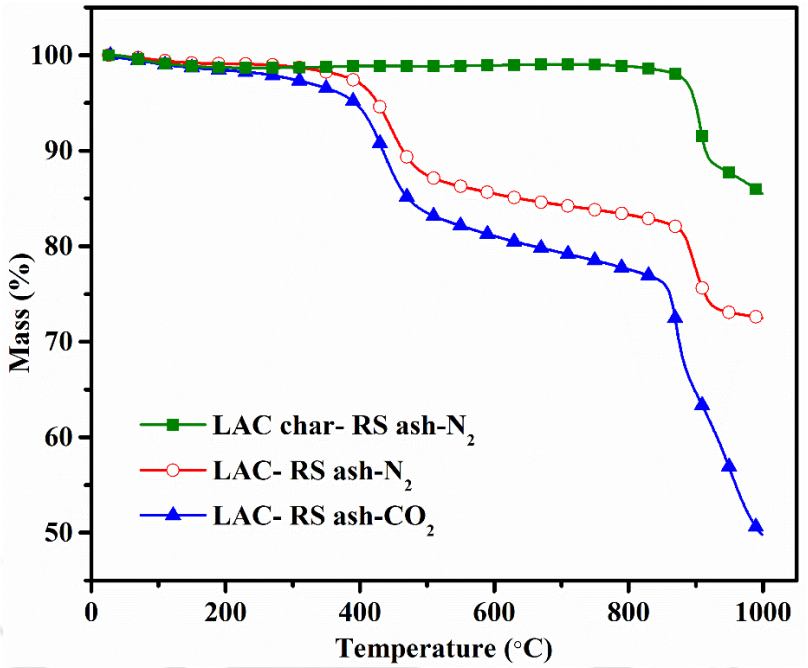

Figure 4.14. TGA analysis on the effect of RS ash on LAC during pyrolysis and gasification.

The reason for the reactivity of RS ash can be understood from the XRD analysis of the RS ash (Figure 4.15a). It is interesting to note the presence of the crystalline phase of $Ca_2Fe_2O_5$, $CaFe_2O_4$, Fe_2O_3, CaO, and Fe_3O_4 in the RS ash. The formation of calcium ferrites in the RS ash could be due to the calcination of CaO with Fe_2O_3 at high temperatures (Eq. 4.6- 4.9) (Ismail et al., 2016). The calcium ferrite in the RS ash can react with char and produces CO (Eq. 4.10-4.11) and thus, the TGA results had shown a mass loss even under N_2 atmosphere at above 800°C (Figure 4.15). FTIR analysis of RS ash is further performed to confirm the presence of calcium ferrites. Figure 4.15 (b) shows the existence of a Ca-Fe bond in the rice straw ash and this could be due to the formation of calcium ferrite. Liu et al. (2018) reported that both the $CaFe_2O_4$ and $Ca_2Fe_2O_5$ can react with carbon at temperatures higher than 710°C. Hence it is clear that the formed calcium ferrite in the ash content enhanced the gasification rate of LAC.

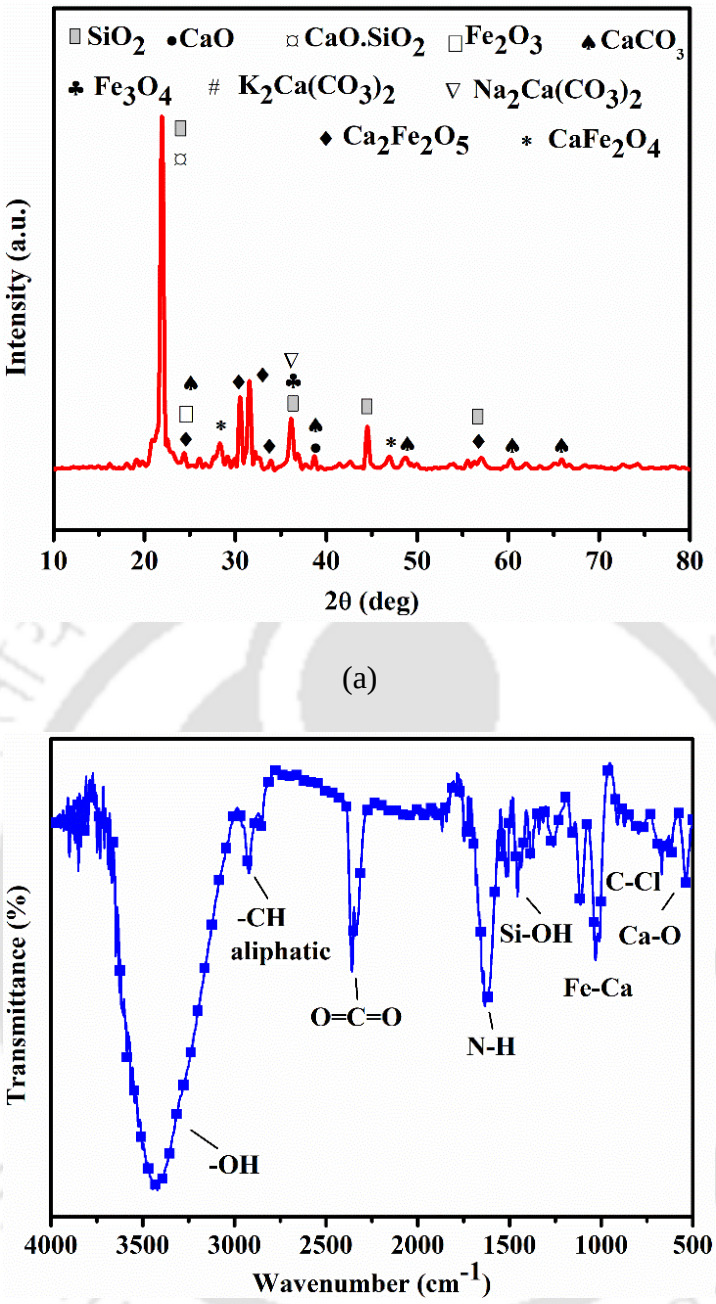

Figure 4.15. Rice straw ash analysis by (a) XRD and (b) FTIR.

The chemical reactions illustrating the formation of calcium ferrites in the ash are shown below. Calcium ferrites mainly exist in the form of $CaO.Fe_2O_3$ ($CaFe_2O_4$) and $2CaO.Fe_2O_3$ ($Ca_2Fe_2O_5$) (Ismail et al., 2016, Liu et al., 2018).

$$CaO + Fe_2O_3 \rightarrow CaFe_2O_4 \quad (4.6)$$

$$2CaO + Fe_2O_3 \rightarrow Ca_2Fe_2O_5 \quad (4.7)$$

$$Ca_2Fe_2O_5 \rightarrow 2Fe + 2CaO + 1.5O_2 \quad (4.8)$$

$$5CaFe_2O_4 \rightarrow 0.5Ca_2Fe_2O_5 + Ca_4Fe_9O_{17} + 0.25O_2 \quad (4.9)$$

The chemical reactions of char with calcium ferrite are as follows (Ismail et al., 2016).

$$3C + CaFe_2O_4 \rightarrow 2Fe + CaO + 3CO \quad (4.10)$$

$$3C + Ca_2Fe_2O_5 \rightarrow 2Fe + 2CaO + 3CO \quad (4.11)$$

D. Synergistic effect of LAC and RS in CLC

Figure 4.16 shows the actual and estimated weight loss of fuels during the co-utilization of LAC and RS in the CLC process. The synergy effect is estimated using Eq. 3.1. It is seen that LAC and RS exhibited a positive synergism with 2.4% excess weight loss under N_2 atmosphere (Figure 4.16a), while it is 7.8% under CO_2 atmosphere (Figure 4.16b). This may be due to two reasons: (a) the presence of alkali and alkaline earth metals in rice straw may act as a catalyst; or (b) formation of calcium ferrite in rice straw ash resulted in an additional mass loss in LAC.

E. Reactivity of char with Fe_2O_3

The solid-solid interaction between char and Fe_2O_3 is analyzed through TGA studies (Figure 4.17). It is seen that LAC char showed a mass loss of about 12%, while RS char displayed 22% mass loss even in the inert atmosphere. It can be concluded that the rice straw char is more reactive than LAC chars resulting in solid-solid interaction at elevated temperatures.

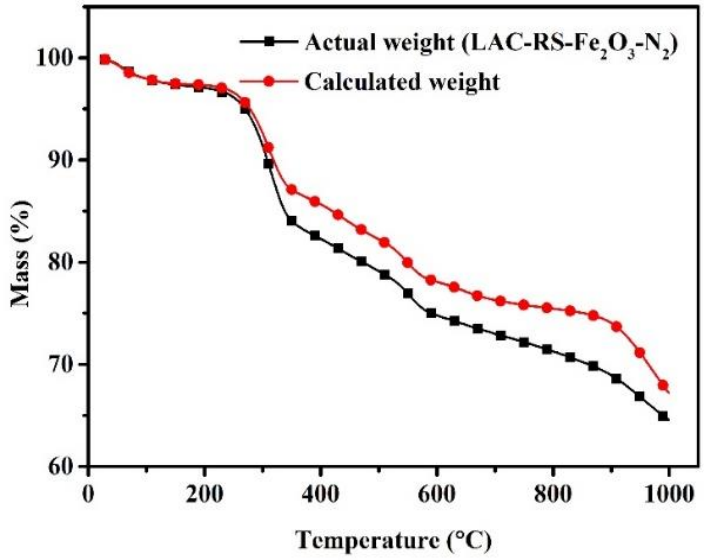

(a)

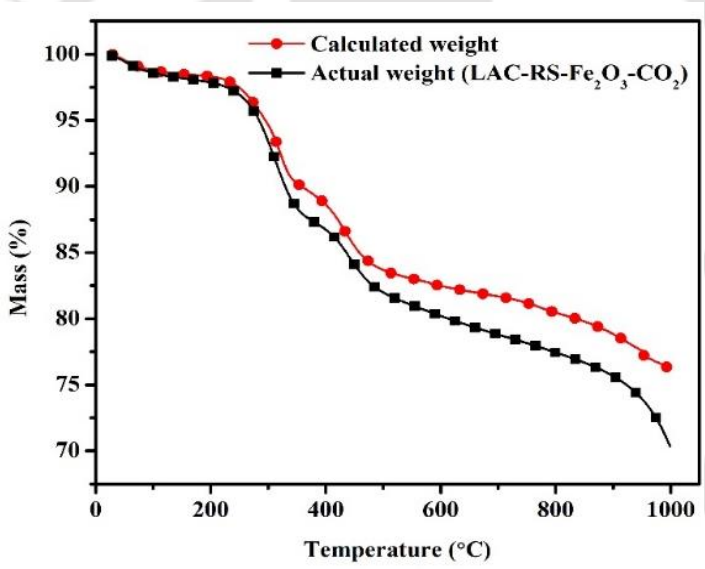

(b)

Figure 4.16. TGA and DTG curve of LAC-Fe_2O_3 mixture under (a) N_2 and (b) CO_2 atmosphere.

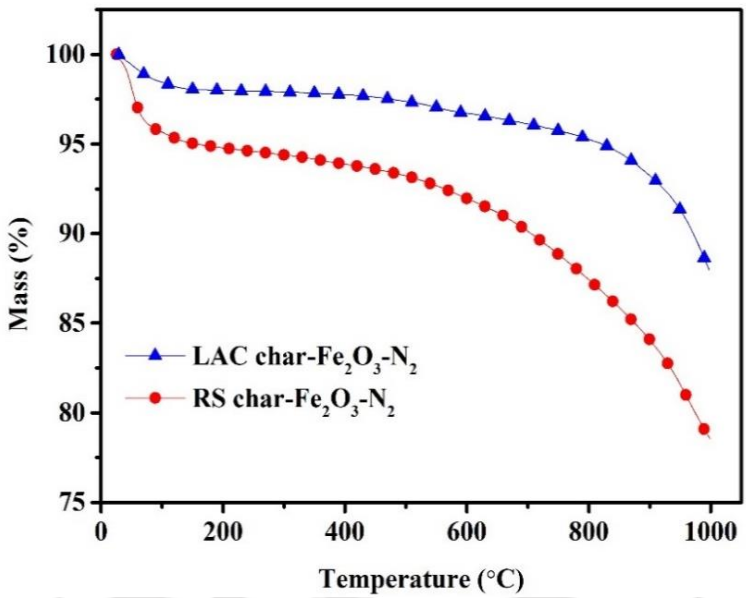

Figure 4.17. TGA and DTG curve of LAC char and RS char with Fe_2O_3 under N_2 atmosphere.

F. Quantitative estimation of oxygen release from Fe_2O_3

The quantity of oxygen reacted from Fe_2O_3 with LAC and RS is estimated by comparing the weight loss of the reaction mixture with and without the presence of Fe_2O_3. Figure 4.18 shows the quantity of O_2 released from Fe_2O_3 in the temperature range of 25-1000°C under N_2 and CO_2 atmosphere. The successive weight loss of LAC/RS-Fe_2O_3 mixture in the TGA analysis denoted the loss due to the coal reactivity with Fe_2O_3, while this weight loss without Fe_2O_3 during TGA gives the quantity of the released volatiles and the gasified char. The difference of this weight loss between these two mixtures measures the quantity of oxygen released in the LAC-Fe_2O_3 mixture. It is taken care that the initial mass of the fuel (coal/rice straw) in both the cases are same for ensuring that the mass difference between these samples is only due to the release of oxygen from the metal oxide. For example, the weight loss at 350°C for the coal-Fe_2O_3 mixture is found to be 0.0046 mg. And, for the coal without Fe_2O_3, the weight loss is accounted as 0.00341mg. The difference in the weight of these mixtures is 0.00119 mg, which is considered as the

quantity of oxygen released during the CLC conditions. This calculation is carried out for each temperature interval to estimate the total quantity of O_2 released.

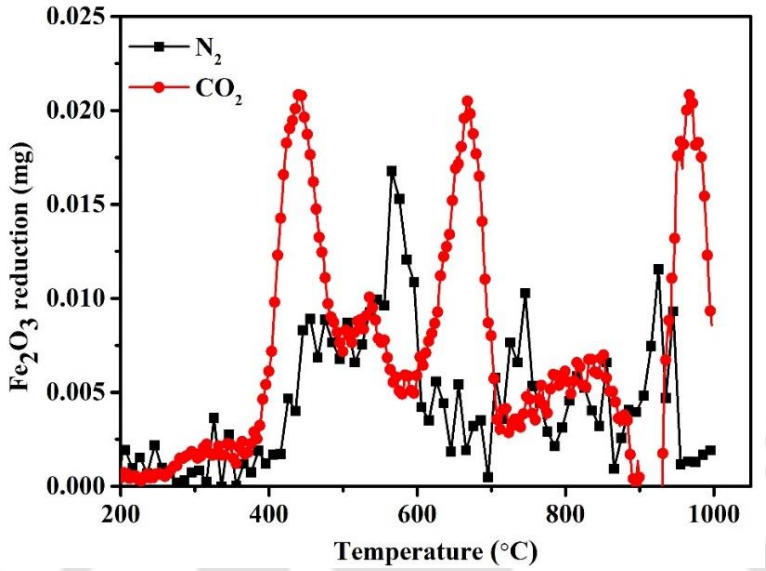

(a)

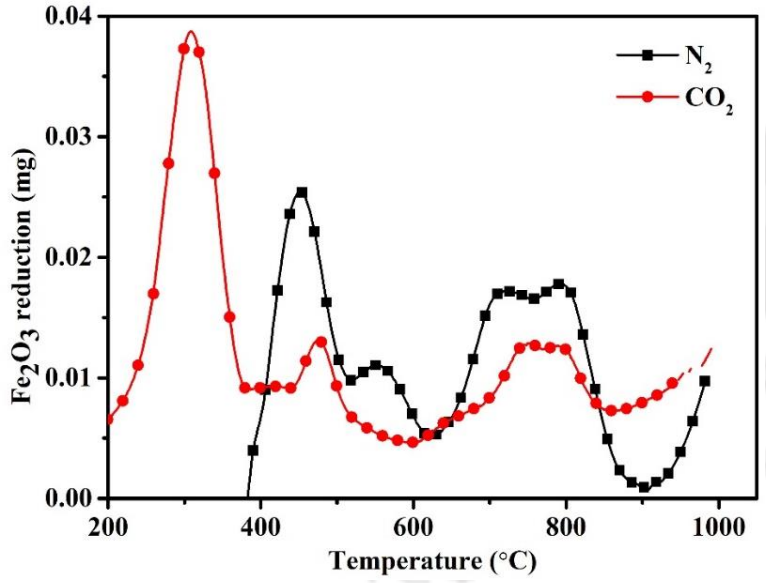

(b)

Figure 4.18. Quantitative analysis of oxygen released from Fe_2O_3 to react with (a) LAC- Fe_2O_3 and (b) RS-Fe_2O_3 under N_2 and CO_2 atmosphere.

Figure 4.18 (a) and Figure 4.18 (b) shows the distinct peaks of the released oxygen from LAC-Fe_2O_3 and RS- Fe_2O_3, respectively, under both N_2 and CO_2 atmosphere. The first

peak denotes the liberation of O_2 due to the reaction between lighter volatiles and Fe_2O_3 particles. Due to the higher content of volatiles in RS, the oxygen released from Fe_2O_3 is 0.04 mg, i.e. 0.015 mg greater than the LAC-Fe_2O_3 case. The second peak refers the reactivity of heavier fraction of the volatiles with O_2 in the temperature range of 600-800°C. The final peak is detected at the temperature interval of 850-1000°C and this is attributed to the reaction between the char-Fe_2O_3. Higher content of fixed carbon in LAC promoted a higher reduction of Fe_2O_3 than in the RS case. Thus, the oxygen released from Fe_2O_3 is almost twice for LAC-Fe_2O_3, compared to RS- Fe_2O_3. It can be noted that a high quantity of O_2 release is observed under the CO_2 atmosphere even at low temperatures. This shows the reactivity of CO_2 with higher volatile gases at lower temperatures.

G. Kinetic analysis

The kinetic parameters of the non-CLC and CLC reactions are evaluated based on the reaction order and shrinking core models. The activation energy is calculated for the non-CLC and CLC based reaction under both N_2 and CO_2 atmosphere and is shown in Tables 4.4 and Table 4.5.

I. Non-CLC reactions (without metal oxides)

The kinetic parameters are calculated based on the temperature intervals of 400-560°C, 600-800°C and 800-1000°C in Table 4.4. The shrinking core model is found to be the best fit for the obtained data based on the regression coefficient (R^2 values). The liberation of volatiles from LAC at 400-560°C has been estimated with an activation energy of 34.5 kJ/mol and 18.7 kJ/mol under N_2 and CO_2 atmosphere, respectively. The activation energy for the release of RS volatiles is found to be 26.1 kJ/mol and 14.6 kJ/mol under N_2 and CO_2 atmosphere, respectively. Mixing LAC with RS has resulted in

a reduction in the activation energy by 10.7 kJ/mol, when compared to RS at 200-400℃ under N_2 atmosphere. Further, the activation energy is found as 89.6 kJ/mol during the LAC char gasification (due to the Boudouard reaction) at 800-1000℃. In this temperature range, the activation energy of LAC is comparatively higher than RS fuel, which illustrates the lower reactivity of LAC than RS. A similar observation is reported by Guo et al. (2020) and Gil et al. (2010). They compared the activation energy of coal and biomass mixture in an oxidizing atmosphere. Guo et al. (2020) obtained an activation energy of 87.9 kJ/mol for bituminous coal and 51.9 kJ/mol for biomass at 500-700℃ in the air atmosphere. Gil et al. (2010) observed decrease in activation energy of blend (bituminous coal and pine) by 11 kJ/mol using diffusion model when compared to pine alone during char oxidation. Wang et al. (2012) estimated the activation energy of coal at 629-758 K to be 44.9 kJ/mol in an inert atmosphere. The values of activation energy are found in line with the reported literature.

II. CLC reactions (with metal oxides)

The estimated activation energy for LAC-Fe_2O_3 due to the interaction of volatiles and Fe_2O_3 at 400-560℃ is found to be 50.8 kJ/mol and 33.5 kJ/mol under N_2 and CO_2 atmosphere, respectively, while the respective activation energy is estimated as 41.8 kJ/mol and 25.3 kJ/mol for the CLC reactions of RS-Fe_2O_3 (Table 4.5). It can be further noted that the activation energy of LAC at 800-1000°C is reduced from 106.8 kJ/mol to 87.3 kJ/mol under the CO_2 atmosphere. The blend of LAC and RS exhibited lower activation energy than the individual feedstock, which indicates positive synergy. Hence, the addition of RS with LAC resulted in the reduction in the activation energy for gasification followed by the CLC reaction.

Table 4.4. Estimation of activation energy for non-CLC reaction of LAC, RS and their blend under N_2 and CO_2 atmosphere.

Fuel	Temperature (°C)	Shrinking core model		1st order reaction model		2nd order reaction model		3rd order reaction model	
		E (kJ/mol)	R^2	E (kJ/mol)	R^2	E (kJ/mol)	R^2	E (kJ/mol)	R^2
LAC-N_2	400-560	34.51	0.98	27.98	0.97	38.58	0.94	55.08	0.95
	600-800	8.14	0.99	8.26	0.98	14.53	0.89	19.47	0.91
LAC -CO_2	400-560	18.72	0.97	18.98	0.96	32.53	0.95	38.58	0.94
	600-800	4.69	0.99	5.35	0.98	8.32	0.99	11.28	0.86
	800-1000	89.57	0.95	109.78	0.93	132.45	0.83	150.11	0.81
RS-N_2	200-400	26.11	0.96	28.93	0.95	37.23	0.95	46.82	0.95
	400-560	8.54	0.98	7.29	0.73	11.94	0.96	26.02	0.97
	600-800	3.47	0.99	13.35	0.89	77.76	0.81	163.09	0.76
RS-CO_2	200-400	14.57	0.97	24.73	0.96	37.52	0.96	47.74	0.95
	400-560	6.25	0.96	5.91	0.95	1.65	0.39	5.57	0.84
	600-800	2.69	0.88	1.66	0.24	14.80	0.85	35.82	0.81
	800-1000	78.59	0.99	35.36	0.98	70.92	0.95	95.62	0.95
LAC-RS-N_2	200-400	18.32	0.91	16.04	0.92	21.79	0.92	28.35	0.93
	400-560	6.09	.54	7.25	0.86	23.87	0.98	45.53	52.21
	600-800	3.29	0.98	2.18	0.99	33.09	.99	33.09	0.99
LAC-RS-CO_2	200-400	15.48	0.93	15.46	0.93	18.62	0.93	22.04	0.93
	400-560	5.96	0.93	4.43	0.82	5.24	0.75	10.96	0.91
	600-800	1.53	0.99	8.42	0.99	4.37	0.99	0.65	0.48
	800-1000	82.40	0.96	52.73	0.63	146.5	0.56	126.94	0.84

Table 4.5. Estimation of activation energy for CLC process using LAC, RS and their blend under N_2 and CO_2 atmosphere.

Fuel	Temperature (°C)	Shrinking core model		1st order reaction model		2nd order reaction model		3rd order reaction model	
		E (kJ/mol)	R^2	E (kJ/mol)	R^2	E (kJ/mol)	R^2	E (kJ/mol)	R^2
LAC- Fe_2O_3-N_2	400-560	50.78	0.99	57.33	0.97	63.17	0.97	69.37	0.98
	600-800	16.31	0.98	9.13	0.93	8.35	0.92	18.58	0.91
LAC - Fe_2O_3 -CO_2	400-560	33.46	0.96	43.46	0.94	50.09	0.95	57.26	0.96
	600-800	13.83	0.92	11.69	0.91	22.04	0.92	20.47	0.96
	800-1000	106.81	0.97	172.14	0.88	193.39	0.86	231.75	0.91
RS- Fe_2O_3-N_2	200-400	41.83	0.92	29.92	0.93	38.91	0.96	47.51	0.93
	400-560	8.46	0.99	3.52	0.67	12.23	0.92	20.05	0.93
	600-800	19.33	0.97	14.87	0.95	79.48	0.80	82.82	0.88
RS- Fe_2O_3-CO_2	200-400	25.27	0.94	26.10	0.94	39.61	0.92	46.23	0.93
	400-560	8.28	0.96	11.62	0.50	14.03	0.95	21.53	0.94
	600-800	9.97	0.98	12.03	0.65	23.88	0.98	42.41	0.98
	800-1000	89.96	0.97	90.79	0.92	79.90	0.84	101.69	0.84
LAC -RS- Fe_2O_3-N_2	200-400	36.85	0.93	19.78	0.93	22.89	0.94	26.29	0.94
	400-560	7.65	0.95	10.07	0.97	18.51	0.99	28.58	0.99
	600-800	5.49	0.33	6.51	0.86	26.81	0.96	53.47	0.97
LAC -RS- Fe_2O_3 -CO_2	200-400	28.07	0.91	14.86	0.91	17.47	0.92	20.33	0.92
	400-560	6.14	0.92	3.55	0.96	8.29	0.99	13.82	0.99
	600-800	4.07	0.94	1.92	0.67	5.98	0.82	15.86	0.92
	800-1000	87.29	0.96	75.82	0.91	254.03	0.79	69.75	0.76

4.3. Conclusions

In-situ CO_2 gasification based direct coal fuelled CLC experiments are conducted using Fe_2O_3 as the oxygen carriers. The reduction and oxidation potential of the oxygen carriers are evaluated using a fixed bed reactor and a TGA apparatus. The following conclusions can be drawn from this chapter.

- The average outlet gas composition is found to be 12.2% H_2, 6.2% CO and 6.8% CH_4 during LAC pyrolysis.
- Around 40-60% of CO is released during LAC-RS gasification at 750-950℃ under the CO_2 atmosphere. Mixing of LAC and RS produced syngas with the calorific value of 6-8 MJ/Nm^3.
- GC-MS analysis of tar obtained during CLC reactions shows the absence of several higher hydrocarbons under the CO_2 atmosphere that highlights the enhanced reactivity between tar and CO_2.
- The fixed bed experiment demonstrated high reactivity of Fe_2O_3 with LAC volatile and char, thereby producing a gas conversion of 89.1% gas conversion and CO_2 yield of 85.8%. Similarly, the CO_2 yield and gas conversion for RS-Fe_2O_3 are 89.6% and 92.4%. Under the co-CLC conditions, the average CO_2 yield has increased to 88.1% and the gas conversion has reached as high as 91.3%.
- The blending of LAC and RS improved the char conversion from 90.9% to 92.7%.
- The FESEM, BET and XRD analysis indicated that no sintering or agglomeration issue has occurred during the complete cycle of LAC, RS and their blend in CO_2 atmosphere.
- It is seen that LAC and RS displayed a positive synergy of 2.4% under N_2 atmosphere, while 7.8% under CO_2 atmosphere when LAC and RS are blended for the CLC process.

- The formation of calcium ferrites ($CaFe_2O_4$, $Ca_2Fe_2O_5$) due to the reaction between CaO in RS ash and Fe_2O_3 enhanced the conversion of LAC under the co-utilization condition.
- The TGA analysis of char-Fe_2O_3 mixture under N_2 atmosphere shows a significant mass reduction of about 12% for LAC, while RS char displayed 22% due to solid-solid interaction.
- The shrinking core model is found to be the best fit for non-CLC and CLC-based reactions under both N_2 and CO_2 atmospheres.

It can be inferred that CO_2 based iG-CLC process is a feasible technology for the efficient utilization of coal with CO_2 capture. However, multiple cycles need to be operated to check its reactivity for long-term use.

References

Cai, J., Wang, Y., Zhou, L., & Huang, Q. (2008). Thermogravimetric analysis and kinetics of coal/plastic blends during co-pyrolysis in nitrogen atmosphere. *Fuel Processing Technology*, *89*, 21–27.

Gil, M. V., Casal, D., Pevida, C., Pis, J. J., & Rubiera, F. (2010). Thermal behaviour and kinetics of coal/biomass blends during co-combustion. *Bioresource Technology*, *101*, 5601–5608.

Guo, F., He, Y., Hassanpour, A., Gardy, J., & Zhong, Z. (2020). Thermogravimetric analysis on the co-combustion of biomass pellets with lignite and bituminous coal. *Energy*, *197*, 1–9.

Ismail, M., Liu, W., Dunstan, M. T., & Scott, S. A. (2016). Development and performance of iron based oxygen carriers containing calcium ferrites for chemical

looping combustion and production of hydrogen. *International Journal of Hydrogen Energy*, *41*, 4073–4084.

Liu, G., Liao, Y., Wu, Y., & Ma, X. (2018). Application of calcium ferrites as oxygen carriers for microalgae chemical looping gasification. *Energy Conversion and Management*, *160*, 262–272.

Liu, T., Yu, Z., Jiao, W., Song, S., Li, C., & Fang, Y. (2020). Interaction of coal ashes with potassium-decorated Fe_2O_3/Al_2O_3 oxygen carrier in coal-direct chemical looping hydrogen generation (CLHG). *Journal of the Energy Institute*, *93*(5), 1790–1797.

Ma, J., Tian, X., Wang, C., Chen, X., & Zhao, H. (2018). Performance of a 50 kW_{th} coal-fuelled chemical looping combustor. *International Journal of Greenhouse Gas Control*, *75*, 98–106.

Pérez-Vega, R., Abad, A., Gayán, P., García-Labiano, F., Izquierdo, M. T., de Diego, L. F., & Adánez, J. (2020). Coal combustion via chemical looping assisted by oxygen uncoupling with a manganese-iron mixed oxide doped with titanium. *Fuel Processing Technology*, *197*, 106184.

Qin, W., Lin, C. F., Long, D. T., Wang, J. Y., & Dong, C. Q. (2016). Activity of Fe_2O_3 with a high index facet for bituminous coal chemical looping combustion: A theoretical and experimental study. *RSC Advances*, *6*, 85551–85558.

Song, T., Wu, J., Zhang, H., & Shen, L. (2012). Characterization of an Australia hematite oxygen carrier in chemical looping combustion with coal. *International Journal of Greenhouse Gas Control*, *11*, 326–336.

Wang, B., Ma, Q., Wang, W., Zhang, C., Mei, D., Zhao, H., & Zheng, C. (2017). Effect

of Reaction Temperature on the Chemical Looping Combustion of Coal with $CuFe_2O_4$ Combined Oxygen Carrier. *Energy and Fuels*, *31*, 5233–5245.

Wang, D., Jin, L., Li, Y., Wei, B., Yao, D., Wang, T., & Hu, H. (2019). Integrated process of coal tar upgrading and in-situ reduction of Fe_2O_3. *Fuel Processing Technology*, *191*, 20–28.

Wang, J., Zhang, S. Y., Guo, X., Dong, A. X., Chen, C., Xiong, S. W., Fang, Y. T., & Yin, W. Di. (2012). Thermal behaviors and kinetics of pingshuo coal/biomass blends during copyrolysis and cocombustion. *Energy and Fuels*, *26*, 7120–7126.

Zhang, K., Li, Y., He, Y., Wang, Z., Li, Q., Kuang, M., Ge, L., & Cen, K. (2018). Volatile gas release characteristics of three typical Chinese coals under various pyrolysis conditions. *Journal of the Energy Institute*, *91*, 1–12.

Zhang, S., Saha, C., Yang, Y., Bhattacharya, S., & Xiao, R. (2011). Use of Fe_2O_3 - containing industrial wastes as the oxygen carrier for chemical-looping combustion of coal: effects of pressure and cycles. *Energy & Fuels*, *25*, 4357–4366.

CHAPTER 4B

EXPERIMENTAL STUDIES OF HAC, RS, AND THEIR BLENDS WITH Fe_2O_3 AS THE OXYGEN CARRIER

In this chapter, the experimental results of chemical looping combustion performance of high ash coal, rice straw and their blend with Fe_2O_3 are discussed. The obtained residue after CLC reaction is analysed using XRD, FESEM, BET, etc. Table 4.6 shows the process parameters of the performed experiments under non-CLC and CLC mode of operation. The re-oxidation of the reduced Fe_2O_3 is performed in the same fixed reactor under air atmosphere and their oxidation potential is evaluated.

Table 4.6. Experimental details of assessing HAC, RS and their blend based fuels in a fixed bed reactor.

Case	Fuel	Operating conditions	
		Fuel Reactor (Temperature, Flow, Fuel: Fe_2O_3)	Air reactor
Expt. 8	HAC	350-950°C, 0.3 LPM-N_2	
Expt. 9	HAC	350-1000°C, 0.3 LPM-CO_2	-
Expt. 10	RS	350-1000°C, 0.3 LPM-CO_2	-
Expt. 11	HAC-RS	350-1000°C, 0.3 LPM-CO_2	-
Expt. 12	HAC	900°C, 0.8 LPM-CO_2, 1:45	900°C, 0.8 LPM-Air
Expt. 13	RS	900°C, 0.8 LPM-CO_2, 1:40	900°C, 0.8 LPM-Air
Expt. 14	HAC-RS	900°C, 0.8 LPM-CO_2, 1:45	900°C, 0.8 LPM-Air

4.4. Results and discussion

4.4.1. HAC pyrolysis (Expt. 8)

The HAC pyrolysis experiment is conducted in the fixed bed reactor to assess the syngas composition. Figure 4.19 displays the composition of obtained syngas under inert atmosphere. A significant amount of calorific valuable gases such as H_2, CO_2, CH_4 and

CO are produced. The average gas composition is found to be 10.3% H_2, 3.2% CO, 5.1% CH_4 and 7.5% CO_2. The gas release has gradually reduced above 800°C due to the significant removal of volatile matter from the char matrix. It is observed that the gas yield of HAC is lower than LAC due to its relatively higher ash and lower carbon content.

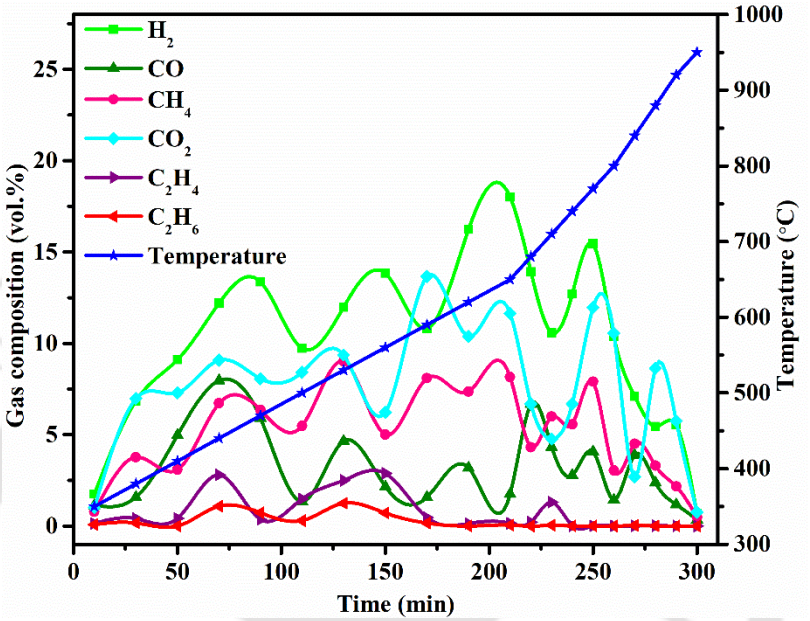

Figure 4.19. Gas composition obtained during the pyrolysis of HAC (on N_2 free basis).

4.4.2. CO_2 gasification of HAC, RS and their blend (Expt. 9, Expt. 10, Expt. 11)

The gas composition obtained during the CO_2 gasification of HAC is shown in Figure 4.20. It is observed that the production of CO and H_2 are found to be the major gases in gasification up to 800°C. As compared to LAC, the production of valuable calorific gases is found to be low due to the lower reactivity of HAC. The average gas composition obtained during of RS gasification is 4.3% H_2, 16.5% CO and 2.2% CH_4. The CO production is the lowest in RS due to low fixed carbon, compared to HAC. The average gas composition obtained during the gasification of HAC-RS blend is found to be 4.96% H_2, 17.9% CO and 3.04% CH_4, which are higher in their percentage composition than that for RS gasification. Similar observations were reported by Zhang et al. (2016), Saw

& Pang (2013). Saw & Pang (2013) assessed the average syngas composition of pinewood and lignite coal during the steam gasification. They concluded that with the increase in the coal/biomass ratio, the production of H_2/CO ratio increases.

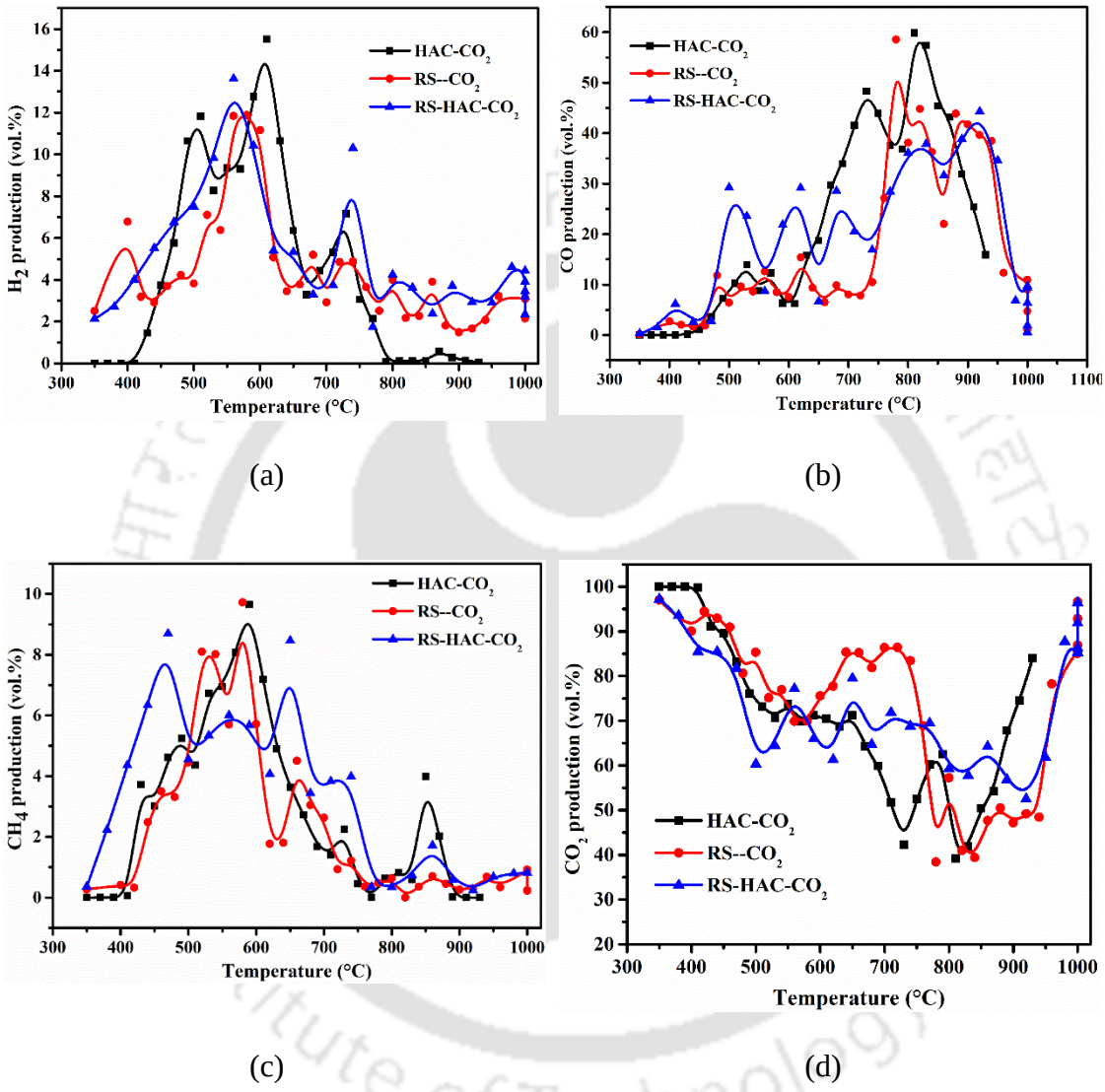

Figure 4.20. Comparison of syngas composition (a) H_2, (b) CO, (c) CH_4 and (d) CO_2 using HAC, RS and their blend in CO_2 atmosphere.

The calorific value of the syngas generated from HAC, RS and this blend is shown in Figure 4.21. The average calorific value of the HAC based syngas is found to be the highest (4.12 MJ/m^3), while RS showed the lowest (3.28 MJ/m^3). The HAC-RS blend

has produced the syngas with the calorific value of 3.91 MJ/m^3. Thus, the blending rice straw with HAC has not reduced the calorific value of syngas drastically, and the detrimental effect of ash on the CLC performance can be minimized.

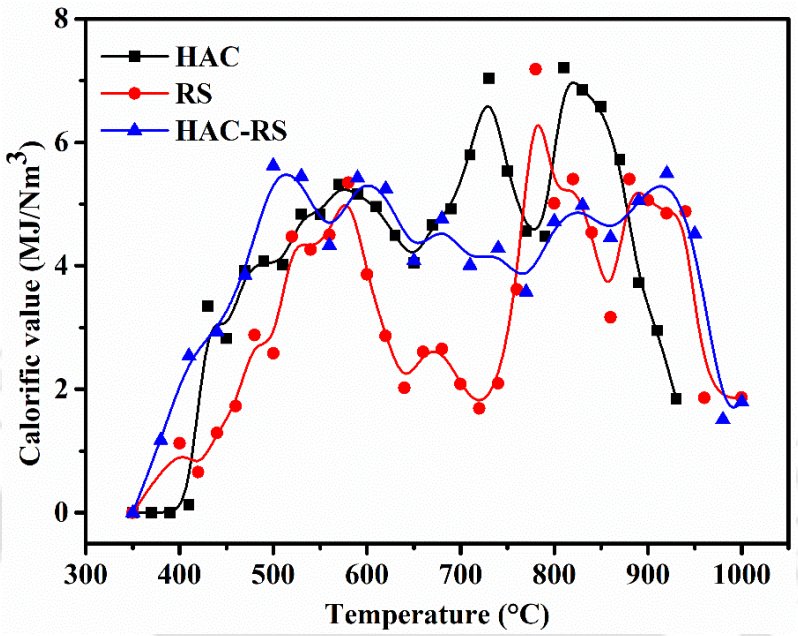

Figure 4.21. Calorific value of the syngas obtained during CO_2 gasification of HAC, RS and their blend.

4.4.3. CLC reactivity of HAC and RS with Fe_2O_3 (Expt. 12, Expt. 13)

The CLC experiments are conducted at 900°C in isothermal mode using HAC, RS and their blends. Figure 4.22 shows the obtained gas composition as a function of time. It is observed that the CLC of HAC has occurred in a residence time of 100 minutes, while it is 80 minutes estimated for RS. The average composition of the unconverted H_2 and CO is found to be 0.5% and 4.8%, respectively, for HAC- Fe_2O_3 (Figure 4.22a). Due to the higher reactivity of RS than HAC, the unreacted gases are found to be slightly low with 0.3% H_2 and 3.6% CO (Figure 4.22b). The liberation of CH_4 and higher hydrocarbons are found to be negligible for all the cases. Overall, the obtained average CO_2 composition is found above 90% for all the cases.

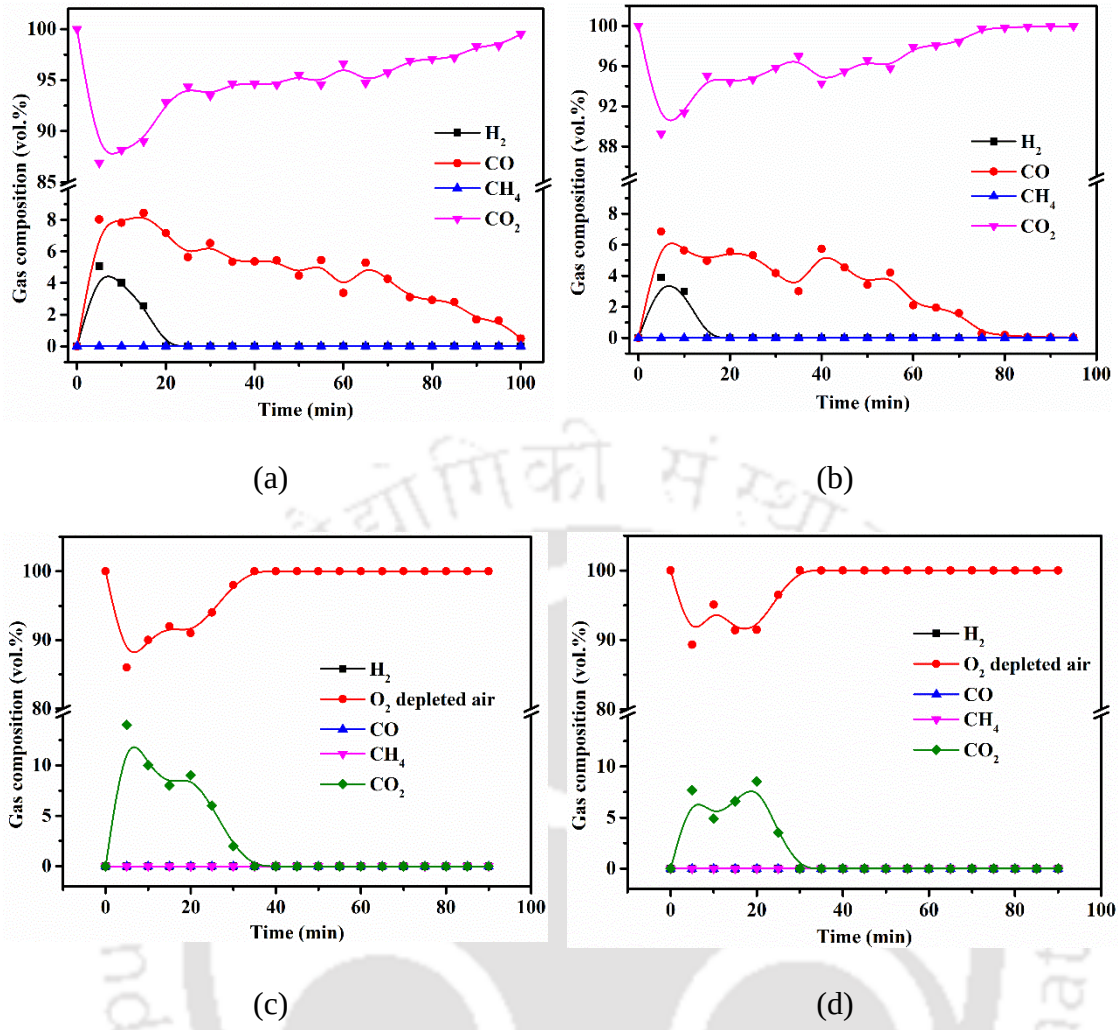

Figure 4.22. The CLC outlet gas composition of (a) HAC-Fe_2O_3 and (b) RS-Fe_2O_3 mixture under CO_2 atmosphere, (c) oxidation of HAC-Fe_2O_3 based residue and (d) oxidation of RS-Fe_2O_3 based residue.

The re-oxidation of the reduced particles from the FR is shown in Figure 4.22 (c-d). The experiments are performed as similar to the LAC case. A 10-16% CO_2 is released during the combustion of the CLC residue of HAC-Fe_2O_3, while it is 5-8% for the case of RS-Fe_2O_3. Due to the lower reactivity of HAC, the leftover char in the residue produces higher percentage of CO_2 by 3-5%, compared to LAC and RS.

4.4.4. CLC reactivity during co-gasification of HAC-RS with Fe_2O_3 (Expt. 14)

Figure 4.23 showed the outlet gas composition during the CLC of HAC-RS blend under the CO_2 atmosphere. The percentage of the unconverted gas is found to be 0.2% H_2 and 4.1% CO. The blending of the fuels has reduced the unconverted gases by 12-14%, compared to unblended conditions. It followed the same trend as that of LAC-RS-Fe_2O_3.

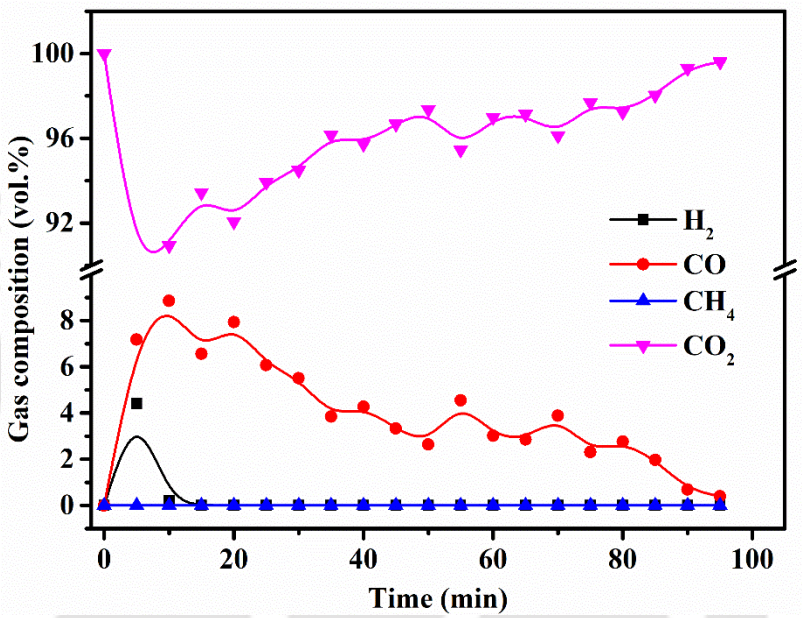

Figure 4.23. The outlet gas composition during the CLC of HAC-RS blend under CO_2 atmosphere

4.4.5. Determination of gas conversion, CO_2 yield and char conversion

The performance parameters such as gas conversion, CO_2 yield, and char conversion for the CLC of HAC, RS and their blend are shown in Figure 4.24. HAC-RS blend increased the CO_2 yield of HAC from 81.2% to 86.3%. The CO_2 yield (89.6%) and gas conversion (92.4%) of RS-Fe_2O_3 are found to be the highest. The CO_2 yield of HAC-Fe_2O_3 is reduced by 4.6%, compared to LAC-Fe_2O_3. The HAC-Fe_2O_3 feed revealed the lowest char conversion of 87.8%, whereas the LAC-Fe_2O_3 attained a higher char conversion by 3.1%, which resulted in the increase in gas conversion in LAC-Fe_2O_3. These performance

parameters are further compared with the reported literature in Table 4.7. It is observed that the CO_2 yield of 92-99% was achieved in a fluidizing bed using iron ore as the oxygen carriers (Xiao et al., 2012, Bayham et al., 2015, Kim et al., 2013). The obtained results are slightly lower than the reported literature results due to the fixed bed operation in the present study.

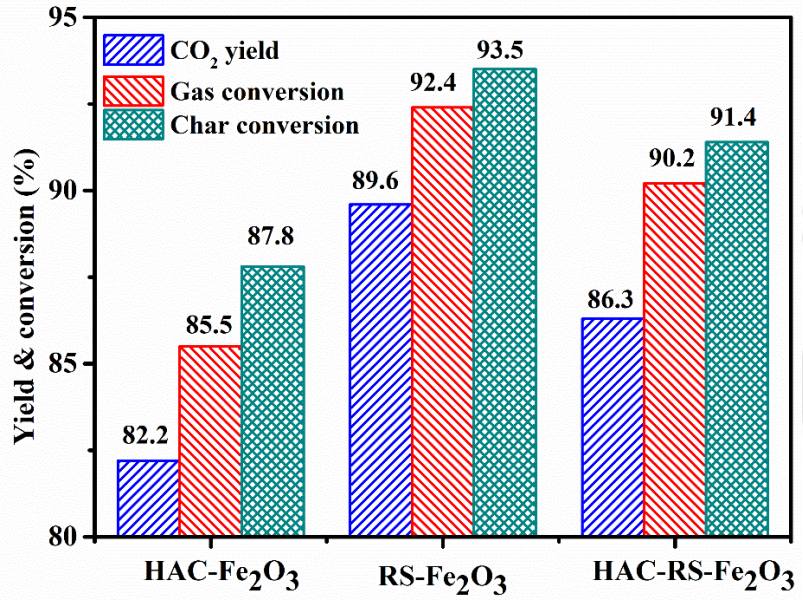

Figure 4.24. Comparison of CO_2 yield, gas conversion and char conversion during the CLC of HAC, RS and their blend under CO_2 atmosphere.

4.4.6. Post characterization of the non-CLC and CLC residue

4.4.6.1. FTIR of raw coal, char and tar

FTIR analysis has been conducted to identify the functional groups present in the raw HAC coal, the obtained char and tar from HAC pyrolysis. The functional groups present in the raw HAC and the obtained char are similar unlike the LAC based results (Figure 4.25). This indicates that the intense release of volatiles from the raw HAC is not achieved, which may be due to the hindrance of ash layer. The functional group, C=C usually found in the heavier hydrocarbons; however, this bond is observed in the char

and tar unlike LAC. A sharp peak at 3800-3300 cm^{-1} represents the gas phase H_2O or phenol group (Meng et al., 2014). C-H bond in CH_4 is identified at 1460 cm^{-1}. C-H aliphatic groups such as carboxylic acid, alcohols, hydrocarbons, etc. (detect at 3300-2800 cm^{-1}) are present for all the cases. C=O in tar suggests the existence of aldehydes, ketones or esters (Lin et al., 2019, Tian et al., 2016).

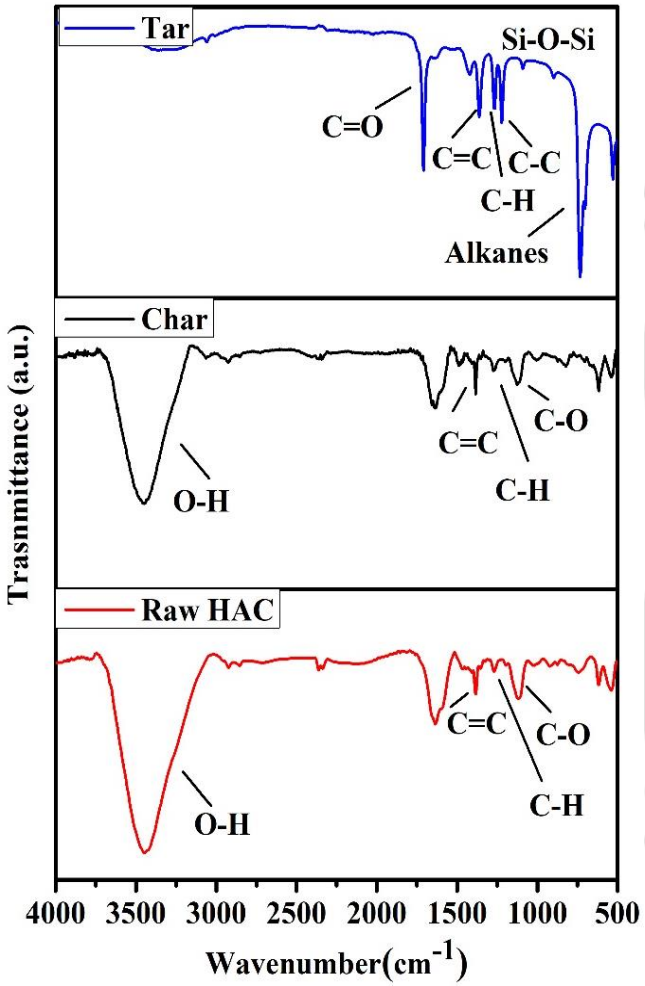

Figure 4.25. FTIR analysis of raw HAC, and its char and tar obtained under N_2 atmosphere

Table 4.7. Comparison of gas conversion, char conversion and CO_2 yield of the present study with literature results.

Fuel- oxygen carrier	FR parameters	CO_2 yield	η_{gc}	X_{char}	References
Bituminous coal (ash 7.8%) - Iron ore	Fluidizing bed, steam, 970°C	92.0%	94.0%		Xiao et al. (2012)
Bituminous coal (ash 15.7%) - Ilmenite	Fluidizing bed, steam, 990°C		90.0%		Pérez-Vega et al. (2016)
Lignite coal (ash 7.1%) - Iron ore	Fixed bed reactor, CO_2, 940°C	99.0%			Bayham et al. (2015)
Sub-bituminous coal (ash 11.3%) - Iron ore	Moving bed, CO_2, 950°C	99.0%			Kim et al. (2013)
Bituminous coal (ash 15.7%)-Ilmenite	Fluidized bed, steam, 990°C			84.7%	Abad et al. (2015)
Pine sawdust (ash 0.4%) – iron ore	Fluidized bed, steam, 915°C			84.0%	Mendiara et al. (2013)
Bituminous coal (ash 4.76%)-Hematite	Fluidized bed, steam, 915°C		96.7%	89.2%	Song et al. (2012)
HAC (ash 33.0%) - Fe_2O_3	Fixed bed, CO_2, 900°C	82.2%	85.5%	87.8%	Present study
RS (ash 12.0%)- Fe_2O_3	Fixed bed, CO_2, 900°C	89.6%	92.4%	93.5%	Present study
LAC (ash 2.1%)-Fe_2O_3	Fixed bed, CO_2, 900°C	85.8%	89.1%	90.9%	Present study

4.4.6.2. GC-MS analysis of HAC based tar

Table 4.8 highlights the tar composition of HAC under N_2 and CO_2 atmosphere. It is seen that alkene content is higher in both the cases, like LAC. The HAC tar components appear different from LAC tar may be due to the change in coal composition and structure. Certain alkene (azafluorene, phenanthrene) and alky groups (benzene 1-methyl-4-phenylmethyl, naphthalene 1,6,7-trimethyl) are found to be negligible in CO_2 atmosphere due to the thermal cracking and CO_2 reforming reactions. Thus, the tar from HAC contains aliphatics (alkane, alkene), aromatics (benzene, naphthalene and its derivatives), oxygenic components (alcohols, ester), and nitrogenous based components (anline, quinoline).

Table 4.8. GC-MS analysis of HAC tar in N_2 and CO_2 atmosphere.

Components	Retention time	Percentage composition (%)	
		N_2 atm.	CO_2 atm.
2,3,5-trimethylphenol	4.35	0.25	0.19
Benzene 1,3 dimethyl	8.75	1.21	1.13
Quinoline	9.23	0.46	0.21
Naphthalene	10.49	1.89	0.51
Aniline	11.02	1.41	0.62
2-methylnaphthalene	12.93	1.06	0.89
6-isopropoxydihydroindole	14.75	0.67	0.12
dibenzofuran	16.00	0.40	0.06
C3 alkyl phenol	16.10	2.35	1.11
n-C16 alkane	17.73	2.58	1.14
Naphthalenecarbonitrile	19.76	2.76	0.42
1,1- biphenyl, 4-methyl	20.34	0.48	0.21
4-nonene,5-butyl	23.65	3.42	2.78
Azulene,1,1-dimethy l-7-(1-methylethyl)	25.44	1.56	1.16
1-octanol,2-butyl	28.71	3.87	1.87

Table 4.8 continued

Components	Retention time	Percentage composition (%)	
		N_2 atm.	CO_2 atm.
7-tetradecene	32.85	0.10	0.04
1,1,4,5,6-pentamethyl-2,3-dihydro-1H-indene	38.79	3.52	2.85
Phenol,2-[(4-hydroxyphenyl)methyl]	34.16	0.68	-
Hexatriacontane	37.41	0.32	-
Azafluorene	17.21	0.55	-
Naphthalene1,6,7-trimethyl	40.21	0.41	-
Benzene1-methyl-4-phenylmethyl	47.28	0.23	-
Phenanthrene	52.27	0.89	-

4.4.6.3. FESEM and BET analysis

The surface morphology of the char produced from pyrolysis is compared with raw HAC in Figure 4.26. Raw HAC is characterized by a smooth surface, while small irregular potholes are observed in the char due to the release of volatiles. This resulted in the increase in the BET surface area from 0.64 m^2/g to 3.07 m^2/g (Table 4.9). The difference in surface area of the gasified HAC and LAC is found to be 2.3 m^2/g, since gasified LAC has a surface area of 13.52 m^2/g. This indicated that the HAC has lower reactivity than LAC.

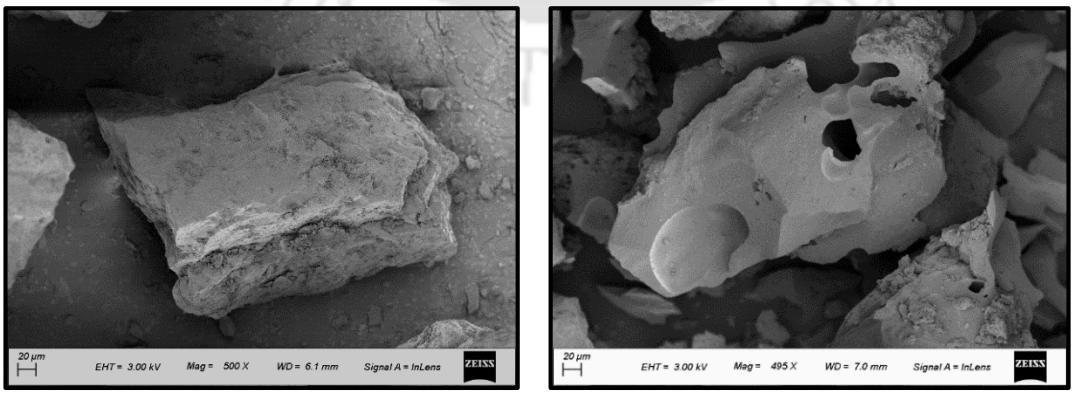

(a) (b)

Figure 4.26. FESEM images of (a) raw HAC, and (b) Pyrolyzed HAC.

The FESEM images of Fe_2O_3 particles after a reduction during the CLC operation are shown in Figure 4.27. The distinct particles of Fe_2O_3 are found as similar to the LAC based CLC residue. In the present study, the oxygen carriers are used for a single run of the CLC operation, which may be the reason for not finding any agglomeration issues with ash. However, these issues may arise during multiple cycle usage of oxygen carriers. Hence, the blend of RS is beneficial during the utilization of HAC.

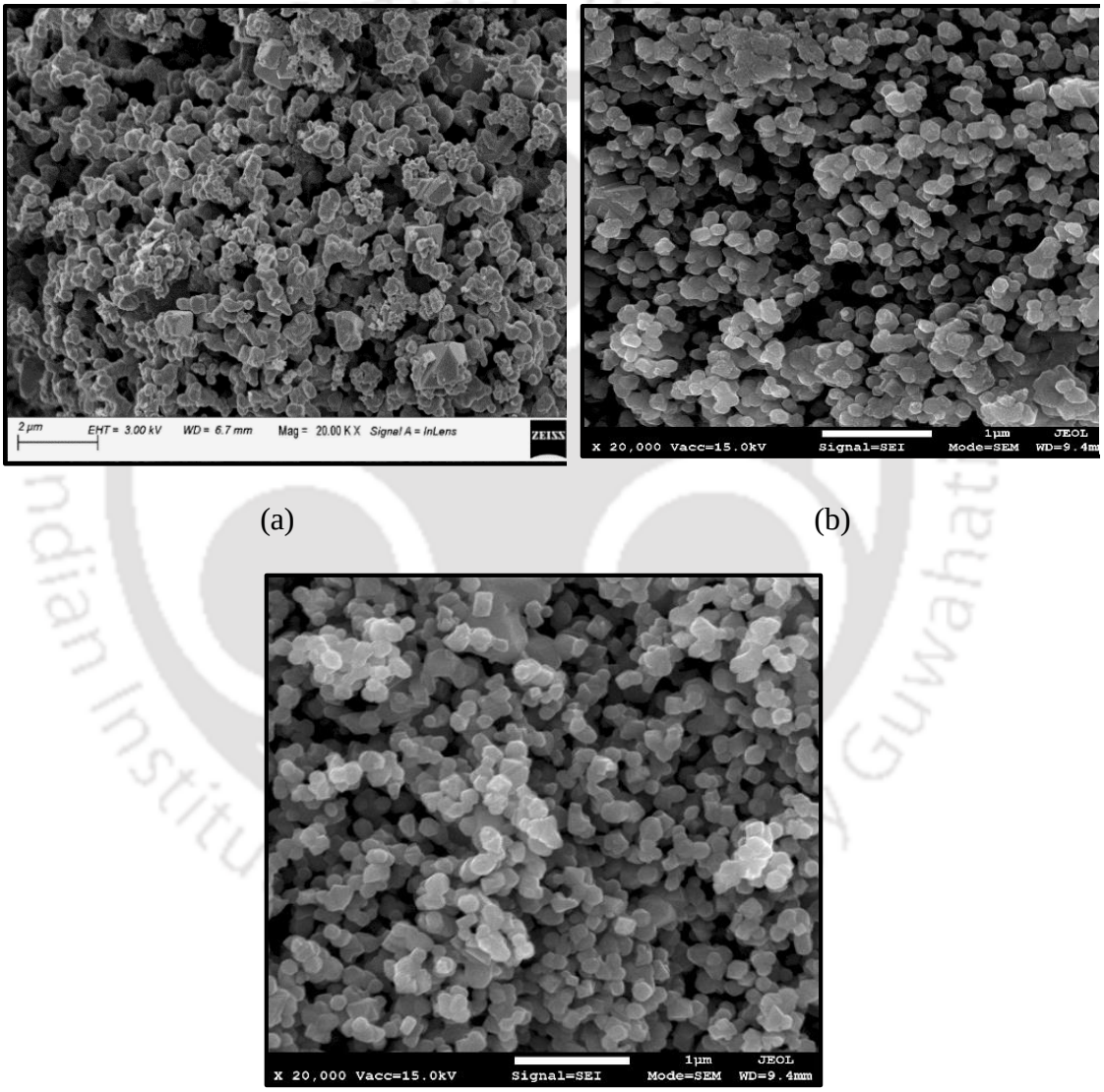

Figure 4.27. FESEM images of the residue obtained during the CLC of (a) HAC-Fe_2O_3, (b) RS- Fe_2O_3, (e) HAC-RS-Fe_2O_3.

The BET analysis of the fresh and the reduced Fe_2O_3 obtained during the CLC operation is shown in Table 4.9. The BET surface area of HAC is 0.6 m^2/g, and thus HAC has a lower surface area than LAC by 0.52 m^2/g. The oxidized Fe_2O_3 particles are found with a higher surface area than the fresh Fe_2O_3. This has occurred mainly due to the enlargement of the pores after the reduction and oxidation process. The surface area of the blend samples has increased by 17-36% after the oxidation process.

Table 4.9. BET Surface area of fresh and reduced residues.

Fuel	Surface area (m^2/g)	Pore volume ($\times 10^{-3}$ cm^3/g)	Pore diameter (nm)
Raw HAC	0.64	3.36	4.59
Pyrolyzed HAC	3.07	4.71	3.9
Gasified HAC	11.25	5.56	3.34
Fresh Fe_2O_3	2.52	5.23	9.34
HAC- Fe_2O_3	2.97	5.48	7.56
RS- Fe_2O_3	3.43	5.77	4.49
HAC-RS- Fe_2O_3	3.11	5.27	5.32

Figure 4.28 shows the photographs of the fresh, reduced and re-oxidized Fe_2O_3 particles. The colour variation in different phases of iron can be observed. Fresh Fe_2O_3 particles (Figure 4.28a) are found red in colour. The reduced particles (Expt. 12) are blackish in colour. However, upon re-oxidation, the colour changes to dark brown. The colour transformation is identical to the residue of LAC-Fe_2O_3 (Expt. 5), RS-Fe_2O_3 (Expt. 6) cases.

(a) (b) (c)

Figure 4.28. Photographs of (a) Fresh Fe_2O_3 with coal (b) CLC residue with reduced Fe_2O_3 (c) reoxidized Fe_2O_3 in air atmosphere.

4.4.6.4.XRD analysis

The fresh HAC and the CLC residue using Fe_2O_3 oxygen carriers obtained during the CLC operations are characterized using the powder XRD. The obtained crystalline peaks of the CLC residue obtained during the reduction (Figure 4.29a) and the oxidation reactions (Figure 4.29b) of the CLC process are found in line with the literature (Song et al., 2012, Zhang et al., 2011). It is observed that there are no complex compounds such as silicates or aluminates formed due to the ash-metal oxide interaction. The characteristic peaks of LAC and HAC are found to be identical. The CLC residue obtained after reduction mainly comprises of Fe_3O_4 and the detection of Al_2O_3 and SiO_2 is due to the ash particles of the fuels. The XRD results of the re-oxidized metal particles confirmed the absence of Fe_3O_4 peaks, and thus complete oxidation may be achieved during the air oxidation process.

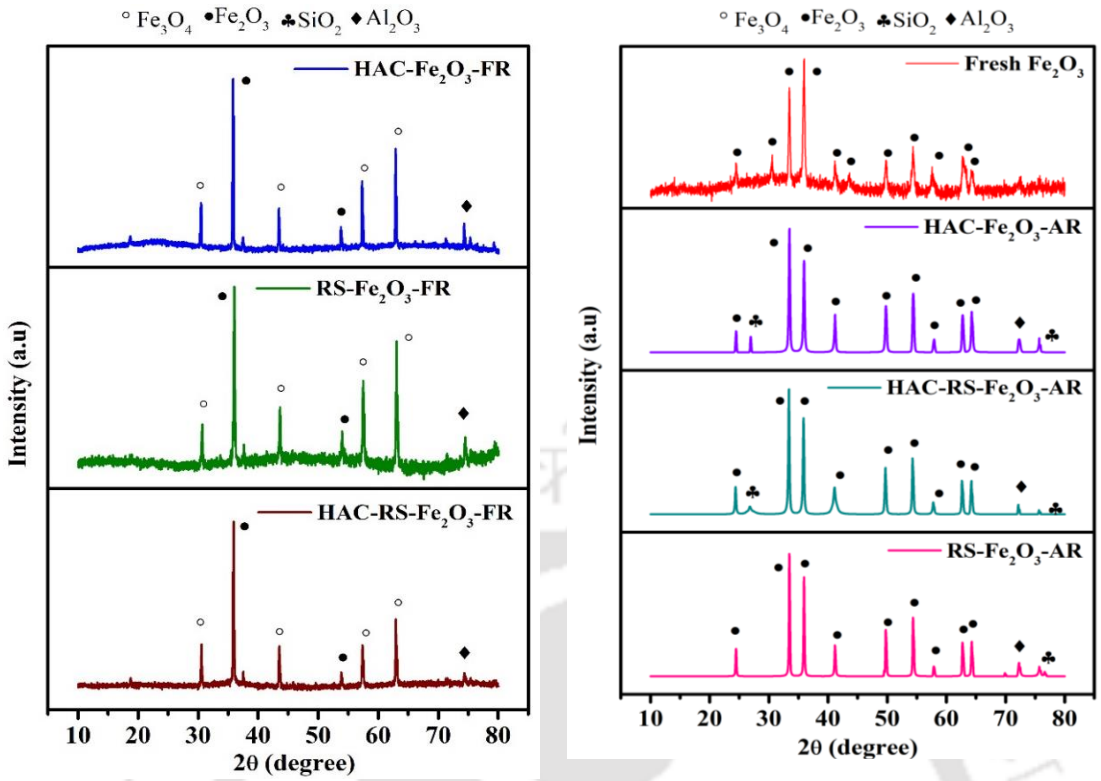

(a) (b)

Figure 4.29. XRD analysis of the residue obtained during (a) HAC-Fe_2O_3 combustion (b) air oxidation of the reduced oxygen carrier.

4.4.6.5. TGA analysis

The CLC process is further conducted in TGA under N_2 and CO_2 atmosphere to evaluate (a) thermal behaviour of fuels (HAC, RS), (b) RS ash-HAC interaction, (c) interaction of released volatiles and syngas with Fe_2O_3 particles, (d) the synergetic effect of HAC and RS in CLC process, (e) solid-solid interaction (char-Fe_2O_3) in inert atmosphere, (f) quantitative analysis of Fe_2O_3 reduction and (g) estimation of activation energy at different temperature intervals using different models.

A. Pyrolysis and gasification of individual fuels- HAC and RS

Figure 4.30 shows the TGA and DTG curves of the raw HAC and RS under N_2 and CO_2 atmosphere. It is interesting to note that the deviation in mass loss between inert and

reactive atmosphere is initiated at 200°C in HAC and continues to increase with an increase in the temperature by 11.5%. However, RS and LAC did not follow the same trend. There is no mass loss deviation till 800°C in both atmospheres. Hence, HAC may contain higher volatiles, which shows reactivity with the supplied CO_2 leading to higher mass loss compared to N_2 pyrolysis. The mass loss in HAC at 800-1000°C (due to the Boudouard reaction) is only 7.3%, while LAC produced a mass loss of 51.3%. A lower degree of conversion is estimated in HAC due to its high ash content. Thus, blending of HAC with RS is appropriate to increase the performance of the gasification process.

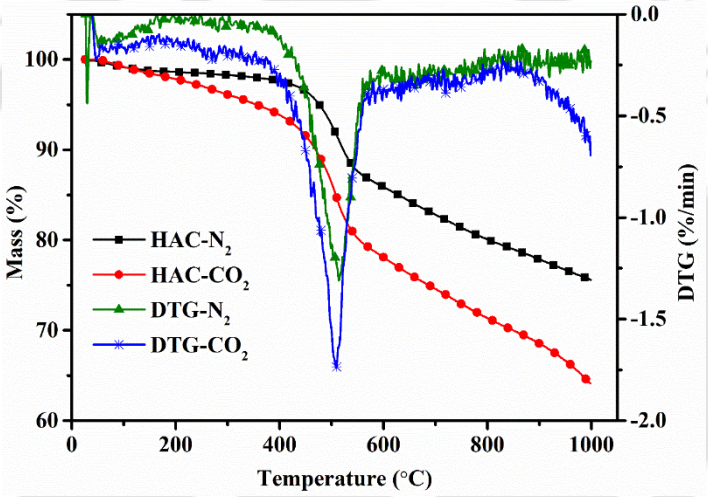

(a)

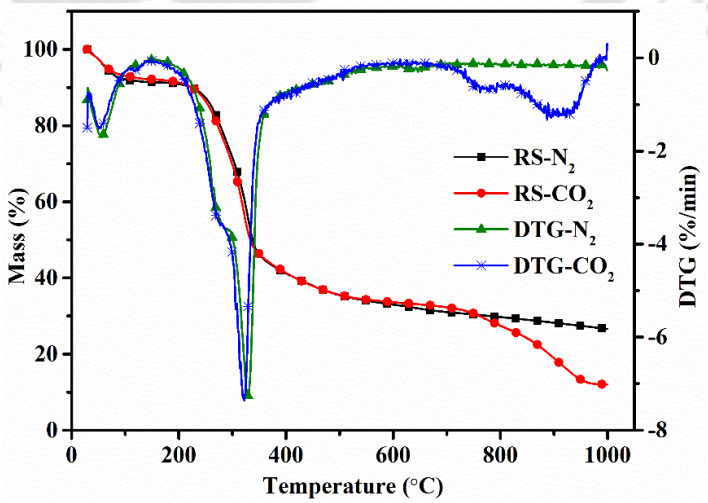

(b)

Figure 4.30. TGA and DTG curve of (a) HAC and (b) RS under N_2 and CO_2 atmosphere.

B. Effect of the addition of RS with HAC in the CLC process

The interaction of HAC with Fe_2O_3 is shown in Figure 4.31 under N_2 and CO_2 atmosphere. The observed mass loss peaks of HAC-Fe_2O_3 are similar to that of LAC-Fe_2O_3.

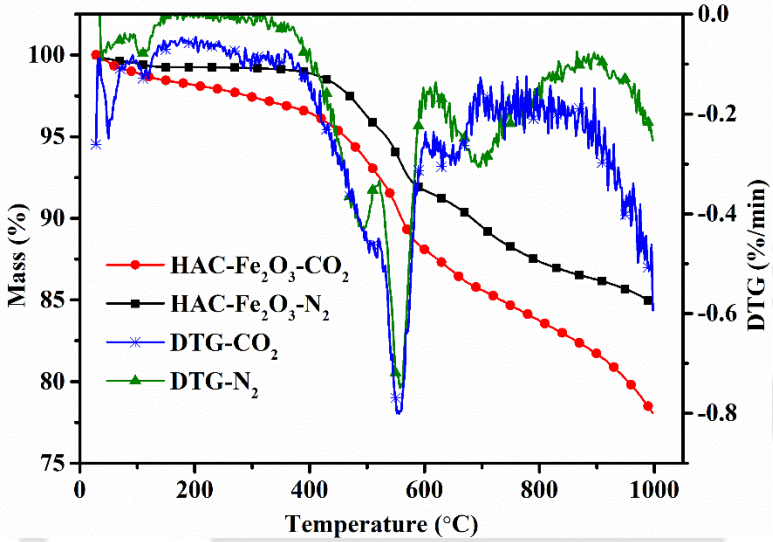

(a)

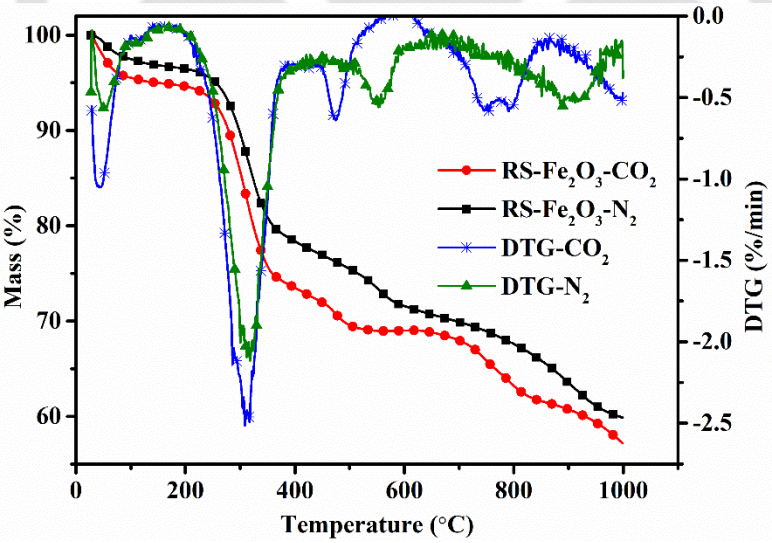

(b)

Figure 4.31. TGA and DTG curve of (a) HAC-Fe_2O_3 and (b) RS-Fe_2O_3 under N_2 and CO_2 atmosphere.

A mass loss of 7-10% at 400-600℃ is noticed due to the interaction of HAC lighter volatiles with Fe_2O_3, while it is 3-5% at 600-800℃ because of the reactivity of heavier volatiles or tar with Fe_2O_3. Finally, the residual char gets gasified with CO_2 and further reacts with the oxygen carriers at 800-1000℃. HAC-Fe_2O_3 and RS-Fe_2O_3 experienced a mass loss of 5.4% and 6.3% at 800-1000℃, respectively, under the CO_2 atmosphere.

C. Effect of RS ash on HAC

Figure 4.32 displays the TGA and DTG curves of HAC with rice straw ash (RSA) in N_2 and CO_2 atmosphere, respectively. The blend of HAC-RSA experienced 20% and 27% mass loss under N_2 and CO_2 atmosphere, respectively. The reactivity between HAC and RSA has exhibited a lower mass loss by 23% than LAC-RSA under CO_2 atmosphere. Further, the interaction of RSA and the char obtained from HAC is tested and a 15% total mass loss in HAC char is accounted. This may be due to the reactivity of calcium ferrite formed in RS with the char content of the HAC (as discussed in the 4A chapter). Hence the ash content of RS is proved to be beneficial even for high ash content coal particles.

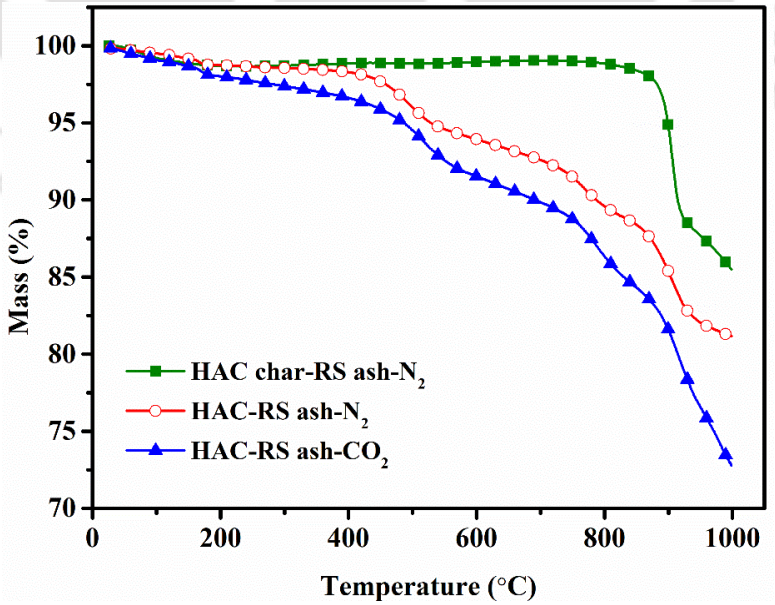

Figure 4.32. TGA analysis on the effect of RS ash on HAC during pyrolysis and gasification.

D. Synergistic effect of HAC and RS in CLC

TGA analysis is conducted for HAC, RS and their blend under CLC conditions to study their synergy. Figure 4.34 shows the actual and estimated weight loss of fuels based on their individual and combined CLC reactivity.

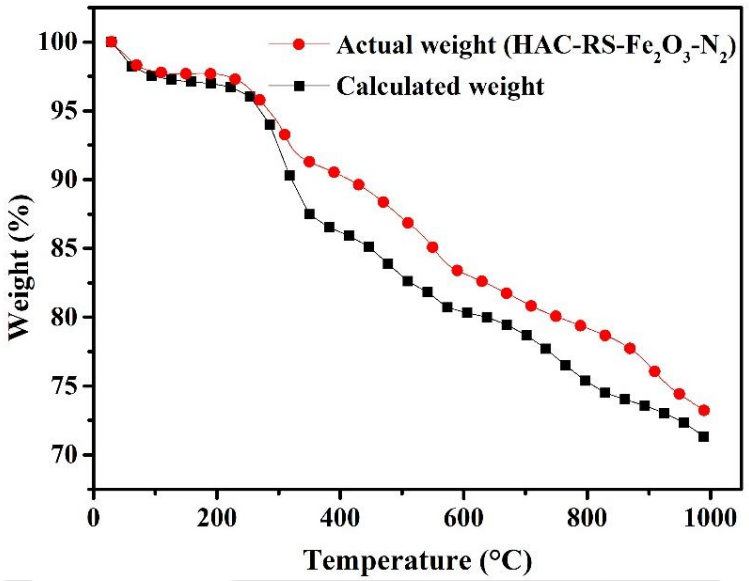

(a)

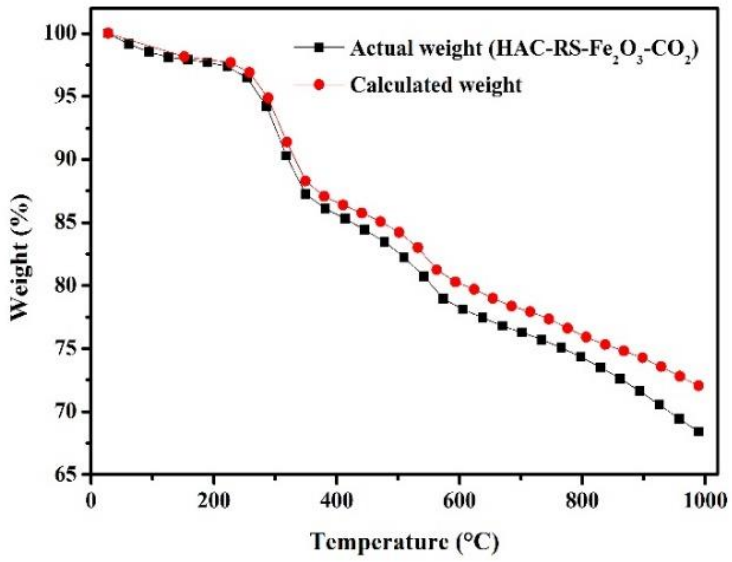

(b)

Figure 4.33. Synergistic effect of HAC blending with RS in CLC mode under (a) N_2 and (b) CO_2 atmosphere.

As similar to LAC-RS blend, it is seen that the HAC-RS blend exhibited a positive synergy with excess weight loss of 1.8% and 3.6% under N_2 and CO_2 atmosphere, respectively. Whereas, LAC-RS-Fe_2O_3 demonstrated a positive synergy with higher weight loss of 2.4% and 7.8% under N_2 and CO_2 atmosphere, respectively. Thus, a higher degree of synergy (4.2%) is observed in the LAC-RS-Fe_2O_3 case, compared to HAC-RS-Fe_2O_3, under CO_2 atmosphere.

E. Reactivity of char with Fe_2O_3

The reactivity of char with Fe_2O_3 is studied under an inert atmosphere to elucidate the solid-solid interaction. It is seen that the HAC char showed a mass loss of 5% in the inert atmosphere, while RS char displayed a mass loss of 21.5% (Figure 4.35). It can be concluded that the rice straw char is more reactive than the coal chars. The LAC char experienced a 7% higher mass loss than the HAC char. The least reactive char is HAC due to its higher ash content. Hence, the addition of RS with HAC would enhance the CLC performance.

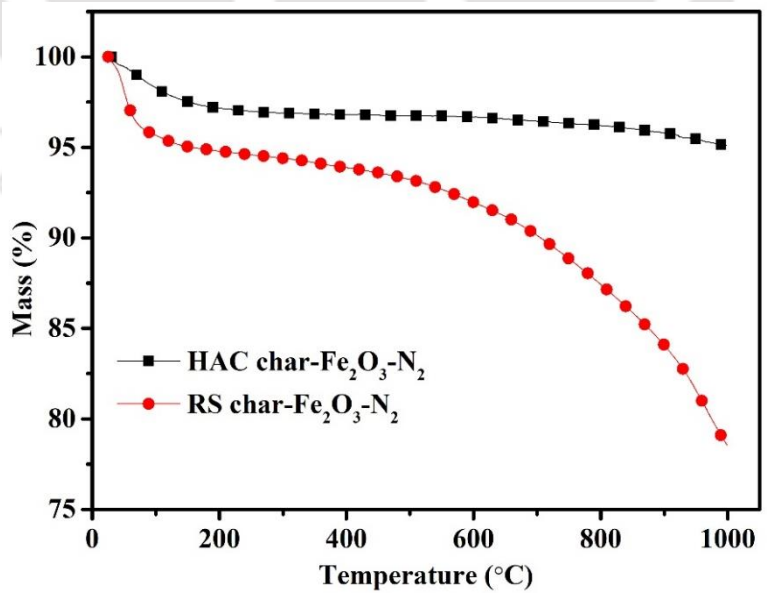

Figure 4.34. TGA analysis of char obtained from HAC and RS with Fe_2O_3 under N_2 atmosphere.

F. *Quantitative estimation of oxygen release from Fe_2O_3*

Figure 4.36 (a) and Figure 4.36 (b) reveal the distinct peaks of the released oxygen during the CLC reactions of HAC-Fe_2O_3 and RS- Fe_2O_3, respectively, under both N_2 and CO_2 atmosphere.

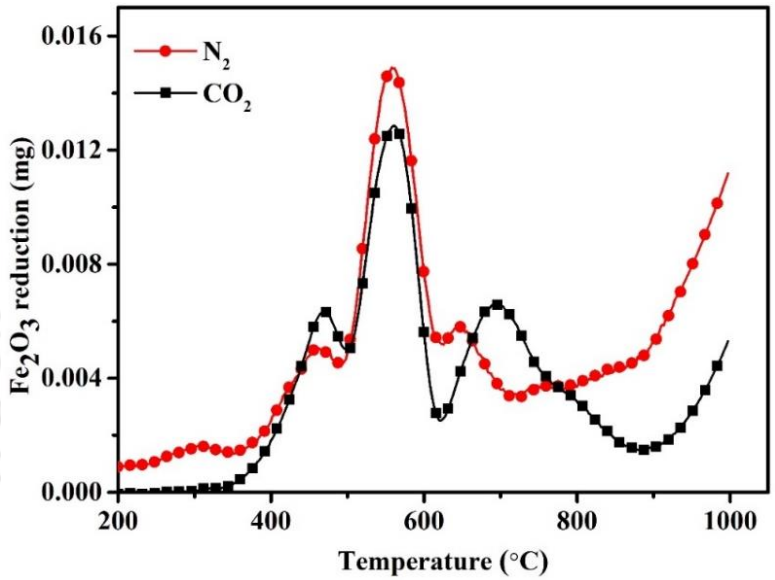

(a)

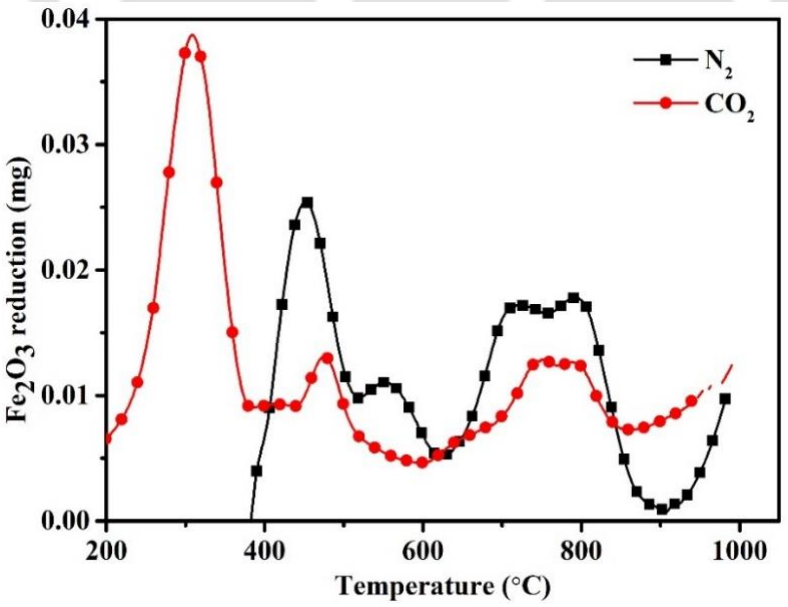

(b)

Figure 4.35. Quantitative analysis of oxygen released from Fe_2O_3 to react with (a) HAC- Fe_2O_3 and (b) RS- Fe_2O_3 under N_2 and CO_2 atmosphere.

The interaction of HAC volatiles with Fe_2O_3 resulted in 0.013-0.016 mg oxygen release from Fe_2O_3 at 400-600°C. The Fe_2O_3 reduction with the HAC is found to be the least, compared to LAC-Fe_2O_3 and RS-Fe_2O_3 cases. Similarly, at elevated temperatures, the released CO due to char gasification reacted with Fe_2O_3 and resulted in metal oxide reduction. The oxygen released from HAC-Fe_2O_3 is found to be 0.011 mg, which is 0.03 mg lower than the RS- Fe_2O_3 case and 0.004 mg lower than the LAC- Fe_2O_3 case. The Fe_2O_3 reduction in HAC-Fe_2O_3 showed an increasing trend even in an inert atmosphere due to the solid-solid interaction. It is seen that reduction of RS-Fe_2O_3 occurred at 900-1000°C even in the N_2 atmosphere. This proves that RS char is more reactive than coal char.

G. Kinetic analysis of coal-Fe_2O_3 reaction

The kinetic analysis of HAC and RS based CLC reactions is carried out using reaction order and shrinking core models. The activation energy is estimated at different temperature intervals at 200-400°C, 400-600°C, 600-800°C and 800-1000°C for the non-CLC and CLC based reactions.

I. Non-CLC reaction (without metal oxides)

Table 4.10 shows the estimated activation energy of HAC, RS and their blends for the models employed under N_2 and CO_2 environment. It is assessed that the shrinking core model (SCM) is found to be the best fit model, compared to the reaction order models at all the temperature intervals based on the correlation coefficient (R^2 values). The activation energy of HAC during devolatilization (400-600°C) is found to be 40.7 kJ/mol and 33.4 kJ/mol under N_2 and CO_2 atmosphere, respectively. It is evident that HAC is the least reactive material since it required higher activation energy than LAC (18.7 kJ/mol) and RS (14.6 kJ/mol). The activation energy at 800-1000°C is found to be 108.1

kJ/mol, which is 18.5 kJ/mol higher than LAC. However, the blend of HAC-RS resulted in the decrease of activation energy from 108.1 to 90.9 kJ/mol.

II. CLC reaction (with metal oxides)

Table 4.11 tabulates the estimated activation energy for the CLC operation under N_2 and CO_2 atmosphere. At 400-600°C, HAC-Fe_2O_3 based CLC reaction required an activation energy of 70.2 kJ/mol and 59.3 kJ/mol, whereas RS-Fe_2O_3 based reaction required 41.8 and 25.3 kJ/mol due to the reactivity of volatiles with Fe_2O_3 under N_2 and CO_2 atmosphere, respectively. Further, the interaction of heavier hydrocarbons from HAC with Fe_2O_3 at 600-800°C resulted in an activation energy of 20.2 kJ/mol and 16.7 kJ/mol under N_2 and CO_2 atmosphere, respectively. The activation energy has increased to 125.6 kJ/mol at 800-1000°C due to the Boudouard reaction and the CO oxidation with Fe_2O_3. The activation energy of HAC-Fe_2O_3 reaction is higher by18.8 kJ/mol than in the case of LAC-Fe_2O_3. The RS exhibited the lowest activation of 87.3 kJ/mol. It is interesting to note that the activation energy of HAC is reduced by 31.7 kJ/mol under blended conditions with RS at 800-1000°C. Hence, the co-utilization of coal and rice straw demonstrated a better reactivity compared to the reactivity of individual fuels.

Table 4.10. Estimation of activation energy for non-CLC reaction of HAC, RS and their blend under N_2 and CO_2 atmosphere.

Fuel	Temperature (°C)	Shrinking core model		1st order reaction model		2nd order reaction model		3rd order reaction model	
		E (kJ/mol)	R^2	E (kJ/mol)	R^2	E (kJ/mol)	R^2	E (kJ/mol)	R^2
HAC-N_2	400-560	40.67	0.97	53.97	0.96	64.73	0.96	76.73	0.95
	600-800	15.23	0.99	9.26	0.99	28.12	0.99	44.87	0.99
HAC -CO_2	400-560	33.38	0.97	36.74	0.97	47.94	0.96	60.75	0.95
	600-800	3.22	0.99	3.47	0.99	15.47	0.99	30.69	0.99
	800-1000	108.12	0.88	93.94	0.84	125.05	0.73	139.26	0.73
RS-N_2	200-400	26.11	0.96	28.93	0.95	37.23	0.95	46.82	0.95
	400-560	8.54	0.98	7.29	0.73	11.94	0.96	26.02	0.97
	600-800	3.47	0.99	13.35	0.89	77.76	0.81	163.09	0.76
RS-CO_2	200-400	14.57	0.97	24.73	0.96	37.52	0.96	47.74	0.95
	400-560	6.25	0.96	5.91	0.95	1.65	0.39	5.57	0.84
	600-800	2.69	0.88	1.66	0.24	14.80	0.85	35.82	0.81
	800-1000	78.59	0.99	35.36	0.98	70.92	0.95	95.62	0.95
HAC-RS-N_2	200-400	23.42	0.98	51.46	0.97	60.36	0.97	70.53	0.97
	400-560	8.10	0.95	6.08	0.82	22.19	0.92	43.27	0.93
	600-800	2.41	0.99	2.28	0.97	25.10	0.99	61.71	0.99
HAC-RS-CO_2	200-400	18.78	0.96	26.25	0.95	30.98	0.95	36.18	0.96
	400-560	1.36	0.97	3.39	0.90	10.59	0.97	19.38	0.97
	600-800	4.35	0.94	10.59	0.86	34.90	0.93	67.03	0.94
	800-1000	90.87	0.80	74.19	0.75	42.63	0.66	75.91	0.76

Table 4.11. Estimation of activation energy for CLC process using HAC, RS and their blend under N_2 and CO_2 atmosphere.

Fuel	Temperature (°C)	Shrinking core model		1st order reaction model		2nd order reaction model		3rd order reaction model	
		E (kJ/mol)	R^2	E (kJ/mol)	R^2	E (kJ/mol)	R^2	E (kJ/mol)	R^2
HAC- Fe_2O_3-N_2	400-560	70.15	0.99	69.31	0.99	80.17	0.99	86.52	0.90
	600-800	20.19	0.99	13.07	0.93	12.53	0.99	48.57	0.95
HAC - Fe_2O_3 -CO_2	400-560	59.26	0.95	42.77	0.93	54.15	0.92	66.79	0.94
	600-800	16.73	0.99	10.19	0.92	26.19	0.99	16.32	0.99
	800-1000	125.59	0.79	132.77	0.74	182.54	0.78	146.26	0.76
RS- Fe_2O_3-N_2	200-400	41.83	0.97	29.92	0.93	38.91	0.96	47.51	0.93
	400-560	8.46	0.99	3.52	0.67	12.23	0.92	20.05	0.93
	600-800	19.33	0.97	14.87	0.95	79.48	0.80	82.82	0.88
RS- Fe_2O_3-CO_2	200-400	25.27	0.94	26.10	0.94	39.61	0.92	46.23	0.93
	400-560	8.28	0.96	11.62	0.50	14.03	0.95	21.53	0.94
	600-800	9.97	0.98	12.03	0.65	23.88	0.98	42.41	0.98
	800-1000	89.96	0.97	90.79	0.92	79.90	0.84	101.69	0.84
HAC -RS- Fe_2O_3-N_2	200-400	48.14	0.94	19.37	0.92	23.47	0.93	28.05	0.93
	400-560	7.88	0.97	3.86	0.86	10.85	0.94	19.32	0.96
	600-800	6.81	0.99	3.76	0.99	21.37	0.99	44.31	0.99
HAC -RS- Fe_2O_3 -CO_2	200-400	32.35	0.97	26.12	0.94	38.60	0.96	44.09	0.96
	400-560	6.5	0.96	6.54	0.79	26.89	0.95	22.89	0.93
	600-800	5.20	0.80	5.15	0.77	38.55	0.78	68.32	0.78
	800-1000	93.91	0.82	75.76	0.81	65.46	0.66	83.35	0.79

4.5. Conclusions

An in-depth analysis of CO_2 based co-utilization of HAC and RS in the CLC process is conducted. The following conclusions can be drawn from these chapters.

- The average gas composition during the HAC pyrolysis is found to be 10.3% H_2, 3.2% CO and 5.1% CH_4.
- The CO_2 yield and gas conversion for HAC-RS based CLC reactions are found as high as 86.3% and 90.2%, respectively. The addition of RS with HAC increased the CO_2 yield and gas conversion by 5.1% and 4.7%, respectively. The char conversion under co-utilization condition is found as 91.4% at 900°C, thereby increasing the char conversion by 3.6% when compared to HAC-Fe_2O_3 case.
- Gas conversion decreased by 3.6% when LAC-Fe_2O_3 is replaced by HAC-Fe_2O_3. CO_2 yield increased by 5.1% for HAC-RS-Fe_2O_3 and 2.3% for LAC-RS-Fe_2O_3 when compared to single feed CLC process.
- No agglomeration or complex formation is observed during the CLC operation of HAC.
- Presence of calcium ferrites ($CaFe_2O_4$, $Ca_2Fe_2O_5$) in RS ash enhanced the CLC reactivity for both the fuels.
- The solid-solid interaction between HAC based char and Fe_2O_3 mixture has resulted in 5% mass loss, while 21.5% loss in RS char is estimated.
- The shrinking core model is the best fitting model for both the non-CLC and CLC based operations.
- The blending of RS with HAC reduces the activation energy by 25.2% at 800-1000 °C.

The present chapter reveals the feasibility of effective utilization of high ash coal with rice straw using Fe_2O_3 as the oxygen carrier. This study has investigated the effect of biomass ash on solid fuels in TGA.

References

Abad, A., Adánez, J., Gayán, P., de Diego, L. F., García-Labiano, F., & Sprachmann, G. (2015). Conceptual design of a 100MW_{th} CLC unit for solid fuel combustion. *Applied Energy*, *157*, 462–474.

Bayham, S., Mcgiveron, O., Tong, A., Chung, E., Kathe, M., Wang, D., Zeng, L., & Fan, L. (2015). Parametric and dynamic studies of an iron-based 25kW_{th} coal direct chemical looping unit using sub-bituminous coal. *Applied Energy*, *145*, 354–363.

Kim, H. R., Wang, D., Zeng, L., Bayham, S., Tong, A., Chung, E., Kathe, M. V., Luo, Chen, D., & Fan, L. S. (2013). Coal direct chemical looping combustion process: Design and operation of a 25kW_{th} sub-pilot unit. *Fuel*, *108*, 370–384.

Lin, B., Zhou, J., Qin, Q., Song, X., & Luo, Z. (2019). Thermal behavior and gas evolution characteristics during co-pyrolysis of lignocellulosic biomass and coal: A TG-FTIR investigation. *Journal of Analytical and Applied Pyrolysis*, *144*, 104718.

Mendiara, T., Diego, L. F. De, Gayán, P., Abad, A., & Adánez, J. (2013). Behaviour of a bauxite waste material as oxygen carrier in a 500W_{th} CLC unit with coal. *International Journal of Greenhouse Gas Control*, *17*, 170–182.

Meng, F., Yu, J., Tahmasebi, A., Han, Y., Zhao, H., Lucas, J., & Wall, T. (2014). Characteristics of chars from low-temperature pyrolysis of lignite. *Energy and Fuels*, *28*, 275–284.

Pérez-Vega, R., Abad, A., García-labiano, F., Gayán, P., Diego, L. F. De, & Adánez, J.

(2016). Coal combustion in a 50 kW_{th} Chemical Looping Combustion unit : Seeking operating conditions to maximize CO_2 capture and combustion efficiency. *International Journal of Greenhouse Gas Control*, *50*, 80–92.

Saw, W. L., & Pang, S. (2013). Co-gasification of blended lignite and wood pellets in a 100 kW_{th} dual fluidised bed steam gasifier: The influence of lignite ratio on producer gas composition and tar content. *Fuel*, *112*, 117–124.

Song, T., Wu, J., Zhang, H., & Shen, L. (2012). Characterization of an Australia hematite oxygen carrier in chemical looping combustion with coal. *International Journal of Greenhouse Gas Control*, *11*, 326–336.

Tian, B., Qiao, Y. Y., Tian, Y. Y., & Liu, Q. (2016). Investigation on the effect of particle size and heating rate on pyrolysis characteristics of a bituminous coal by TG-FTIR. *Journal of Analytical and Applied Pyrolysis*, *121*, 376–386.

Xiao, R., Chen, L., Saha, C., Zhang, S., & Bhattacharya, S. (2012). Pressurized chemical-looping combustion of coal using an iron ore as oxygen carrier in a pilot-scale unit. *International Journal of Greenhouse Gas Control*, *10*, 363–373.

Zhang, S. S. S., Rajendran, S., Henderson, S., Zeng, D., Xiao, R., Linderholm, C. J., Chiron, F., Patience, G. S., Luo, M., Wang, S. S., Wang, L. L., Lv, M., Qian, L., Fu, H., Perejón, A., Romeo, L. M., Lara, Y., Lisbona, P., Martínez, A., Zou, J. (2016). Characterisation of tars from biomass gasification : Effect of the operating conditions. *Fuel*, *157*, 181–189.

Zhang, S., Saha, C., Yang, Y., Bhattacharya, S., & Xiao, R. (2011). Use of Fe_2O_3-Containing Industrial Wastes As the Oxygen Carrier for Chemical-Looping Combustion of Coal: Effects of Pressure and Cycles. *Energy & Fuels*, *25*, 4357–4366.

CHAPTER 5

Utilization of Discarded E-waste as Oxygen Carrier in Co-CLC Technology

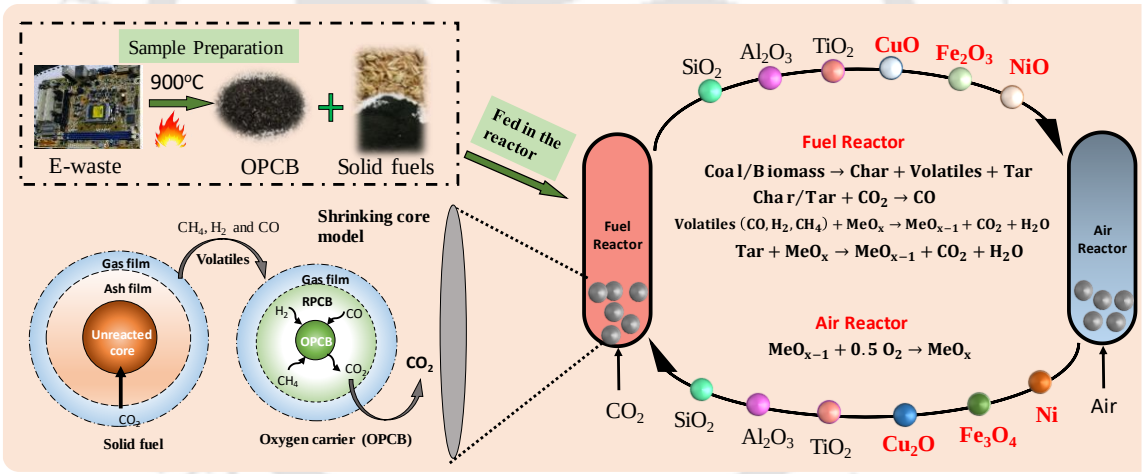

CHAPTER 5

UTILIZATION OF DISCARDED E-WASTE AS AN OXYGEN CARRIER IN CO-CLC TECHNOLOGY

This work discusses the chemical reactivity of coals (LAC, HAC) and rice straw (RS) using the metals extracted from a printed circuit board (PCB) as the oxygen carrier. In the first step, a series of experiments such as pyrolysis, gasification and combustion process has been performed in a fixed bed reactor using the PCB to prepare the oxygen carrier. In the second step, the oxidized printed circuit board based metal oxides (OPCB) are used for the CLC process with coals and rice straw as the fuels mixed in various mass ratios. Further, thermogravimetric analyzer (TGA) studies are conducted to assess the activation energy of the CLC reactions between the fuel and the oxidized e-waste under N_2 and CO_2 atmosphere.

5.1. Experimental description

In this chapter, the performance of e-waste as an oxygen carrier is tested using different fuels viz LAC, HAC, RS and their blend under CO_2 atmosphere. As discussed in Chapter 2, there is no literature available on the utilization of e-waste as an oxygen carrier. The major components in a PCB are indicated in Figure 5.1. Several components such as heat sink, connectors, CPU socket, fan etc. are manually removed prior to the pyrolysis. The photographic of the step-wise procedure for metal oxide preparation is shown in Figure 5.2. The PCB comprises of metallic (metals) and non-metallic components (resins) (Figure 5.2a). The PCB board is first dismantled from the desktop and is sliced into long strips, as shown in Figure 5.2 (b,c,d). The specific sites rejected (marked) in the PCB for the pyrolysis and gasification processes are shown in Figure 5.2(a). The un-marked

sections in the PCB are sliced and used in the pyrolysis. Before pyrolysis, the sliced PCB composed of plastics and metals are mixed at equal proportions (Figure 5.2d). The evenly mixed materials are used in the CLC experiments. The polymers and other volatile components are completely removed by thermal treatment processes (pyrolysis, gasification and further oxidation). The thin strips are then manually cut into small pieces (Figure 5.2e). Pyrolysis followed by gasification processes are conducted to extract the metals from the PCB. During the pyrolysis step, the gas volatiles are liberated and the retained char is gasified during the CO_2 gasification process. The metallic components retained in the residue after gasification is separated out from the non-metallic fractions. The obtained OPCB is further screened to 213 µm size for the CLC operation conducted at 900°C. The pyrolysis and gasification of PCB were carried out to extract the value added chemicals and gases from the wastes. During pyrolysis, the volatiles in the form of H_2, CO, CH_4 etc. are released. After pyrolysis, the retained char is gasified to convert into CO and other gases using CO_2. These calorific valuable gases (H_2, CO, CH_4 etc.) can be used as co-fuels with coal for effective utilization of solid fuels. Also these gases are beneficial since they can be used in spark-ignition engines or power plants (after proper treatment) (Ghodke et al., 2021). Thus, the total output energy of the process can be enhanced by either generating electricity in small facilities or by producing organic components (dimethyl ether, methanol etc.), or biofuels (Condori et al., 2021a, Veses et al., 2021). These high-value added products will compensate the energy penalty (total production cost) of OPCB production. However, the utilization of syngas from PCB is not studied in the present work. Further, Weiland et al. (2021) observed that gasification of plastic waste resulted in lower dioxin production than direct combustion, thereby reducing the environmental issues. Thus, gasification is preceded by combustion to prevent dioxin release.

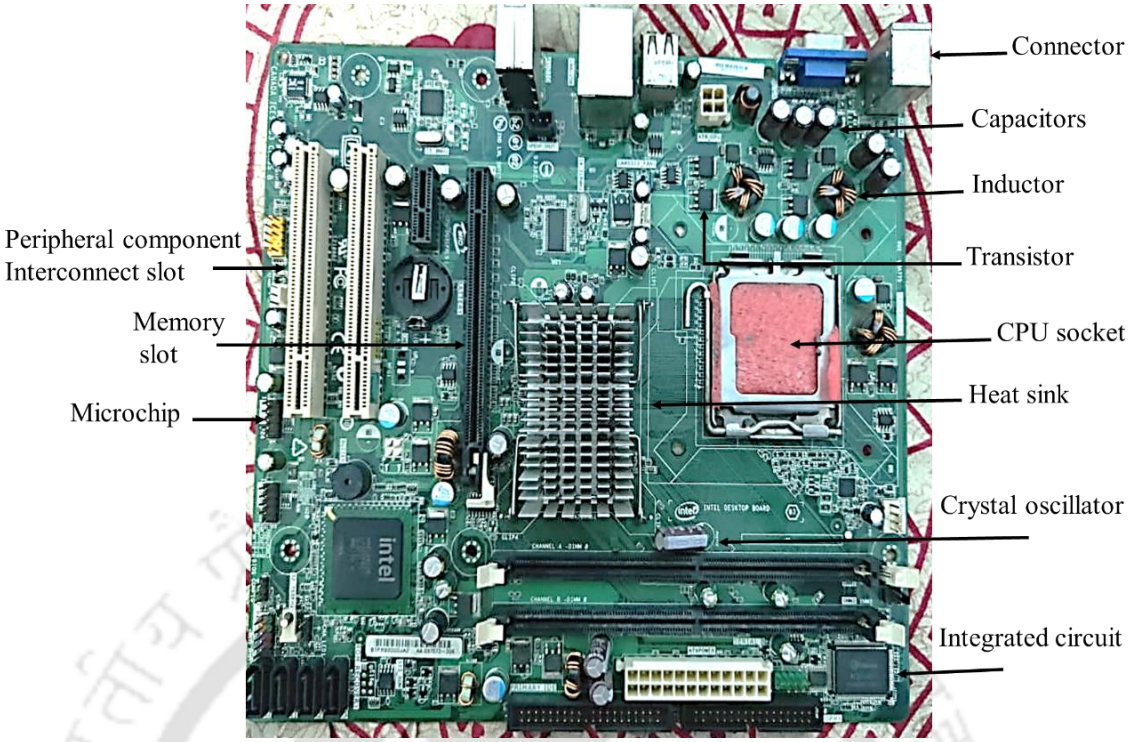

Figure 5.1. Parts of components mounted on desktop's printed circuit board.

Table 5.1 shows the six cases of experiments conducted in the fixed bed reactor with a CO_2 flow rate of 0.8 litre per minute (LPM). Case 1 is the thermal treatment process for preparing oxygen carriers from PCB materials. Case 2 to Case 6 are the CLC based experiments using different fuels under the CO_2 atmosphere. LAC (Case 2), HAC (Case 3) and RS (Case 4) are separately mixed with OPCB at different mass ratios to evaluate the solid fuel conversion. Further, a blend of LAC with RS (Case 5) and HAC with RS (Case 6) is used in the co-combustion process. The theoretical oxygen-carrying capacity of OPCB particles is estimated as 3.65 wt. %. The stoichiometric ratios of OPCB (fuel: OPCB) required are calculated as 1:57 for LAC, 1:45 for HAC and 1:35 for RS. And under co-combustion conditions, it is estimated as 1:50 for LAC-RS: OPCB and 1: 45 for HAC-RS: OPCB for complete oxidation of the fuel. OPCB are solid particles and direct interaction of OPCB with solid fuel (coal, rice straw) is difficult and their solid-solid reactivity would be very poor. Hence the coal needs to be converted into syngas to

further react with OPCB. Hence CO_2 or steam is essential for in-situ gasification based CLC reaction. As stated earlier, CuO liberated their oxygen directly into the gas phase whereas Fe_2O_3 oxidize syngas directly and produce CO_2 and H_2O. The OPCB contains 21.5% Fe_2O_3 and 22.8% CuO, hence it is essential to supply CO_2 for char gasification.

Table 5.1. Summary of the experiments conducted in the fixed bed reactor.

Case No.	Sample	Fuel: OPCB ratio
Case 1	PCB-N_2/CO_2/O_2	-
Case 2	LAC: OPCB-CO_2/air	1:10, 1:20, 1:30, 1:60
Case 3	HAC: OPCB-CO_2/air	1:10, 1:20, 1:30, 1:40, 1:50
Case 4	RS: OPCB-CO_2/air	1:10, 1:20, 1:30, 1:40
Case 5	LAC-RS: OPCB-CO_2/air	1:50
Case 6	HAC-RS: OPCB-CO_2/air	1:45

5.2. Results and discussion

The experimental section comprises of (a) preparation of oxygen carriers from e-waste material by thermal treatment, (b) testing the potential of the e-waste as oxygen carrier with HAC and RS in a fixed bed reactor under CO_2 atmosphere, and (c) estimation of activation energy of HAC, RS with e-waste at different temperature intervals using TGA.

5.2.1. Pyrolysis and gasification of PCB

Table 5.2. Product yield of PCB during pyrolysis at different operating temperatures

Temperature (°C)	Solid yield (wt. %)	Liquid yield (wt. %)	Gas yield (wt. %)
500	75.2	4.6	20.2
700	73.6	5.5	20.9

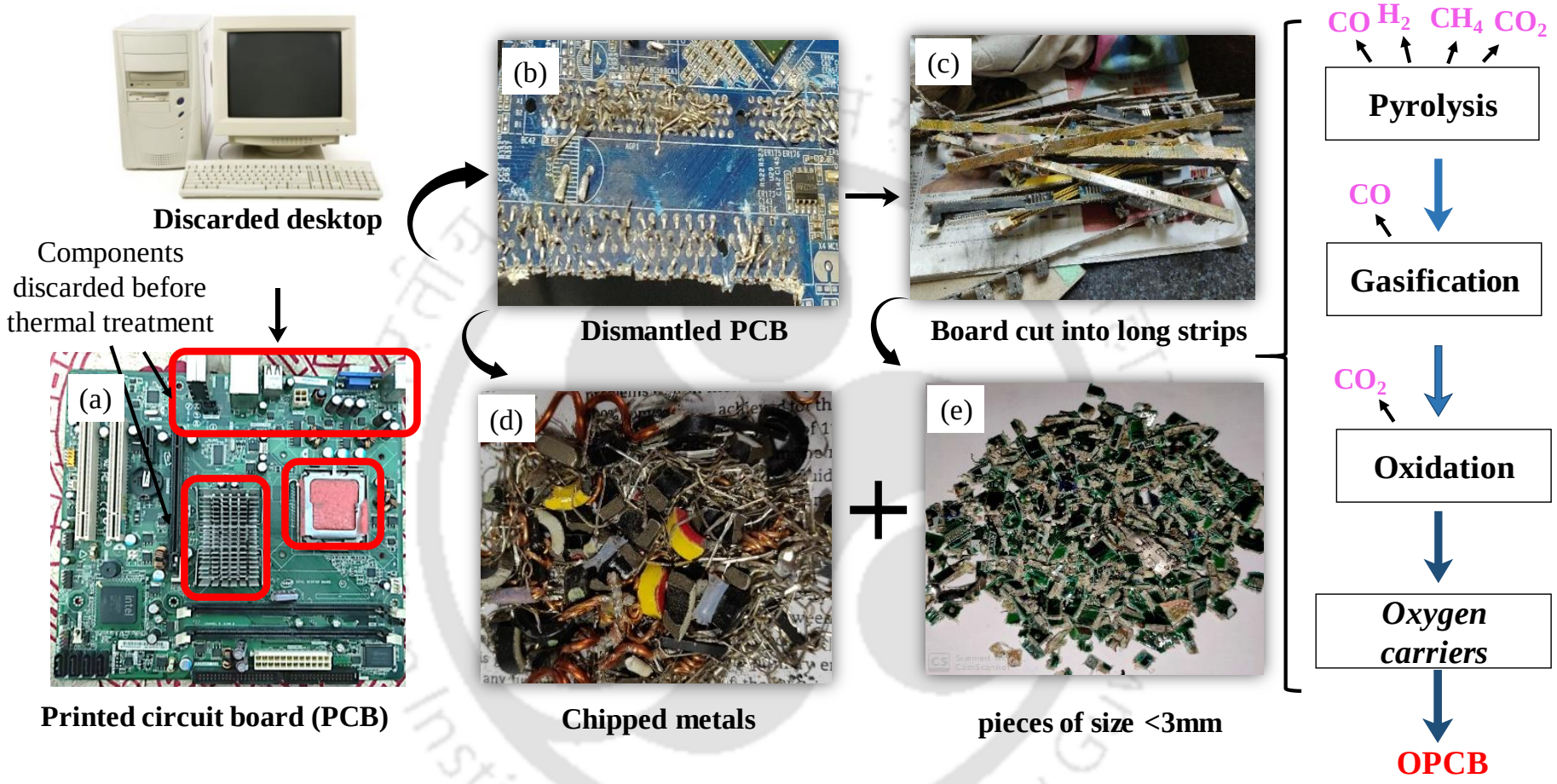

Figure 5.2. Step wise procedure to prepare oxygen carrier from PCB based e-waste.

The yield of solid, liquid and gaseous components obtained during the PCB pyrolysis under isothermal conditions at 500°C and 700°C is reported in Table 5.2. It is observed that there is a slight increase in the liquid and gas yield by 0.7-1.1% (by weight) at 700°C due to the tar cracking reaction. The calorific value of the liquid oil obtained during the PCB pyrolysis is found as 19.9 MJ/kg.

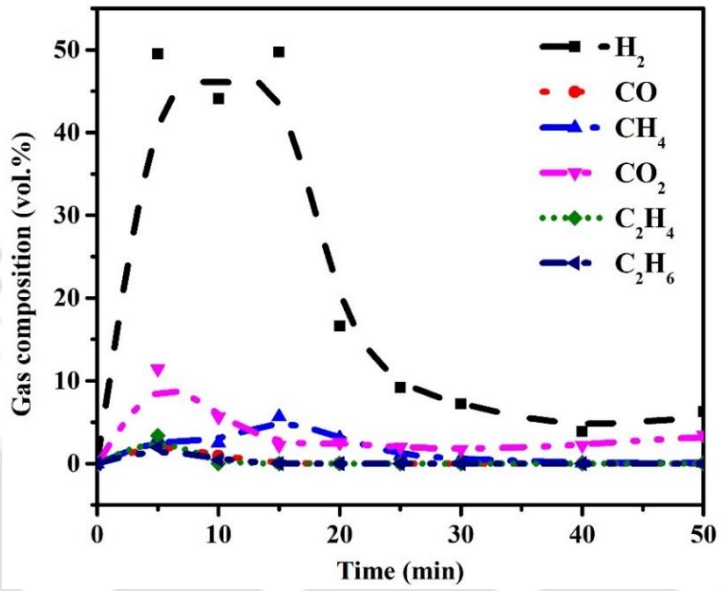

(a)

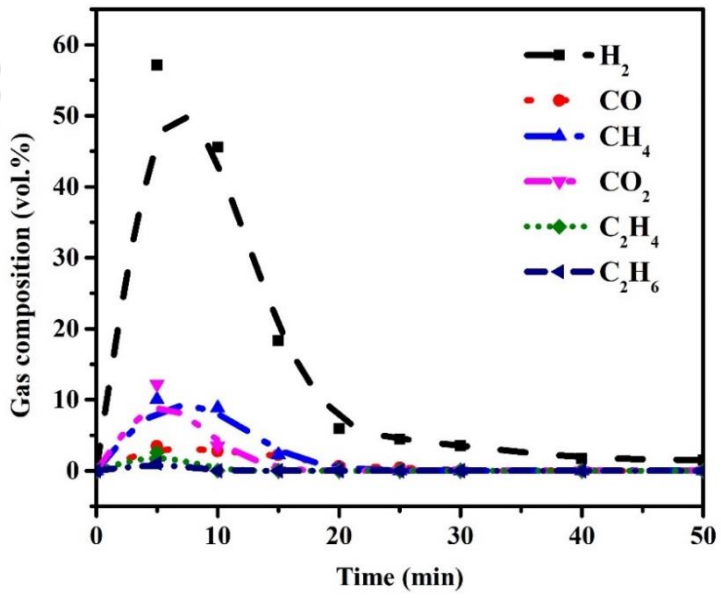

(b)

Figure 5.3. PCB pyrolysis at (a) 500°C and (b) 700°C under N_2 atmosphere.

Figure 5.4 shows the gas composition obtained during the gasification of PCB at 900°C under CO_2 atmosphere. It can be noticed that the H_2 and CH_4 gas are liberated in the range of 20-60% at the beginning of the first 50 min. This could be due to the CO_2 cracking reactions in the retained plastic residues (Eq. 5.1-5.2) (Saad & Williams, 2016, Straka & Bičáková, 2014). Further, the CO is found in the range of 60% in the outlet gas after 50 minutes of the operation due to the char gasification reaction. The CO production is sustained for 175 minutes and declined due to the complete gasification of the residual char.

$$C_xH_y \rightarrow C_{x-(1-4)}H_{(y-n)} + C_{(1-4)}H_n \quad (5.1)$$

$$C_xH_y + xCO_2 \rightarrow 2xCO + (y/2)H_n \quad (5.2)$$

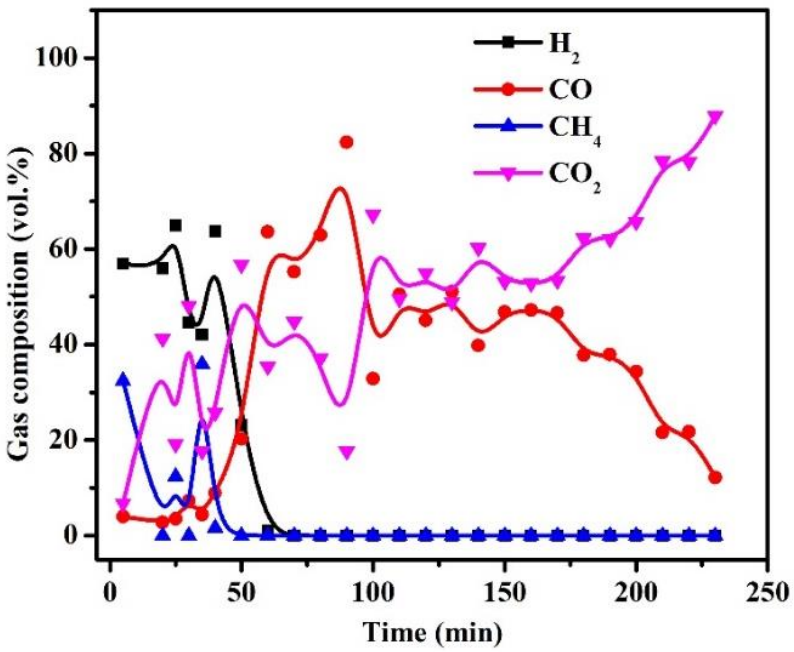

Figure 5.4. PCB gasification at 900°C under CO_2 atmosphere.

The calorific value of the syngas obtained during the PCB pyrolysis (at 500°C, 700°C) and PCB gasification (900°C) is shown in Figure 5.5. It can be seen that the PCB pyrolysis process produced syngas with a calorific value of 6-9 MJ/ m^3 at the beginning

due to the release of H_2 (50-60 vol.%). However, the generation of calorific value gases has decreased drastically within 20 minutes. The average calorific value of the syngas during PCB gasification is found as 6.3 MJ/m^3.

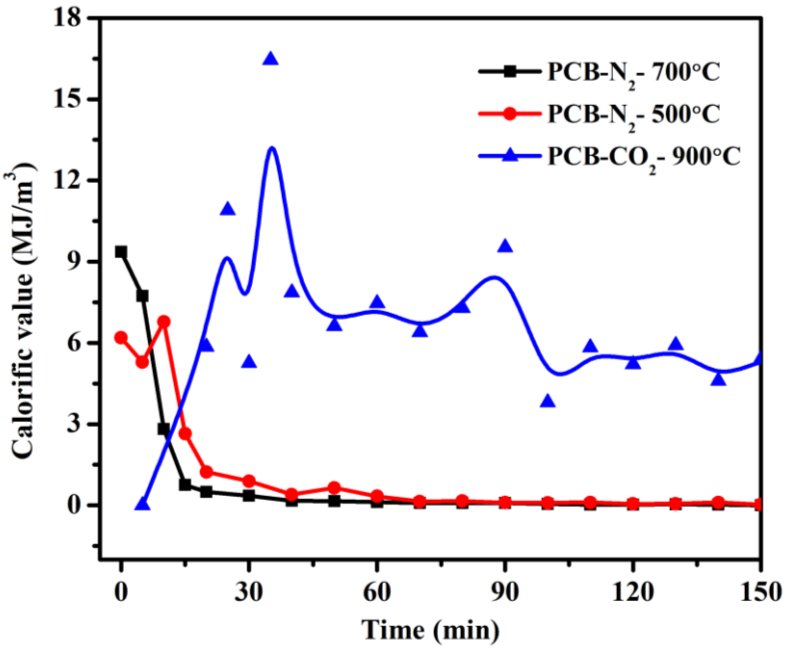

Figure 5.5. Calorific value of the syngas generated from PCB pyrolysis and PCB gasification.

After the gasification process, the retained solid fraction is a mixture of flame retardants, metals and ash. The residues of the PCB based pyrolysis and combustion reactions are shown in Figure 5.6. Figure 5.6(a) shows the pyrolyzed residue containing chunks of flame retardants with metallic components. Figure 5.6(b) shows the gasified residue containing negligible char. Further, the retained metal components are oxidized using atmospheric air for CLC reaction (Figure 5.6c). During the combustion process, the unreacted char is combusted, and the residue is left with only metal-oxide particles. It can be seen that the flame retardants are converted into fine particles. The obtained particles are further screened to a size of 213 µm to remove unconverted resins and products with uneven size (Figure 5.6d).

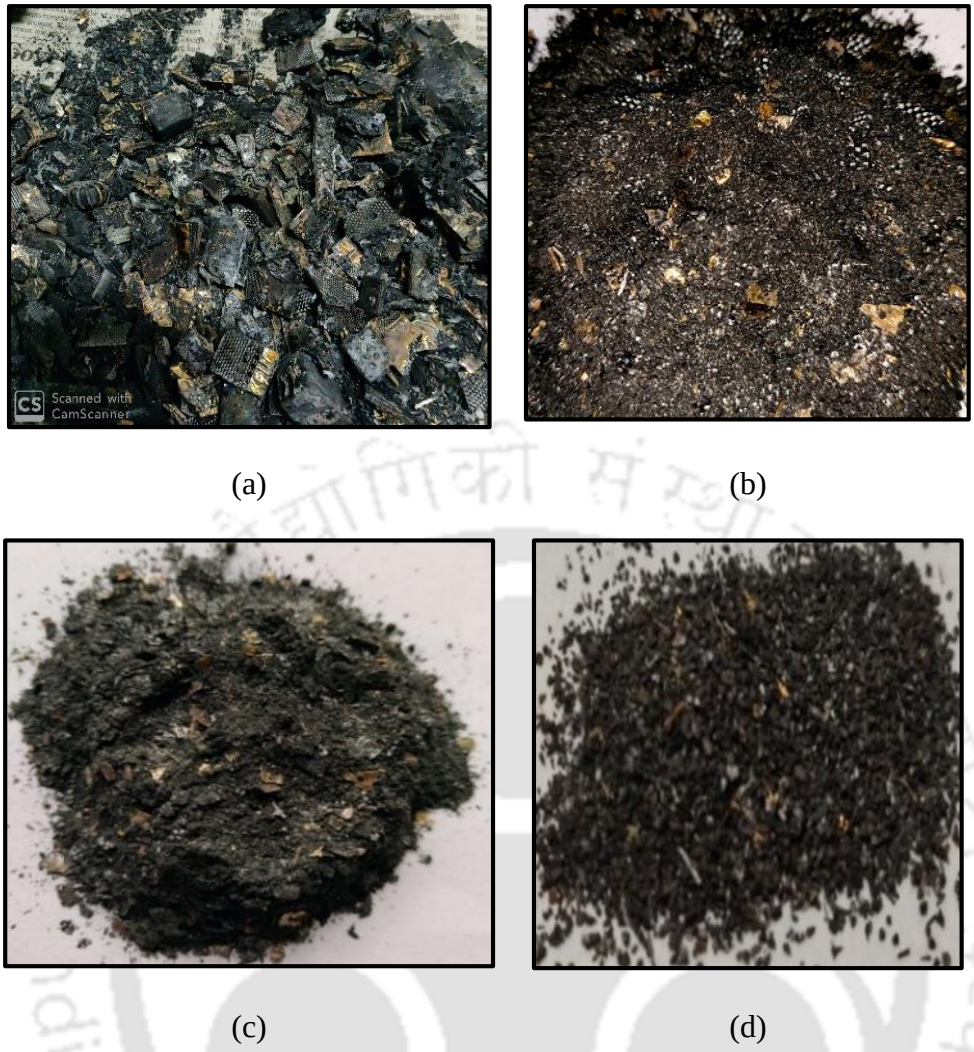

Figure 5.6. Snapshot of residue retrieved after (a) pyrolysis, (b) gasification, (c) combustion, and (d) screening of OPCB after combustion.

The composition of the oxidized residue obtained under the air atmosphere is analyzed using an X-ray fluorescence (XRF) equipment to detect the metal oxides. The e-waste based metal oxides are termed as an oxidized printed circuit board (OPCB). The role of each component in the OPCB mixture during the CLC process is indicated in Table 5.3. The OPCB contains an equal mass of Fe_2O_3 and CuO. As detected by the XRF, the OPCB contains other metal oxides such as ZnO, ZrO_2, Nb_2O_5, As_2O_3, K_2O, SnO_2, PbO, Cr_2O_3 etc. Other metal oxides, excluding Fe_2O_3, CuO and NiO, constitute of 9.4% of the total content. Some of these metal oxides are beneficial as they play multiple roles in the CLC

process such as oxygen carrier, inert support and catalyst. The heavy metal oxides present in the OPCB are PbO (0.98%), Cr_2O_3 (2.84%), Nb_2O_5 (0.17%) and As_2O_3 (0.19%), which are in minor quantities. However, the presence of these fractions has been proved to be beneficial since they act as oxygen carriers in the CLC process (Santos et al., 2019, Bhosale et al., 2020, Sarafraz et al., 2017). As the amount of these components are lower, their role is not significant in the present study. The presence of As_2O_3 in the OPCB is detrimental, however, the CaO (9.58%) present in OPCB can absorb As_2O_3 (Fan et al., 2019). This absorption reaction usually occurs from 600 to 1000°C in oxygen atmosphere (Jadhav & Fan, 2001). The reactivity of SnO_2, PbO and Cr_2O_3 with gaseous fuels has already been reported in the literature (Sarafraz et al., 2017a, Sarafraz et al., 2017b). These metal oxides showed good reactivity with gaseous fuels even after multiple redox cycles. However, PbO has a low melting point that may create agglomeration issues. (Liu et al., 2019). ZnO in the OPCB acts as an inert support for calcium ferrite based oxygen carriers since ZnO has low redox activity. Similarly, Sun et al. (2020) used ZrO_2 as support for Cu-based oxygen carriers. CaO in the OPCB has the ability to adsorb arsenic (Fan et al., 2019) and thus, no hazardous materials may liberate during the CLC operation. Nb_2O_5 particles can exist as oxygen carriers and catalysts in the CLC process (Santos et al., 2019).

As the OPCB is a mixture of metal oxides such as Fe_2O_3, CuO and NiO, the individual oxygen carrying capacity ($R_{o,i}$) of these metal oxides is used to calculate the overall capacity of OPCB ($R_{o,mixture}$). m_{ox} and m_{red} are the mass of the metal oxide under oxidized and reduced state, respectively.

$$R_0 = (m_{ox} - m_{red})/m_{ox} \quad (5.3)$$

Table 5.3. X-Ray fluorescence analysis of oxidized printed circuit board (OPCB) and the roles of each component in the CLC process.

Oxides	OPCB (wt. %)	Role in the CLC process	Reactions	References
Fe_2O_3	21.50	Oxygen carrier, catalyst	$\text{Volatiles } (CO,\ H_2, CH_4) + Fe_2O_3 \rightarrow Fe_3O_4 + CO_2 + H_2O$	Wang et al. (2011), Ma et al. (2021)
CuO	22.83	Oxygen carrier	$\text{Volatiles } (CO,\ H_2, CH_4) + CuO \rightarrow Cu_2O + CO_2$	Dai & Whitty (2019), Wang et al. (2018)
NiO	3.01	Oxygen carrier, catalyst	$\text{Volatiles } (CO,\ H_2, CH_4) + NiO \rightarrow Ni + CO_2 + H_2O$	Chen et al. (2012), Dueso et al. (2010)
CaO	9.58	CO_2 sorbent, catalyst, adsorbs As_2O_3	$CaO + CO_2 \rightarrow CaCO_3$	Rydén & Ramos (2012), Peng et al. (2016), Fan et al. (2019)
Cr_2O_3	2.84	Oxygen carrier	$\text{Volatiles } (CO,\ H_2, CH_4) + Cr_2O_3 \rightarrow Cr + CO + H_2$	Bhosale et al. (2020)
SnO_2	1.62	Oxygen carrier	$\text{Volatiles } (CO,\ H_2, CH_4) + SnO_2 \rightarrow SnO + CO_2 + H_2O$	Sarafraz et al. (2017b), Abanades (2012)

Table 5.3 continued

Oxides	OPCB (wt. %)	Role in the CLC process	Reactions	References
PbO	0.98	Oxygen carrier	$\text{Volatiles } (CO,\ H_2, CH_4) + PbO \rightarrow Pb + CO_2 + H_2O$	Sarafraz et al. (2017b) Sarafraz et al. (2017a)
Nb_2O_5	0.15	Oxygen carrier, catalyst	$\text{Volatiles } (CO,\ H_2, CH_4) + Nb_2O_5 \rightarrow NbO_2 + CO_2 + H_2O$	Santos et al. (2019)
Al_2O_3	10.45	Inert support, catalyst	-	Izquierdo et al. (2021), Shahbaz et al. (2017)
SiO_2	22.56	Inert support	-	Song et al., (2014)
TiO_2	0.62	Inert support	-	Tian et al. (2017)
MgO	1.02	Catalyst, Inert support	-	Hussain et al. (2019)
ZnO	1.77	Catalyst, Inert support	-	Liu et al. (2019)
K_2O	0.19		Catalyst for gasification	Li et al. (2020)

Table 5.3 continued

Oxides	OPCB (wt. %)	Role in the CLC process	Reactions	References
ZrO_2	0.07	Catalyst (improves steam cracking reaction), inert support	-	Wang et al. (2019)
As_2O_3	0.19	Toxic gas can be adsorbed by CaO	-	Fan et al. (2019)
P_2O_5	0.21	Adverse effect due to low melting point, formation of K-Ca phosphates	-	He et al. (2020)
SO_3	0.37	Pollutant, adverse effect with oxygen carriers	-	Pachler et al. (2019)
Cl	0.04	Corrosion agent	-	Aho et al. (2008)

The oxygen carrying capacity of Fe_2O_3, CuO and NiO is evaluated as 3.33%, 10.06% and 21.42%, respectively. The OPCB contains 21.5% Fe_2O_3, 22.8% CuO and 3.01% NiO. Thus, the mass of each metal oxide is taken into account as per the following equation,

$$R_{0,mixture} = x_i . R_{0,i} \quad (5.4)$$

'x_i' is the mass fraction of the individual metal oxides. The $R_{0,\ mixture}$ is calculated as 0.0365 g of O_2/g of OPCB. The amount of oxygen required by the coal as per the ultimate analysis is 2.09 g. Hence, the stoichiometric amount of the fuel to oxygen carriers is found to be 1:57.4 for LAC-OPCB, 1:44.8 for HAC-OPCB and 1:34.6 for RS-OPCB.

5.2.2. Effect of mass ratio of OPCB and solid fuels

To study the CLC behaviour of the oxidized e-waste (OPCB), the solid fuels (LAC/HAC/ RS) are mixed with OPCB at different mass ratios. The obtained outlet gas composition of the reactor with time is shown in Figure 5.7. By changing the mass ratios of OPCB and fuels, the lattice oxygen supplied to the fuel is regulated. As mentioned earlier, the stoichiometric ratios of fuel and OPCB required is 1:57 (LAC: OPCB) for LAC, 1:45 (HAC: OPCB) for HAC and 1:35 for RS: OPCB. Thus, the CLC performances of LAC: OPCB are tested using 1:10, 1:20, 1:30 and 1:60 mass ratios, while HAC: OPCB are tested using 1:10, 1:20, 1:30, 1:40 and 1:50. Similarly, the RS is mixed with OPCB in the mass ratios of 1:10, 1:20, 1:30 and 1:40.

A typical result can be seen that the carbon conversion is significantly improved with an increase in the amount of OPCB. The increase in the quantity of the OPCB particles shows the progress of CLC reactions leading to a decrease in the unreacted CO from 27.4% at 1:10 ratio to 3.4% at 1:60 ratio for LAC (Figure 5.7a), while in the case of HAC, the CO is reduced from 20.4% at 1:10 ratio to 4.2% at 1:50 for the HAC (Figure 5.7b). Similarly, the unconverted CO from RS has reduced from 17.8% to 3.3% when the mass

ratio is increased from 1:10 to 1:40 (Figure 5.7c). The H_2 gas also exhibited a similar trend in the composition like CO in all the fuels. One can notice that the CH_4 gas is oxidized quickly, and the higher hydrocarbons could not be observed in the outlet gas.

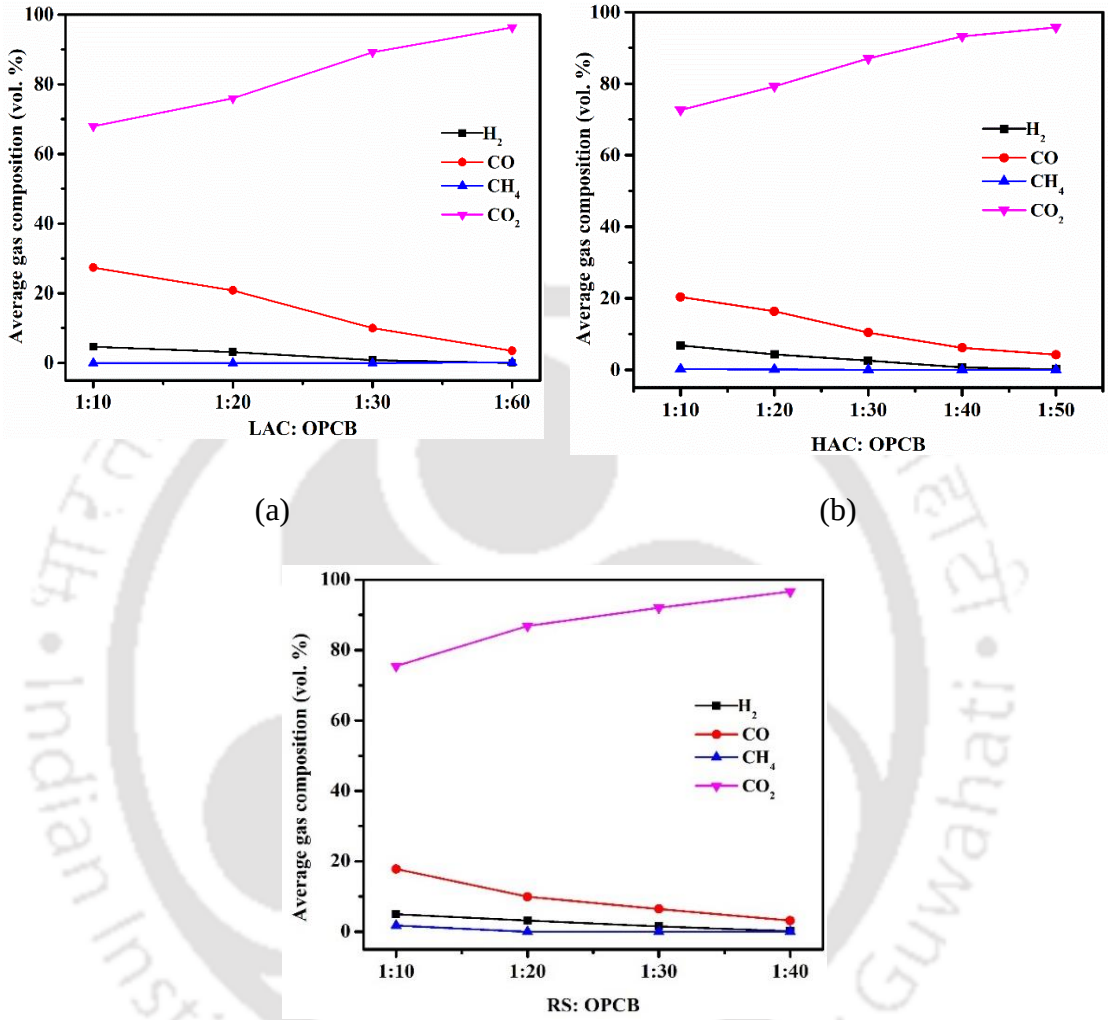

Figure 5.7. The obtained gas composition at different mass ratios using (a) LAC: OPCB and (b) HAC: OPCB and (c) RS: OPCB.

The CO_2 concentration had increased with the increase in mass ratios of OPCB for all the cases. The CO_2 concentration has increased from 67.9% at 1:10 ratio to 96.8% at 1:60 ratio in the case of LAC-OPCB mixture, while it is increased from 72.6% to 95.7% when the mass ratio of HAC to OPCB mixture is increased from 1:10 to 1:50. In the case of

RS, the CO_2 concentration has increased from 75.5% to 96.7% at the OPCB mass ratios increased from 1:10 to 1:40.

5.2.3. CLC reactivity during co-gasification of coal and RS with OPCB

The reactivity of OPCB particles with the blended fuels at equimass ratio (1:1) is assessed. The comparison of the blends (LAC-RS, HAC-RS) with the pure are shown in Figure 5.8. A mass ratio of 1:50 (LAC- RS: OPCB) and 1:45 (HAC-RS: OPCB) are used in the co-CLC study. The fuel-OPCB ratio is maintained as per the stoichiometric amount as discussed in Table 5.1. As the RS has an ability to release volatiles earlier than the HAC, the CLC reaction of volatile oxidation in RS required lower residence time (75 min) than the coal based CLC combustion (100 min). The mixing of RS with LAC and HAC has increased the reactivity, compared to the coal alone as fuel. The average composition of the unconverted H_2 and CO is found to be 0.08% and 3.4% during the co-CLC process (HAC-RS: OPCB), which resulted in reducing the unconverted fractions by 13% and 18%, compared to HAC as the fuel. The gas concentration profiles from Figure 5.8 are compared with Xiao et al. (2010). They conducted the CLC process in a fixed bed reactor using coal and iron ore with steam as the gasifying agent at 970°C. The obtained residence time (80-100 min) is found to be higher by 25min than the reported literature. The deviation between the results could be due to differences in the operating conditions: (a) operating temperature was 70°C higher in the reported literature, (b) inlet gas flow was 1L/min, while 0.8 L/min is maintained in the present study and (c) coal size of 180µm and iron ore of 125µm were taken by Xiao et al. (2010), while we maintained the particle size somewhat larger (212µm). Similarly, LAC-RS: OPCB reduced the unreacted CO by 19%. Thus, the blend of HAC with RS and LAC with RS showed better performance than the pure HAC and LAC as the fuels.

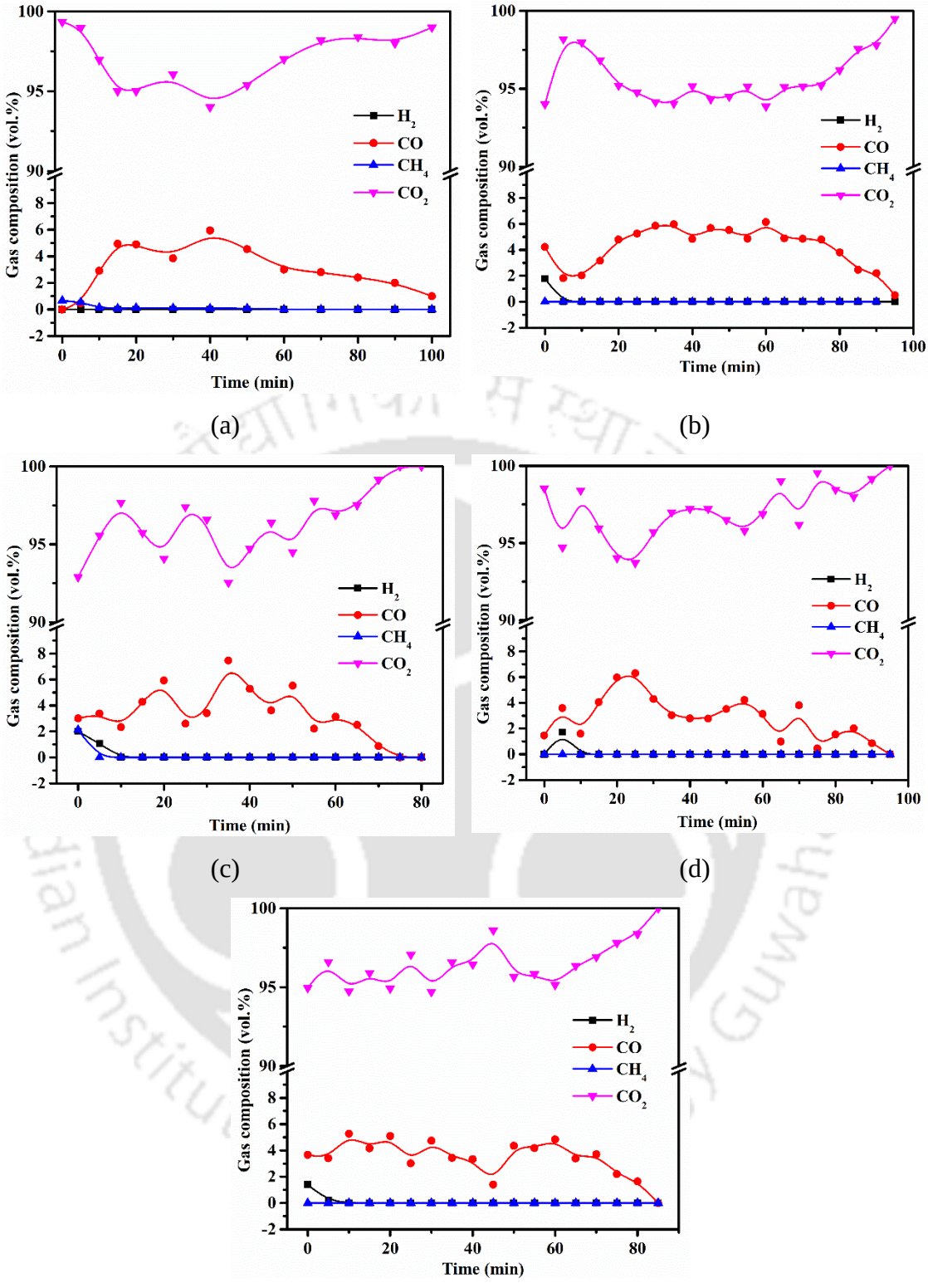

Figure 5.8. Variation of gas composition for (a) LAC-OPCB (1:60), (b) HAC-OPCB (1:50), (c) RS-OPCB (1:40), (d) LAC-RS-OPCB (1:50) and (e) HAC-RS-OPCB (1:45).

5.2.4. Determination of gas conversion, CO_2 yield, char conversion

Gas conversion, CO_2 yield and char conversion are evaluated to examine the reactivity of the OPCB based oxygen carriers. The variation of the key parameters during the co-CLC process is shown in Figure 5.9. The results clearly indicate the positive effect of using blend instead of coal alone as the fuel. The gas conversion and CO_2 yield are found to be 93.8% and 90.4% for LAC fuel, 90.6% and 86.1% for HAC fuel, while 96.5% and 93.8% for RS, respectively. The CO_2 yield is improved from 90.4% to 92.8% when LAC is replaced by LAC-RS mixture, while 86.1% to 90.9% when HAC is replaced by HAC-RS mixture. The average gas conversion is also found to be increased by 1.9-3.5% for the blended fuels. The deviation in CO_2 yield between the two coals is 4.3%. It is due to high ash content in the coals leading to hindrance for complete fuel conversion. The char conversion is found to be above 94% for the LAC-based fuels, while 90% for HAC-based fuels. However, under blended conditions, the conversion has increased by 2.5% for LAC-RS, 3.6% for HAC-RS blended fuels.

The obtained values are in concordance with the results obtained by Cuadrat et al. (2011), Abad et al. (2012). Cuadrat et al. (2011) obtained a char conversion of 82% at 950°C using a bituminous coal with ilmenite as oxygen carriers. Abad et al. (2012) used coal and CuO as the feed mixture and obtained 95.8% char conversion and 96% CO_2 yield. It is usually seen that the Cu-based oxygen carriers achieve a higher fuel conversion rate than the Fe-based oxygen carriers due to their CLOU nature. The OPCB showed slightly higher reactivity than pure Fe_2O_3 for all the fuels. It is seen that the CO_2 yield has increased for OPCB oxygen carriers by 4.6% for LAC, 3.9% for HAC and 4.2% for RS, compared to Fe_2O_3 alone as the metal oxides. This is due to the CLOU nature of CuO present in the OPCB. It is seen that the overall CO_2 yield in OPCB-based CLC increased by 5% approx. when compared to Fe_2O_3, since the contribution of CuO in OPCB is only

23% (Table 3.2). Hence, e-waste based oxygen carriers have shown equivalent performance in the CLC reactions to that of Fe_2O_3 particles.

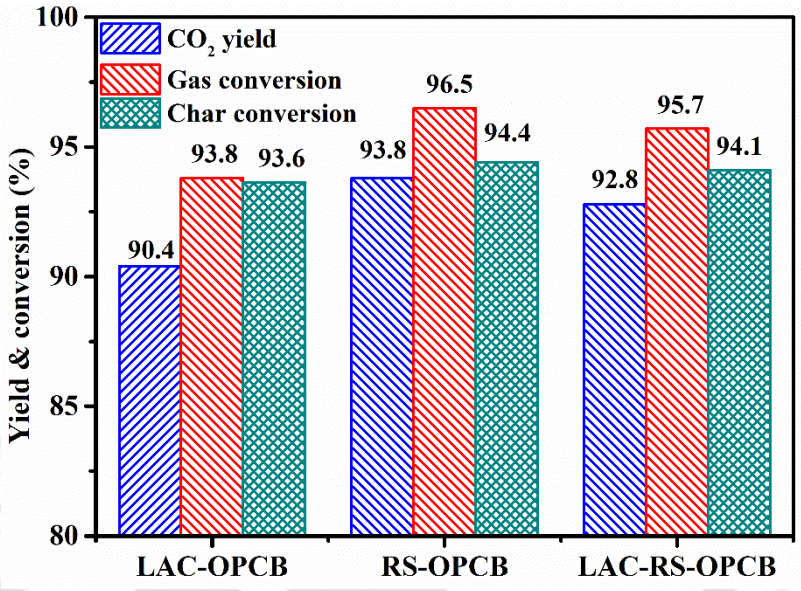

(a)

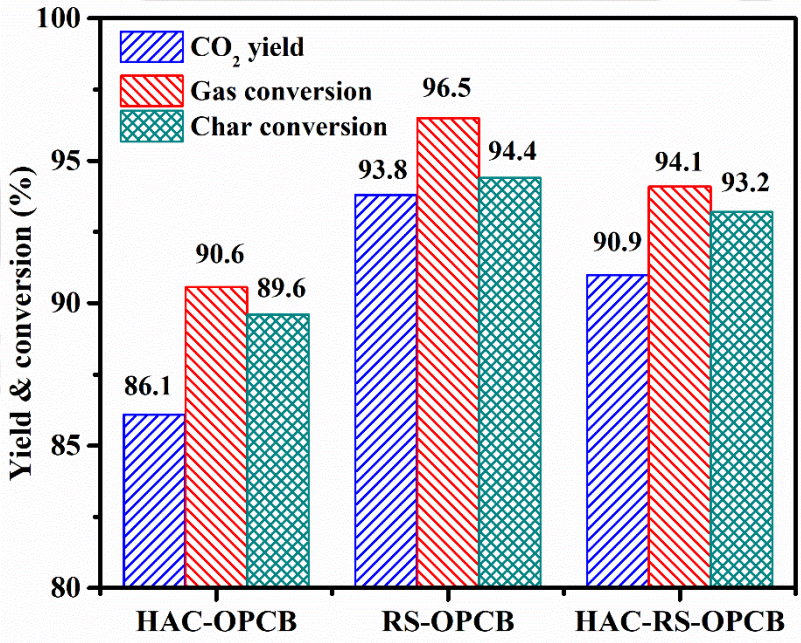

(b)

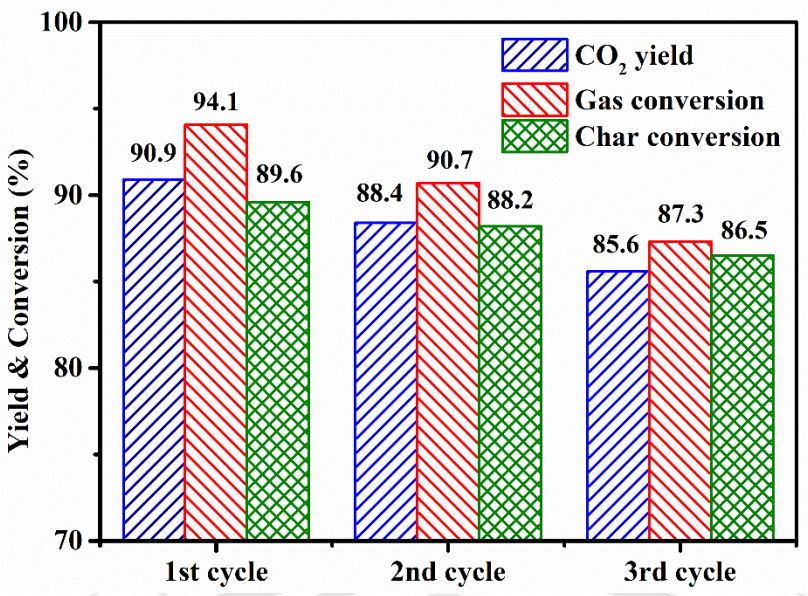

(c)

Figure 5.9. Variation of CO_2 yield, gas conversion and char yield with different feedstock using (a) LAC, RS and their blend, (b) HAC, RS and their blend and (c) multiple cycles of oxidation and reduction at co-combustion conditions with 0.5:0.5:45 mass ratio of HAC-RS-OPCB.

5.2.5. Post-CLC characterization of OPCB

5.2.5.1. XRD analysis of raw PCB and its residue

Figure 5.10(a) provides the XRD analysis of the PCB samples taken at different locations of the board. It is observed that the metallic portion of PCB is masked by the polymers. Thus, the obtained peaks are not sharp in most of the cases as the polymers are amorphous in nature. It is observed that the Cu, Ni, Fe metals in the PCB are not found in the oxidized form (Figure 5.10a). The XRD peaks of pyrolyzed PCB and their oxidized residue are shown in Figure 5.10(b). The pyrolyzed residue had shown the peaks mainly for Cu, Ni, Sn, CuO, Fe_3O_4 and FeSi. Further, the oxidized PCB residue is found with the oxidized form of metals such as Fe_2O_3, CuO, PbO, SnO_2.

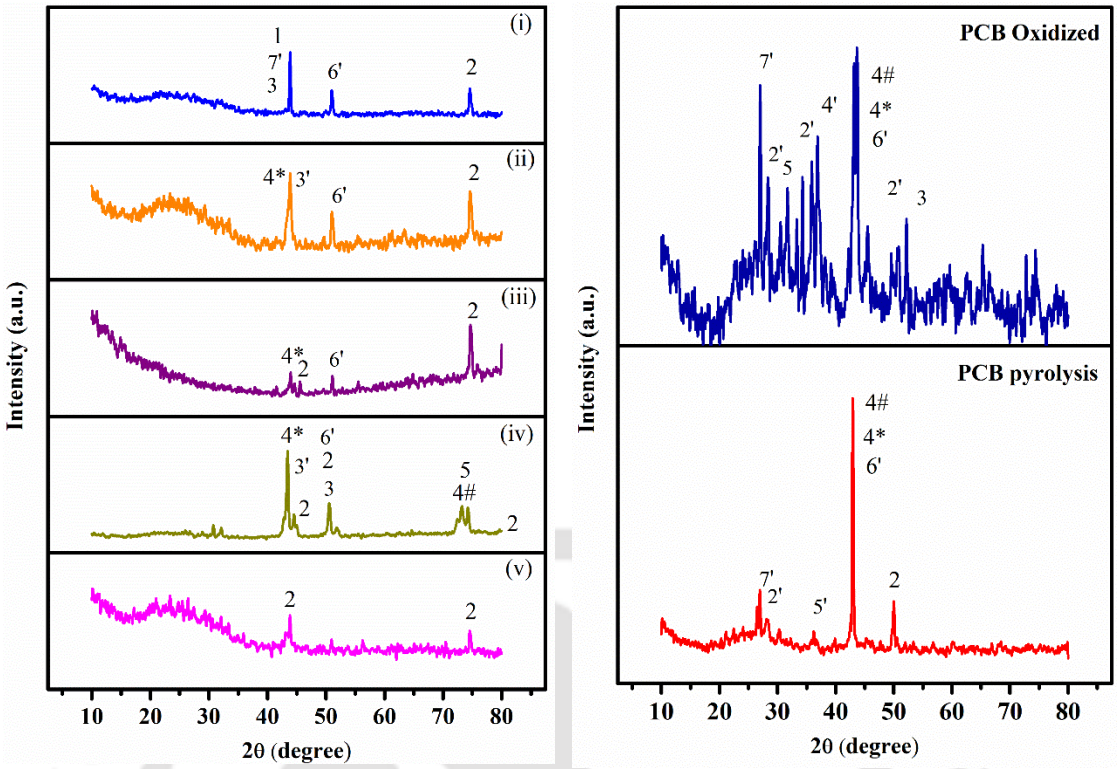

(a) (b)

Figure 5.10. XRD analysis of (a) raw PCB taken from different locations of the board (i-v), (b) residue of PCB pyrolysis and its subsequent oxidation (1 Hg, 2 Cu, 2' CuO, 2* CuSn, 3 Ni; 3' NiO; 4 Fe; 4' Fe_2O_3; 4# Fe_3O_4; 4* FeSi; 5 Sn; 5' SnO_2; 6 Si; 6' SiO_2; 7 Pb; 7' PbO; 7# $PbSO_4$).

5.2.5.2. FESEM and BET analysis

Figure 5.11 shows the surface morphologies at a magnification of 20,000X for different residues obtained after the CLC reactions. The OPCB particles are found spherical in shape (Figure 5.11a). Figure 5.11 (b-f) shows the abundant fine particles embedded over the OPCB oxygen carriers having no cohesion between the ash and the OPCB particles. The sintering phenomena could not be observed even for the residue of coal with high ash content. Discrete OPCB particles are observed in each case, indicating the thermal stability of the OPCB particles. This could be attributed to the presence of 33.63% of SiO_2, Al_2O_3 and TiO_2 in the OPCB, which prevented the agglomeration and sintering

issues. Thus, the limitation of Cu-based oxygen carrier (agglomeration) can be mitigated by the mixed metal oxides. Similar observations are reported by Wang et al., (2010) as they observed a lower agglomeration tendency of CuO-Fe_2O_3 mixture, compared to CuO alone. Thus, the OPCB containing mixed metal oxides with inherent inert materials has proved to be beneficial for the CLC process.

Table 5.4 shows the BET surface area of the OPCB particles before and after the oxidation test. The BET surface area of the pyrolyzed and the gasified PCB is 13.8 m^2/g and 19.5 m^2/g due to the formation of the porous structure as compared to the raw PCB. During the char gasification, the CO_2 gas diffused into the pores and reacted with fixed carbon in the pyrolyzed PCB. This has increased the BET surface area by 5.7 m^2/g. The BET surface area of the fresh OPCB particles is found to be 7.1 m^2/g. Thus, the surface area of OPCB is 4.6 m^2/g higher than pure Fe_2O_3 (Table 4.2), thereby signifying higher porosity. An interesting result is that the surface area of the re-oxidized OPCB particles after the reduction process are found to be increased by 21.6% (LAC-OPCB), 14.5% (HAC-OPCB), 26.0% (RS-OPCB), 31.1% (LAC-RS-OPCB) 24.9% (HAC-RS-OPCB) as compared with the fresh OPCB. This may be due to the (i) enlargement of the existing pores in OPCB particles or (ii) the formation of new pores. This indicates that the OPCB particles are well regenerated without facing any sintering issues. The average pore volume of the oxidized residue particles is larger than the raw OPCB particles. This has enabled higher diffusion of gases, thereby enhanced the reactivity. As there is no reduction in the surface area of OPCB particles, it confirms that there is no ash deposition on the oxygen carriers (OPCB), as confirmed by the BET results.

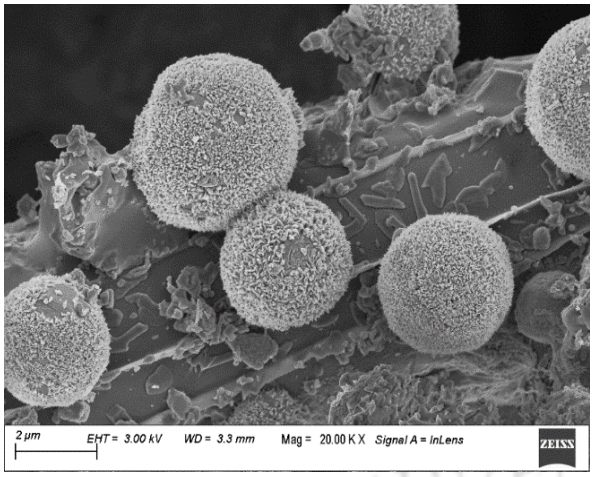

(a)

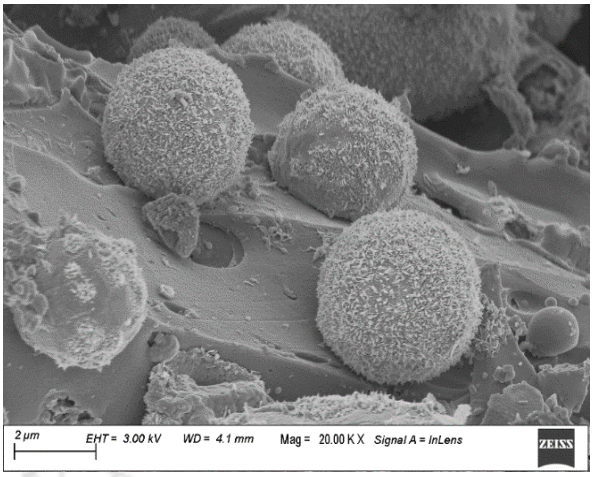

(b)

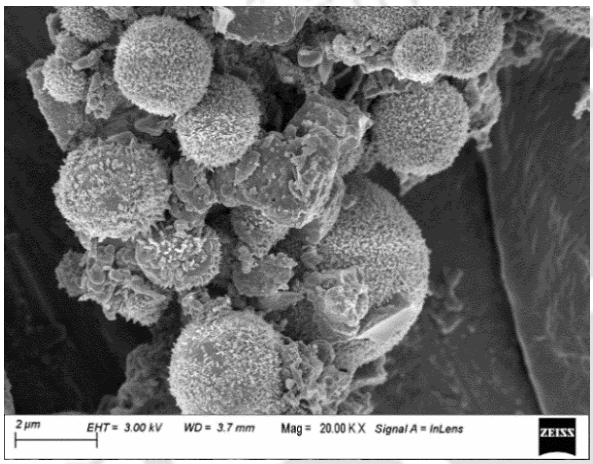

(c)

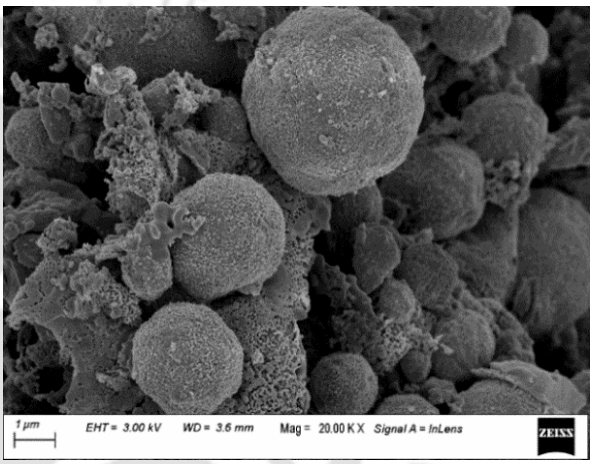

(d)

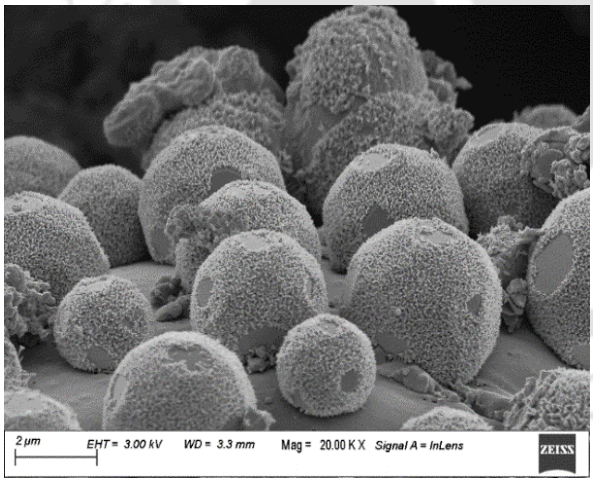

(e)

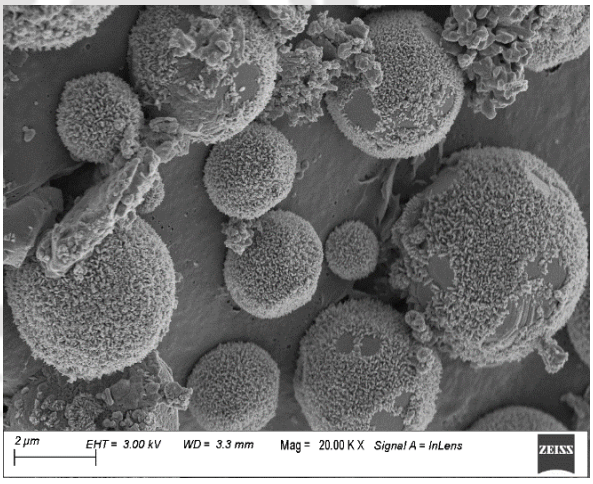

(f)

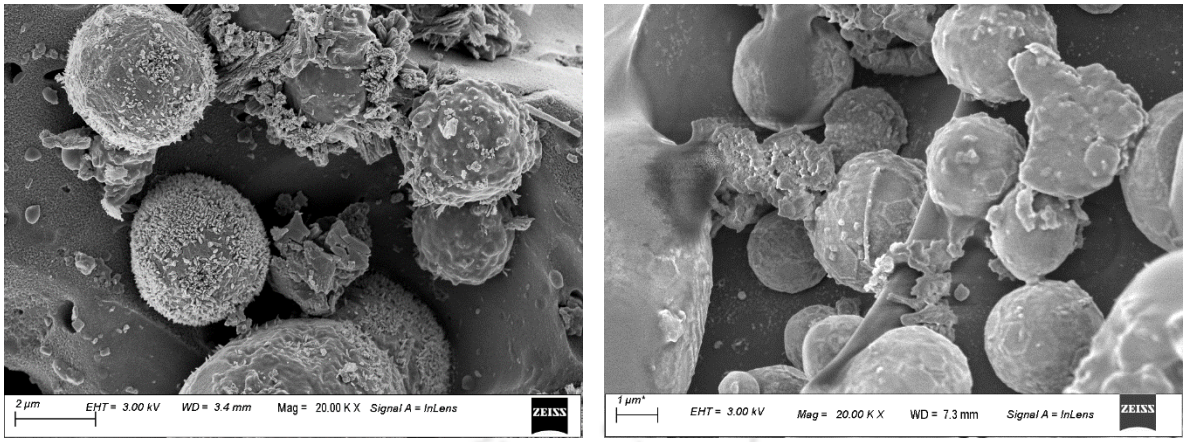

Figure 5.11. FESEM images of the residue of (a) OPCB, (b) LAC-OPCB, (c) HAC-OPCB, (d) RS-OPCB, (e) LAC-RS-OPCB and (f) HAC-RS-OPCB under CO_2 atmosphere, (g) HAC-RS-OPCB (2^{nd} cycle) and (h) HAC-RS-OPCB (3^{rd} cycle).

Table 5.4. BET analysis of the residue.

Residue	BET (m^2/g)	Pore volume ($\times10^{-3}$ cm^3/g)	Pore diameter (nm)
Circuit board	8.97	9.87	4.39
Pyrolyzed PCB	13.87	11.35	3.28
Gasified PCB	19.51	16.71	3.42
OPCB	7.11	5.56	3.13
LAC-OPCB (1:60)-AR	8.65	9.97	5.80
HAC-OPCB (1:50)-AR	8.14	7.16	4.02
RS-OPCB (1:40) -AR	8.96	10.8	6.39
LAC-RS-OPCB (1:50) -AR	9.32	8.42	3.26
HAC-RS-OPCB (1:45) -AR	8.88	9.2	4.74

5.2.5.3. XRD analysis

The residues obtained at the post-operation of the CLC are examined in XRD to detect the changes observed in the chemical structure of OPCB (oxygen carrier) after reduction and oxidation cycles. The residues are scanned from 10-80° with a step size of 0.03°. Figure 5.12 (a-b) shows the XRD analysis of the LAC, RS and their blend, while Figure

5.13 (a-b) highlights the crystalline peaks of HAC, RS and their mixture. The fresh OPCB indicated the presence of Fe_2O_3, CuO, NiO, PbO which is consistent with Table 5.3. In the residue obtained after the CLC reaction, the phases corresponding to Cu_2O, Fe_3O_4 are detected for all the cases along with the peaks of Al_2O_3, SiO_2 (Figure 5.12a, 5.13a). The presence of Cu_2O, Fe_3O_4 indicated the reduction of OPCB particles under the CO_2 atmosphere. The typical minerals (Al, Si, Fe) present in the fuel ash (LAC/ HAC/ RS) are detected and are observed in the form of Al_2O_3, SiO_2 and Fe_2O_3. Figure 5.12(b) and 5.13(b) compared the re-oxidized OPCB particles with the fresh OPCB. The re-oxidation peaks are found to be similar to that of the fresh OPCB indicating the complete oxidation of the metal particles. Several authors reported the formation of complex components such as $CuAlO_2$, $CuAl_2O_4$, Fe_2SiO_4, K_3FeO_2, alumina-silicates or magnesio-ferrites etc. during the interaction of solid fuels and oxygen carriers in the CLC reactions, and these complex components thereby reduce the CLC performance (Siriwardane et al., 2009, Bao et al., 2014, and Ilyushechkin et al., 2016). But these compounds are not observed in the present study in any of the obtained residues, indicating no ash interaction with the oxygen carriers.

Formation of spinel structure of NiO and CuO is beneficial since the properties (reactivity, thermal stability) are enhanced than the single metal oxides (Azad et al., 2013, Siriwardane et al., 2013). Usage of CuO alone is limited due to its low melting point which causes agglomeration and sintering. Thus, mixed metal oxides with CuO are preferred to overcome this issue as discussed in Section 2.1.3 (Chapter 2). Further, Wang et al. (2016) observed higher reactivity of $CuFe_2O_4$ than Fe_2O_3 with no agglomeration at 900°C during cyclic operation. The hydrogen yield was found to be 4 times higher with $NiFe_2O_4$ (11 mol H_2 approx.) than Fe_2O_3 under same operating conditions (Aston et al., 2013). Thus, spinel formations are favoured since they act as promising oxygen carriers

in the CLC process. Presence of $NiFe_2O_4$ and $CuFe_2O_4$ could be detected in the residue after the oxidation. It is observed that presence of $NiFe_2O_4$ and $CuFe_2O_4$ is detected in the residue (coal-OPCB) from the XRD analysis during multiple cycles (Figure 5.13c).

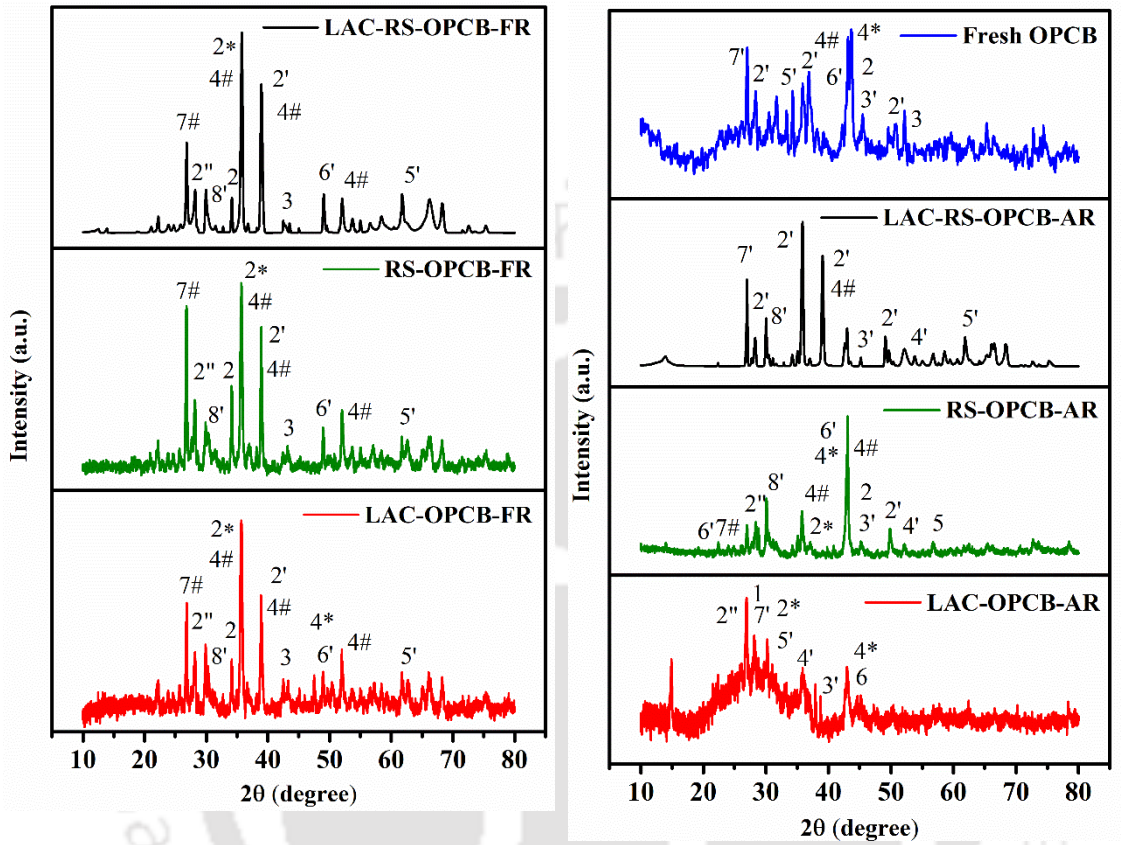

(a) (b)

Figure 5.12. XRD analysis of the residue obtained after (a) CLC reaction for LAC cases, (b) air oxidation for LAC cases. [2 $Cu(OH)_2$; 2' CuO; 2'' Cu_2O; 2* CuSn; 3 Ni; 3' NiO; 4 Fe; 4' Fe_2O_3; 4# Fe_3O_4; 4* FeSi; 5 Sn; 5' SnO_2; 6' SiO_2; 7 Pb; 7# $PbSO_4$; 8' Al_2O_3].

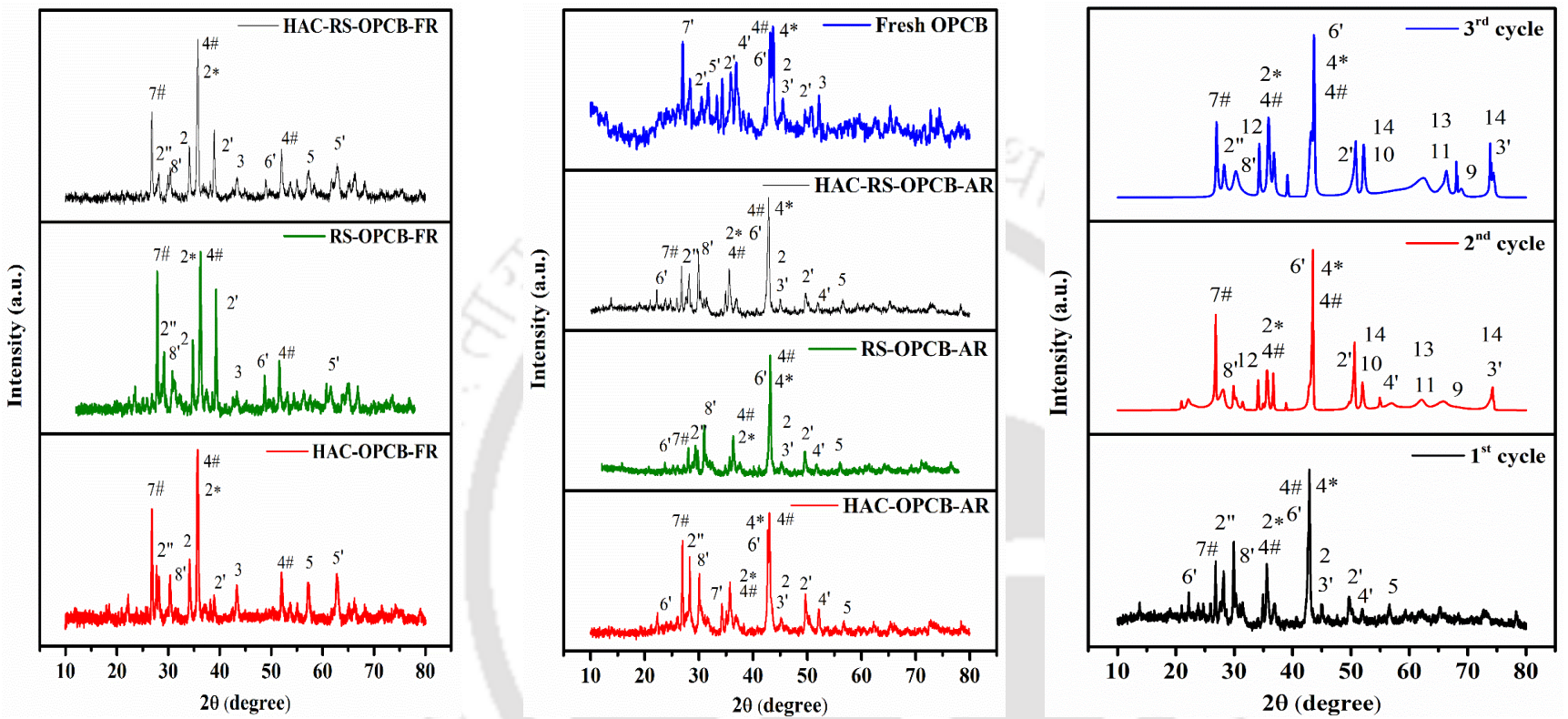

(a) (b) (c)

Figure 5.13. XRD analysis of the residue obtained after (a) CLC reaction for HAC cases, (b) air oxidation for HAC cases, **(c).** XRD analysis of the residue obtained after (c) three cycles of HAC-RS-OPCB in AR [2 $Cu(OH)_2$; 2' CuO; 2'' Cu_2O; 2* CuSn; 3 Ni; 3' NiO; 3* FeNi, 4' Fe_2O_3; 4# Fe_3O_4; 4* FeSi; 5 Sn; 5' SnO_2; 6' SiO_2; 7' PbO 7# $PbSO_4$; 8' Al_2O_3, 9 Fe_2SiO_4, 10 $CuFeO_2$, 11CuSi, 12 $CaCu_2O_3$, 13 $NiFe_2O_4$ and 14 $CuFe_2O_4$].

5.2.5.4. TGA analysis

TGA analysis of the e-waste based PCB is conducted at a heating rate of 10 K/min under N_2 and CO_2 atmosphere. As a typical result, the pyrolysis of PCB took place at 200-400°C, while the char gasification had occurred at 800-1000°C as seen in Figure 5.14. It is observed that the rate of mass loss is found similar up to 800°C under both N_2 and CO_2 atmospheres. At elevated temperatures (800-1000°C), an additional mass loss of about 4% occured due to char gasification in the CO_2 atmosphere.

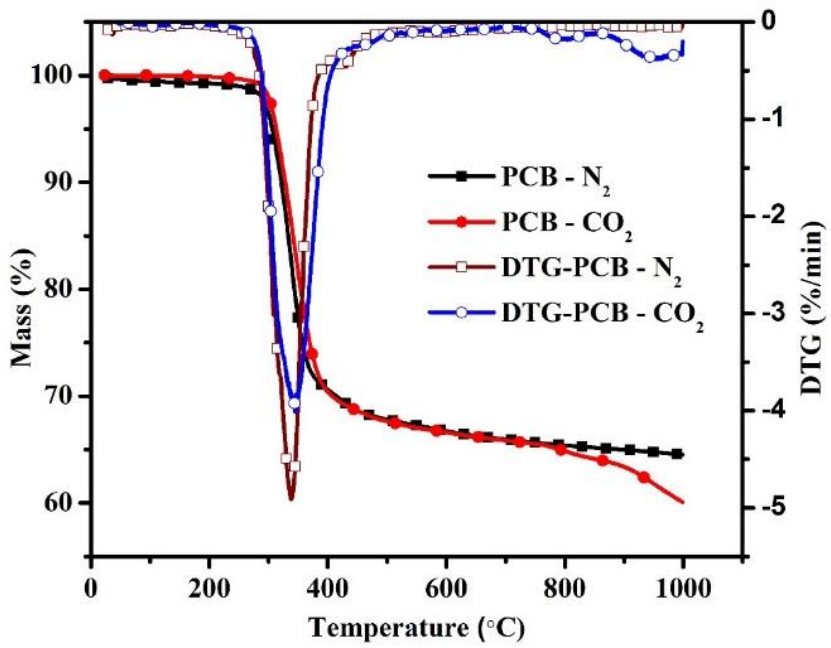

Figure 5.14. TGA and DTG curves of raw PCB under N_2 and CO_2 atmosphere.

A. Synergistic effect in CLC process

The co-combustion behaviour of coals (LAC, HAC) and RS are tested in the TGA under N_2 and CO_2 atmosphere. As observed in Figure 5.15, the blended fuel of LAC, HAC with RS in the CLC process displayed a positive synergetic effect under both the gas atmospheres. The synergy is estimated using Eq. (3.1). The mass loss in the blended condition is higher than the predicted values (based on the individual CLC behaviour of fuels). This confirms the positive synergy due to the interaction of the fuels. The deviation

between the actual and the predicted values is initiated from 300°C and accelerated with the increase in temperature under the CO_2 atmosphere. The deviations in the mass loss between the actual and predicted values at 1000°C are found to be 1.6% and 4.6% for LAC-RS-OPCB, while 2.5% and 4.9% for HAC-RS-OPCB under N_2 and CO_2 atmosphere, respectively.

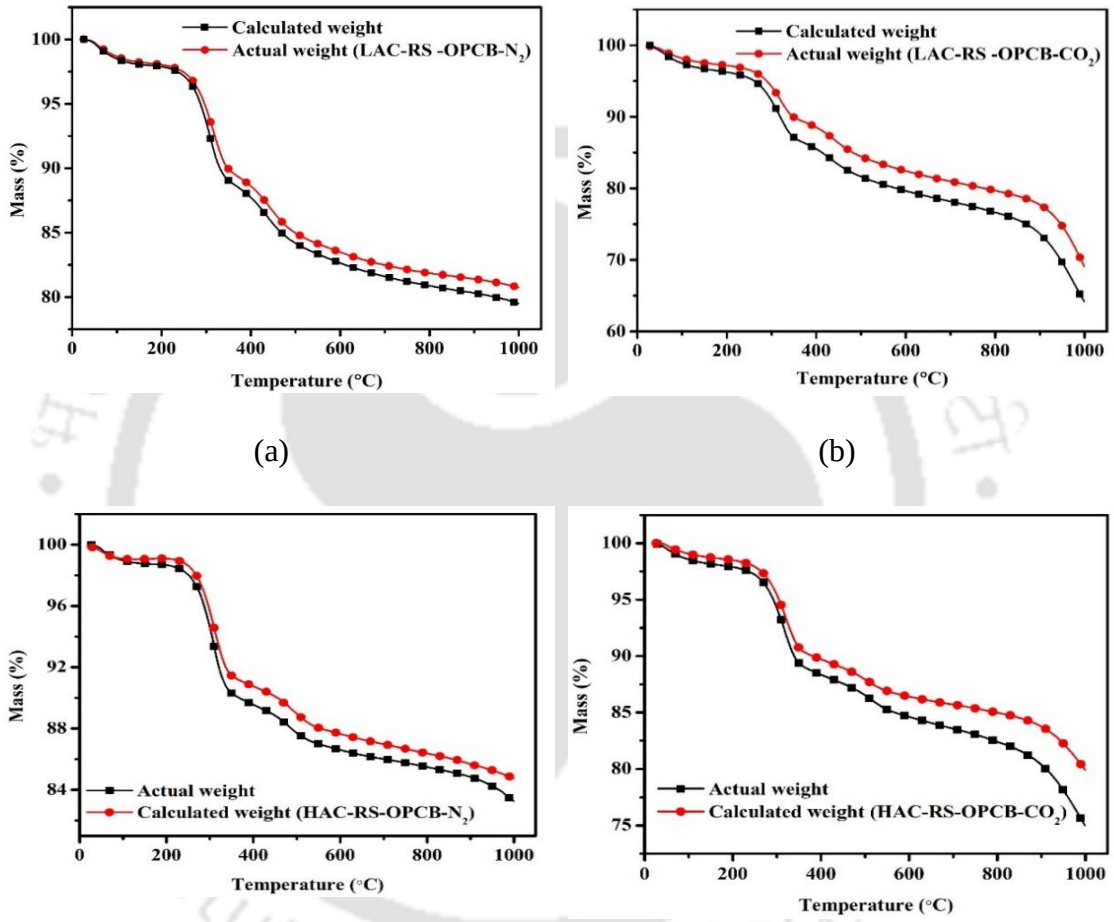

Figure 5.15. Synergetic effect of (a) LAC-RS-N_2, (b) LAC-RS-CO_2, (c) HAC-RS-N_2 and (d) LAC-RS-CO_2 during the CLC process.

It is postulated that larger pores may be formed due to their interaction, which resulted in higher mass loss deviation under the CO_2 atmosphere. The total mass loss of HAC-RS blend is found to be 20% for LAC-RS-OPCB mixture, while it is 15% for HAC-RS-OPCB mixture under N_2 atmosphere. In CO_2 atmosphere, an additional mass loss of 17%

is obtained for LAC-RS-OPCB mixture, while it is 6% for HAC-RS-OPCB mixture is noted due to the reactions of char gasification and OPCB reduction with syngas.

The oxidation of char (LAC, HAC, RS) using OPCB particles is further tested in an N_2 atmosphere to study the solid-solid interaction between char and oxygen carriers. The coal char exhibited a mass loss of 5.2% for LAC and 2.3% for HAC, while RS char showed 7.7% mass loss with OPCB particles (Figure 5.16). This indicates the interaction of char particles with OPCB even in the inert atmosphere. Due to the CLOU nature of the CuO, the released oxygen in the gas phase directly reacted with char.

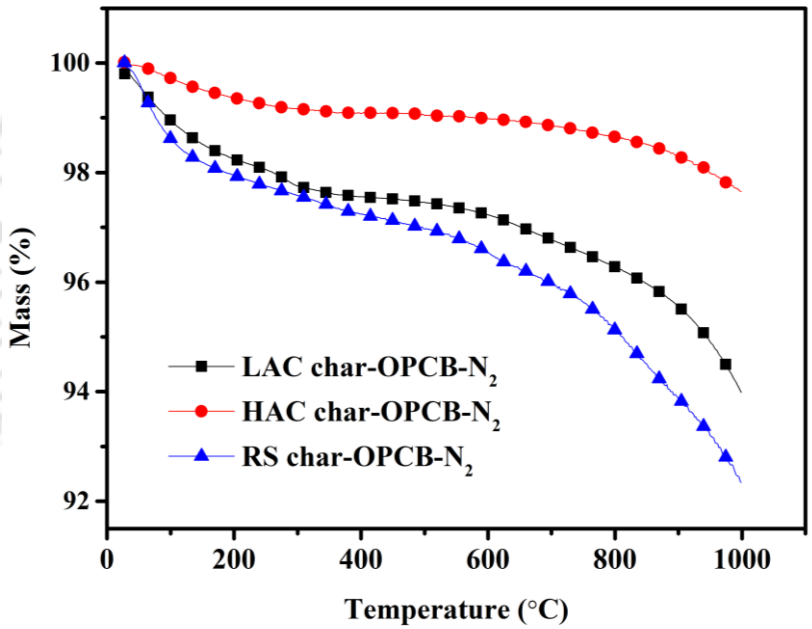

Figure 5.16. TGA analysis of LAC, HAC, RS char-OPCB under N_2 atmosphere.

B. Kinetic analysis

The activation energy with regression coefficient at various temperature intervals is assessed and summarized in Table 5.5. The shrinking core model is found to be the best fit for all the cases (based on the R^2 values). The activation energy for the reaction of LAC volatiles with OPCB particles at 400-600℃ is found to be 44.2 kJ/mol and 28.3

kJ/mol under N_2 and CO_2 atmosphere, respectively. The activation energy for HAC-OPCB during the reaction between the volatiles and OPCB at 400-600℃ is 66.9 kJ/mol and 50.3 kJ/mol under N_2 and CO_2 atmosphere. Thus, LAC fuel required lower activation energy than HAC coals during the devolatilization stage by 22.0 kJ/mol. Further, it is observed that the activation energy for the CLC reactions with OPCB is 7-25% lower than the Fe_2O_3 based CLC process due to the presence of CuO (Table 4.3). Highly reactive volatiles in RS resulted in lowering the activation energy. Under the co-CLC conditions, the blended fuels (LAC-RS, HAC-RS) have shown lower activation energy than their individual OPCB based CLC reaction. The activation energy decreased by 6.5 kJ/mol in LAC-RS-OPCB mixture, while 3.5 kJ/mol in HAC-RS-OPCB mixture at 200-400°C. At the temperature range of 600 to 800°C, the higher hydrocarbons could release and interact with the OPCB particles. In this temperature range, the activation energy under CO_2 atmosphere is lower than (~30 to 60%) that of the reaction under N_2 atmosphere. Further, the CLC reaction at 800 to 1000°C is due to the char gasification and further the oxidation of the released CO by OPCB particles. In this temperature range, the LAC-OPCB mixture required an activation energy of 97.5 kJ/mol, while the addition of the RS reduced the activation energy to 78.6 kJ/mol at 800 to 1000°C under CO_2 atmosphere. Similarly, the HAC-RS-OPCB mixture reduced the activation energy from 111.9 kJ/mol to 86.4 kJ/mol. Hence the blended feed reduced the activation energy by 18.9 kJ/mol and 25.5 kJ/mol, compared to unblended LAC and HAC fuels, respectively.

Table 5.5. Reduction kinetics of OPCB particles with different fuels under N_2 and CO_2 atmosphere.

Fuel	Temperature (°C)	Shrinking core model		1st order reaction model		2nd order reaction model		3rd order reaction model	
		E (kJ/mol)	R^2	E (kJ/mol)	R^2	E (kJ/mol)	R^2	E (kJ/mol)	R^2
LAC-OPCB-N_2	400-560	44.17	0.96	46.76	0.96	45.08	0.96	46.21	0.96
	600-800	12.80	0.99	10.69	0.84	18.40	0.99	17.83	0.99
LAC-OPCB-CO_2	400-560	28.25	0.89	29.75	0.89	24.52	0.89	29.75	0.89
	600-800	8.27	0.95	0.48	0.79	6.54	0.99	13.18	0.90
	800-1000	97.49	0.82	54.99	0.79	132.45	0.70	233.29	0.77
HAC-OPCB-N_2	400-560	66.97	0.95	30.86	0.86	43.05	0.91	57.28	0.93
	600-800	14.36	0.98	12.84	0.84	17.32	0.96	30.96	0.97
HAC-OPCB-CO_2	400-560	50.29	0.96	10.29	0.90	14.96	0.92	20.18	0.95
	600-800	5.21	0.99	4.41	0.99	0.75	0.61	5.72	0.98
	800-1000	111.92	0.90	159.45	0.83	140.06	0.80	145.24	0.87
RS-OPCB-N_2	200-400	38.75	0.97	42.78	0.95	57.26	0.95	74.68	0.95
	400-560	7.82	0.99	1.62	0.88	12.55	0.97	31.55	0.99
	600-800	11.78	0.99	9.09	0.99	4.19	0.78	21.93	0.96
RS-OPCB-CO_2	200-400	21.06	0.94	23.49	0.94	31.88	0.94	41.61	0.94
	400-560	5.19	0.99	6.04	0.98	1.64	0.69	3.98	0.89
	600-800	9.46	0.99	10.17	0.99	5.03	0.91	1.71	0.95
	800-1000	77.22	0.83	37.40	0.76	137.21	0.74	268.99	0.74

Table 5.5 continued

Fuel	Temperature (°C)	Shrinking core model		1st order reaction model		2nd order reaction model		3rd order reaction model	
		E (kJ/mol)	R^2	E (kJ/mol)	R^2	E (kJ/mol)	R^2	E (kJ/mol)	R^2
LAC-RS-OPCB-N_2	200-400	32.47	0.91	16.37	0.91	19.40	0.91	22.71	0.91
	400-560	4.96	0.97	3.56	0.68	9.08	0.92	15.60	0.96
	600-800	6.25	0.99	6.85	0.99	1.77	0.97	4.57	0.98
LAC-RS-OPCB-CO_2	200-400	20.76	0.93	21.77	0.93	29.49	0.93	32.31	0.93
	400-560	4.39	0.74	8.66	0.91	25.48	0.98	47.34	0.99
	600-800	3.38	0.99	1.26	0.89	22.88	0.99	55.26	0.99
	800-1000	78.57	0.84	89.53	0.56	110.9	0.53	205.73	0.53
HAC-RS-OPCB- N_2	200-400	35.21	0.94	27.32	0.94	34.30	0.94	42.43	0.94
	400-560	4.19	0.99	8.53	0.91	25.75	0.98	48.18	0.99
	600-800	8.36	0.99	1.11	0.95	23.92	0.99	57.45	0.99
HAC-RS-OPCB-N_2	200-400	24.47	0.94	26.12	0.94	31.79	0.94	37.92	0.93
	400-560	5.26	0.96	0.58	0.92	5.52	0.89	13.07	0.94
	600-800	5.79	0.99	5.66	0.99	2.76	0.86	13.70	0.97
	800-1000	86.44	0.89	92.27	0.85	99.73	0.85	103.96	0.85

5.3. Conclusions

The feasibility of utilizing e-waste based PCB oxygen carriers in the CLC operation is assessed using a fixed bed reactor. The following conclusions can be drawn from the experimental investigation.

- The OPCB contains metal oxides with CLC (Fe_2O_3, NiO) and CLOU behaviour (CuO). The combined chemical behaviour of these metals enhanced the CO_2 yield, syngas and char conversion. Further, the inherent presence of inerts such as Al_2O_3, SiO_2 etc., in the OPCB is highly beneficial for the CLC reaction. These could be a low cost oxygen carrier for the CLC of the high ash fuels for economical operation.
- The gas conversion and CO_2 yield are found to be 93.8% and 90.4% for LAC fuel, 90.6% and 86.1% for HAC fuel, while 96.5% and 93.8% for RS, respectively. The CO_2 yield is improved from 90.4% to 92.8% when LAC is replaced by LAC-RS mixture, while 86.1% to 90.9% when HAC is replaced by HAC-RS mixture. The overall yield in OPCB-based CLC process has increased by 5% approx. when compared to Fe_2O_3, since the contribution of CuO in OPCB is 23%.
- The surface area of OPCB is 4.6 m^2/g higher than pure Fe_2O_3, thereby signifying higher porosity and reactivity.
- A positive synergistic effect is observed between the coal sample (LAC, HAC) and RS in terms of higher mass loss in TGA. The deviations in the mass loss between the actual and predicted values at 1000°C are found to be 1.6% and 4.6% for LAC-RS-OPCB, while 2.5% and 4.9% for HAC-RS-OPCB under N_2 and CO_2 atmosphere, respectively.

- FESEM, BET and XRD analysis showed that the structural and morphological changes during the reduction and oxidation process did not show any sign of agglomeration issues.
- The shrinking core model is found to be the best fit among other models. The activation energy of the CLC is found low under the blended condition of the fuels, compared to the unblended conditions.

The production of harmful gases during PCB pyrolysis and combustion is not analyzed in the present study. Thus, further investigation needs to be conducted to study the environmental impact during the thermal degradation of e-waste (PCB). In the present study, the products from the e-waste pyrolysis and gasification (mainly metallic fraction) are proven to be beneficial for the CLC process. The pyrolyzed and gasified PCB generated H_2, CO and tar, which can be used as a potential chemical feedstock.

References

Abad, A., Gayán, P., García-labiano, F., Diego, L. F. De, & Adánez, J. (2012). Demonstration of chemical-looping with oxygen uncoupling (CLOU) process in a 1.5kW_{th} continuously operating unit using a Cu-based oxygen-carrier. *International Journal of Greenhouse Gas Control*, *6*, 189–200.

Abanades, S. (2012). CO_2 and H_2O reduction by solar thermochemical looping using SnO_2/SnO redox reactions: thermogravimetric analysis. *International Journal of Hydrogen Energy*, *37*, 8223–8231.

Aho, M., Vainikka, P., Taipale, R., & Yrjas, P. (2008). Effective new chemicals to prevent corrosion due to chlorine in power plant superheaters. *Fuel*, *87*, 647–654.

Azad, A.-M., Hedayati, A., Rydén, M., Leion, H., & Mattisson, T. (2013). Examining

the Cu-Mn-O spinel system as an oxygen carrier in chemical looping combustion. *Energy Technology*, *1*(1), 59–69.

Bao, J., Li, Z., & Cai, N. (2014). Interaction between iron-based oxygen carrier and four coal ashes during chemical looping combustion. *Applied Energy*, *115*, 549–558.

Bhosale, R., AlMomani, F., & Takalkar, G. (2020). Thermodynamic analysis of solar-driven chemical looping steam methane reforming over Cr_2O_3/Cr redox pair. *International Journal of Hydrogen Energy*, *45*, 10370–10380.

Chen, D. Q., Shen, L. H., Xiao, J., Song, T., Gu, H. M., & Zhang, S. W. (2012). Experimental investigation of hematite oxygen carrier decorated with NiO for chemical looping combustion of coal. *Journal of Fuel Chemistry and Technology*, *40*, 267–272.

Condori, O., García-Labiano, F., de Diego, L. F., Izquierdo, M. T., Abad, A., & Adánez, J. (2021). Biomass chemical looping gasification for syngas production using LD Slag as oxygen carrier in a 1.5 kW_{th} unit. *Fuel Processing Technology*, *222*, 106963.

Cuadrat, A., Abad, A., García-Labiano, F., Gayán, P., de Diego, L. F., & Adánez, J. (2011). The use of ilmenite as oxygen-carrier in a 500W_{th} Chemical-Looping Coal Combustion unit. *International Journal of Greenhouse Gas Control*, *5*, 1630–1642.

Dai, J., & Whitty, K. J. (2019). Predicting and alleviating coal ash-induced deactivation of CuO as an oxygen carrier for chemical looping with oxygen uncoupling. *Fuel*, *241*, 1214–1222.

Dueso, C., Abad, A., García-Labiano, F., De Diego, L. F., Gayán, P., Adánez, J., & Lyngfelt, A. (2010). Reactivity of a NiO/Al_2O_3 oxygen carrier prepared by impregnation for chemical-looping combustion. *Fuel*, *89*, 3399–3409.

Fan, Y., Weng, Q., Zhuo, Y., Dong, S., Hu, P., & Li, D. (2019). Theoretical study of As_2O_3 adsorption mechanisms on CaO surface. *Materials*, *12*, 677–690.

Ghodke, P. K., Sharma, A. K., Pandey, J. K., Chen, W.-H., Patel, A., & Ashokkumar, V. (2021). Pyrolysis of sewage sludge for sustainable biofuels and value-added biochar production. *Journal of Environmental Management*, *298*, 113450.

He, Z., Saw, W. L., Van Eyk, P. J., Nathan, G. J., & Ashman, P. J. (2020). Effect of calcium and phosphorus on interactions between quartz sand and K-salt-doped wood under both steam gasification and combustion atmospheres. *Energy and Fuels*, *34*, 3210–3222.

Hussain, M., Tufa, L. D., Yusup, S., & Zabiri, H. (2019). Characterization of coal bottom ash & its potential to be used as catalyst in biomass gasification. *Materials Today: Proceedings*, *16*, 1886–1893.

Ilyushechkin, A. Y., Kochanek, M., & Lim, S. (2016). Interactions between oxygen carriers used for chemical looping combustion and ash from brown coals. *Fuel Processing Technology*, *147*, 71–82.

Izquierdo, M. T., García-Labiano, F., Abad, A., Cabello, A., Gayán, P., de Diego, L. F., & Adánez, J. (2021). On the optimization of physical and chemical stability of a Cu/Al_2O_3 impregnated oxygen carrier for chemical looping combustion. *Fuel Processing Technology*, *215*, 106740.

Jadhav, R. A., & Fan, L. S. (2001). Capture of gas-phase arsenic oxide by lime: Kinetic and mechanistic studies. *Environmental Science and Technology*, *35*(4), 794–799.

Li, X. M., Zhang, H., Liu, M. J., Zhi, L. F., Bai, J., Bai, Z. Q., & Li, W. (2020). Investigation of coal-biomass interaction during co-pyrolysis by char separation and

its effect on coal char structure and gasification reactivity with CO_2. *Journal of Fuel Chemistry and Technology*, *48*, 897–907.

Liu, G., Liao, Y., Wu, Y., & Ma, X. (2019). Enhancement of $Ca_2Fe_2O_5$ oxygen carrier through Mg/Al/Zn oxide support for biomass chemical looping gasification. *Energy Conversion and Management*, *195*, 262–273.

Ma, Z., Wang, J., Liu, G., Zhang, H., Lu, Y., Xiong, J., Xie, C., & Zou, C. (2021). Regeneration of deactivated Fe_2O_3/Al_2O_3 oxygen carrier via alkali metal doping in chemical looping combustion. *Fuel Processing Technology*, *220*, 106902.

Pachler, R. F., Penthor, S., Mayer, K., & Hofbauer, H. (2019). Fate of sulfur in chemical looping combustion of gaseous fuels using a Perovskite oxygen carrier. *Fuel*, *241*, 432–441.

Peng, W., Xu, Z., & Zhao, H. (2016). Batch fluidized bed test of SATS-derived CaO/TiO_2-Al_2O_3 sorbent for calcium looping. *Fuel*, *170*, 226–234.

Rydén, M., & Ramos, P. (2012). H_2 production with CO_2 capture by sorption enhanced chemical-looping reforming using NiO as oxygen carrier and CaO as CO_2 sorbent. *Fuel Processing Technology*, *96*, 27–36.

Saad, J., & Williams, P. T. (2016). Pyrolysis-Catalytic-Dry Reforming of Waste Plastics and Mixed Waste Plastics for Syngas Production. *Energy & Fuels*, *30*, 3198–3204.

Santos, P. H., Nowak, S., Lau-Truong, S., Blanchard, J., Beaunier, P., Rodrigues, J. A. J., & Brayner, R. (2019). Preparation of niobium-based oxygen carriers by polyol-mediated process and application to chemical-looping reforming. *Journal of Nanoparticle Research*, *21*, 88–104.

Sarafraz, M. M., Jafarian, M., Arjomandi, M., & Nathan, G. J. (2017a). Potential use of

liquid metal oxides for chemical looping gasification: A thermodynamic assessment. *Applied Energy*, *195*, 702–712.

Sarafraz, M. M., Jafarian, M., Arjomandi, M., & Nathan, G. J. (2017b). The relative performance of alternative oxygen carriers for liquid chemical looping combustion and gasification. *International Journal of Hydrogen Energy*, *42*(26), 16396–16407.

Shahbaz, M., Yusup, S., Inayat, A., Patrick, D. O., & Ammar, M. (2017). The influence of catalysts in biomass steam gasification and catalytic potential of coal bottom ash in biomass steam gasification: A review. *Renewable and Sustainable Energy Reviews*, *73*, 468–476.

Siriwardane, R., Tian, H., Richards, G., Simonyi, T., & Poston, J. (2009). Chemical looping combustion of coal with metal oxide oxygen carriers. *Energy Fuels*, *23*, 3885–3892.

Siriwardane, R. V., Ksepko, E., Tian, H., Poston, J., Simonyi, T., & Sciazko, M. (2013). Interaction of iron-copper mixed metal oxide oxygen carriers with simulated synthesis gas derived from steam gasification of coal. *Applied Energy*, *107*, 111–123.

Song, H., Shah, K., Doroodchi, E., & Moghtaderi, B. (2014). Development of a Cu-Mg-based oxygen carrier with SiO_2 as a support for chemical looping air separation. *Energy and Fuels*, *28*, 163–172.

Straka, P., & Bičáková, O. (2014). Hydrogen-rich gas as a product of two-stage co-gasification of lignite/waste plastics mixtures. *International Journal of Hydrogen Energy*, *39*, 10987–10995.

Sun, Z., Zhang, X., Li, H., Liu, T., Sang, S., Chen, S., Duan, L., Zeng, L., Xiang, W., &

Gong, J. (2020). Chemical looping oxidative steam reforming of methanol: A new pathway for auto-thermal conversion. *Applied Catalysis B: Environmental*, *269*, 118758.

Tian, X., Wei, Y., & Zhao, H. (2017). Evaluation of a hierarchically-structured $CuO@TiO_2$-Al_2O_3 oxygen carrier for chemical looping with oxygen uncoupling. *Fuel*, *209*, 402–410.

Veses, A., Sanahuja-Parejo, O., Martínez, I., Callén, M. S., López, J. M., García, T., & Murillo, R. (2021). A pyrolysis process coupled to a catalytic cracking stage: A potential waste-to-energy solution for mattress foam waste. *Waste Management*, *120*, 415–423.

Wang, B., Wang, W., Ma, Q., Lu, J., Zhao, H., & Zheng, C. (2016). In-Depth Investigation of Chemical Looping Combustion of a Chinese Bituminous Coal with $CuFe_2O_4$ Combined Oxygen Carrier. *Energy and Fuels*, *30*(3), 2285–2294.

Wang, B., Yan, R., Zheng, Y., Zhao, H., & Zheng, C. (2011). Mechanistic investigation of chemical looping combustion of coal with Fe_2O_3 oxygen carrier. *Fuel*, *90*, 2359–2366.

Wang, P., Means, N., Howard, B. H., Shekhawat, D., & Berry, D. (2018). The reactivity of CuO oxygen carrier and coal in Chemical looping with oxygen uncoupled (CLOU) and in-situ gasification chemical looping combustion (iG-CLC). *Fuel*, *217*, 642–649.

Wang, S., Wang, G., Jiang, F., Luo, M., & Li, H. (2010). Chemical looping combustion of coke oven gas by using Fe_2O_3/CuO with $MgAl_2O_4$ as oxygen carrier. *Energy and Environmental Science*, *3*, 1353–1360.

Wang, T. T., Li, Y., Jin, L. J., Wang, D. C., Yao, D. M., & Hu, H. Q. (2019). Upgrading of coal tar with steam catalytic cracking over Al/Ce and Al/Zr co-doped Fe_2O_3 catalysts. *Journal of Fuel Chemistry and Technology*, *47*, 287–296.

Weiland, F., Lundin, L., Celebi, M., van der Vlist, K., & Moradian, F. (2021). Aspects of chemical recycling of complex plastic waste via the gasification route. *Waste Management*, *126*, 65–77.

Xiao, R., Song, Q., Song, M., Lu, Z., Zhang, S., & Shen, L. (2010). Pressurized chemical-looping combustion of coal with an iron ore-based oxygen carrier. *Combustion and Flame*, *157*, 1140–1153.

CHAPTER 6

Techno-Economic Evaluation of Electronic Waste Based Oxygen Carriers for CLC Integrated Combined Cycle Power Plants

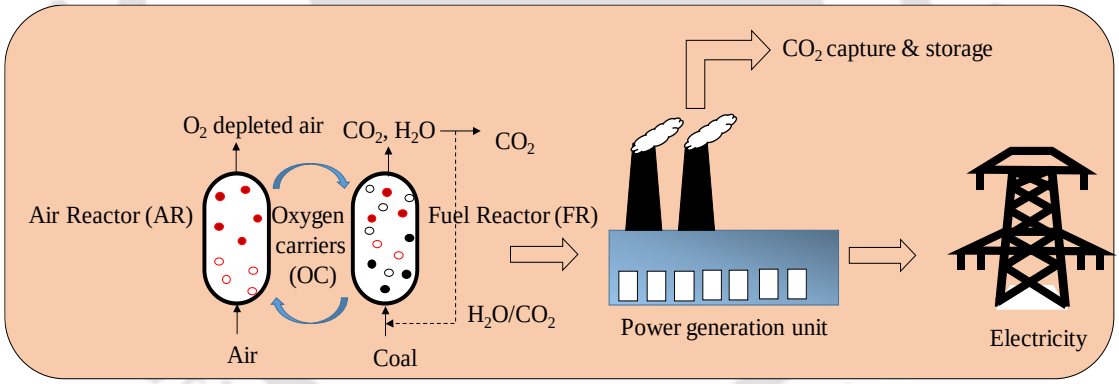

CHAPTER 6

TECHNO-ECONOMIC EVALUATION OF ELECTRONIC WASTE BASED OXYGEN CARRIERS FOR CLC INTEGRATED COMBINED CYCLE POWER PLANTS

The present chapter evaluates the CLC performance using different oxygen carriers (e-waste, Fe_2O_3, CuO) in fuel blends for the energy generation. The novelty of the present study is to assess the economic impact of utilizing e-waste based metal oxides in the CLC process for the production of electricity. In this study, the e-waste based CLC process is integrated with the combined cycle power plant for electricity production using Indian coals and rice straw as fuels. The impact of co-feeding of coal and rice straw on the net thermal efficiency of the power plants is investigated with the estimation of levelized cost of electricity (LCOE) by economic assessment.

6.1. Model description of the combined cycle power plant

In the present study, the combined cycle power plant simulations are performed by using pure and commercial based metal oxides and e-waste based mixed metal oxides. The following cases of metal oxides are considered in the present study with solid fuels used under blended and non-blended conditions.

(i) Pure Fe_2O_3 metal oxide

(ii) Pure CuO metal oxide

(iii) OPCB based metal oxide obtained from the present experimental study

(iv) Mixed metal oxide obtained from Molto et al. (2009)

Table 6.1. Composition of electronic waste obtained experimentally (OPCB: oxidized printed circuit board) using X-ray fluorescence (XRF) analysis.

Oxides	OPCB (wt. %)	(Molto et al., 2009) (wt. %)
Fe_2O_3	21.50	4.66
CuO	22.83	38.20
NiO	3.01	3.08
CaO	9.58	6.50
Al_2O_3	10.45	3.04
SiO_2	22.56	32.4
TiO_2	0.62	4.15
P_2O_5	0.21	0.17
SO_3	0.37	1.21
Cl	0.04	0.02
SnO_2	1.62	3.5
PbO	0.98	0.54
Cr_2O_3	2.84	0.1
MgO	1.02	0.2
ZnO	1.77	0.27
ZrO_2	0.07	0.03
Nb_2O_5	0.15	0.03
As_2O_3	0.19	0.3
K_2O	0.19	-
Sb_2O_3	-	0.84
Ag_2O	-	0.19
BaO	-	0.5
SrO	-	0.07

Table 6.1 shows the metal oxides obtained using the PCB. Also, the composition of the metal oxides (by XRF analysis) reported in the literature, Molto et al. (2009), is compared with the present study. The metal oxide obtained by Molto et al. (2009) had a higher fraction of CuO, followed by Fe_2O_3 and NiO, while the OPCB contains an equal mass fraction of Fe_2O_3 and CuO. In the present study, the obtained OPCB and the metal oxides

obtained by Molto et al. (2009) are used for the simulation studies. The global e-waste production was 44.7 million tonnes (Mt) in 2016, where India alone contributed 2 Mt (Kiran et al., 2021). Shittu et al. (2021) estimated that the annual global quantity of e-waste production was 54 million tons and it is further expected to increase by 70% in the year 2050. India is the fourth largest country to generate e-waste after China, the United States and Japan in 2019 (Vries & Stoll, 2021). Ahirwar & Tripathi (2021) considered landfilling as not the economical way to handle e-waste due to the heavy metals. India generated 2 million tons of e-waste in 2017 (Kiran et al., 2021). The typical ash content (metal and non-metals) in e-waste ranges from 10-70% (Borthakur & Govind, 2018, Chen et al., 2021), thus enormous amount of mixed metal oxides can be produced using thermal treatment. A portion of the total extracted metal oxides will be utilized in the CLC process, while the rest amount will be stored for commercial purposes. Hence, it is possible to run a large number of CLC plants since CLC process circulates the same oxygen carrier until its reactivity is detoriated. This clearly illustrates that utilization of OPCB as oxygen carriers is highly encouraged in CLC based power plants.

Table 6.2. Oxygen carrying capacity of different metal oxides and synthesized OPCB.

Oxygen carrier	Oxygen carrying capacity (wt. %)
$NiO \rightarrow Ni + O_2$	21.42
$CuO \rightarrow Cu_2O + O_2$	10.06
$6\ Fe_2O_3 \rightarrow 4\ Fe_3O_4 + O_2$	3.33
(Fe_2O_3:CuO: NiO) (21.5:22.83:3.01) (wt. %) (OPCB)	3.57
(Fe_2O_3:CuO: NiO) (4.66:38.2:3.08) (wt. %) Molto et al. (2009)	4.66

The oxygen carrying capacity of various oxygen carriers is summarized in Table 6.2. It can be seen that NiO has higher oxygen carrying capacity than Cu and Fe-based oxygen carriers. The oxygen carrying capacity of metal oxides is found in the following order:

NiO/Ni > CuO/Cu_2O > Fe_2O_3/Fe_3O_4. The oxygen carrying capacity of the prepared OPCB is found as 3.6%, which is higher than the pure Fe_2O_3 based metal oxides.

Table 6.3 shows the heat of reactions for different oxygen carriers at 900°C. The heat of reaction is evaluated from the literature Barin, (1995). The net reaction in the FR is found exothermic in nature for all the cases except for methane based reduction reactions. The reduction reactions using CuO are mostly exothermic in nature since it liberates molecular oxygen, unlike Fe_2O_3 and NiO. It is observed that the Fe and Ni-based oxygen carriers have a higher heat of reaction (ΔH_r) than Cu-based oxygen carrier during oxidation reaction.

Table 6.3. Heat of reaction for the reduction and oxidation reactions of syngas and char using different metal oxides at 900°C.

Oxygen carriers	Standard heat of reactions (ΔH_r^0)				
	Reducing reactions				Oxidizing reaction
	H_2	CO	CH_4	C	O_2
Fe_2O_3	-11.6	-42.7	216.0	89.2	-472.4
CuO	-120.2	-151.3	107.4	-133.3	-259.1
NiO	-16.1	-47.2	211.6	73.6	-466.5

The detailed layout of the power plant is shown in Figure 6.1. The complete flow sheeting of the power system consists of several components: a fuel reactor, an air reactor, a desulfurization unit, a pump, a gas turbine, three steam turbines, a heat recovery steam generator (HRSG) unit, and a carbon capture and storage (CCS) unit. The CLC process is initiated by feeding 4.6 to 7 kg/s of coal or 8.5 kg/s of rice straw into the RGibbs reactor after passing through the RYield reactor. The RYield reactor decomposes the fuel into its elements based on the ultimate analysis. The feed rate is maintained based on the gross

chemical energy of the fuel (150 MW) for all the cases. A pressurized stream of recycled CO_2 (30 bar) is used as a gasifying agent for the in-situ gasification of char. The amount of CO_2 required for LAC, HAC and RS are 8.9 kg/s, 11.5 kg/s and 3.2 kg/s, respectively. The oxygen carriers are marked by 'M', gaseous stream by 'G', air by 'A', steam flow by 'S'. The flow rate of OPCB is adjusted such that a negligible amount of unconverted gases are present at the FR outlet. The outlet stream of the FR (G1 & M1) is sent to a solid-gas separator (G-S-Sep1) to separate the gaseous stream from the solid residues (reduced metal oxide and ash). The G1 stream from the FR is sent to an HRSG unit to extract the residual heat. The HRSG unit exchanges the heat from the high temperature exhaust gas from the FR and the AR in order to produce steam for electricity generation. Before sending the flue gas (G2 stream) to the CO_2 capture unit, it is sent to a gas cleaning unit to remove H_2S, HCl, SO_2 contaminants.

The solid stream from the FR outlet (M1) is fed into a cyclone separator to separate the metal particles from the ash residue. Ash from the FR is drained out, and the thermal energy in the ash is recovered by a cold stream through a heat exchanger. The separated metal particles (M1) are then circulated into the AR for oxidation. The air flow rate is maintained to achieve complete conversion of oxygen carriers. The compressed air at 30 bar (A10) oxidizes the OPCB metal particles, which are then transported to the gas-solid separator (G-S-Sep2). A high temperature and high pressure gas stream (A11) from the outlet of the AR is sent to an air turbine for electricity generation. The outlet stream of the air (A12) is sent to the HRSG unit to recover the residual heat for steam generation. The oxidized particles from the AR (M2) are then circulated to the FR. The AR was operated at 1000°C to limit any agglomeration and sintering issues. The flow sheets for the co-CLC process are prepared using Aspen Plus software with a similar configuration for various solid feeds such as LAC, HAC, RS, LAC-RS and HAC-RS.

6.2. Model validation

The developed model in the present study is validated under similar operating conditions with the results obtained by Surywanshi et al. (2019). The accuracy of the model is verified by comparing the breakdown of the total energy production in the combined cycle, which is shown in Table 6.3.

$$\text{Error deviation}\,(\%) = \frac{\text{Literature value - model value}}{\text{Literature value}} \times 100 \qquad (6.1)$$

Table 6.4. Comparison of net efficiency, power output and LCOE for model validation.

	(Surywanshi et al., 2019)	Present study	Error deviation (%)
Input energy (MW)	1286.9	1286.9	0
Total power output (MW)	488.3	494.8	-1.31
Net power output (MW)	449.9	455.1	-1.16
Net efficiency (%)	34.9	35.4	-1.42
LCOE ($/MWh)	113.63 (*€ converted to $)*	105.95	6.76

It is found that the deviation of the net power output is 1.2%, suggesting that the obtained results are in line with the corresponding values reported by Surywanshi et al. (2019). The deviation in the values of LCOE is found as 6.8%. The variation may be due to the consideration of the capital cost of the equipment based on their various reference capacity and their costs.

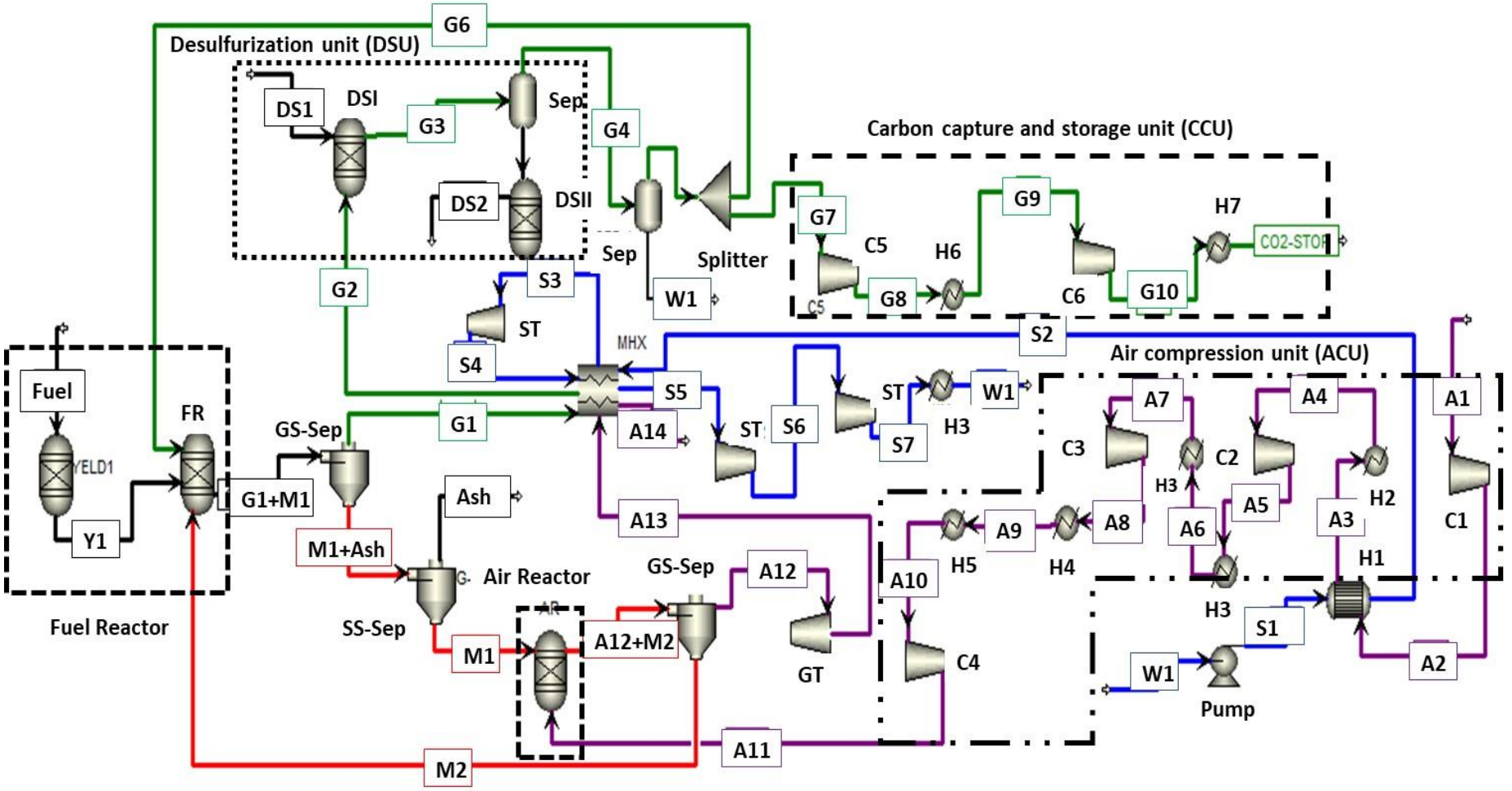

Figure 6.1. Detailed Aspen plus flow sheeting based on direct coal fuelled CLC process integrated combined cycle power plant (Oxygen carriers are marked by 'M', gaseous stream by 'G', air by 'A' and steam flow by 'S').

6.3. Results and discussion

A comparative analysis using electronic waste (e-waste) based oxygen carriers is performed using Aspen Plus software. The chemical energy input to the CLC system is 150 MW in all cases. The performance of the power system is compared for OPCB, pure Fe_2O_3 and CuO based oxygen carriers. Figure 6.2 shows the effect of OPCB-fuel ratio on the flue gas composition at the FR outlet at a constant flow rate of the solid fuels. The gases such as CH_4 and H_2 are almost negligible in the flue gas in all the cases. The production of H_2O is higher in the case of RS due to the higher content of H_2 and O_2 compared to the coals (LAC and HAC). It can be observed that the CO_2 content increases with increasing the OPCB content to some extent and becomes constant with a further increase in the mass ratio of the oxygen carrier. Thus, the optimum values are selected as 1:70 for LAC: OPCB (Figure 6.2a), 1:45 for HAC: OPCB (Figure 6.2b) and 1:35 for RS: OPCB fuels (Figure 6.2c). The mass flow rates of OPCB are 319.9 kg/s, 305.1 kg/s and 298.2 kg/s for LAC, HAC and RS fuels, respectively.

The gas composition obtained at the FR outlet for the CLC reaction conducted at the optimal ratio of fuel and oxygen carriers is shown in Table 6.5. The LAC based syngas (without any oxygen carrier) produced in the FR contains H_2, CH_4, CO as 0.29 kg/s, 0.023 kg/s and 15.84 kg/s, respectively. These gases have reacted with the oxygen carriers and the resultant flue gas holds a trace amount of CO, H_2 and CH_4 below 2000 ppm. A complete conversion of the solid fuels is found with the e-waste based oxygen carrier. The CO and H_2S in the flue gas should be less than 2000 ppm and 200 ppm for storage, respectively (Fan et al., 2017). The quantity of pollutants such as SO_x, NO_x and HCl is estimated for the gases at the FR outlet (Table 6.5). HCl is formed due to the presence of chlorine in the raw PCB material. The nitrogen in the fuel is liberated in the form of N_2 rather than NO, NO_2 or N_2O. As these pollutant concentrations are below 2000 ppm, no

further treatment is required. Hence the flue gas is sent to the desulfurization unit for H_2S removal. Finally, the flue gas enriched in CO_2 is sent for storage. The CO_2 capture efficiency (η_{CC}) was found to be ~100% for all the cases suggesting the complete conversion of fuel into CO_2 and H_2O in the fuel reactor, as shown in Table 6.5

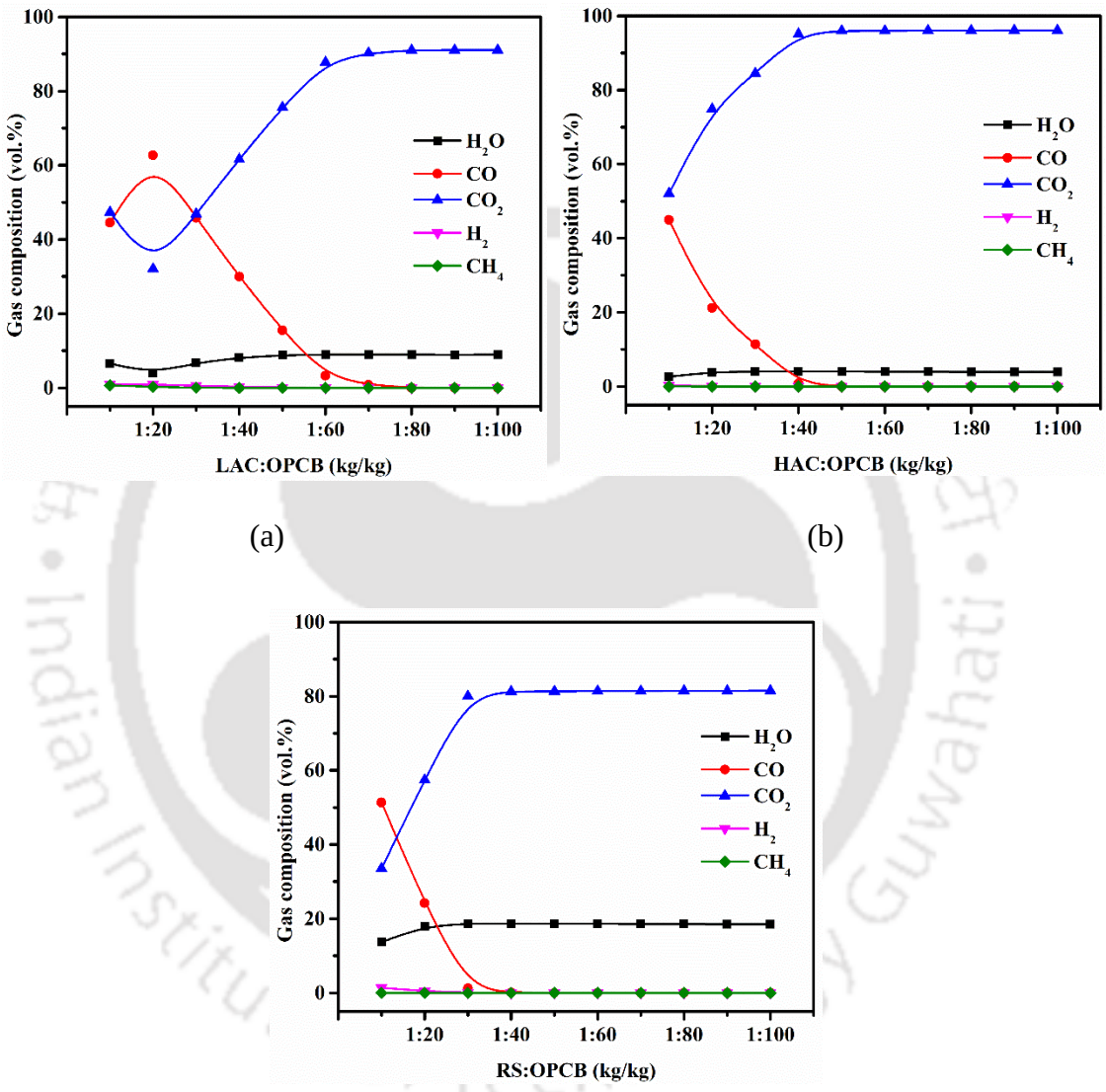

Figure 6.2. Effect of OPCB oxygen carriers on the flue gas composition at the fuel reactor outlet using (a) LAC-OPCB, (b) HAC-OPCB and (c) RS-OPCB.

Table 6.5. Gas composition at the FR outlet using OPCB as the oxygen carrier.

Gases	LAC	LAC	HAC	HAC	RS	RS	LAC-RS	LAC-RS	HAC-RS	HAC-RS
	OPCB	Molto et al. (2009)	OPCB	Molto et al. (2009)	OPCB	Molto et al. (2009)	OPCB	Molto et al. (2009)	OPCB	Molto et al. (2009)
					Gas composition (vol. %)					
H_2	Trace	Trace	Trace	Trace	Trace	Trace	Trace	Trace	Trace	Trace
CH_4	Trace	Trace	Trace	Trace	Trace	Trace	Trace	Trace	Trace	Trace
H_2S	0.21	0.22	-	-	0.004	0.004	0.11	0.11	0.002	0.002
H_2O	8.91	9.22	4.04	4.38	18.65	18.81	12.29	12.50	10.54	10.67
CO	Trace	0.004	0.008	0.002	0.004	0.004	0.004	0.004	0.004	0.005
CO_2	90.88	90.55	95.95	95.61	81.34	81.18	87.59	87.38	89.45	89.32
η_{CC} (%)	99.99	99.99	99.99	99.99	99.98	99.99	99.99	99.99	99.99	99.99
					Pollutant formation (ppm)					
HCl	80.13	78.51	61.29	58.06	61.73	61.11	78.32	69.21	49.19	45.16
N_2	47.47	46.51	50.71	48.05	35.74	35.38	39.36	34.79	48.10	44.16
SO_x	31.21	32.73	-	-	13.70	13.84	21.56	22.45	6.69	6.85

6.3.1. Energy analysis of the power plants

The comparison of the performance of the power plants in terms of their power production, power consumption and thermal efficiency for different fuels employed using OPCB as the oxygen carrier is shown in Table 6.6. The quantity of the oxygen carriers is calculated based on the minimal quantity of unconverted syngas at the outlet. Rice straw based power system exhibited the lowest thermal efficiency among all the cases. However, the blending of rice straw with coal had resulted in an increase in the net efficiency by 1-3%. The net power produced in the LAC, HAC and RS based power system using OPCB as the oxygen carriers are 63.5 MW, 60.8 MW and 56.9 MW, respectively. The blending of LAC and HAC with RS increased the net power production by 4.7 MW for LAC-RS and 1.3 MW for HAC-RS, compared to the power system based on rice straw. The power consumption in the air compression unit is found to be varied based on the air requirement for maintaining the operating temperature of the AR at 1200°C. It can be seen that there is negligible power consumption in the water pumping unit in the range of 0.52-0.59 MW. The net thermal efficiency varies in each case of the power plant due to the variation in their fuel properties and the oxygen carrier used.

Table 6.6. Plant performance based on energy analysis of the CLC process using e-waste based OPCB as the oxygen carrier.

Data	LAC	LAC	HAC	HAC	RS	RS	LAC-RS	LAC-RS	HAC-RS	HAC-RS
Oxygen carrier	OPCB	Molto et al. (2009)	OPCB	Molto et al. (2009)	OPCB	Molto et al. (2009)	OPCB	Molto et al. (2009)	OPCB	Molto et al. (2009)
Air compression (MW)	37.07	36.19	32.81	31.62	31.93	31.36	35.33	34.27	32.59	31.85
Water pump (MW)	0.59	0.58	0.58	0.57	0.57	0.56	0.55	0.53	0.54	0.52
CO_2 compression (MW)	0.92	0.92	0.80	0.80	0.73	0.72	0.89	0.88	0.74	0.73
Total power consumed (MW)	38.58	37.69	34.18	32.99	33.23	32.65	36.78	35.68	33.88	33.10
Air turbine (MW)	75.18	74.18	71.19	70.24	68.01	66.18	73.84	72.65	68.12	67.11
Steam turbine (MW)	26.92	26.05	23.88	22.79	22.18	21.96	24.64	24.32	24.04	23.32
Total power produced (MW)	102.1	100.23	95.07	92.05	90.19	88.15	98.48	96.97	92.16	90.43
Gross efficiency (%)	68.07	66.82	63.38	61.36	60.13	58.77	65.65	64.65	61.44	60.29
Net efficiency (%)	42.37	41.70	40.59	39.73	37.97	36.99	41.13	40.86	38.86	38.22

6.3.2. Effect of fuel properties

The fuel flow rate is calculated based on the chemical energy of the fuel used (150 MW). Due to the lower heating value (17.6 MJ/kg), a higher flow rate of biomass (8.52 kg/s) is maintained. The highest net efficiency is found to be 42.4% for LAC fuel, while the RS had shown the lowest thermal efficiency of 37.9% using OPCB as the oxygen carrier. As RS has higher oxygen content than the coals, a smaller amount of oxygen carrier (35 kg/s) is needed in the fuel reactor, as discussed earlier (Figure 6.2c). The simulation results indicated that the power required for CO_2 compression dropped by 0.19 MW by switching the fuel from LAC to RS due to the lower carbon content in the RS. The ash plays a significant role in the CLC process. It can be noticed that 1.04 MW of heat loss from the slag has occurred in the HAC, while 0.07 MW is accounted for the case of LAC. The heat loss in the rice straw ash slag is 0.44 MW. The co-firing of RS with HAC reduced the heat loss in the ash slag to 0.65 MW. The blending of LAC and HAC with rice straw has resulted in a higher net thermal efficiency by 3.2% and 0.9%, respectively, compared to RS as the fuel.

6.3.3. Effect of ash on OPCB metal oxide

Thermogravimetric analysis (TGA), energy dispersive X-ray (EDX) and X-ray diffraction (XRD) analyses are performed to examine the interaction of ash with OPCB. Figure 6.3 shows the TGA analyses of fuel ash and OPCB. A negligible mass loss of 3% is obtained till 800°C and a sudden drop in the weight loss is observed above 800°C due to the release of lattice oxygen from CuO, which possesses CLOU. It can be noted that irrespective of ash percentage of the fuels, the mass loss trend is found to be similar in all the cases. Table 6.6 shows the EDX analysis of ash content of fuels. It can be observed that the HAC ash contains lower content of Fe and Ca than LAC and RS. However, the

HAC is enriched with silica and alumina, which could be the potential inert supports for the metal oxides. Further, a higher quantity of silica (~25%) and alumina (~18%) in HAC possess a high melting point and would prevent the agglomeration issues. Further, in order to find out the detrimental effect of ash on the OPCB, their interaction is experimentally conducted in a muffle furnace. The XRD analyses of the resultant residues are shown in Figure 6.3. It is found that no complex components such as Fe_2SiO_4, $MgFe_2O_4$, $NaFe(SiO_3)_2$, $Fe(Mg)_3O_4$, $2FeO.2Al_2O_3.5SiO_2$ are detected. Thus, the ash and the OPCB did not interact to form any detrimental complex for all the cases.

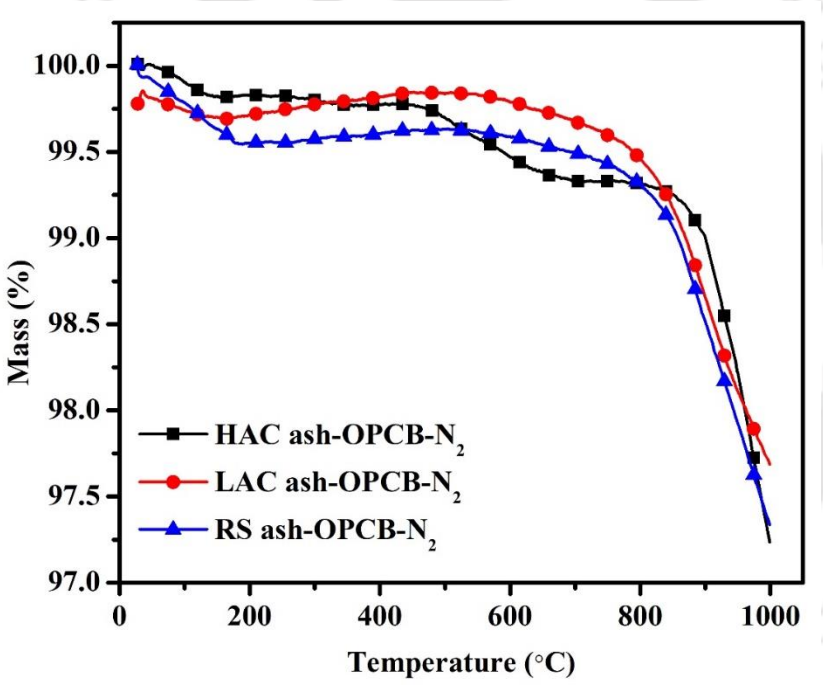

Figure 6.3. Interaction of ash with oxygen carriers using TGA under N_2 atmosphere.

Table 6.7. EDX analysis of ash.

Fuels	O	Si	K	Ca	Mg	Fe	S	Na	Al	Mn	P
LAC	53.12	15.1	0.75	0.35	0.22	18.3	0.12	0.02	12.00	0	0.02
HAC	53.69	25.06	1.25	0.05	0.25	0.90	0.10	0	18.40	0	0.30
RS	47.50	23.30	7.90	13.00	1.00	0.60	1.20	3.60	0.30	1.20	0.40

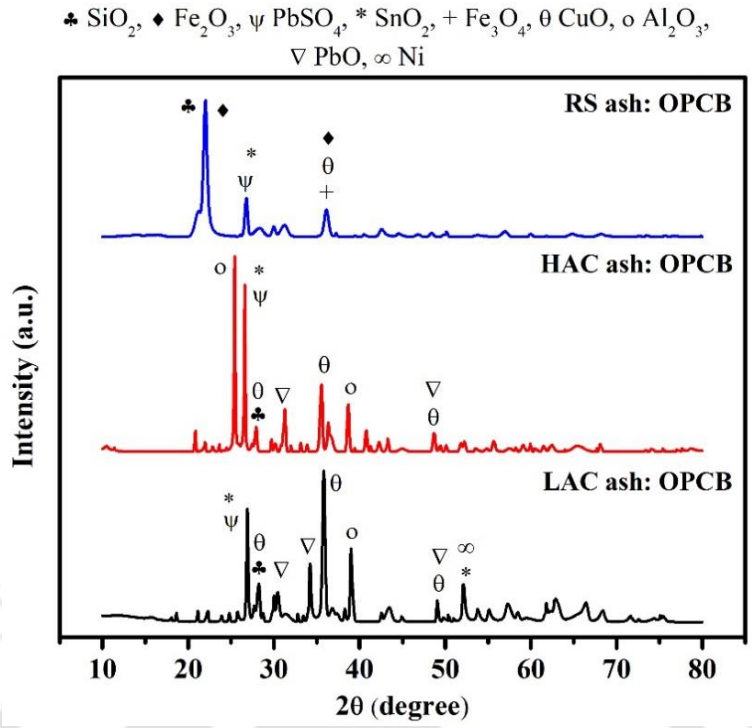

Figure 6.4. XRD analysis of the residue for ash-oxygen carrier (OPCB) interaction.

6.3.4. Effect of oxygen carrier

The conversion of CuO into Cu_2O instead of Cu allows the flexibility to operate the AR at a higher temperature of 1000 °C as the melting point of Cu_2O is 1235°C and 1084°C for Cu. The liberation of oxygen molecules from CuO is initiated at 850°C (Zang et al., 2018). The net thermal efficiency of LAC based power system is the highest among others for Fe_2O_3 oxygen carriers, as shown in Table 6.8 and Figure 6.5. The oxidation of metal is an exothermic reaction, and the reaction enthalpy is found as 480.4 kJ/mol for Fe_3O_4 oxidation and 192.5 kJ/mol for Cu_2O at 1000°C. Thus, a higher amount of thermal energy is generated (91.2-102.8 MW) in the case of pure Fe-based oxygen carriers. Therefore, the total power production using Fe_2O_3 is found to be 4% higher than CuO. Due to the high calorific value of LAC, the net efficiency is enhanced by 1.7%-4.3%, compared to HAC and RS feedstock. As a consequence, the highest of 76.2 MW of electricity is produced in the air turbine in the case of LAC-Fe_2O_3. RS-CuO mixture

showed the lowest efficiency of 37.3%. Hence, the blend of coal and RS is preferred to increase the net power production compared to utilizing RS alone. The amount of Fe_2O_3 with Al_2O_3 required for LAC, HAC and RS is 176.9 kg/s, 100.4 kg/s and 75.4 kg/s, respectively, to achieve complete conversion of fuel into CO_2. The flow rate of CuO with Al_2O_3 is estimated as 59.7 kg/s, 34.7 kg/s and 25.1 kg/s for LAC, HAC and RS fuel, respectively. The oxygen carrying capacity of Fe_2O_3 is lower than the CuO and thus a higher content of Fe_2O_3 is used as discussed in Table 3.3.

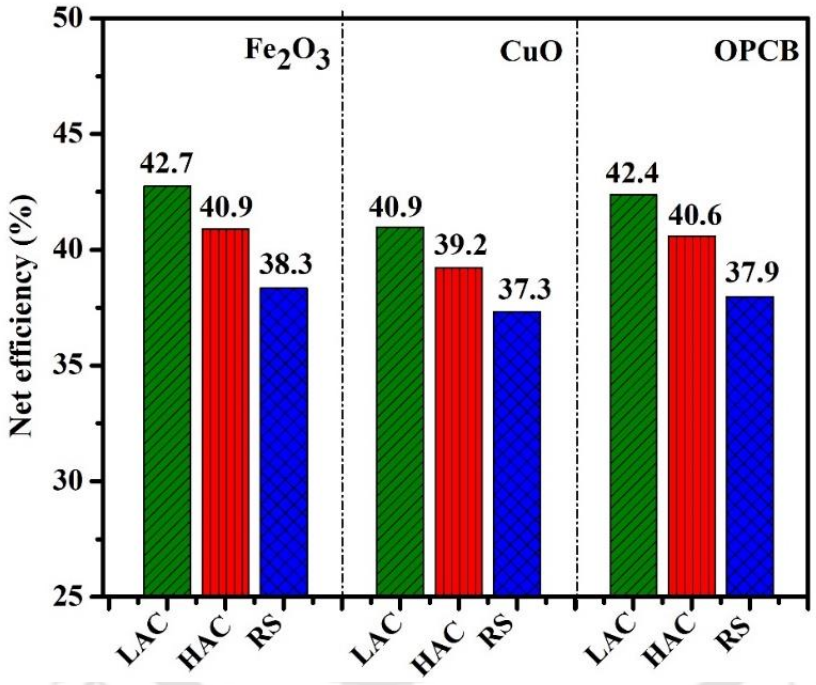

Figure 6.5. Plant performance based on net efficiency of the CLC process using OPCB, Fe_2O_3 and CuO as the oxygen carriers.

In the case of LAC, the OPCB oxygen carriers based power system had achieved a net efficiency of 42.4%, which is almost equivalent to that of the system using commercial Fe_2O_3 oxygen carriers (42.7%), as seen in Figure 6.5. Also, the LAC-OPCB based system achieved a higher efficiency (42.4%) by 1.5% than the pure CuO based power system. It is found that a higher quantity of air is required to balance the heat in the AR, and the oxidation of Fe_2O_3 required a higher quantity of air for all the cases. This is due to their

higher oxidation reaction enthalpy and lower oxygen carrying capacity than other metal oxides. It is estimated that the LAC- Fe_2O_3 required 3.6 kmol/s air and when switching it to the fuel HAC and RS, the air requirement is reduced to 3.4 kmol/s and 3.3 kmol/s, respectively. A similar trend is observed for CuO based oxygen carriers. The total quantity of air required using CuO as the oxygen carrier is 3.4 kmol/s, 3.2 kmol/s and 3.0 kmol/s for LAC, HAC and RS, respectively. Hence in the case of Fe_2O_3 metal oxides, a higher quantity of oxygen depleted air is obtained at a higher temperature at the AR outlet. This resulted in the higher power production in the air turbine by 1.8-3.5 MW, compared to CuO oxygen carriers.

Table 6.9 provides a comparative analysis of net thermal efficiency of the combined cycle power plants reported in various literature for the CLC system for different metal oxides. It can be seen that Fe-based oxygen carriers were mostly chosen because of their higher reactivity and easy availability. It can be seen in the literature that the coal with high ash content of 48.8% resulted in the lowest net thermal efficiency of 38% (Surywanshi et al., 2019); whereas the OPCB-HAC (33% ash) based power system achieved a net thermal efficiency of 42.6%. This shows that the proposed OPCB system has the equivalent potential in a chemical looping combustion unit as that of Pure Fe_2O_3 as metal oxides. Fan et al. (2017) investigated the performance of ilmenite based oxygen with coals of varying ash content. It can be seen that the net efficiency is reduced by 5.0% with the increase in the ash content of coals from 14.9 wt. % to 28.8 wt. %. In the present study, the difference in the net thermal efficiency of the OPCB based power system between the LAC and HAC is found to be 1.8%.

Table 6.8. Plant performance based on the energy analysis of the CLC process using Fe_2O_3 and CuO as the oxygen carriers.

Data	LAC	LAC	HAC	HAC	RS	RS
Oxygen carrier	Fe_2O_3	CuO	Fe_2O_3	CuO	Fe_2O_3	CuO
Air compression (MW)	37.44	35.32	32.91	31.28	32.45	29.88
Water pump (MW)	0.59	0.58	0.58	0.57	0.56	0.53
CO_2 compression (MW)	0.92	0.92	0.80	0.80	0.73	0.73
Power consumed (MW)	*38.96*	*36.82*	*34.28*	*32.65*	*32.74*	*31.14*
Air turbine (MW)	76.23	73.31	71.73	68.19	68.80	63.34
Steam turbine (MW)	26.57	24.98	23.88	23.29	22.40	23.81
Power produced (MW)	*102.80*	*98.29*	*95.62*	*91.48*	*91.20*	*87.14*
Gross efficiency (%)	68.53	65.53	63.75	60.98	60.80	58.09
Net efficiency (%)	42.56	40.97	40.88	39.25	38.31	37.33

Table 6.9. Comparison of the performance of e-waste based power plants with literature results.

Fuel	Oxygen carrier	Operating parameters	Plant configuration	Net efficiency (%)	References
Coal (Ash 16.75%)	Fe_2O_3	CO_2, T_{FR}: 850-910°C, T_{AR}: 940-950°C, P:1 atm.	Brayton cycle	41.3%	Chen et al. (2018)
Coal (Ash 9.7%)	Fe_2O_3	CO_2, T_{FR}: 1100-1300°C, T_{AR}: 1300°C, P:30 atm.	Combined cycle	44.4%	Mukherjee et al. (2015)
Coal (Ash 48.87%)	Fe_2O_3	T_{FR}: Adiabatic, T_{AR}: 900°C, P:10 bar	Combined cycle	38.2%	Surywanshi et al. (2019)
Lignite Coal (Ash 28.8%)	Ilmenite	Steam, T_{FR}: 900-940°C, T_{AR}: 1050°C, P:15 atm.	Combined cycle	39.0%	Fan et al. (2017)
Bituminous Coal (Ash 14.9%)	Ilmenite	Steam, T_{FR}: 900-940°C, T_{AR}: 1050°C, P:15 atm.	Combined cycle	44.0%	Fan et al. (2017)
Sawdust (Ash 0.9%)	Ilmenite	Steam, T_{FR}: 650-900°C, T_{AR}: 800-1000°C, P:38 bar	Combined cycle	42.5%	Cormos (2015)
LAC (Ash 2.1%)	OPCB	CO_2, T_{FR}: 900°C, T_{AR}: 1000°C, P:30 bar	Combined cycle	42.4%	Present study
HAC (Ash 33.0%)	OPCB	CO_2, T_{FR}:900°C, T_{AR}: 1000°C, P:30 bar	Combined cycle	40.6%	Present study

6.3.5. Economic analysis of the power plants

The economic indicators used in the e-waste based CLC processes are capital cost, specific investment cost and LCOE. The total capital cost is estimated based on the reactor cost, solid fuel handling system, power generating equipment cost and their utilities. The accessories cost includes the cost of heat exchangers, fans, cyclone separators and condensers. The LCOE assessment of the CLC power plants is shown in Table 6.10. It can be observed that the cost of the CLC reactors for biomass is found to be higher than the coal based CLC reactors. It is due to the higher mass flow rate of rice straw with 8.52 kg/s, while the coal flow rate is found in the range of 4.6-6.8 kg/s. At these flow rates, the RS fuel cost is higher than the HAC cost by 0.99 M$/year. The fuel cost is accounted as 6.81 M$/year for LAC and 5.25 M$/year for HAC. The production cost of OPCB from e-waste is included in terms of the capital cost of a combustor. The capital cost of the OPCB production consists of a combustor unit in which the series processes such as pyrolysis, gasification and combustion of PCB is carried out. The cost of the combustor unit is estimated based on the reference, Jiang & Bhattacharyya, (2017). The equipment cost of the fans and cyclone separator is calculated using the data from Wu et al. (2020). Solids handling cost includes the pre-treatment cost for moisture removal and the crushing cost to reduce the size of solid fuel before feeding into the fuel reactor. Due to the high energy consumption in biomass processing, the solid handling cost of RS is estimated as 8.8 M$, while this cost accounting for LAC and HAC is 5.8 M$ and 7.7 M$, respectively. The LCOE of LAC-OPCB is found to be 85.9 $/MWh, while the LCOE of RS-OPCB is higher than LAC-OPCB system by 8.3 $/MWh. This is due to the low net power production in the case of RS. The addition of the coal to the RS biomass had resulted in the LCOE of about 90.2 $/MWh for LAC-RS, while it is 91.4

$/MWh for HAC-RS. The lowest LCOE of 85.9 $/MWh is estimated for LAC-OPCB fuel and the highest LCOE of 94.3 $/MWh is found for RS-OPCB fuel.

The net electrical efficiency is estimated for the power plants operating with AR temperatures ranging from 950°C to 1200 °C. The variation in the net efficiency and LCOE with the operating temperature of the AR is shown in Figure 6.6. The net efficiency is found to be increased by 3.95% with an increase in the operating temperature from 950°C to 1200°C. The LCOE of LAC-OPCB is reduced from 88.2 $/MWh to 80.6 $/MWh by increasing the operating temperature from 950°C to 1200°C. The operating temperature of the CLC process depends on the melting point of the metal oxides in the OPCB. The melting point of CuO is 1232°C, which is lower than the melting point of Fe_2O_3 (1565°C) and NiO (1959°C). In order to address the sintering and self-heating issues, the operating temperature of the AR is to be maintained at 1000°C.

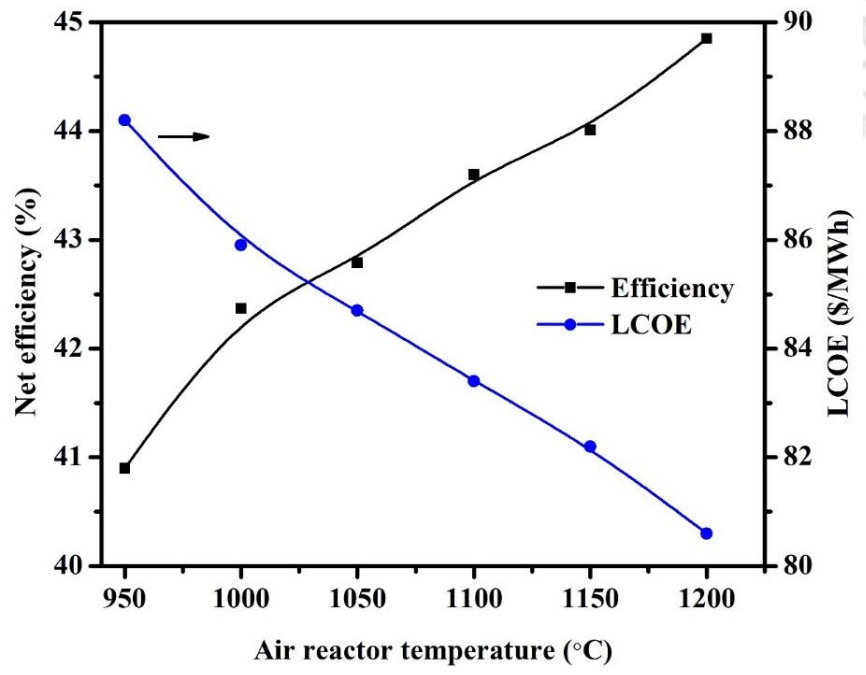

Figure 6.6. Effect of air reactor temperature on net energy efficiency and LCOE for LAC-OPCB case.

Table 6.10. Plant performance based economic analysis of the CLC power systems using e-waste as the oxygen carrier ([a] - data taken from aspen).

Cost analysis	LAC	LAC	HAC	HAC	RS	RS	LAC-RS	LAC-RS	HAC-RS	HAC-RS
Oxygen carrier	OPCB	Molto et al. (2009)	OPCB	Molto et al. (2009)	OPCB	Molto et al. (2009)	OPCB	Molto et al. (2009)	OPCB	Molto et al. (2009)
CLC – FR (M$)	9.02	9.02	11.88	11.88	13.42	13.42	10.72	10.72	12.60	12.60
CLC – AR (M$)	3.00	3.00	3.96	3.96	4.47	4.47	3.57	3.57	4.20	4.20
PCB combustor (M$)	2.59	2.59	2.51	2.51	2.47	2.47	2.53	2.53	2.49	2.49
Power generating systems (M$)	60.27	59.61	57.75	57.00	55.57	55.19	58.98	58.43	56.68	56.04
Solids handling	5.81	5.81	7.77	7.77	8.82	8.82	6.96	6.96	8.26	8.26
Accessories costs (M$)	100.78	99.82	97.97	97.68	92.62	90.45	96.16	95.28	92.72	92.54
Owners cost (M$)	15.10	14.96	14.65	14.64	13.82	13.56	14.42	14.28	13.90	13.87
Land purchase, surveying etc.	5.04	4.99	4.88	4.88	4.61	4.52	4.81	4.76	4.63	4.62
Utilities (M$)[a]	25.62	25.57	23.89	23.05	21.63	20.8	24.68	24.48	22.34	22.31
Total capital cost (M$)	227.23	225.37	225.26	223.37	217.43	213.7	222.83	221.01	217.82	216.93
Labor cost, Maintenance cost, overhead charges (M$/year)[a]	4.89	4.77	4.69	4.69	3.98	3.91	3.48	3.20	3.26	3.16
Fuel cost (M$/year)	6.81	6.81	5.25	5.25	6.24	6.24	6.53	6.53	5.75	5.75
Slag disposal cost (M$/year)	0.04	0.04	0.79	0.79	0.34	0.34	0.15	0.15	0.59	0.59
CO_2 transport and storage cost (M$/year)	17.41	17.41	17.17	17.01	15.80	15.66	17.23	16.95	15.74	15.93
Total operating cost	29.03	28.91	27.91	27.75	27.16	26.95	27.76	27.19	25.66	25.74
LCOE ($/MWh)	85.99	86.90	88.27	89.46	94.31	94.82	90.22	90.98	91.38	92.89

A comparative study is shown in Figure 6.7 for the LCOE of different oxygen carriers based power systems. It can be seen that the LCOE of LAC-OPCB is the lowest at 85.9 \$/MWh, compared to the LCOE of LAC-Fe_2O_3 and LAC-CuO. The LAC-OPCB system decreased the LCOE by 8.9 \$/MWh and 15.3 \$/MWh, compared to the pure metal oxide based LAC-Fe_2O_3 and LAC-CuO power systems, respectively. A similar trend is observed for HAC and RS fuel. The variation in the LCOE is due to the oxygen carrier cost. As the quantity of metal oxides required varies depending on the fuel, the total estimated price of Fe_2O_3 has also varied in the range of 86.7 M\$, 60.7 M\$ and 52.0 M\$ for LAC, HAC and RS, respectively. This has increased the capital cost of LAC-Fe_2O_3 system (313.2 M\$), compared to LAC-OPCB based system (227.2 M\$). Due to the higher cost of CuO, the cost of oxygen carriers has increased by 17.4 M\$, 15.3 M\$ and 11.1 M\$ for LAC, HAC and RS, respectively. Though the total cost of oxygen carriers is higher for the LAC fuel, the LCOE is the lowest compared to other fuels due to the higher net power production.

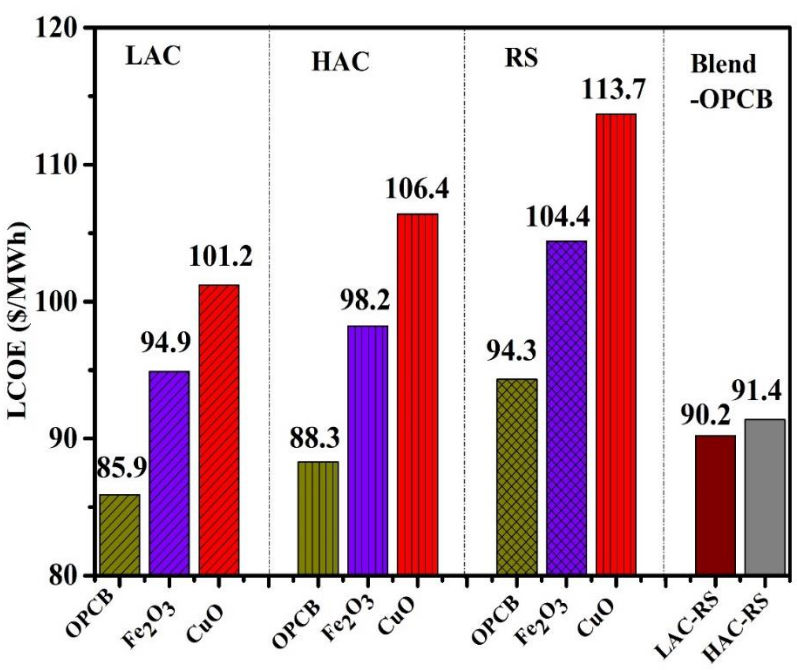

Figure 6.7. Comparison of LCOE based on different metal oxides in the CLC integrated power systems.

The specific net investment cost for all the cases of the power plants is shown in Figure 6.8. The co-utilization of coal with rice straw impacts the net investment cost, which is decreased by 241.3 $/KW and 136.6 $/KW for LAC-RS and HAC-RS system, compared with the RS system, respectively. It can be seen that the net investment cost of the OPCB based LAC system has decreased by 1002.6 $/kW and 1354.6 $/kW, compared to Fe_2O_3 and CuO based LAC systems, respectively. A similar trend is observed for HAC and RS. The net investment has decreased by 988.5 $/kW for HAC-$Fe_2O_3$ and 947.4 $/kW for RS-$Fe_2O_3$, while it is 1253.9 $/kW for HAC-CuO and 1276.5 $/kW for RS-CuO. The net investment has decreased by 1000 $/kW and 1300 $/kW (approx.) by switching from Fe_2O_3 and CuO based oxygen carriers to OPCB, respectively. Hence, the utilization of e-waste based oxygen carrier effectively reduced the investment cost.

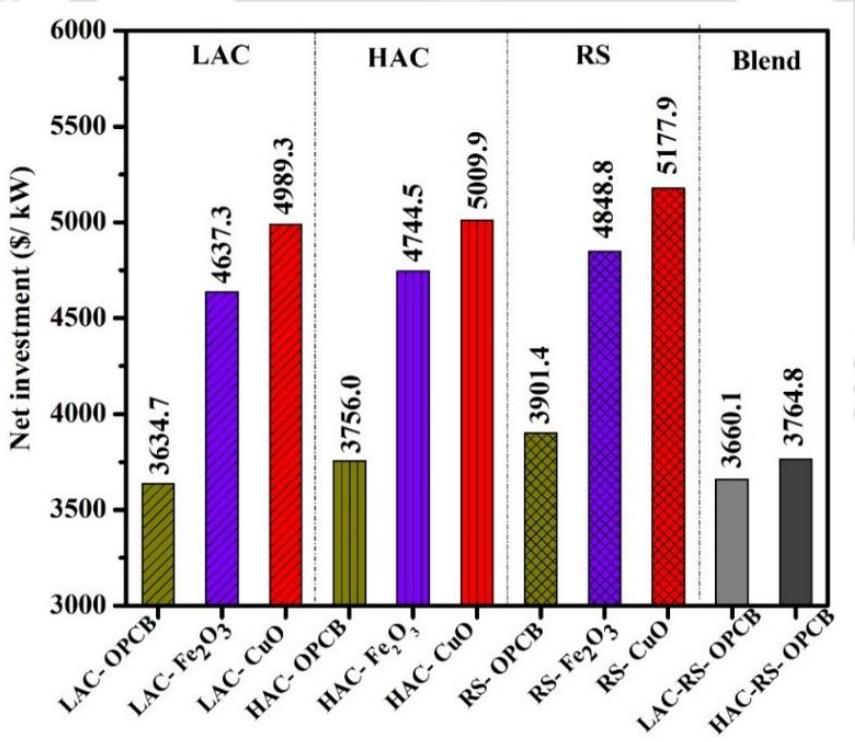

Figure 6.8. Comparison of net investment cost of different fuel-metal oxide combination in CLC integrated combined cycle power systems.

6.4. Conclusions

Using e-waste based oxygen carriers, energy and economic analysis are performed for the direct coal fuelled CLC integrated combined cycle power system with CO_2 as the gasifying agent. Rice straw is used as the co-feed with coal for alternate and carbon neutral feedstock for energy production. The following conclusions are obtained from the present study.

- E-waste based metal oxides (OPCB) employed CLC-combined cycle power system achieved a net thermal efficiency of 42.4%, 40.6% and 37.9% for LAC, HAC and RS based fuels, respectively.
- The LAC-OPCB based power system attained an equivalent net thermal efficiency of 42.4%, compared to the LAC-Fe_2O_3 system.
- The LCOE of OPCB based combined cycle power system is found to be 85.9 $/MWh for LAC, 88.3 $/MWh for HAC and 94.3 $/MWh for RS.
- The LAC-OPCB system had achieved the lowest LCOE of 85.9 $/MWh, compared to LAC-$Fe_2O_3$ and LAC-CuO with a difference of 8.9 $/MWh and 15.3 $/MWh, respectively.
- The 50% addition of rice straw with LAC and HAC had decreased the net thermal efficiency of the OPCB power plants only with a marginal difference of 1.2% and 1.7%, respectively, compared to the LAC and HAC based power system without blending.
- The blending of RS with LAC and HAC had resulted in a decrease of LCOE from 94.3 $/MWh to 90.2 $/MWh and 91.4 $/MWh, respectively, compared to the RS based power system without blending.

The economic analysis showed that the e-waste based oxygen carriers could achieve a net thermal efficiency equivalent to commercial oxygen carriers (Fe_2O_3, CuO) based power systems with a lower LCOE in the CLC process.

References

Ahirwar, R., & Tripathi, A. K. (2021). E-waste management: A review of recycling process, environmental and occupational health hazards, and potential solutions. *Environmental Nanotechnology, Monitoring and Management*, *15*, 100409.

Barin, I. (1995). *Thermochemical Data of Pure Substances* (Third). VCH.

Borthakur, A., & Govind, M. (2018). Public understandings of E-waste and its disposal in urban India: From a review towards a conceptual framework. *Journal of Cleaner Production*, *172*, 1053–1066.

Chen, S., Soomro, A., Yu, R., Hu, J., Sun, Z., & Xiang, W. (2018). Integration of chemical looping combustion and supercritical CO_2 cycle for combined heat and power generation with CO_2 capture. *Energy Conversion and Management*, *167*, 113–124.

Chen, Y., Liang, S., Xiao, K., Hu, J., & Hou, H. (2021). A cost-effective strategy for metal recovery from waste printed circuit boards via crushing pretreatment combined with pyrolysis : Effects of particle size and pyrolysis temperature. *Journal of Cleaner Production*, *280*, 124505.

Cormos, C. (2015). Biomass direct chemical looping for hydrogen and power co-production : Process configuration, simulation, thermal integration and techno-economic assessment. *Fuel Processing Technology*, *137*, 16–23.

De Vries, A., & Stoll, C. (2021). Bitcoin's growing e-waste problem. *Resources,*

Conservation and Recycling, *175*, 105901.

Fan, J., Zhu, L., Hong, H., Jiang, Q., & Jin, H. (2017). A thermodynamic and environmental performance of in-situ gasification of chemical looping combustion for power generation using ilmenite with different coals and comparison with other coal-driven power technologies for CO_2 capture. *Energy*, *119*, 1171–1180.

Jiang, Y., & Bhattacharyya, D. (2017). Techno-economic analysis of direct coal-biomass to liquids (CBTL) plants with shale gas utilization and CO_2 capture and storage (CCS). *Applied Energy*, *189*, 433–448.

Kiran, M., Shanmugam, P. V., Mishra, A., Mehendale, A., & Nadheera Sherin, H. R. (2021). A multivariate discrete grey model for estimating the waste from mobile phones, televisions, and personal computers in India. *Journal of Cleaner Production*, *293*, 126185.

Molto, J., Font, R., Galvez, A., & Conesa, J. A. (2009). Pyrolysis and combustion of electronic wastes. *Journal of Analytical and Applied Pyrolysis*, *84*, 68–78.

Mukherjee, S., Kumar, P., Yang, A., & Fennell, P. (2015). Energy and exergy analysis of chemical looping combustion technology and comparison with pre-combustion and oxy-fuel combustion technologies for CO_2 capture. *Journal of Environmental Chemical Engineering*, *3*, 2104–2114.

Shittu, O. S., Williams, I. D., & Shaw, P. J. (2021). Global E-waste management: Can WEEE make a difference? A review of e-waste trends, legislation, contemporary issues and future challenges. *Waste Management*, *120*, 549–563.

Surywanshi, G. D., Pillai, B. B. K., Patnaikuni, V. S., Vooradi, R., & Anne, S. B. (2019). 4-E analyses of chemical looping combustion based subcritical, supercritical and

ultra-supercritical coal-fired power plants. *Energy Conversion and Management*, *200*, 112050.

Wu, S., Zhou, C., Doroodchi, E., & Moghtaderi, B. (2020). Techno-economic analysis of an integrated liquid air and thermochemical energy storage system. *Energy Conversion and Management*, *205*, 112341.

Zang, G., Jia, J., Tejasvi, S., Ratner, A., & Silva, E. (2018). Techno-economic comparative analysis of biomass integrated gasification combined cycles with and without CO_2 capture. *International Journal of Greenhouse Gas Control*, *78*, 73–84.

CHAPTER 7

Conclusions
&
Future Work

CHAPTER 7

CONCLUSIONS & FUTURE WORK

This chapter draws the overall conclusions of the CLC performance. It further indicates some recommendations for future research.

7.1. Major conclusions

The electronic waste based oxygen carriers showed a better reactivity with coals, rice straw and their blends. The major conclusions of the thesis are as follows:

- Using the commercial Fe_2O_3 based oxygen carriers, the fixed bed reactor experimental studies confirmed the higher CO_2 yield, which is increased from 85.8% to 88.1% by blending LAC with rice straw. Similarly, the blend of HAC-RS- Fe_2O_3 increased the CO_2 yield by 5.1%.
- The gas conversion of LAC-Fe_2O_3 mixture is found to be 89.1%. This conversion is further increased to 91.3% by blending with RS. Due to the lower reactivity of HAC with Fe_2O_3, the gas conversion (~ 85.5%) is found lower than that of LAC-Fe_2O_3, achieving 89.1% of gas conversion.
- The char conversion has decreased from 90.9% (LAC-Fe_2O_3) to 87.8% (HAC-Fe_2O_3) by switching the fuel from LAC to HAC. The blend of RS increased the char conversion from 90.9% to 92.7% in the case of LAC-RS-Fe_2O_3 and 87.8% to 91.4% for HAC-RS-Fe_2O_3.
- The formation of calcium ferrite from RS ash is beneficial as an oxygen carrier, resulting in 15% mass loss in HAC char and 18% in LAC char under inert atmosphere.

- With the use of e-waste, potential metals such as Cu, Fe, and Ni could be obtained from the PCB of a computer for CLC operation. The interesting fact is that the extracted metal from PCB contains 22% CuO, 21% Fe_2O_3 and 3% NiO along with inert supports such as alumina and silica about 33%. The composition of the metal and inert supports in the OPCB is highly suitable for the CLC operation.
- The BET surface area of the OPCB oxygen carriers obtained from the e-waste is found to be 7.11 m^2/g, which is 4.59 m^2/g higher than the commercial Fe_2O_3 (2.52 m^2/g). The surface area is found to be increased from 7.11 to 10.6 m^2/g upon re-oxidation.
- The unconverted CO is reduced from 20.4% to 4.2% with increase in the OPCB mass ratio from 1:10 to 1:60 (LAC: OPCB). As a result, the gas conversion of LAC-OPCB reached to 93.8% at 1:60 mass ratio. The presence of mixed metal oxides in the OPCB resulted in the increase in the gas conversion by 3.6%, compared to LAC-Fe_2O_3 case. The blend of LAC-RS-OPCB further increased the CO_2 yield by 2.4% than LAC-OPCB case.
- The char conversion in the mixture LAC-OPCB case is found to be 93.6%, which is 4% higher than the HAC-OPCB case. This resulted in an increase in the gas conversion by 3.2% for LAC-OPCB. The CO_2 yield of LAC-RS-OPCB is 92.8%, which is 2.4% higher than LAC-OPCB case.
- The CLC performance of OPCB is found to be higher than the commercial Fe_2O_3 in all the cases. The CO_2 yield for LAC-RS-OPCB (92.8%) is 3.7% higher than LAC-RS-Fe_2O_3 case. Similarly, HAC-RS-OPCB mixture increased the CO_2 yield by 2.9%, compared to HAC-RS-Fe_2O_3 case.
- The blends of the coal-RS reduced the activation energy from 33.5 kJ/mol to 28.1 kJ/mol in the case of LAC-Fe_2O_3, whereas it is reduced by 45.4% in the case of

HAC-RS blend at 400-600℃. The activation energy of blends has declined by 18.3% for LAC-RS and 25.2% for HAC-RS, compared to LAC-Fe_2O_3 and HAC-Fe_2O_3 at 800-1000℃.

- In the case of the OPCB oxygen carriers, a similar trend in the reduction of activation energy is assessed. LAC-RS and HAC-RS blends reduced the activation energy by 26.5% and 51.3%, respectively, at 400-600℃ compared to the coals. However, the OPCB further reduces the activation energy by 7-25% due to the improved surface morphology and the presence of CuO.
- The net efficiency of the OPCB based combined cycle power plant is found to be 42.4%, 40.6% and 37.9% for LAC, HAC and RS based feedstock, respectively. The estimated efficiencies based on OPCB are found to be equivalent with the net thermal efficiency of the Fe_2O_3 based CLC system. The performance of OPCB based system is found 0.6%-1.5% higher than the CuO based CLC power plants.
- Blending of RS with LAC and HAC has resulted in the decrease in the LCOE from 94.3 $/MWh to 90.2 $/MWh (LAC-RS-OPCB) and 91.4 $/MWh (HAC-RS-OPCB).
- The LAC-OPCB system has achieved the lowest LCOE of 85.9 $/MWh, compared to LAC-$Fe_2O_3$ and LAC-CuO feedstock with a difference of 8.9 $/MWh and 15.3 $/MWh, respectively.

7.2. Future scope of the study

The future work is intended to improve the performance of the CLC process for commercial implementation. The potential aspects of the CLC process need to be further studied as:

- In order to ensure the stability of OPCB particles, multiple redox cycles of e-waste as oxygen carriers with coal/ rice straw need to be performed for stability purposes.
- The syngas generated during pyrolysis and gasification of metal extraction processes can be used as a co-feed along with high ash coal for better reactivity. Aspen plus process simulation needs to be carried out to evaluate the impact of reducing the LCOE of the power plants.
- The feasibility of integrating continuous metal extraction units with CLC based power plants can be examined by process simulation.
- The effect of harmful gases generated during PCB pyrolysis and its impact on the CLC performance needs to be assessed.
- The effect of high sulphur coal on the CO_2 yield of the CLC process needs to be evaluated.

RESEARCH OUTPUTS

RESEARCH OUTPUT FROM THE THESIS

Refereed journal papers

1. **Bhui, B**. and Vairakannu, P., 2019. Experimental and kinetic studies on in-situ CO_2 gasification based chemical looping combustion of low ash coal using Fe_2O_3 as the oxygen carrier. ***Journal of CO_2 Utilization***, 29,103-116. (Impact Factor 7.132).

2. **Bhui, B**. and Vairakannu, P., 2019. Prospects and issues of integration of co-combustion of solid fuels (coal and biomass) in chemical looping technology. ***Journal of Environmental Management***, 231, 1241-1256. (Impact Factor 6.789)

3. **Bhui, B**. and Vairakannu, P., 2020. Co-chemical looping combustion of high ash Indian coal and rice straw operating under CO_2 in-situ gasification mode. ***Journal of the Energy Institute***, 94, 176-190. (Impact Factor 6.186)

4. **Bhui, B**. and Vairakannu, P., 2021. Experimental investigations on electronic waste based oxygen carriers for direct coal fuelled chemical looping combustion process**.** ***Fuel***, 305, 121535. (Impact Factor 6.609)

5. **Bhui, B**. and Vairakannu, P., 2021. Techno-economic evaluation of electronic waste based oxygen carriers for co-chemical looping combustion of coal and biomass integrated combined cycle power generating systems. ***Energy Conversion and Management***, 236, 114075. (Impact Factor 9.709)

6. **Bhui, B**. and Vairakannu, P., 2021. Electronic waste metals as novel oxygen carriers for chemical looping combustion of high ash Indian coals. ***Waste Management,*** 138, 199-209. (Impact Factor 7.145)

Other research outputs

1. Mishra, N., **Bhui, B**. and Vairakannu, P., 2019. Comparative evaluation of performance of high and low ash coal fuelled chemical looping combustion integrated

combined cycle power generating systems. ***Energy,*** 169, 305-318. (Impact Factor 7.147).

2. Rai, C., **Bhui, B**. and Vairakannu, P., 2022. Techno-economic analysis of e-waste based chemical looping reformer as hydrogen generator with co-generation of metals, electricity and syngas. ***Internal Journal of Hydrogen Energy***- *Accepted*, (Impact Factor 5.816)

Book chapter publication

1. **Bhui, B.** and Vairakannu, P., 2018. Chemical Looping and Plasma Technologies for Gasification of Coal and Biomass. In *Coal and Biomass Gasification* (pp. 499-520). Springer, Singapore.

2. **Bhui, B.,** Pathak, SJ and Vairakannu, P., 2022. Effective utilization of e-waste in advanced energy technology processes. In Electronic Waste Management: Policies, Processes, Technologies and Impact. ***Wiley*** (under preparation).

Conference proceedings

1. **Bhui, B.** and Vairakannu, P., Thermo-gravimetric analyzer studies on direct coal fuelled chemical looping combustion under N_2 and CO_2 atmosphere. Proceeding of *Sustainable Energy and Environmental Challenges (SEEC-2018)* 31st December, 2017-3rd January, 2018 Indian Institute of Science, Bangalore, India (Best oral presentation award).

2. **Bhui, B.** and Vairakannu, P., Co-chemical looping combustion of high ash Indian coal and rice straw with Fe_2O_3 as the oxygen carrier using fixed bed reactor and thermogravimetric analyzer. *International Conference on Coal Science & Technology (ICCS&T 2019).* 24th November-28th November, 2019. Krakow, Poland.

3. **Bhui, B.** and Vairakannu, P., Electronic waste based oxygen carriers for direct coal fueled chemical looping combustion technology. *Sustainable Energy and Green Technology 2019 (SEGT 2019).* 11th December-14th December, 2019, Bangkok.

4. **Bhui, B.** and Vairakannu, P., Thermochemical interaction of biomass ash with Indian coals in the context of chemical looping combustion technology under N_2 atmosphere. 3rd Sustainable Waste Management Conference 2021. 4th August-6th August, 2021. AICHE (Selected for oral presentation by virtual mode).

5. **Bhui, B.** and Vairakannu, P., Investigation of biomass ash as an affordable oxygen carrier for the chemical looping process using TGA. *Advances in Sustainable Research for Energy and Environmental Management 2021 (ASREEM 2021).* 6th August-8th August, 2021. NIT Surat, India (Selected for oral presentation by virtual mode).